U.S.NRC
United States Nuclear Regulatory Commission
Protecting People and the Environment

NUREG/CR-7231

Modeling of Radionuclide Transport in Freshwater Systems Associated with Nuclear Power Plants

Office of Nuclear Regulatory Research

AVAILABILITY OF REFERENCE MATERIALS IN NRC PUBLICATIONS

NRC Reference Material

As of November 1999, you may electronically access NUREG-series publications and other NRC records at NRC's Library at www.nrc.gov/reading-rm.html. Publicly released records include, to name a few, NUREG-series publications; *Federal Register* notices; applicant, licensee, and vendor documents and correspondence; NRC correspondence and internal memoranda; bulletins and information notices; inspection and investigative reports; licensee event reports; and Commission papers and their attachments.

NRC publications in the NUREG series, NRC regulations, and Title 10, "Energy," in the *Code of Federal Regulations* may also be purchased from one of these two sources.

1. **The Superintendent of Documents**
   U.S. Government Publishing Office
   Mail Stop IDCC
   Washington, DC 20402-0001
   Internet: bookstore.gpo.gov
   Telephone: (202) 512-1800
   Fax: (202) 512-2104

2. **The National Technical Information Service**
   5301 Shawnee Rd., Alexandria, VA 22312-0002
   www.ntis.gov
   1-800-553-6847 or, locally, (703) 605-6000

A single copy of each NRC draft report for comment is available free, to the extent of supply, upon written request as follows:

Address: **U.S. Nuclear Regulatory Commission**
Office of Administration
Publications Branch
Washington, DC 20555-0001
E-mail: distribution.resource@nrc.gov
Facsimile: (301) 415-2289

Some publications in the NUREG series that are posted at NRC's Web site address www.nrc.gov/reading-rm/doc-collections/nuregs are updated periodically and may differ from the last printed version. Although references to material found on a Web site bear the date the material was accessed, the material available on the date cited may subsequently be removed from the site.

Non-NRC Reference Material

Documents available from public and special technical libraries include all open literature items, such as books, journal articles, transactions, *Federal Register* notices, Federal and State legislation, and congressional reports. Such documents as theses, dissertations, foreign reports and translations, and non-NRC conference proceedings may be purchased from their sponsoring organization.

Copies of industry codes and standards used in a substantive manner in the NRC regulatory process are maintained at—

The NRC Technical Library
Two White Flint North
11545 Rockville Pike
Rockville, MD 20852-2738

These standards are available in the library for reference use by the public. Codes and standards are usually copyrighted and may be purchased from the originating organization or, if they are American National Standards, from—

American National Standards Institute
11 West 42nd Street
New York, NY 10036-8002
www.ansi.org
(212) 642-4900

Legally binding regulatory requirements are stated only in laws; NRC regulations; licenses, including technical specifications; or orders, not in NUREG-series publications. The views expressed in contractorprepared publications in this series are not necessarily those of the NRC.

The NUREG series comprises (1) technical and administrative reports and books prepared by the staff (NUREG–XXXX) or agency contractors (NUREG/CR–XXXX), (2) proceedings of conferences (NUREG/CP–XXXX), (3) reports resulting from international agreements (NUREG/IA–XXXX), (4) brochures (NUREG/BR–XXXX), and (5) compilations of legal decisions and orders of the Commission and Atomic and Safety Licensing Boards and of Directors' decisions under Section 2.206 of NRC's regulations (NUREG–0750).

U.S.NRC
United States Nuclear Regulatory Commission
Protecting People and the Environment

NUREG/CR-7231

Modeling of Radionuclide Transport in Freshwater Systems Associated with Nuclear Power Plants

Manuscript Completed: November 2016
Date Published: April 2017

Prepared by: S. B. Yabusaki, B. A. Napier,
W. A. Perkins, M. C. Richmond, C. L. Rakowski,
S. F. Snyder, and L. F. Hibler

Pacific Northwest National Laboratory
Richland, Washington 99352

Mark Fuhrmann, Project Manager

NRC Job Code V6366

Office of Nuclear Regulatory Research

ABSTRACT

The potential consequences of radionuclides that have been directly released into a surface water body, as happened in the 2011 Fukushima Daiichi nuclear power plant accident, are not well understood, especially for the lake and river settings where most U.S. nuclear power plant reactors are sited. Accordingly, hypothetical scoping analyses have been performed to better understand how radionuclide transport in freshwater systems might be affected by the interaction of radionuclide-specific decay and sorption with hydrologic and sediment conditions.

Eight radionuclides, ^{137}Cs, ^{134}Cs, ^{131}I, ^{90}Sr, ^{3}H, ^{106}Ru, ^{125}Sb, and ^{144}Ce, were selected for these analyses based on a methodology that estimated the partitioning of the reactor core inventory to water as a function of reactor type, mass of uranium fuel, and fuel burnup. Transport simulations for each radionuclide were based on the release of a 10-day pulse of 1,000 m^3 of water with 1 Bq of activity into small lake, small river, and large river settings. The small lake setting was based on a reservoir impounded by a dam on a river that provided a large water volume but limited transport, which led to high concentrations at early times. The small river setting examined relatively low flow and slow average velocity conditions, which resulted in less dilution (i.e., higher concentrations) and longer transit times for the 10-day radioactive release. The large river scenario examined conditions where relatively high flow resulted in lower concentrations but faster downriver transport.

Bathymetric data and hydraulic parameters were adapted and modified from actual lake and river systems. Consistent with the scoping level of analysis, steady-state hydraulics were used with the rivers simulated in two dimensions (depth-averaged) and the lake in three dimensions. Modeled transport processes included advection, mixing/dispersion, decay, sediment transport, and sediment-radionuclide interaction (i.e., adsorption/desorption); modeled features included the impact of tributaries, dams, and impoundments.

FOREWORD

Over the years, the NRC has analyzed many hypothetical severe accidents involving releases of radionuclides. Most of these analyses assessed the impact of releases to the atmosphere because air-borne contaminants can be transported rapidly over a large area. Several studies (e.g., NUREG/CR–4251 and NUREG-0140) examined radionuclides carried in water, but these studies assumed that the molten core material breached the basemat of the reactor building and came into contact with soil and groundwater. Contaminants distributed in groundwater would move slowly due to groundwater flow rates and reactions with the soil. In this current study, contaminated water is assumed to have been released directly to the water body, much like the observed release to the ocean during the Fukushima Daiichi accident.

The Fukushima Daiichi nuclear reactor accident of March 2011 resulted in leakage of more than 1,000 m^3 of highly contaminated water directly into the Pacific Ocean. This type of direct leakage path had not been analyzed by the U.S. Nuclear Regulatory Commission (NRC). As a result, the Office of Nuclear Regulatory Research contracted with the staff at Pacific Northwest National Laboratory to produce this exploratory study entitled, *Modeling of Radionuclide Transport in Freshwater Systems Associated with Nuclear Power Plants.*

This report presents state-of-the-art hydrologic transport modeling results for leakage of waterborne radionuclides directly into a freshwater body. The study postulates releases to three types of freshwater settings typical of NPPs within the United States: a large river, a small river, and a small lake. Two- and three-dimensional modeling is used to explore the concentrations of radionuclides as they are transported through the three freshwater bodies. The approach is to determine how advection, dilution/dispersion, radioactive decay, and adsorption/desorption processes affect concentrations of each of the transported radionuclides under the hypothetical conditions in each freshwater setting. Although the study results do not apply to the Great Lakes or to estuary settings because of their different hydrological conditions, they do help define transport distributions and rates, effects of sediment-contaminant interactions, and the behavior of contaminants in rivers with and without dams.

NRC's interest is in the methodology and the overall insights provided on contaminant transport in the freshwater systems that were modeled. The eight radionuclides studied are associated with aqueous releases expected from damaged light water reactor fuel. Results are presented for a set of hypothetical locations as Bq/m^3 based on the initial release of a 1 Bq source term. Because these results scale linearly, these fractional concentrations can be multiplied by any source term of interest. Results cannot be taken as representative of any particular nuclear power reactor facility as the modeling parameters and data are highly site specific. However, the observations of the movement of a relatively high concentration pulse of contaminants, the long distances it can be transported in rivers, and the possibility of long-term sediment/water/contaminant interactions are important general insights from this study.

Accident scenarios capable of producing significant aqueous radionuclide source terms are expected to be very unlikely occurrences at any individual nuclear power plant location. Specifically, an accident resulting in core damage (a rare event) would need to occur in combination with the loss (or bypass) of the reactor containment and the existence of a leakage path for contaminated water to flow into a nearby water body. Reactor containment and potential leakage paths were not a subject of this study because they are highly scenario- and site-specific. It should be noted that a number of factors could mitigate aqueous releases such as water hold-up in plant systems or buildings, settling or plate-out of radionuclides, relative

elevation differences between in-plant leakage sources and nearby water bodies, and operator actions to reduce leakage rates or delay the timing of releases. Moreover, actions taken since the accident at Fukushima Dai-ichi by the NRC and the nuclear industry have enhanced safety and reduced both the likelihood and potential consequences of severe core damage events. Although a significant aqueous radionuclide release is expected to be a rare event, this project provides an improved understanding of the potential behavior of these releases and can better inform plans to control and minimize impact to public health and safety and the environment.

This report has been subject to external peer review by a panel of experts in the fields of reactor core inventories, flow and transport processes in open channels, and reactor accident consequences. Their comments as well as those from the many reviewers within the NRC improved the technical basis of this work.

TABLE OF CONTENTS

LIST OF FIGURES

LIST OF TABLES

EXECUTIVE SUMMARY

The Fukushima Daiichi nuclear power plant accident in March 2011 highlighted a surface water contamination scenario not currently addressed in the NRC's severe accident consequence analysis. The purpose of this study is to perform exploratory transport analyses of a direct release of radionuclides to surface water, similar to the Fukushima scenario. Transported radionuclide activity is simulated in hypothetical river and lake systems typical of U.S. nuclear power plant sites. It must be emphasized that the types of scenarios discussed in this report are expected to be very rare events requiring a number of unlikely failures in engineered systems. It was assumed that these failures resulted in an accumulation of contaminated water in the structures of the nuclear power plant and that some of that water leaked to a freshwater body.

This study has three principal tasks: 1) develop a radionuclide source term consistent with the Fukushima reactor type, uranium fuel mass, and fuel burnup status, along with the volume, rate, and duration of the March 2011 release; 2) design radionuclide release scenarios and specifications of processes, properties, and conditions for hypothetical freshwater settings typical of U.S. nuclear power plant sites; and 3) simulate flow and the transport of radionuclides released into the hypothetical freshwater systems.

The selection of radionuclides to be included in the source term is based on the partitioning of the reactor core inventory to the cooling water in the Three Mile Island Unit 2 basement water. The eight radionuclides selected were ^{134}Cs, ^{131}I, ^{137}Cs, ^{90}Sr, ^{3}H, ^{106}Ru, ^{125}Sb, and ^{144}Ce. Radionuclide-specific behavior is differentiated by half-life and sorption distribution coefficient, K_d. The source term volume and release rate were consistent with published estimates of the release to the ocean from the Fukushima Daiichi nuclear power plant accident in the aftermath of the March 11, 2011 earthquake and tsunami. For each of the selected radionuclides, a hypothetical 1 becquerel (Bq) activity source was associated with 1,000 m^3 of water released over a 10-day period.

Three hypothetical freshwater settings were addressed: 1) small lake, 2) small river, and 3) large river. The lake setting, about 11 mi long and 0.62 mi wide, provided a large water volume (130,000 ac-ft) but limited transport. The small river setting examined relatively low flow [5,000 cubic feet per second (cfs)] and slow average velocity conditions, which resulted in less dilution (i.e., higher concentrations) and longer transit times for the 10-day radioactive release. The large river scenario examined conditions where a relatively high 100,000 cfs discharge (118,000 cfs with downstream tributary inflows) resulted in lower concentrations but faster downriver transport. Bathymetric data and hydraulic parameters were adapted and modified from actual lake and river systems. Consistent with the objective of a scoping level of analysis, steady-state discharge rates were used in all scenarios, with the rivers simulated in two dimensions (depth-averaged) and the lake in three dimensions.

The transport studies were driven by a shoreline release of the 8-radionuclide source term. Advection, mixing, and radioactive decay were simulated for all settings; radionuclide-sediment interaction and sediment transport processes were simulated in the small and large river settings for 50 mi downstream from the radionuclide release point. Simulations designed to capture the transport of the radionuclide release pulse through the three freshwater settings were used to explore the impact of radionuclide decay and partitioning to sediment. Subsequent transport simulations of the three freshwater settings were extended out to one year for the four most important radionuclides: ^{134}Cs, ^{131}I, ^{137}Cs, and ^{90}Sr. The large river setting was then lengthened from 50 mi to a dam 103 mi from the radionuclide release point.

Downstream of this dam, two flow scenarios were examined for the next 190 river mi (for a total of 293 mi): 1) unimpounded free-flowing conditions and 2) impounded conditions with three intervening dams.

Based on the modeling of the flow, specified source term, and radionuclide transport in the three freshwater settings, the following important conclusions were made:

- Of the three hydrologic settings, the small lake scenario results in the highest radionuclide concentrations. Most of the lake volume available for dilution is not accessed at early times because transport is essentially limited to dispersion. As a result, radionuclide concentrations remain high.
- In the river settings, the 10-day pulse of released activity remains largely intact for the entire length of the river, which for the extended large river model is 293 mi. Depending on the amount of activity in the release, radionuclide concentrations in the water could be high enough to require emergency measures for long distances downstream. Dams can slow the river transit considerably. In the extended large river simulation, first arrival of contaminants over a 190-mi reach took 4.4 days without dams and 14.2 days with three intervening dams. Over the 293-mi extent of the large river, transit of the full pulse, including the passage of the trailing end, took up to 50 days.
- Radionuclide sorption onto sediment is most significant in the presence of the pulse of released radionuclides. After the passage of the pulse, desorption from the bed sediments becomes a longer-term, widespread source as the sorbed contaminants are driven to re-equilibrate with the cleaner overlying water. The resulting water column concentrations are significantly lower than the pulse but may persist for extended time.
- A key feature of the river transport model is the downstream persistence of higher concentrations along the near shore of the radionuclide release. There can be orders of magnitude differences in near-shore versus far-shore concentrations. In the case of the large river scenario, complete mixing across the river may not occur until 50 mi downstream. In the small river scenario, complete mixing occurs after 10 mi of transport.
- Depending on the magnitude of radioactivity released, concentrations of radionuclides sorbed to bed sediments, especially at low water stages, could have long-term impacts on shoreline use. This could potentially be an issue along the entire length (up to 293 mi) of the analyzed river settings.
- The simulated space- and time-dependent aqueous and sorbed activity concentrations in this study are based on a 1 Bq source term for each radionuclide in the 10-day release. The functionally linear transport and sediment-radionuclide interaction process models used in this study allow the simulated concentrations to be scaled for any magnitude of released activity simply by multiplying the presented radionuclide concentrations, which are per unit activity, by the desired radionuclide activity (Bq) in the source term. For example, increasing radionuclide activity in the source term by a factor of 3 results in activity concentrations 3 times higher.

ACKNOWLEDGMENTS

This project significantly benefitted from the comments, insights and discussions provided by the external Peer Review Panel: J. Van Ramsdell, Jr.; Forrest M. Holly, Jr.; and Tracy A. Ikenberry.

This report underwent substantial internal review by NRC staff from the Office of Nuclear Regulatory Research (RES), the Office of Reactor Regulation (NRR), the Office of New Reactors (NRO), and the Office of Nuclear Security and Incident Response (NSIR); we thank all who contributed. Special thanks to Don Marksberry, Keith Compton, Mike Salay, Tom Nicholson, Meredith Carr, Tom Aird, Stephanie Bush-Goddard, Rebecca Tadesse, Don Palmrose, Trish Milligan, William Ott, Chuck Norton, and Steve LaVie. We thank Dana Powers and the members of the Advisory Committee on Reactor Safeguards subcommittee on Radiation Protection and Nuclear Materials for their helpful comments.

Massively parallel processing flow and transport simulations were performed using PNNL Institutional Computing at Pacific Northwest National Laboratory.

ABBREVIATIONS

^{3}H	tritium
ac-ft	acre-feet
Ag	Silver
Ba	Barium
Bq	Becquerel (one disintegration/second)
BWR	boiling water reactor
CDS	central differencing
Ce	Cerium
CFD	computational fluid dynamics
cfs	cubic feet per second
cm	centimeter
Co	Cobalt
Cs	Cesium
DOE	U.S. Department of Energy
EIS	environmental impact statement
EPA	U.S. Environmental Protection Agency
FD	Fukushima Daiichi
FLEX	Diverse and Flexible Mitigation Strategies
ft	feet
GWd/MTU	Gigawatt day per Metric Ton of Uranium
I	Iodine
IAEA	International Atomic Energy Agency
K_d	Distribution or Partitioning Coefficient
kg	kilogram
kgf	kilogram-force
km	kilometer
L	Liter
La	Lanthanum
m	meter
mg	milligram
mi	mile or miles
mL	milliliter
Mo	Molybdenum
MPI	Message Passing Interface
MTU	Metric Tons of Uranium
MUSCL	Monotonic Upstream-Centered Scheme for Conservation Laws
MWd/MTU	Megawatt-day per Metric Ton of Uranium
NRC	U.S. Nuclear Regulatory Commission

NVSF	normalized variable and space formulation
PBq	Petabecquerel (1×10^{15} becquerel)
PNNL	Pacific Northwest National Laboratory
PORV	pressure-operated relief valve
PWR	pressurized water reactor
RCS	Reactor Coolant System
Ru	Ruthenium
s	second
SAC	System Assessment Capability
Sb	Antimony
SIMPLE	Semi-Implicit Method for Pressure Linked Equations
Sr	Strontium
Tc	Technetium
Te	Tellurium
TEPCO	Tokyo Electric Power Company
TETHYS	Transient Energy Transport HYdrodynamics Simulator
TMI	Three Mile Island
UN	United Nations
UNSCEAR	United Nations Scientific Committee on the Effects of Atomic Radiation
USGS	United States Geological Survey
μm	micrometer or micron

1. INTRODUCTION

Historically, the surface water pathway for exposure to radioactive material from hypothetical nuclear reactor accidents has not received as much attention as the atmospheric pathway. The immediacy and unconstrained dispersal of an atmospheric release during a severe accident can lead to the potential for significant doses to exposed individuals (Gudiksen et al. 1989; Chernobyl Forum 2005). However, exposure from a radioactive release to surface water, while often considered to be smaller and less likely than an atmospheric release, may still have important consequences.

1.1 Background and Motivation

The accident at the Fukushima Daiichi (FD) nuclear power plant in 2011 resulted in the accumulation of highly contaminated water in the reactor and turbine buildings during emergency cooling of the reactor fuel. Some of this water is known to have leaked into the ocean. The leak was discovered three weeks after the earthquake and tsunami, and was contained several days later. While the duration of the leak is not known, the source term could be estimated from the monitoring of radionuclide concentrations off the coast of Fukushima. Credible estimates ranged from 0.2 to 0.9 percent of the reactor core radionuclide inventory (UN 2014).

The FD accident demonstrated that such an event could result in a substantial release of radioactivity directly into an adjacent surface water body. It highlighted a rare surface water contamination scenario that is not currently addressed in the U.S. Nuclear Regulatory Commission's (NRC's) severe accident consequence analysis. Most of the operating nuclear reactors in the United States are sited near freshwater bodies. This project is motivated by the need to assess a Fukushima-like scenario where contaminated water is directly released to freshwater settings. The basic conceptual model is one in which the released materials are transported in surface water from the point of release to locations where people and the environment are exposed via various pathways. The potential radiation doses to individuals that could result from a release of radioactive materials would be mitigated by federal, state, and local responses.

It is likely that the onset of an aqueous release from a severe power plant accident would be relatively slow. An unlikely series of failures of engineered systems would be needed for contaminated water to begin to accumulate in plant structures. However rare, the 1979 Three Mile Island (TMI) Unit 2 and 2011 FD accidents illustrate that such potential exists. Under these conditions it would likely take several days to weeks to accumulate sufficient water for a direct release to a water body. Subsurface leakage is also possible. This type of release has been discussed by Niemczyk et al. (1981) and Oberlander et al. (1985); the impacts in this case would be relatively slow and less severe because of attenuation by radionuclide interactions with the soil.

The methodology presented here does not address the events and processes leading up to the radionuclide release to the environment (e.g., mechanics of the accident, core meltdown, and breach of containment). Nor does it address the various mitigative strategies that would be used, such as emergency operating procedures, severe accident management guidelines, and Diverse and Flexible Mitigation Strategies (FLEX) (NEI 2015). It is expected that these strategies would preclude the accident or minimize the impact of a radionuclide release.

1.1.1 Purpose

Scoping analyses were performed to calculate the transport of radionuclides released from a hypothetical reactor accident into freshwater settings that are typical of U.S. nuclear power plant sites. These analyses were used to determine how advection, dilution/dispersion, radioactive decay, and sorption processes affect activity concentrations for each of the transported radionuclides under the specified conditions in each freshwater setting. Scoping analyses addressed the speed and distances of transport in the assumed scenarios, as well as the fate of dissolved and sediment-sorbed radionuclides in river water columns and beds.

1.1.2 Scope

The exploratory nature of this study is reflected in the small number of hypothetical freshwater settings considered, use of steady flow conditions, simple release scenario, and limited variation in sediment and transport conditions. However, this study differs from previous studies in that the simulations use a higher level of detail and the source term was informed by observations from actual nuclear power plant accidents:

- multidimensional modeling was used to account for three-dimensional bathymetry, spatially varying flow fields, tributaries, dams and impoundments, transport of radionuclides and sediment, and sediment-radionuclide interactions;
- the aqueous radionuclide inventory in the release was estimated with a methodology based on reactor type, mass of uranium fuel, and fuel burnup, which was developed, in part, using observations of aqueous partitioning of the reactor core inventory in the TMI contaminated building water;
- the volume, rate, and duration of the release were based on observations during the FD accident that included radioactivity measured in seawater near FD; and
- the release of radionuclides to surface water was not assumed to first pass through the subsurface environment as in earlier studies. Instead release was made consistent with observations of radioactivity entering the marine environment from FD.

1.2 Approach

The three principal tasks of this study included the following: 1) develop a radionuclide source term consistent with the FD reactor type, uranium fuel mass, and fuel burnup, along with the volume, rate, and duration of the March 2011 release; 2) design radionuclide release scenarios and specifications of processes, properties, and conditions for hypothetical freshwater settings typical of U.S. nuclear power plant sites; and 3) simulate flow and the transport of radionuclides released into the hypothetical freshwater systems.

1.2.1 Source Term

The source term for the environmental transport modeling is a specified set of radionuclides that is associated with a liquid volume, release rate, and duration. A methodology to estimate the aqueous radionuclide inventories for severely damaged reactors is presented in this report.

The first step in the methodology is to determine the reactor core inventory as a function of reactor type (i.e., pressurized water reactor [PWR] or boiling water reactor [BWR]), amount of uranium fuel, and burnup (Ramsdell et al. 2001). This is followed by the determination of the potential aqueous radionuclide inventory (i.e., building water) following a severe nuclear power plant reactor accident. In this case, radionuclide measurements of contaminated water that

accumulated in buildings in the aftermath of the 1979 TMI nuclear power plant accident provide a basis for partitioning individual radionuclides between the nuclear reactor core and the water phase. Attributes of the March 2011 FD reactor core and post-accident measurements of radionuclide concentrations in the building water were used to test and evaluate the methodology.

The FD source term scenario assumes a direct release of a fraction of the estimated aqueous radionuclide inventory consistent with estimates of activity released into the marine system offshore from the FD nuclear power plant. The activity in the source term is assumed to be associated with a liquid volume and release period, which are consistent with the generation of contaminated water during emergency measures at TMI and FD.

1.2.2 Freshwater Settings

For this exploratory analysis, hypothetical freshwater settings were limited to three of the most common surface water situations for operating nuclear power plants in the United States: small lake, small river, and large river. For the selection of the hypothetical lake setting, the most common situation was a reservoir impounded by a dam on a river. While the three selected freshwater settings account for the most common situations for nuclear power plants in the United States, they do not address the Great Lakes, estuaries, or coastal settings.

Bathymetric data and hydraulic parameters were adapted and modified from actual lake and river systems. Steady hypothetical water levels and discharge were used in all scenarios, with the lake simulated in three dimensions and the rivers in two dimensions (depth-averaged). The lake scenario examined a large water volume (i.e., large dilution potential) where limited transport leads to very high radionuclide concentrations until more of the lake volume participates in mixing. The small river scenario examined conditions where a relatively low flow rate minimizes dilution of the released radioactivity pulse. Conversely, the large river scenario examined conditions where a relatively high discharge results in higher dilution of the released pulse of radioactivity, but faster downriver transport.

The initial small and large river domains addressed 50 mi of downstream transport from the source term release point. In subsequent analyses, the large river domain was extended from 50 mi to a dam 103 mi from the radionuclide release point. This extension included the influx of 2 tributaries that added 20 percent more flow to the large river. Downstream of this dam, two flow scenarios were examined for the next 190 river mi (for a total of 293 mi): 1) unimpounded free-flowing conditions and 2) impounded conditions with three intervening dams.

1.2.3 Flow and Transport

The objective of the simplified and generic scoping analyses was to identify the transport consequences when a source term containing the predominant dose-contributing radionuclides was transported in lake and river settings. The analyses were based on a set of radionuclides, release volume, and duration developed for the FD source term scenario.

The simulated space- and time-dependent aqueous and sorbed activity concentrations in this study were based on a 1 becquerel (Bq) activity source term for each radionuclide. The functionally linear transport and sediment-radionuclide interaction process models used in this study make it possible for others to scale the presented concentrations, which are per unit activity, for any magnitude of released activity. This can be accomplished simply by multiplying the simulated concentrations from this report by the desired radionuclide activity (Bq) in the source term.

The initial modeling analyses addressed aqueous-only transport with radionuclide-specific decay using steady nonuniform flow fields for the three freshwater settings. The multidimensional simulations were designed to resolve spatial variations in the radioactive plume, such as the persistence of higher radionuclide concentrations along the same shore as the release. Bed and suspended sediment transport with radionuclide-sediment interactions were included in the subsequent river simulations to examine the behavior of radionuclides with different sorption distribution coefficients (i.e., K_ds) in the context of the small and large river flow regimes. Sorption during the passage of the released radionuclide pulse followed by longer-term desorption from bed sediments was of particular interest. The extension of the large river modeling domain to a downstream dam 103 mi from the radionuclide release point incorporated the impact of two tributaries and backwater effects on the distribution of aqueous and sorbed radionuclides. The final 190-mi extension downstream from this dam was modeled two different ways: as a free-flowing reach without impoundments and as a sequence of impoundments with intervening dams. These two different extended large river scenarios were used to compare the transport of radionuclides with and without the effect of dams and the wide, deep impoundments behind them. Of particular interest were 1) comparisons of large and small river mixing processes and their impact on near-shore versus far-shore concentration profiles with downstream distance, 2) transit times of the pulse of released radionuclide activity and their effect on the concentrations of short-lived radionuclides (e.g., ^{131}I), and 3) radionuclide-specific bed sediment interactions and the corresponding impact on longer-term concentrations of radionuclides in the water column due to sorption and desorption.

Massively parallel processing was necessary to address the high-performance computing and large memory requirements for the multidimensional modeling of coupled flow with sediment and radionuclide transport and interaction. These processes were resolved in modeling domains represented by up to 2.4 million mesh cells and year-long simulations requiring over 1 million time steps.

1.3 Report Sections

The report continues with Section 2, Aqueous Source Term Estimation Methodology, which describes the procedure for calculating the aqueous radionuclide inventory, the fraction released, and the volume and duration of the release. Section 3, Freshwater Settings, describes the small lake, small river, and large river systems as well as the hydraulic modeling approach and radionuclide-specific properties. Section 4, Flow and Transport Modeling, describes the processes, governing equations, and simulators used to model the scenarios, and the results of the flow and non-radionuclide transport modeling. Section 5, Radionuclide Transport Modeling Results, describes the results of the simulated transport of radionuclide activity. Section 6, Conclusions, summarizes the approach and provides an overview of the findings. Finally, Section 7 is a list of references.

2. AQUEOUS SOURCE TERM ESTIMATION METHODOLOGY

2.1 Introduction

The generation of large volumes of highly contaminated waste water is common to both the Three Mile Island TMI and FD accidents. This section outlines a methodology used to estimate aqueous concentrations of radionuclides in accidents with severe fuel damage. This could be useful when measurements for only a limited set of radionuclides are reported. For example, early in the FD accident, obtaining wastewater data was difficult for radionuclides other than ^{131}I, ^{134}Cs, and ^{137}Cs. The method detailed in this section enables estimates for other potentially important radionuclides in the aqueous phase, which was necessary for this project to determine concentrations for radionuclides that are difficult to analyze or require longer time for analysis.

2.2 Analysis of Historical Accidents

This methodology develops a relationship between the reactor core inventory and the concentrations of radionuclides in an accident-generated water release as a function of the age/condition of the reactor fuel. The 1979 TMI and 2011 FD accidents provided information useful in developing aqueous source terms for hypothetical waterborne release scenarios. The accident at TMI Unit 2 in 1979 resulted in a large amount of radioactive water accumulating in the basement of the reactor building and in adjacent buildings, although no release of this material to the environment occurred. The accident at FD also resulted in accumulations of contaminated water in the basements of the reactor buildings, adjacent buildings, and the tunnels between them; some of this water was accidentally released into the Pacific Ocean.

2.2.1 Three Mile Island Unit 2, 1979

The TMI Unit 2 had been operating about three months when the series of events that led to the accident began at 0400 on March 28, 1979. Reactor Building basement water sources included the reactor coolant system, spray system, air coolers, and inleakage of river water. The description of the sources in the next paragraphs is adapted from McIsaac and Keefer (1984).

When a pressure-operated relief valve (PORV) opened, reactor coolant began to escape from the Reactor Cooling System (RCS). The lost coolant flowed to the Reactor Coolant Drain Tank located in the basement. As a consequence of rapid pressurization, the rupture disk on this tank soon burst and coolant escaped to the basement floor. Coolant continued to escape to the Reactor Building basement via this pathway until the PORV block valve was closed. Additional coolant, in the form of steam and water, and hydrogen gas escaped through the PORV when the block valve was intermittently opened to regulate RCS pressure. An estimated 1×10^6 L of reactor coolant was released to the basement via this pathway during the first three days following the onset of the accident.

In addition to the 1×10^6 L of RCS water released during the accident, an average of 29.4 L/h flowed through the PORV block valve for more than two years following the accident. This leakage contributed 6.74×10^5 L of RCS water to the basement water volume. Thus the total volume of RCS water that escaped to the basement was approximately 1.67×10^6 L, which is about 69 percent of the total volume of water released to the basement as of September 23, 1981.

A pressure spike that occurred as a result of a hydrogen burn in containment on the day of the accident activated the Reactor Building spray system, which remained on for almost 6 minutes. During that time, the system discharged an estimated 6.43×10^4 L of chemically treated water, containing boron and sodium hydroxide, into the Reactor Building. Most of this water would have eventually drained to the basement.

Further increases in the basement water level after the accident are attributed to leakage from the river water cooling system of the Reactor Building air cooling assembly. The leakage is suspected to have been from a relief valve on the assembly cooling coils. Based on back projections of water level and reconstruction of events associated with water inventory, an estimated 6.81×10^5 L of river water was released to the basement from this source before it was secured. The river water from this source represents about 28 percent of the maximum basement water inventory prior to September 1981. Thus, in this accident, over 1,000 tons of water accumulated within the first three days, and continuing in-plant and external sources more than doubled that within three years.

Measurements were made of the concentrations of radioactive contaminants in the water in the TMI Unit 2 basement at various times. These are summarized in McIsaac and Keefer (1984); Table 2-1 reproduces their summary. Table 2-2 shows a back-calculation of these results to the date of the accident, March 28, 1979. These back-calculations have not been adjusted for the slowly increasing volume of water. The radionuclides listed are those reported by McIsaac and Keefer (1984); they represent those most likely to be found (^{3}H, ^{137}Cs, ^{90}Sr), a good surrogate for short-lived ^{131}I (^{129}I), and the major refractory fission products (^{106}Ru, ^{125}Sb, ^{144}Ce).

Various estimates of the amount of radioactive material immediately released to the water in the lower levels of the TMI containment are available. An estimate was made by the NRC for the environmental impact statement (EIS) related to decontamination and decommissioning of the reactor (NRC 1981) using an average of measured concentrations and an estimated water volume. This estimate is presented in Table 2-3. An estimate of the total release to basement waters may also be made using the data of McIsaac and Keefer (1984) as described in Section 2.2 of this report; this estimate is presented in Table 2-4. These two estimates are reasonably similar.

Particle size distributions of the sediment solids were determined by analyzing 500X photomicrographs of the material filtered from the samples following ultrasonic treatment (McIsaac and Keefer 1984). Measurements were made in 2-μm intervals, and did not include particles under 1 μm. By number, about 12 percent of the particles collected from the sump were larger than 10 μm. About 39 percent of the sump particles were in the 1- to 3-μm size range. On a population basis, the mean particle size measured in the sump samples was 6.2 μm. In another sample from the floor, the particle size distribution measured was found to contain very few particles larger than 10 μm. The mean particle size on a volume basis was measured to be about 20 μm, and on a population basis it was about 4 μm. A total of 65 percent of the particles in this sediment sample exhibited sizes between 1.5 and 3 μm, and only 1.5 percent were found to be larger than 10 μm. These very small particles would be easily transported by surface water.

Table 2-1. Measured Concentrations of Radionuclides in Various Locations of the TMI Unit 2 Basement at Various Times (Bq/mL)

Nuclide	8/28/79	11/15/79	5/14/81	9/24/81	6/23/82	6/23/82	1/11/83	1/11/83	1/11/83	8/22/83	12/12/83
^{3}H	3.81E+04	3.85E+04	2.23E+04	2.17E+04	--	--	--	--	--	--	1.30E+03
^{90}Sr	1.04E+05	8.51E+04	1.92E+05	1.78E+05	2.58E+05	2.15E+05	9.21E+04	8.73E+04	1.28E+05	2.26E+05	9.29E+04
^{106}Ru	2.59E+02	1.15E+02	--	--	<1.3E+03	9.62E+01	<5.8E+02	<1.4E+03	<3.5E+02	--	<1.0E+03
^{125}Sb	5.55E+02	8.51E+02	1.11E+03	<7.4E+02	<1.1E+02	9.62E+02	<2.6E+02	<7.4E+02	<1.8E+02	--	2.37E+02
^{129}I	5.11E-01	--	1.59E-01	7.40E-01	<2E-4	--	4.00E-02	4.11E-02	1.51E-02	--	1.44E-02
^{134}Cs	1.48E+06	1.19E+06	7.10E+05	5.99E+06	5.18E+05	5.18E+05	3.63E+04	2.48E+04	2.44E+04	2.28E+05	2.86E+03
^{137}Cs	6.51E+06	5.99E+06	5.29E+06	5.07E+06	5.59E+06	5.88E+06	4.44E+05	3.04E+05	3.06E+05	3.53E+06	4.55E+04
^{144}Ce	2.33E+02	3.22E+01	--	<1.3E+03	--	--	<1.6E+02	<4.4E+02	<1.1E+02	--	<5.5E+02

Source: McIsaac and Keefer 1984

Table 2-2 Concentrations of Radionuclides in Various Locations of the TMI Unit 2 Basement at Various Times Back-Decayed to March 28, 1979 (Bq/mL)

Nuclide	8/28/79	11/15/79	5/14/81	9/24/81	6/23/82	6/23/82	1/11/83	1/11/83	1/11/83	8/22/83	12/12/83
^{3}H	3.90E+04	3.99E+04	2.52E+04	2.50E+04							1.69E+03
^{90}Sr	1.05E+05	8.64E+04	2.03E+05	1.89E+05	2.79E+05	2.32E+05	1.01E+05	9.58E+04	1.40E+05	2.51E+05	1.04E+05
^{106}Ru	3.45E+02	1.78E+02			(a)	8.93E+02	(a)	(a)	(a)		(a)
^{125}Sb	6.16E+02	9.98E+02	1.89E+03	(a)	(a)	2.17E+03	(a)	(a)	(a)		7.71E+02
^{129}I	5.11E-01		1.59E-01	7.40E-01	(a)		4.00E-02	4.11E-02	1.51E-02		1.44E-02
^{134}Cs	1.70E+06	1.47E+06	1.45E+06	1.39E+07	1.54E+06	1.54E+06	1.30E+05	8.87E+04	8.74E+04	1.00E+06	1.39E+04
^{137}Cs	6.58E+06	6.08E+06	5.56E+06	5.37E+06	6.02E+06	6.34E+06	4.84E+05	3.32E+05	3.33E+05	3.91E+06	5.07E+04
^{144}Ce	3.39E+02	5.67E+01		(a)			(a)	(a)	(a)		(a)

(a) less than values not back-decayed

Table 2-3. NRC Estimate of Radioactive Material Released to TMI Unit 2 Accident Waters

Nuclide	Inventory (Bq)	
	As Reported 9/30/1980	Back-decayed to 3/28/1979
^{3}H	9.3E+13	1.0E+14
^{137}Cs	1.6E+16	1.6E+16
^{134}Cs	2.4E+15	4.1E+15
^{90}Sr	2.6E+14	2.7E+14
^{89}Sr	7.0E+12	1.3E+16
Others	2.8E+12	--

Source: NRC 1981

Table 2-4. Derived Estimate of Radioactive Material Released to TMI Unit 2 Basement Waters

Nuclide	TMI Core Inventory, 8/28/1979 (Bq)	Release Fraction	TMI Core Inventory Back-Decayed to 3/28/1979 (Bq)	Estimated Release to Basement (Bq)
^{3}H	1.4E+14	0.57	1.4E+14	7.9E+13
^{90}Sr	2.8E+16	0.017	2.9E+16	4.9E+14
^{106}Ru	9.0E+16	0.00004	1.2E+17	4.8E+12
^{125}Sb	1.9E+15	0.003	2.1E+15	6.2E+12
^{129}I	7.2E+09	0.14	7.2E+09	1.1E+09
^{131}I	4.8E+12	0.2	2.5E+18	5.1E+17
^{134}Cs	6.9E+15	0.42	7.9E+15	3.3E+15
^{137}Cs	3.1E+16	0.41	3.1E+16	1.3E+16
^{144}Ce	6.0E+17	0.00001	8.7E+17	8.7E+12

Based on release fraction information in McIsaac and Keefer 1984

2.2.2 Fukushima Daiichi, 2011

The tsunami at FD resulted in flooding of the lower levels of the reactor buildings with sea water. Loss of groundwater control systems allowed the influx of groundwater. The highly contaminated water in the lower levels of the Fukushima reactor buildings resulted from emergency attempts to cool the reactors and fuel storage pools allowing the contaminated water to accumulate in basement areas. Much of this injected water subsequently drained into the turbine building basements and other structures. Measurements made of radionuclides in standing water in the basements of the turbine buildings are shown in Table 2-5 (TEPCO 2011a). These measurements indicated that the highest concentrations existed in the basement of Unit 2.

Table 2-5. Radionuclide Concentrations in FD Turbine Hall Basement Waters

	Concentration of Radioactivity (Bq/mL)			
	Unit 1	Unit 2	Unit 3	Unit 4
Nuclide	Sampled on March 26, 2011	Sampled on March 26, 2011	Sampled on March 26, 2011	Sampled on March 24, 2011
^{56}Co	N.D.	1.60E+05	N.D.	N.D.
^{58}Co	N.D.	N.D.	N.D.	2.70E-01
^{60}Co	N.D.	N.D.	2.70E+02	N.D.
^{99}Mo	N.D.	N.D.	N.D.	1.00E+00
^{99m}Tc	N.D.	8.70E+04	2.20E+03	6.50E-01
^{106}Ru	N.D.	N.D.	N.D.	3.30E+00
^{108m}Ag	N.D.	2.50E+05	N.D.	N.D.
^{129}Te	N.D.	N.D.	N.D.	2.60E+01
^{129m}Te	N.D.	N.D.	N.D.	1.30E+01
^{132}Te	N.D.	N.D.	N.D.	1.40E+01
^{131}I	1.50E+05	1.30E+07	3.20E+05	3.60E+02
^{132}I	N.D.	N.D.	N.D.	1.30E+01
^{134}I	N.D.	N.D.	N.D.	N.D.
^{134}Cs	1.20E+05	2.30E+06	5.50E+04	3.10E+01
^{136}Cs	1.10E+04	2.50E+05	6.50E+03	3.70E+00
^{137}Cs	1.30E+05	2.30E+06	5.60E+04	3.20E+01
^{140}Ba	N.D.	4.90E+05	1.90E+04	N.D.
^{140}La	N.D.	1.90E+05	3.10E+03	7.40E-01

N.D. = Not Detected

Some of this turbine hall basement water appears to have leaked into the ocean by way of a utility tunnel (cable storage pit) or its gravel base mat. Water measured in, and just outside, the tunnel, had concentrations of ^{131}I at 5.2 × 10^6 Bq/mL, ^{134}Cs at 1.9 × 10^6 Bq/mL, and ^{137}Cs at 1.9 × 10^6 Bq/mL (TEPCO 2011b). This water had radionuclide concentrations about one-half that of the water in the Unit 2 turbine hall basement; it may have been diluted with groundwater or mixed with water from one of the other nearby reactors. The leak was discovered on April 2, 2011 and successfully stopped on April 5, 2011. It is not known how long after the March 11, 2011 accident that the leak began before being found. Contaminated water leaking through a 20-cm crack in the concrete wall and falling directly into the seawater was observed. The observed leak had a flow roughly equivalent to several garden hoses. Initial analyses by TEPCO indicated that perhaps 520 m^3 of water containing a combined total of about 4.7 PBq of ^{131}I, ^{134}Cs, and ^{137}Cs escaped (TEPCO 2012). Later evaluations by others based on ocean dispersion estimates resulted in radionuclide release estimates about four times higher (Kawamura et al. 2011; Tsumune et al. 2012; Estournel et al. 2012; Buesseler 2013; Miyazawa et al. 2013), although the uncertainties are large and the estimate could be even higher (Charette 2013).

Using the sampling results from the basement of Unit 2 (the most likely source of the leak), the ratios of other radionuclides to cesium and iodine derived from Table 2-5 may be used to estimate the composite release from FD to the ocean. Isotopes of strontium and technetium were not initially measured; Bailly du Bois et al. (2012) indicates that the isotopic ratios (^{90}Sr/^{137}Cs) and (^{99}Tc/^{137}Cs) were around 0.02 and 0.01 respectively. These ratios differ significantly from the initial ratios in the fuel because of different vapor pressures and solubilities. Using this information and concentration ratios derived from Table 2-5 with the release estimates of Kawamura et al. (2011), Tsumune et al. (2012), Estournel et al. (2012), and Miyazawa et al. (2013), the total release to the ocean from the Fukushima leak may be estimated as shown in Table 2-6. The United Nations Scientific Committee on the Effects of

Atomic Radiation (UNSCEAR) in its 2013 Report to the General Assembly (UN 2014) also evaluated the direct release to the ocean and concluded that about 3 to 6 PBq of ^{137}Cs and 10 to 20 PBq of ^{131}I were released. The magnitude of the strontium estimate generated in this way is corroborated by Buesseler (2013) and Casacuberta et al. (2013). The estimate of the total release to the basement in Table 2-6 is based upon the measurements of Estournel et al. (2012) multiplied by a factor accounting for the ratio of the amount of water in the basement (10,000 m^3) to that released (520 m^3) and a factor of two for the apparent dilution seen in the cable pit.

Table 2-6. Estimated Release from the Fukushima Cable Pit Leak to the Pacific Ocean (Pbq) Based on Different Sources, and Extrapolated Total Release from Unit 2 Core to Basement Waters

	Release to Pacific Ocean				Estimated Inventory in Basement Waters
Nuclide	TEPCO 2012	Kawamura et al. 2011	Tsumune et al. 2012	Estournel et al. 2012	
^{56}Co	0.065	0.278	0.250	0.285	11.0
^{99m}Tc	0.035	0.151	0.136	0.155	5.96
^{108m}Ag	0.102	0.435	0.391	0.446	17.2
$^{90}Sr/^{90}Y$	0.019	0.080	0.072	0.082	3.15
^{99}Tc	0.009	0.040	0.036	0.041	1.58
^{131}I	2.810	11.0	11.00	12.3	473
^{134}Cs	0.936	4.00	3.50	4.10	158
^{136}Cs	0.102	0.435	0.391	0.446	17.2
^{137}Cs	0.936	4.00	3.60	4.10	158
^{140}Ba	0.199	0.852	0.767	0.873	33.6
^{140}La	0.077	0.330	0.297	0.339	13.0

2.3 A Generalized Approach to Aqueous Source Term Development

A generalized approach to estimating the aqueous source term from a reactor accident can be developed based on the experience gained during the events at TMI and FD. This calculation is needed to estimate concentrations of radionuclides in the leaked water because at FD only a limited number of radionuclides were initially reported. The approach is based upon release of radionuclides from the reactor to waters collected in the building substructures, followed by a loss of some fraction of that water to the environment. A simplified schematic of such a process is given in Figure 2-1. The evaluation includes consideration of the total amount of radioactive material in the reactor at the time of the accident, the fractional release of that material to the confines of the reactor buildings, dilution in waters derived from the accident and the responses to it, and subsequent leakage from the reactor complex to the aquatic environment.

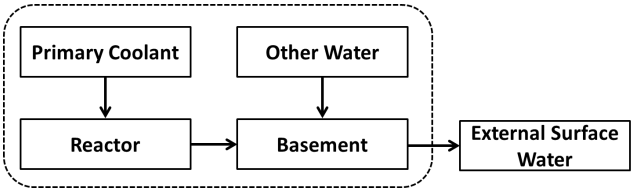

Figure 2-1. Schematic Process for Estimating Radionuclide Releases to Surface Water From a Severe Reactor Accident.

The evaluation procedure first requires an estimate of reactor core radionuclide contents. As reactors operate, energy is liberated by the fission of fuel nuclei, reducing the amount of fuel and increasing the content of fission products. A common measure of fuel usage is termed "burnup" and is reported in units of megawatt-days per metric ton of uranium fuel (MWd/t). The reactors at FD were BWRs that had been running for many months on reloaded fuel elements, and thus had an average high burnup. The reactor at TMI was a PWR that had only been operating for three months, and thus had a low fuel burnup. Reactor type, size, and operating history all have an influence on the total amount of radioactive material available for a release. Previous research for the NRC resulted in tabulations of reactor fuel inventories for various fuel burnup levels in units of Bq per metric ton of uranium (Ramsdell et al. 2001). The Ramsdell et al. (2001) reference provides values for BWRs and PWRs for a range of burnup from 22 to 75 gigawatt days per metric ton of uranium fuel (GWd/MTU). These are summarized in Appendix A.

The next step in the evaluation procedure requires information about the transfer of radioactive material from the reactor to the confines of the reactor complex. After the TMI accident, extensive post-accident analyses were conducted and it was determined that large fractions of some radionuclides were released into the water that spilled into the lower levels of the reactor and turbine building basements. The total release fraction of various materials from the core to the water was determined by McIsaac and Keefer (1984). Their estimates of the fraction of materials in the water are given in Table 2-7. Similar fractions of radionuclides released are seen at FD; the UNSCEAR 2013 Report to the General Assembly (UN 2014) notes that "several tens of per cent of the inventories of the more volatile elements (i.e., hydrogen/tritium, iodine and cesium) in the cores of the three damaged reactors have been found … in stagnant water, mainly in the basements of the turbine and reactor buildings but also in surrounding areas. Less volatile elements (e.g., strontium, barium and lanthanum) were also found but at levels that were between about one and ten percent of those for the more volatile elements in terms of their relative inventories." While these FD release fractions have yet to be refined, the preliminary results indicate that the use of similar release fractions in severe reactor accidents has merit.

Table 2-7. Fraction of Reactor Core Inventory Released to Water in the Basement at TMI

Material	Fraction	Material	Fraction
^{3}H	0.57	Pu	0.000006
^{90}Sr	0.017	Cr	0.005
^{106}Ru	0.00004	Fe	0.01
^{125}Sb	0.003	Ni	0.008
^{129}I	0.14	Zr	0.000004
^{131}I	0.2	Ag	0.002
^{134}Cs	0.42	Cd	0.003
^{137}Cs	0.41	In	0.009
^{144}Ce	0.00001	Sn	0.0007
U	0.000008	Gd	0.001

Source: McIsaac and Keefer 1984

The 94 MTU of fuel in Unit 2 at FD had a burnup of about 35 GWd/MTU, based on the ratio of ^{134}Cs to ^{137}Cs of about 1.0 (Pretzsch et al. 2011). Using the TMI-derived release fractions, 94 MTU in the core, and an interpolated core inventory from Ramsdell et al. (2001), the total inventory released to the FD Unit 2 building water may be estimated as shown in Table 2-8. Comparing this estimate with that derived in Table 2-6, it may be seen that the two agree to well

within a factor of 2. Thus, the methodology was able to provide estimates that compared reasonably well with the only available independent measurements of an aqueous radionuclide inventory from a severe nuclear power plant reactor accident. An assumed release fraction to the environment from the basement completes the assessment.

Table 2-8. Comparison of Fukushima Daiichi Aqueous Radionuclide Inventories Derived from TMI Release Fractions and Ocean Measurements

Nuclide	TMI Release Percentage	FD Core Inventory (PBq from 94 MTU at 35 MWd/MTU)	PBq Estimated in FD Basement Using Release Fractions	PBq Estimated in FD Basement Using Ocean Release	Ratio of Ocean / Fractions Methods
^{90}Sr	1.7	305	5.19	3.15	0.61
^{131}I	20	2,040	408	473	1.16
^{134}Cs	42	431	181	158	0.87
^{137}Cs	41	391	160	158	0.98

2.3.1 Comparison of TMI Unit 2 and FD Waste Water

The estimates derived in this report using the methods of Section 2.2 for masses of radioactive material in accident-generated water in the basement of TMI Unit 2 and FD Unit 2 are given in Table 2-9. There are significant differences in the events at TMI Unit 2 and FD. The initiating event at FD (i.e., the tsunami) introduced a large amount of seawater to the lower levels of the reactor complex, and the inleakage of groundwater and input of cooling water both continued at relatively high rates; thus, the amount of water at FD was larger. Beyond the differences of reactor type (i.e., BWR at FD and PWR at TMI Unit 2), additional differences existed in the radionuclide inventories in the reactors just prior to the accident. TMI Unit 2 had been running only a few months and the fuel burnup ranged from about 900 to 6,000 MWd/MTU (Schnitzler and Briggs 1985), averaging about 2,500 MWd/MTU. This is about one-tenth the burnup of the FD Unit 2 fuel (Pretzsch et al. 2011).

The levels of fuel damage caused by the accidents at TMI Unit 2 and FD Unit 2 appear similar. The amounts of uranium dioxide fuel were approximately the same (about 94 metric tons in each reactor). The differences in fuel burnup account for most of the difference in the releases to basement water seen in Table 2-9 between TMI Unit 2 and Fukushima. The concentrations of shorter-lived radionuclides (e.g., ^{131}I) in fuel are determined more by power level than burnup, and should be similar.

Table 2-9. Comparison of Major Radionuclides in Accident-Generated Water at TMI Unit 2 and FD

Nuclide	TMI (PBq)	Fukushima (PBq)	Ratio Fukushima/TMI
^{3}H	0.079	0.95	12
^{90}Sr	0.49	5.2	10.6
^{106}Ru	0.0048	0.047	9.7
^{125}Sb	0.0062	0.074	11.9
^{131}I	510	410	0.8
^{134}Cs	3.3	180	54.5
^{137}Cs	13	160	12.5
^{144}Ce	0.0087	0.030	3.4

The concentrations of long-lived radionuclides (^{3}H, ^{90}Sr, ^{137}Cs) in fuel are determined mostly by burnup, and ought to differ by about the ratio of burnups (i.e., one order of magnitude). Intermediate-lived radionuclides (^{144}Ce) should be in between. This is the behavior noted in Table 2-9. The only radionuclide concentration not immediately obvious is ^{134}Cs, which is produced both directly as a fission product and via neutron capture from nonradioactive ^{133}Cs, which is a common fission product. As a result, ^{134}Cs increases at a rate greater than a simple burnup ratio.

An independent assessment of the amounts of water, ^{131}I, and ^{137}Cs in the lower levels of FD Units 1, 2, and 3 was recently published (Hidaka and Ishikawa 2014). The estimate of ^{131}I normalized to March 11, 2011 in water beneath Unit 2 is 1,700 PBq, which may be decayed to April 1, 2011 of the cable pit leak to 280 PBq. The estimate for ^{137}Cs is 99 PBq. These are both within 50 percent of their respective values in Table 2-8 derived using the methods of Section 2.2, and also are similar to the results in Table 2-6 derived from ocean measurements. Substantial uncertainty still exists regarding the actual amounts of radioactivity released from the reactors during the accidents, but the various approximation techniques produce similar results.

2.4 Surface Water Source Term

Because the reactor and turbine buildings are robust and partially subterranean, it is unlikely that all of the water could escape the buildings to surface water even in the severest of accidents. As noted above, the release rate of water seen leaking directly to the ocean during the FD accident was the rough equivalent of several garden hoses. Thus, a fractional release of that material must be hypothesized.

Evaluations based on ocean dispersion estimates resulted in radionuclide release estimates shown in Table 2-10 (Kawamura et al. 2011; Tsumune et al. 2012; Estournel et al. 2012; the UN (2014) estimate is an expert summarization of these references) for the direct release (not including fallout from the atmospheric releases), although the uncertainties are large and the estimate could be even higher (Charette et al. (2013) indicate 11 to 16 PBq of ^{134}Cs; Bailly du Bois et al. (2012) estimate 12 to 41 PBq of ^{137}Cs – although these estimates are somewhat confounded by an atmospheric component). The values in Table 2-10 represent about 2.5 percent of the entire amount available in the water in the FD buildings (Section 2.3); those of Charette et al. (2013) and Bailly du Bois et al. (2012) represent from 11 to 25 percent.

The leak at FD was relatively small and may have been undetected for several days. It took almost 3 days to contain the leak from the time of discovery. It appears that about 2.5 percent of the available aqueous radionuclide inventory was released. Equivalently, the activity in the released water was about 0.3 percent of their aggregate activity in the reactor core inventory.

Table 2-10. Estimates of Direct Release of Radionuclides to the Ocean from Fukushima (PBq)

	Release to Pacific Ocean				
Nuclide	TEPCO 2012	Kawamura et al. 2011	Tsumune et al. 2012	Estournel et al. 2012	UN 2014
^{131}I	6.8	11	11	12.3	9 – 18
^{134}Cs	1.2	4.0	3.5	4.1	3 – 6
^{137}Cs	1.2	4.0	3.6	4.1	3 – 6

In addition to a fractional release, a period of time over which the release occurs is also required for the specification of the source term. The primary direct leak was discovered on April 2, 2011 and successfully stopped on April 5, 2011. It is not known how long after the March 11 accident the leak began before being found; however, the amount of radioactive material released into the ocean was estimated for TEPCO (2012) by the Central Research Institute of Electric Power Industry based on the monitoring data of radioactivity concentration of materials in the seawater near the north/south water discharge channels at the power station. This analysis found that the largest releases began about March 26, 2011. This would indicate that the major releases occurred over a period of approximately 11 to 12 days. For the initial scoping analysis, a 10-day radionuclide release duration is assumed.

To transport the radioactive material from the reactor buildings to the adjacent surface water body, there must be a water volume associated with the release. Initial TEPCO analyses suggested that the major leak at FD to the ocean in March and April 2011 consisted of about 520 metric tons (m^3) of water (TEPCO 2012); subsequent analyses indicated that the radionuclide release could have been up to 4 times greater, which could indicate that larger amounts of water were involved (i.e., up to 2,000 m^3). The water in the FD buildings resulted from not only reactor coolant and injected water but also the residuals from the tsunami and groundwater inleakage. Estimates of the quantity of water that accumulated in the buildings associated with Units 1, 2, and 3 ranged up to 55,000 m^3 in the months following the accident (Hidaka and Ishikawa 2014). The total amount of water in the TMI Unit 2 basements was about 1,000 m^3 in the first three days (McIsaac and Keefer 1984) from the reactor coolant system via the open PORV and Reactor Building spray system, after which most water accumulation was slowed or stopped. This provides a reasonable lower bound to the amount of water that could be released to the environment. For the initial scoping analysis, it is assumed that the radionuclide release be associated with 1,000 m^3 of water.

In summary, the methodology to develop an aqueous radionuclide source term for environmental release was demonstrated for the 2011 FD reactor accident. The first step was to determine the reactor core inventory based on the reactor type (single BWR), mass of uranium fuel (94 metric tons), and fuel burnup (35 GWd/MTU) using the approach of Ramsdell et al. (2001). Then, the aqueous radionuclide inventory (i.e., concentrations in building water) was calculated using the reactor core inventory and the partitioning of radionuclides to water observed following the 1979 TMI nuclear power plant accident. For the FD event, the aqueous radionuclide inventory comprised eight radionuclides: ^{3}H, ^{90}Sr, ^{106}Ru, ^{125}Sb, ^{131}I, ^{134}Cs, ^{137}Cs, and ^{144}Ce. A direct release of 2.5 percent of the predicted aqueous radionuclide inventory (~0.3 percent of the reactor core inventory) was shown to be consistent with activity estimates in the marine system offshore from the FD nuclear power plant in the wake of the March 11, 2011 earthquake and tsunami. Finally, the hypothetical source term was associated with 1,000 m^3 of water released over a 10-day period, which was intended to account for the generation of contaminated water during emergency measures in a severe reactor accident.

3. FRESHWATER SETTINGS

This section describes the physical hydrologic settings and radionuclide characteristics used in the fate and transport calculations for the scoping analysis. The prototype lake and river model environments will receive radionuclides via the liquid release described in the previous section.

The attributes of these freshwater settings are informed by characteristics of existing nuclear power plant sites to simulate reasonably representative conditions. Processes controlling the transport and mobility of the target radionuclides in the lake and river environments include hydrodynamics, transport of dissolved constituents (i.e., advection and mixing), sediment transport, reactions with bed and suspended sediments, transport of dissolved and sediment-sorbed radionuclides, and radioactive decay. This scoping analysis uses three freshwater data sets (i.e., small lake, small river, and large river) that include bathymetry, hydrologic conditions, sediment conditions, and radionuclide transport properties.

The scope of this study is the examination of freshwater settings and conditions controlling the aqueous transport of radionuclides from a severe reactor accident scenario. Of the operating nuclear power plant reactors in the United States, 83 are associated with freshwater bodies.[1] Of the reactors sited near freshwater bodies, 51 are sited near largely free-flowing sections of rivers and 32 are sited near lakes or reservoirs—including the 12 associated with the Great Lakes. Most of the lakes or reservoirs proximate to reactor sites are artificial impoundments on rivers controlled by dam operations. Large rivers (annual average flow greater than 50,000 cfs) with nuclear reactors include the Mississippi River (e.g., Grand Gulf Nuclear Station), the Columbia River (e.g., Columbia Generating Station), and the Missouri River (e.g., Callaway Nuclear Power Plant). Reactors using recirculating (as opposed to once-through) cooling water systems minimize water use, allowing them to be sited on river sections with small discharges (annual average flow less than 10,000 cfs) such as the Schuylkill River (i.e., Limerick Generating Station), Colorado River (i.e., South Texas Project), Rock River (i.e., Byron Nuclear Generating Station), and Savannah River (i.e., Vogtle Electric Generating Plant).

3.1 Specifications for Hypothetical Freshwater Settings

This study uses three hypothetical freshwater settings for a severe reactor accident radionuclide release. All three cases use the same 10-day radionuclide activity release. Consequently, differences in radionuclide concentrations and exposure are dictated by the transport and transformation conditions for each modeled setting and the radionuclide-specific distribution coefficients (K_d) and half-lives (Table 3-1). One lake/reservoir setting was considered; however, as most reactors are sited near rivers, two river settings were considered corresponding to small and large discharges that include free-flowing reaches.

Lake/Reservoir. The lake setting was intended to examine conditions where the potentially large volume of water available to dilute the radionuclide release was offset by less dynamic flow conditions, which limited transport to primarily mixing rather than advection. The selected lake setting was an impoundment behind a dam with a small nominal 100 cfs flow. The lake was modeled to be about 6,000 ac with an approximate volume of 130,000 ac-ft; measuring about 1.2 mi (2 km) at its widest and about 11 mi (17.7 km) long. Volumetrically, the modeled lake system is over 3 orders of magnitude smaller than Lake Erie, the smallest of the Great Lakes.

[1] http://www.nrc.gov/info-finder/reactor/

Table 3-1. Radionuclide Partition Coefficient (K_d) and Half-Life Values

Nuclide	K_d (L/kg)	Half-life (years)
^{3}H	NA	12.32
^{90}Sr	2.3E+2	28.79
^{106}Ru	1.1E+4	1.02
^{125}Sb	5.5E+2	2.75
^{131}I	5.9E+1	0.022
^{134}Cs	1.6E+3	2.07
^{137}Cs	1.6E+3	30.17
^{144}Ce	4.2E+4	0.78

Small Discharge River. The small discharge river setting was intended to be used to examine conditions where lower volumetric flow rates limit dilution and lead to relatively slower transport. In this case, the river setting was modeled with a nominal 5,000 cfs discharge and 50 mi of downstream transport from the shoreline release point.

Large Discharge River. The large discharge river setting was intended to be used to examine conditions where higher volumetric flow rates result in faster transport and generally lower radionuclide concentrations. In this case, the river setting was modeled with a nominal 100,000 cfs discharge for 50 mi of downstream transport from the shoreline release point.

Bathymetry is the primary data required to represent the shape of the river and lake bottoms in the specification of the model geometry. Typically, multiple data sources are integrated into a single bathymetric surface. The extents of the simulated domain are defined, and then the bathymetric surface is used to create the computational mesh for the hydrodynamic and transport modeling.

The lake/reservoir setting was based on an impoundment behind a dam. The modeled lake/reservoir width was approximately 2,000 to 6000 ft wide with variable water depths and a maximum depth of 85 ft. The small river was given a pool/riffle configuration. The large river settings addressed free-flowing and impounded scenarios, including tributaries. All data sets were modified from actual geometries to better suit the hypothetical and scoping nature of these hydrodynamic and transport analyses (Figure 3-1, Figure 3-2, and Figure 3-3).

The fate of a radionuclide in a water body can sometimes depend on its interaction with other constituents, including sediment or biota. In this work, radionuclide interaction with sediment or biota was not considered in the lake setting. Sediment interaction was considered in the river settings, but biota was not. Suspended sediment characteristics in rivers and lakes can vary widely depending on location and geologic characteristics of the watersheds in the river basin.

Deposition of contaminated sediments can affect the magnitude and timing of downstream radionuclide concentrations and lead to longer-term dose consequences. If more study is warranted, the attenuation and chronic source associated with sediment-radionuclide interaction and deposition are candidates for further exploration. Future work looking at long-term (i.e., years) transport processes in an actual river with annual hydrographs and flood/drought cycles may need to include bedload transport, both erosion and deposition, and a multi-layer sediment bed, especially in alluvial rivers.

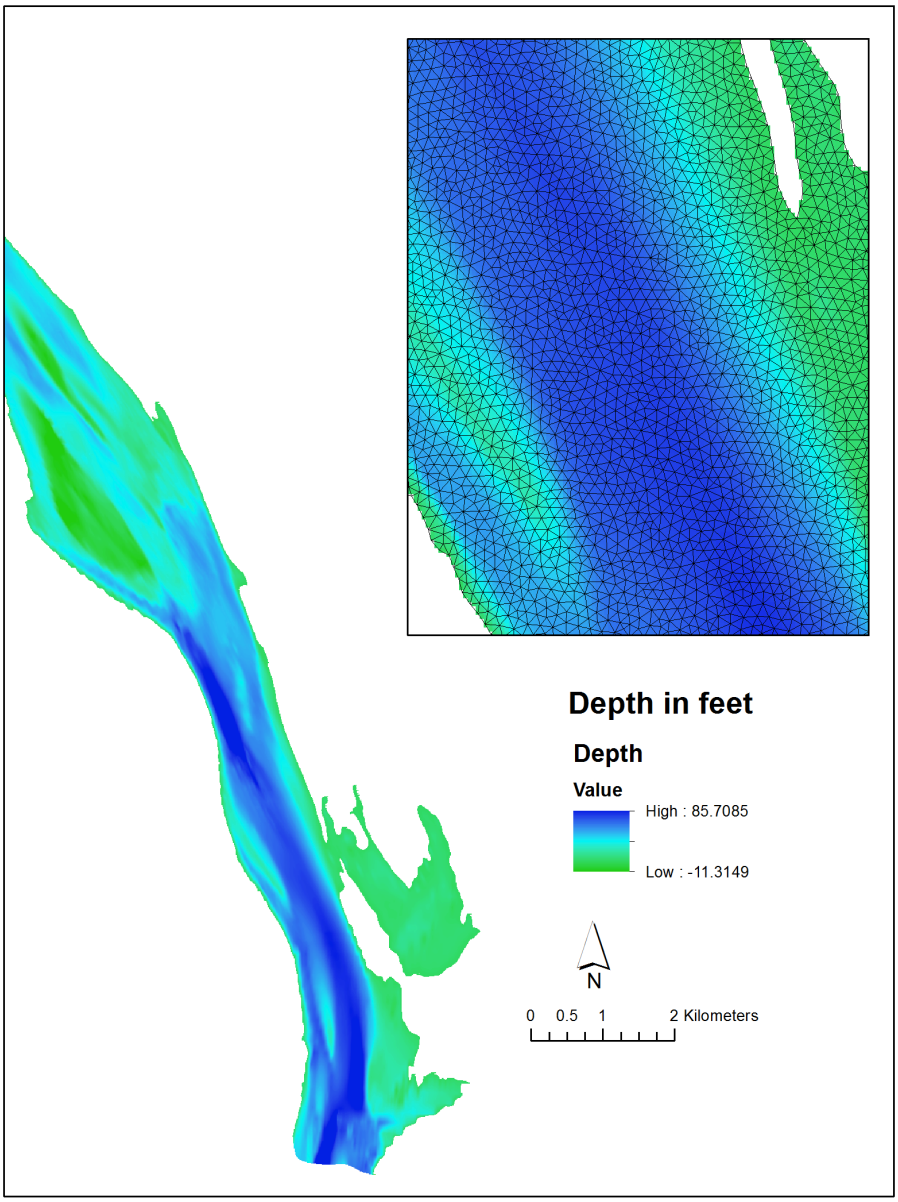

Figure 3-1. Reservoir/Lake Bathymetry Showing the Variable Water Depth. ***The inset shows an example of a typical computational mesh (horizontal layer) used for three-dimensional (3D) hydrodynamics and transport modeling.***

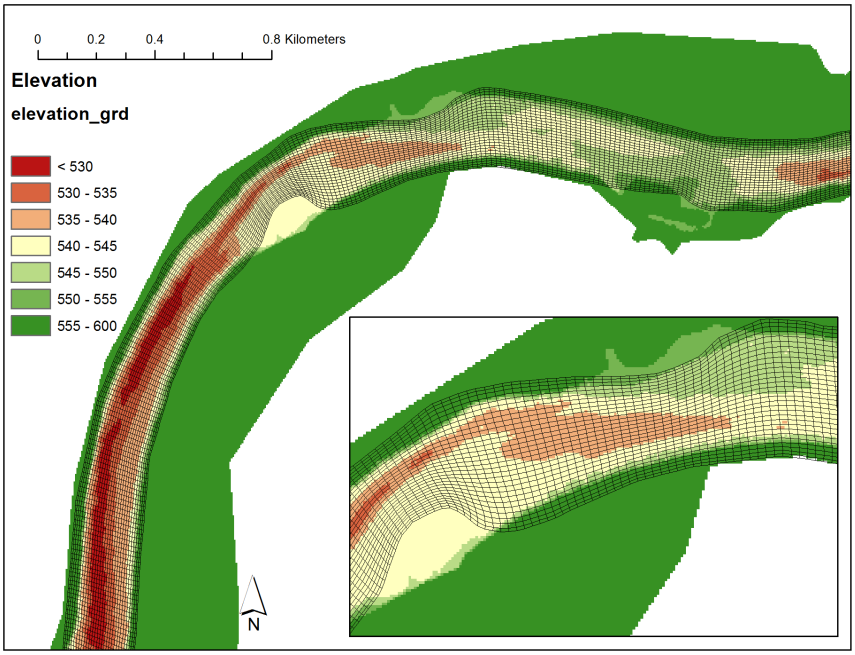

Figure 3-2. An Example of a Section of the Small River Bathymetry. ***A typical computational mesh is also shown overlaid on the bathymetry. Elevation units are feet.***

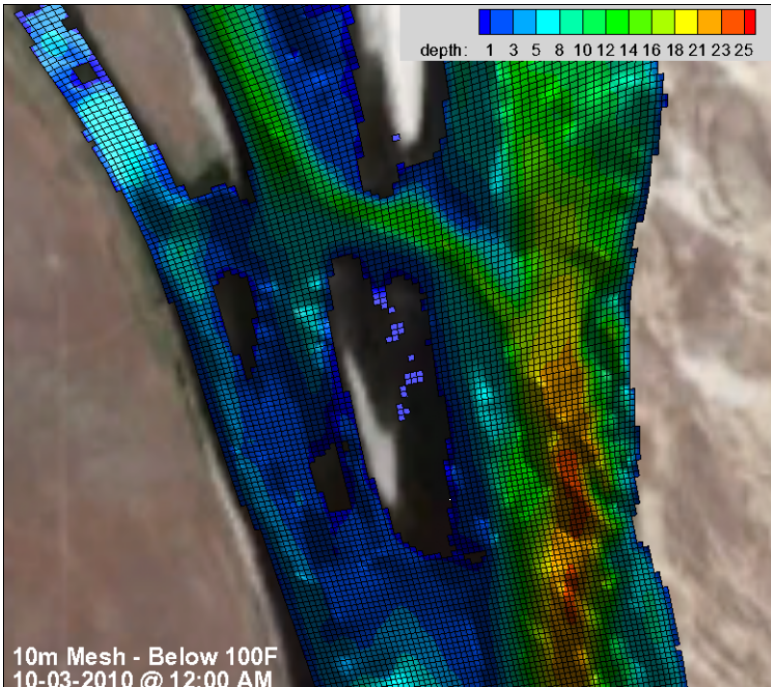

Figure 3-3. Example of a Large River Section with Bathymetry. ***Also shown is the computational mesh for a 2-D depth-averaged model. Each mesh cell is approximately 10 m on a side. Depth units are feet.***

3.2 Examples of Release Pulses Transported in Rivers

The intent for modeling the transport of a hypothetical pulse of radionuclides released into riverine settings is to better understand the collective and systematic impact of processes, properties, and conditions on downstream radionuclide concentrations. As the radionuclide pulse moves downstream, lateral mixing eventually leads to fully mixed conditions across the channel cross-section, whereas longitudinal mixing tends to dissipate peak concentrations by spreading out the length of the pulse. A key outcome is determining the timing of downstream arrivals and the extent of radionuclide activity attenuation from dilution, sorption, and decay processes. The transport of instantaneous and pulse releases in rivers has been observed in dye and tracer experiments and in many inadvertent releases of materials into rivers. Several examples are discussed below, focusing on radionuclide releases and dye tests.

Releases of ^{131}I occasionally took place from the Hanford plutonium production reactors to the Columbia River, when a fuel element failed. Nelson et al. (1966) measured ^{131}I concentrations at various locations downstream of the Hanford D Reactor following several releases. Time-dependent concentration plots of the downstream arrival of the releases show substantial attenuation of peak concentrations and spreading of the pulse during transport through impoundments behind dams. For the Columbia River, the ^{131}I concentration was reduced by about a factor of 8 over approximately 250 mi. The time histories of observed ^{131}I concentrations at downstream locations (Figure 3-4) show the transport of a distinct concentration peak as a result of the relatively instantaneous nature of the release. In contrast, a controlled radionuclide release with constant concentration over a period of several days (e.g., the source term used in this study) would result in the transport of a concentration pulse resembling a square wave at downstream locations. Spreading from longitudinal mixing tends to smooth out the front and trailing edges of the square wave pulse. Nelson et al. (1966) calculated time of travel from the D Reactor to a site about 200 mi downstream to vary from about 9.5 days during average flow (102,000 cfs) to about 2.3 days under very high-flow conditions (627,000 cfs); or 21.1 and 87.0 mi/day, respectively.

In 1996, a flood on the Pripyat River Floodplain in the area of Chernobyl inundated contaminated soils, releasing ^{90}Sr to the water. This contaminant flowed downstream through the Dnieper River system and was sampled at several locations (IAEA 2006). This pulse of ^{90}Sr took more than 6 months to flow about 560 mi and concentrations were reduced by a factor of three (Figure 3-5). The very slow travel time is because of the large size of the reservoirs in the system, especially the Kakhovka reservoir which has a volume of 13 million ac-ft.

Tests using Rhodamine BA dye on the lower reaches of the Missouri River were conducted in 1966 by the United States Geological Survey (USGS 1969). For the section of the river illustrated in Figure 3-6, the dye was injected into the river at Sioux City and detected at three locations over a total distance of about 84 mi. Tests conducted in October and December resulted in significantly different transit times and concentrations for the peak arrivals of dye at the same downstream sampling locations (i.e., Decatur, Blair, and Omaha, Nebraska). For the December test, peak arrival concentrations in Omaha, Nebraska doubled and travel time increased by 40 percent. Similar data are available for a number of river systems.

The Missouri River study also provided a set of tables of travel times and water velocities between different sampling points. Table 3-2 extracts a small example of those data for the distance of 84 mi between Sioux City and Blair, illustrating that as discharge varies so too will travel times and velocities of dissolved chemicals.

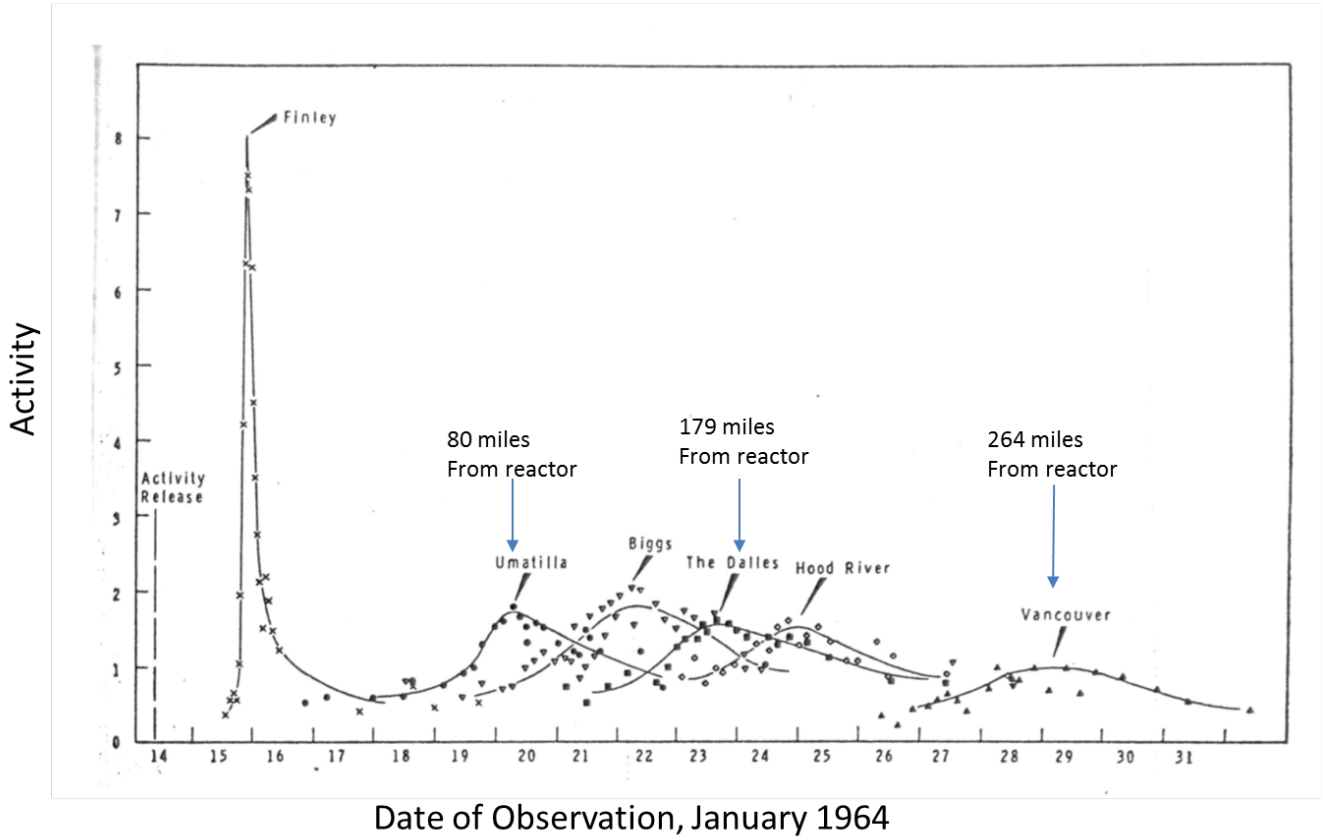

Figure 3-4. Observations of ^{131}I Pulse as It Travels Downstream on the Columbia River (Nelson et al. 1966).

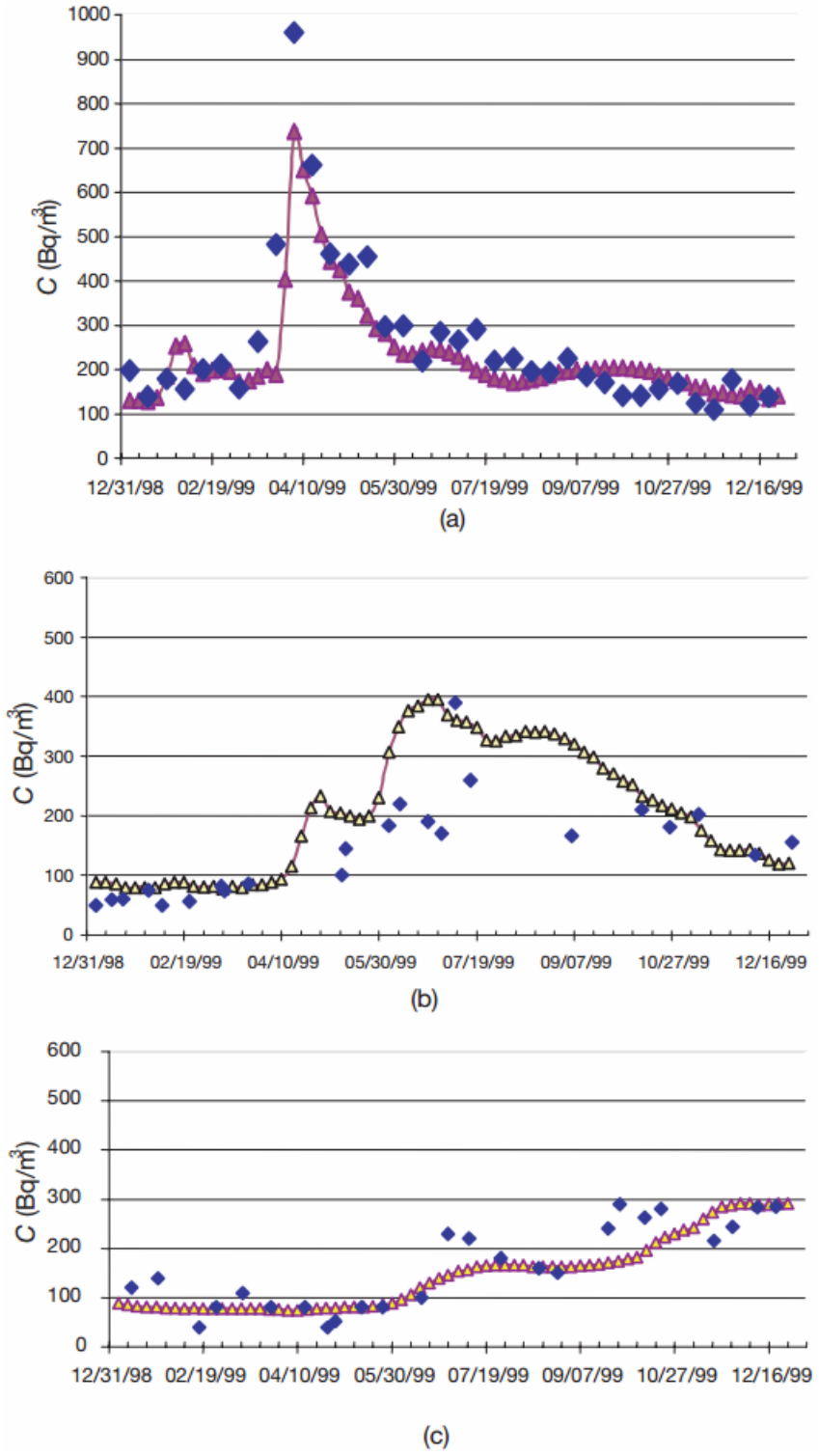

Figure 3-5. Ten Day Averaged Activity Concentrations (blue diamonds) of ^{90}Sr at Three Dams along the Dnieper River: (a) Kiev Reservoir, (b) Zaporozhe Reservoir, and (c) Kakhovka Reservoir (IAEA 2006). *Triangles represent simulated concentrations*.

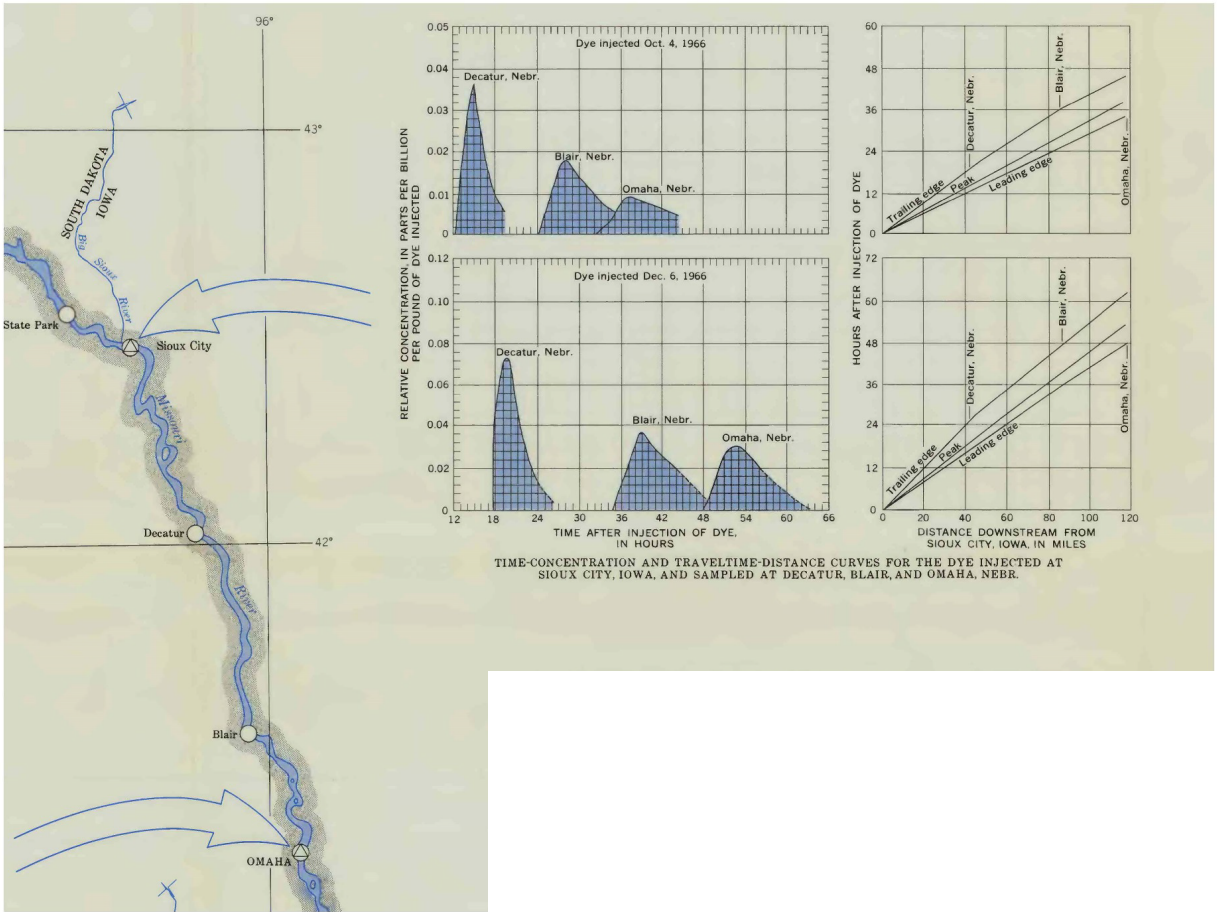

TIME-CONCENTRATION AND TRAVELTIME-DISTANCE CURVES FOR THE DYE INJECTED AT SIOUX CITY, IOWA, AND SAMPLED AT DECATUR, BLAIR, AND OMAHA, NEBR.

Figure 3-6. Data from a Tracer Test on the Lower Missouri River. ***Tracer was injected at Sioux City and sampled downstream at Decatur, Blair and Omaha. Graphs showing the arrival concentration profiles at the three locations for tests in October and December 1966 (USGS 1969).***

Table 3-2. Travel Time and Velocity of Solute in the Missouri River between Sioux City and Blair (USGS 1969).

Discharge (CFS)	Time (hours)	Velocity (MPH)
10,000	44.0	1.90
20,000	33.0	2.52
50,000	22.7	3.68
100,000	17.0	4.90

Other studies on several rivers using dyes showed similar behavior on stretches of the Missouri River (Yotsukura et al. 1970), the Ohio River (Wiley 1997), and the Potomac River (Taylor et al. 1985). In addition to determinations of contaminant travel time, these studies allow analysis of longitudinal dispersion. Other tracer tests have provided transit rates that include: 3.1 mi/day for 70 mi of the upper Ohio River (Wiley 1997), 5.5 mi/day for the Potomac from Cumberland to Point of Rocks (Taylor et al. 1985), 5.6 mi/day for the upper Hudson River (above Troy, NY) (Caplow et al. 2004) and 55.9 mi/day for a 298 mi stretch of the lower Mississippi (USGS, 1976). These travel time examples vary depending on discharge rates, channel geometries, and the operations of dams.

In summary, travel times of contaminants downstream depend on the discharge and velocity of the river, which can vary substantially in time and space (e.g., effect of tributaries, dams, and reservoirs). Water column concentrations are generally reduced by dilution, dispersion, decay, and sediment interaction, yet coherent pulses of dissolved contaminants with relatively high concentrations have been observed hundreds of miles from their sources.

3.2.1 Long-Term Impacts of a Large Radionuclide Release

A large release of radionuclides to a small river (25 to 200 cfs) occurred in the early 1950s (Napier 2014). Beginning in 1948, the Soviet Union initiated a program for production of nuclear materials for a weapons program. The first facility for production of plutonium was constructed in the central portion of the country east of the southern Ural Mountains, about halfway between the major industrial cities of Ekaterinburg and Chelyabinsk. The facility, now known as the Mayak Production Association, and its associated town, now known as Ozersk, were built to irradiate uranium in reactors, separate the resulting plutonium in reprocessing plants, and prepare plutonium metal in the metallurgical plant. The rush to production, coupled with inexperience in handling radioactive materials, led to large radiation exposures, not only to the workers in the facilities, but also to the surrounding public. Designed disposals of low- and intermediate-level liquid radioactive wastes, and accidental releases via cooling water from tank farms of high-level liquid radioactive wastes, into the small Techa River caused significant contamination and exposures to residents of numerous small riverside villages downstream of the site. Discovery of the magnitude of the aquatic contamination in late 1951 caused revisions to the waste handling regimes, but not before about 100 PBq (3 million Ci) of fission product radionuclides (with large contributions of ^{90}Sr and ^{137}Cs) were released – about 3 times the estimated release from the FD accident presented in Section 2.2.2, but of a different radionuclide mix. Although use of the Techa River was prohibited following discovery of the magnitude of the releases, residents up to 150 mi downstream received chronic bone doses of up to 2 Sv (200 rem) because they were ignoring the prohibition on river shoreline use. Over 50 years later, the dose rate in the river sediments was still sufficiently high above background that villages remained evacuated.

The low flow and small profile of the Techa River minimized dilution and maximized sorption. Sorption of radionuclides to sediments along the shoreline and in the river bed during the passage of these releases resulted in a distributed radioactive source with long-term consequences. In this case, the primary pathway for exposure involved uncontrolled access to the river shoreline. The sediment-sorbed activity was immobile and subject to decay and desorption into the water column. However, the radionuclides were sufficiently long-lived (e.g., ^{137}Cs and ^{90}Sr) and strongly sorbed to create a chronic exposure scenario that required access restrictions long after the passage of the radionuclide releases in the water column.

4. FLOW AND TRANSPORT MODELING

This section describes the processes, governing equations, and simulators used to model the scenarios, the modeling approach, and the results of the flow and non-radionuclide transport modeling. The various scenarios were modeled using simulators (Section 4.3) that solve the governing equations of mass, momentum, and transported scalar conservation. For brevity, the details of mass and momentum simulation will be omitted. Detailed descriptions can be found in citations mentioned in the model descriptions below. In this work, the fate and transport of sediment and radioactive species is described, for which some details require discussion.

4.1 Mixing and Transport

When a contaminant is introduced into a flowing river it first experiences mixing due to its buoyancy and initial momentum forming into a "cloud" of concentration. After the initial discharge, the contaminant undergoes several mechanisms of mixing and transport, detailed here with increasing magnitude: molecular diffusion, turbulent diffusion, advective dispersion, and advection. Due to the high turbulence in even the most quiescent flow, turbulent diffusion is far larger than molecular diffusion, though it is modeled in much the same way with mass flux proportional to the concentration gradient by a mixing coefficient. Advective dispersion is caused by the cross-channel variation in velocity and turbulent diffusion, spreading the cloud out in the longitudinal, or stream-wise, direction. In general, the largest mechanism of contaminant transport is advection, or the movement due to the downstream velocity of the water in which the contaminant cloud resides (Fischer et al. 1979, Rutherford 1994, Martin et al. 2012).

In natural rivers, where depth is generally much smaller than width, and width is much smaller than length, vertical diffusion occurs the most quickly, with concentrations rapidly becoming vertically well-mixed by the turbulent diffusion. Complete transverse mixing occurs next, with turbulent diffusion causing the contaminant to be mixed across the cross section of the river as a function of the distance across and the turbulence of the flow. Once the contaminant is well-mixed in both the vertical and transverse directions, the continued turbulent mixing across the cross section causes the contaminant to "sample" different velocities (e.g., higher in the middle, lower near the shore), stretching the cloud along the direction of flow (i.e., the longitudinal direction). While all this is occurring, the mass of the water and the contaminant are being advected, or moved downstream by the flow of the water. The magnitude of both the turbulent diffusion and advective dispersion can be affected by the shape of the bed; the bends in the river; and the presence of zones of low velocity, typically found near the shore. The contaminant can also experience other mechanisms that affect its concentration and transport (e.g., chemical or radioactive decay, sorption, or precipitation).

4.2 Theory

This section briefly summarizes the theory behind the fate and transport simulations performed in this work. As with the hydrodynamic modeling, details can be found in the model citations.

The governing equation for transport of a scalar φ (amount of transported constituent per unit volume) in the water column is

$$\frac{\partial}{\partial t}\int_V \varphi dV + \int_S \varphi \mathbf{v}\cdot\mathbf{n} dS = \int_S \varepsilon_\varphi \nabla\varphi\cdot\mathbf{n}\, dS + \int_V q_\varphi dV \qquad (4\text{-}1)$$

where V is volume; S is surface area; **v** is the fluid velocity vector with components u_i; **n** is the surface area outward-directed unit normal; q_φ is a source term; and ε_φ is the turbulent mixing coefficient of φ.

The source term of Equation (4-1) represents processes that increase or decrease constituent mass or activity in the water column. This includes sediment erosion and deposition, decay of aqueous and sediment-sorbed radionuclides, erosion and deposition of sediment-sorbed radionuclides, and direct sorption to the bed sediment. The mathematical representation of the important source term components is described below for the different scalar types. The representation of suspended and bed sediment and radionuclide interaction with sediment was used in the river settings only (i.e., sediment interaction was not considered in the lake setting).

4.2.1 Sediment

When the fate and transport of suspended sediment is modeled by Equation (4-1), the contribution to the source term consists of rates of erosion from and deposition to the bed. The source term contribution from net deposition is represented as

$$q_{\varphi_{sed}} = E - D \tag{4-2}$$

where $q_{\varphi_{sed}}$ has dimensions of mass per unit bed area per time. E is the erosion rate, given for example by (Partheniades 1962):

$$E = \begin{cases} \left(\frac{\tau_b}{\tau_e} - 1\right) E_o ; if\, \tau_b > \tau_e \\ 0; if\, \tau_b \le \tau_e \end{cases} \tag{4-3}$$

where τ_b is the bed shear computed from the hydrodynamic state, E_o is the erodibility coefficient, and the critical erosion shear stress, τ_e, represents the shear at which erosion is initiated. The erosion rate computed using Equation (4-3) is limited by the availability of sediment in the bed. In this work, the sediment was assumed to be non-cohesive and only deposition was considered, as reflected in the adoption of zero erodibility ($E_o = 0$).

D is the sediment deposition rate, given for example by (Krone 1962)

$$D = \begin{cases} \left(1 - \frac{\tau_b}{\tau_d}\right) w \varphi_{sed} ; if\, \tau_b < \tau_d \\ 0; if\, \tau_b \ge \tau_d \end{cases} \tag{4-4}$$

where φ_{sed} is the volumetric sediment concentration, w is the particle settling velocity, and τ_d is the critical deposition shear stress. The parameters w, τ_e, and τ_d are sediment-specific properties. Their values will vary depending on the sediment particle size, chemical composition of the sediment, and other local conditions. Consequently, they are usually

determined by calibration guided by reported values from the literature. Although a plethora of alternative formulations for erosion and deposition are available (see for example García 2008), the formulations adopted herein are appropriate and demonstrative for establishing the methodology of the scoping study.

4.2.2 Dissolved Radionuclide

The dissolved radionuclide (or aqueous phase) is affected by decay, sorption to and desorption from suspended sediment, and direct sorption to and desorption from the bed surface (radionuclide interaction with biota is not considered in this work). The source term in Equation (4-1) is represented as

$$q_\varphi = -\lambda_\varphi \varphi + K_\varphi \left(K_{d_\varphi} \varphi_{sed} \varphi - \varphi_{part} \right) + \varrho_{sed} D_{50} (1-p) K_\varphi \left(K_{d_\varphi} \varphi - \varphi_{bed} \right) \quad (4\text{-}5)$$

The first term describes radioactive decay, where λ_φ is the decay rate (1/T), which is computed from the half-life, $t_{\varphi_{1/2}}$, as

$$\lambda = \frac{\ln 2}{t_{\varphi_{1/2}}} \quad (4\text{-}6)$$

The second term on the right-hand side of Equation (4-5) represents the exchange with the suspended particulate phase of φ. K_{d_φ} is a partitioning coefficient specific to the scalar φ and sediment size and type (Onishi and Thompson 1984). The value of K_{d_φ} is the ratio of particulate to dissolved contaminant when they are in equilibrium

$$K_{d_\varphi} = \frac{\varphi_{part}}{\varphi_{sed} \varphi} \quad (4\text{-}7)$$

where φ_{part} is the volumetric concentration of particulate or sorbed radionuclide and φ_{sed} is the volumetric concentration of suspended sediment. The magnitude of the exchange is governed by the dissolved/particulate imbalance and the rate K_φ at which contaminant is exchanged between phases, which has dimensions of 1/T.

The third term on the right-hand side of Equation (4-5) similarly represents the exchange of dissolved contaminant within the water column with any particulate contaminant on the bed surface. φ_{bed} is the bed concentration of φ and p is the bed porosity. The exchange is assumed to be limited to the surface of the bed, or the mass of sediment occupying a thickness of one sediment grain diameter, D_{50}, at the top of the bed.

4.2.3 Suspended Sediment-Sorbed Radionuclides

When suspended sediment-sorbed radionuclides (or particulate phase) are simulated, the source term for Equation (4-1) includes the loss of mass due to sediment deposition and interaction with the aqueous phase. The source term takes the form

$$q_{\varphi_{part}} = -\lambda_{\varphi}\varphi_{part} - K_{\varphi}\left(K_{d_{\varphi}}\varphi_{sed}\varphi - \varphi_{part}\right) + \left(\varphi_{bed}E - \frac{D\varphi_{part}}{\varphi_{sed}}\right) \quad (4\text{-}8)$$

The first term on the right-hand side of Equation (4-8) represents decay, as in Equation (4-5). The second term represents exchange with the dissolved phase and corresponds to the second term of Equation (4-5). The third term represents the particulate mass deposited to or eroded from the bed, as described above.

4.2.4 Bed Representation

This section describes the representation of sediment and sorbed radionuclides in the river bed in Modular Aquatic Simulation System in 2 Dimensions (MASS2) (Section 4.3.2). MASS2 can represent multiple sediment size fractions and multiple bed layers, but for this work bed sediment was represented with a single sediment size fraction in a single well-mixed layer with a specified, spatially and temporally constant porosity, p, and a variable layer depth, d_{bed}. The bed sediment is stored as mass per unit bed area, M_{sed}. The depth of the bed is computed as

$$d_{bed} = \frac{M_{sed}}{\varrho_b} \quad (4\text{-}9)$$

where ϱ_b is the bed bulk density,

$$\varrho_b = \varrho_s (1-p)$$

and ϱ_s is the sediment solids (or particle) density.

At the end of a simulation time step, Δt, the deposition rates computed during the suspended sediment transport solution are added to the bed mass

$$M_{sed} = \left(M_{sed}\right)_{old} + \Delta t\,(D-E)h_1h_2$$

where h_1h_2 is the plan-view surface area of the cell. This is an approximate time integration of the source term in Equation (4-2).

Transported scalar quantities are also accounted for in the bed, both in a dissolved phase within the bed pore water and particulate phase(s) sorbed to bed sediments. Dissolved scalar quantities are stored as mass per unit bed area, $M_{\varphi_{pore}}$. When necessary, a pore concentration is computed as

$$\varphi_{pore} = \frac{M_{\varphi_{pore}}}{pd_{bed}}$$

Particulate scalar quantities are also stored as mass per unit bed area, $M_{\varphi_{bed}}$. The ratio of scalar to sediment mass is necessary

$$\varphi_{bed} = \frac{M_{\varphi_{bed}}}{M_{sed}}$$

At the end of the time step, all other direct exchange with the water column is accounted for. This takes two forms. First, any particulate contaminant eroded or deposited with sediment is subtracted or added to the current particulate mass

$$M_{\varphi_{bed}} = \left(M_{\varphi_{bed}}\right)_{old} + \Delta t \left(\frac{D\varphi_{part}}{\varphi_{sed}} - \varphi_{bed} E \right) h_1 h_2$$

which is a time integration of the third term of Equation (4-8). Second, any exchange of particulate contaminant on the bed surface with the water column is accounted for

$$M_{\varphi_{bed}} = \left(M_{\varphi_{bed}}\right)_{old} + \Delta t \left(\varrho_s D_{50} (1-n) K_{\varphi} \left(K_{b_{\varphi}} \varphi - \varphi_{bed} \right) \right) h_1 h_2,$$

which is a time integration of the third term of Equation (4-5). The exchange is assumed to be limited to the surface of the bed, or the mass of sediment occupying a thickness of one sediment grain width, D_{50}, at the top of the bed.

Those scalar quantities that decay in the water column also decay in the bed. This decay is accounted for at the end of each time step, after any exchange with the water column has been considered. The masses of dissolved scalar quantities are decayed using

$$M_{\varphi_{pore}} = \left(M_{\varphi_{pore}}\right)_{old} \exp\left(-\lambda_{\varphi} \Delta t\right) \tag{4-10}$$

Similarly, each particulate phase is decayed using

$$M_{\varphi_{bed}} = \left(M_{\varphi_{bed}}\right)_{old} \exp\left(-\lambda_{\varphi} \Delta t\right) \tag{4-11}$$

Radionuclides sorbed to bed sediments are assumed to be instantaneously in equilibrium with their dissolved counterparts in the bed pore water

$$\varphi_{pore} = \frac{\varphi_{bed}}{K_{d_{\varphi}}}$$

This is enforced at the end of each computational time step after the fluxes described above are considered.

4.3 Simulators

Two simulators, MASS2 and Transient Energy Transport HYdrodynamics Simulator (TETHYS), are used to model the various scenarios in this scoping study. Both models solve the momentum and scalar transport equations discretized using the finite-volume method (Ferziger and Perić 2002; Versteeg and Malalasekera 2007).

4.3.1 MASS2

MASS2 is a two-dimensional, depth-averaged hydrodynamic and transport model (Perkins and Richmond 2004a, 2004b). The model simulates time-varying distributions of depth-averaged velocities, water surface elevations, suspended sediment, and water-quality constituents. MASS2 is applicable to a wide variety of environmental analyses of rivers and estuaries where vertical variations in the water column are negligible or unimportant.

MASS2 uses a boundary-fitted, orthogonal, curvilinear computational mesh. A key feature is the use of multiple computational mesh blocks. Multiple blocks allow MASS2 to be applied to complex domains. Blocks can be connected to each other with cells having a one-to-one or one-to-many correspondence. This allows the use of a high-density mesh where detailed results are needed and coarser meshes elsewhere. MASS2 is designed for execution on desktop to massively parallel processing computing architectures. The source code is written in standard Fortran 90 using the Message Passing Interface (MPI) (MPI Forum 2009) and the Global Array toolkit (Nieplocha et al. 1996, 2006) for interprocess communication, and the Portable, Extensible, Toolkit for Scientific Computation (PETSc) (Balay et al. 2014) for the solution of linear equation systems.

The code can simulate a wide variety of hydrodynamic conditions, including supercritical flow and hydraulic jumps. MASS2 can also be used to simulate advection, mixing, decay, sediment transport, and sediment-contaminant interaction. Any number of conservative or decaying scalar quantities (e.g., salinity or radionuclides) may be simulated simultaneously with hydrodynamics or using precomputed hydrodynamics. In addition, MASS2 has the ability to simulate water-quality parameters (e.g., total dissolved gas, temperature, and suspended sediment). Advective fluxes are computed using deferred correction (Ferziger and Perić 2002) with the choice of several high-resolution schemes (e.g., central differencing [CDS], second-order upwind, and the monotonic upstream-centered scheme for conservation laws [MUSCL]). These are implemented using the normalized variable and space formulation (NVSF) of Darwish and Moukalled (1994). The equations of mass, momentum, and species conservation are discretized using the finite-volume method (Patankar 1980) and solved using iterative solution procedures. The coupling of the momentum and mass conservation (continuity) equations is achieved using a variation of the Semi-Implicit Method for Pressure Linked Equations (SIMPLE) algorithm (Patankar 1980) extended to shallow-water flows.

The small river and large river settings were simulated using the MASS2 simulator.

4.3.2 TETHYS

The TETHYS (Yang et al. 2013; Richmond et al. 2013) simulator solves the governing equations of mass, momentum, and scalar conservation on an unstructured mesh. The finite-volume method (Ferziger and Perić 2002) is used to discretize the governing equations on a computational mesh consisting of arbitrarily shaped three-dimensional cells (e.g., hexahedral and tetrahedral). A co-located storage scheme is used where all computed variables are

defined at the centroid of each mesh cell. Advective fluxes are computed using deferred correction (Ferziger and Perić 2002) with the choice of several high-resolution schemes such as CDS, second-order upwind, and MUSCL. These are implemented using the NVSF of Darwish and Moukalled (1994) modified for unstructured meshes (Darwish and Moukalled 2003). Coupling between the pressure and velocity fields is done using the iterative SIMPLE algorithm (Patankar 1980) modified for co-located variables on unstructured meshes using Rhie-Chow interpolation (Ferziger and Perić 2002). Discretizing the governing equations and implementing the SIMPLE algorithm results in systems of linear algebraic equations that are solved using iterative methods available in PETSc (Balay et al. 2014). TETHYS is designed for execution on desktop to massively parallel processing computing architectures. The source code is written in C++ and uses the MPI (MPI Forum 2009) and the Global Array toolkit (Nieplocha et al. 1996, 2006) for its parallel interprocess communication and PETSc (Balay et al. 2014) for linear system solution.

The lake setting was simulated using the TETHYS simulator.

4.4 Software History and Model Testing

The process models and simulators applied in this work have been developed, enhanced, and maintained by the Pacific Northwest National Laboratory (PNNL) for many years. They are a part of a longer history of sediment and radionuclide transport modeling in surface water systems at PNNL going back to the 1970s. As part of the Hanford Environmental Dose Reconstruction Project (Walters et al. 1996), an unsteady flow and transport model including radioactive decay, was used to simulate the transport of radionuclides (^{24}Na, ^{32}P, ^{65}Zn, ^{76}As, and ^{239}Np) released to the Columbia River from the operation of reactors at the Hanford Site. The model was applied to the river from Priest Rapids Dam to the vicinity of Portland, Oregon, from January 1950 through January 1971. Model validation was accomplished by comparing computed water depths and ^{51}Cr concentrations to historical river monitoring data.

4.4.1 History

The MASS2 simulator was initially developed in 1997 to model fully coupled hydrodynamics, water temperature, and dissolved gas transport in open rivers and reservoirs (Richmond et al. 1999). Since that time, additional transport processes have been added and a parallel version of the code was developed. The TETHYS simulator is a newer computational fluid dynamics (CFD) code that PNNL developed to address the need to simulate fully 3D flows based on solutions of the Navier-Stokes equations (Richmond et al. 2013). Development of TETHYS began in 2006 and is currently continuing with the addition of new capabilities to simulate coupled geochemistry, multiphase flow (e.g., water, air, and oil) phenomena, and enhanced river-reservoir simulations where non-hydrostatic density stratification effects are important.

4.4.2 Testing and Applications

The documentation for MASS2 (Perkins and Richmond 2004a, 2004b) present several cases that are used to regularly test the code as part of the code configuration management. In addition, MASS2 has been extensively validated against observed field data in river and reservoir systems as part of several applications on the Columbia River and Snake River systems. These studies include simulating water temperature and dissolved gas transport (Richmond et al. 2000), time-varying salmon habitat (Hanrahan and Richmond 2008), stranding caused by discharge fluctuations (Perkins et al. 2004), and radionuclide transport (Kincaid et al. 2000). Validation simulations are typified by Richmond et al. (1999) and Niehus et al. (2014)

who demonstrated model fidelity for spatial and temporal distributions of simulated quantities for a number of river-reservoir systems. Furthermore, water surface elevations and velocities compared favorably with measured tailwater elevations at dams using velocities measured with an acoustic doppler current profiler (Niehus et al. 2014). Simulated and observed time-varying water temperature and total dissolved gas also compared favorably over a wide range of locations. For radionuclide transport, the MASS2 code was used as the river transport simulator in the System Assessment Capability project for the U.S. Department of Energy Hanford Site (Kincaid et al. 2000). The simulated contaminant concentrations from the MASS2 model were compared to measurements for two separate time periods: 1964 to 1966, when radionuclides were directly discharged to the river from once-through cooled plutonium production reactors and 1992 to 1996, when contaminants entered the river from groundwater sources and upstream inputs. The results of these comparisons showed reasonable agreement with the available field data.

TETHYS is currently being applied to simulate flow and transport across a wide range of spatial and temporal scales. Basic test cases for steady and unsteady flows in 3D and two-dimensional (2D) geometries are described by Richmond et al. (2013). In addition to surface water systems, the fundamental CFD formulation of TETHYS allows it to be used to simulate flow and transport in explicit pore-scale geometries consisting of individual sediment grains for DOE Office of Science applications (Oostrom et al. 2016; Scheibe et al. 2015; Yang et al. 2015). At the scales of meters to tens of kilometers, density stratified flows in Dworshak and Lower Granite Reservoirs on the Snake and Clearwater Rivers are being simulated to help understand the relationships between water temperatures and migration behavior of salmon (Bellgraph et al. 2009).

Verification tests using surface water geometries and conditions similar to two of the freshwater scenarios were designed to test MASS2 and TETHYS against analytical solutions for radionuclide transport and decay. Comparisons were generally excellent and are summarized in Appendix A, Sections A.1 and A.2.

4.5 Modeling Approach

4.5.1 Source Term

The source term release volume (1,000 m^3), rate (100 m^3/d), and duration (10 d) described in Section 2 are used for all simulations of the freshwater settings and scenarios in this report. For each freshwater setting, the source term is released into a single internal grid cell along the shore. For each radionuclide, the 10-day source term is associated with the release of 1 Bq (unit) of activity. In absolute terms, 1 Bq is an extremely minute amount of activity; e.g., over 15 orders of magnitude smaller than the estimated release to surface water for the 2011 FD accident. There are two principal advantages for this radionuclide source term implementation. First, using the same activity release allows a common basis for comparing transport behaviors of different radionuclides at specific times and locations. In this case, differences in simulated activity concentrations are a direct consequence of the sorption and decay parameterizations that are radionuclide-specific. But second, and more importantly, the unit activity release allows the space- and time-dependent aqueous and sorbed activity concentrations presented in this report to be scaled for any 10-day activity release simply by multiplying by the desired source activity (Bq). This is because of the functionally linear transport and sediment-radionuclide interaction process models used in this study. For example, increasing radionuclide activity in the source term by a factor of 3 results in activity concentrations 3 times higher.

4.5.2 Lake/Reservoir

The geometry of the lake model domain was adapted from bathymetric data for a large river impoundment. Physical extent and mesh dimensions of the lake setting are summarized in Table 4-1. The interior of the model domain was discretized using a surface triangular mesh with a resolution of about 100 ft. This was extruded down to the bottom elevation at 1 ft intervals, forming a 3D prism-celled mesh. An inlet boundary was defined at the northwest corner of the domain. At this boundary, a constant discharge of 100 cfs was imposed. The outlet was defined at the southwest end. Hydrodynamics were simulated with a "rigid lid," i.e., the top boundary was a slip wall. All other boundaries were nonslip walls.

Table 4-1. Transport Simulation Approximate Domain Physical and Mesh Dimensions

		Freshwater Settings		
Dimension	**Units**	**Lake**	**Large River**	**Small River**
Length	mi	11	60	60
Nominal Width	ft	3,300	1,800	650
Average Depth	ft	24	15	7
Discharge	cfs	100	100,000	5,000
Maximum Velocity	ft/s		13	26
Mesh Cells		1.4M	714K	2.4M
Mesh Resolution	ft	105	30	14
Vertical Mesh Resolution		1.0	N/A	N/A
Transit time	hr	N/A	17	25

Transport simulations for an actual lake could include the representation of several transport mechanisms (e.g., wind, wave action, thermal buoyancy, and sorption to and desorption from sediment and biota). The data required to represent these mechanisms are very site-specific. Consequently, for this scoping study, these mechanisms were lumped into a single constant turbulent mixing coefficient. A value of 0.04 m^2/s was chosen. This is a measured value for Lake Huron (Fischer et al. 1979) and within the range measured by Peeters et al. (1996) in smaller lakes. The initial lake case was simulated for 30 days total: 10 days during the release and for 20 days afterward. Simulation output was sampled at discrete locations near the release site and along the shore at a radius of 0.5 and 1.0 mi from the release point (Figure 4-1). Subsequent lake simulations that were extended to one year, were based on the same boundary conditions, parameters, and sampling locations; however, a coarser mesh with 400 ft horizontal resolution and 3 ft vertical resolution was necessary to maintain turnaround times.

4.5.3 River Settings

It was assumed that the hypothetical river cases in this work were well-mixed vertically. This assumption has been reasonable for past water quality and transport modeling in these settings. Consequently, the river cases were simulated as 2D depth-averaged flow and transport with MASS2.

Structured curvilinear meshes were prepared for about 60 mi in each river setting to model 50 mi of transport downstream from the point of release (this distance was later extended for the large river, see below). The approximate resolutions used are shown in Table 4-1.

Steady-state hydrodynamics were simulated first. Discharge was imposed as the upstream boundary condition. An appropriate stage was imposed as the downstream boundary condition. The most important parameters for the hydrodynamic simulations were channel roughness and

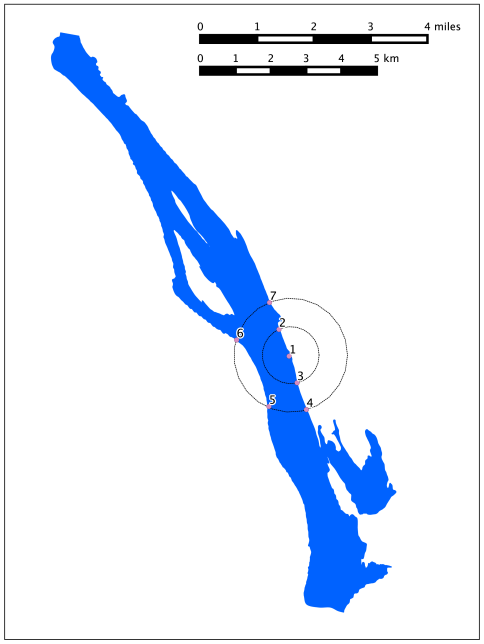

Figure 4-1. Sampling Locations for the Lake Simulation. ***Circles represent 0.5 and 1.0 mi radii centered about release point for radionuclides.***

turbulent eddy viscosity. Normally, these are determined through calibration. In the large river case, these values were available from a previous calibration: turbulent eddy viscosity (both transverse and longitudinal) was 0.0186 m^2/s and Manning's roughness coefficient varied from 0.027 to 0.038. Because no calibrated values for turbulent eddy viscosity and roughness were available for the small river, some reasonable values were chosen: 0.06 m^2/s for turbulent eddy viscosity and 0.027 for Manning's roughness coefficient, which are within the range of observed values presented by Fischer et al. (1979) for eddy viscosity and Chow (1959) for Manning's roughness.

Table 4-1 summarizes the physical dimensions of the river cases and some hydrodynamic results. Both river cases had islands and some braiding of the main channel. The small river was dominated by pool and riffle sequences: deeper, slower stretches (around 3 ft/s) alternated with short, shallow, faster stretches (some small areas with velocities higher than 20 ft/s). The small river required a much higher resolution mesh in order to adequately resolve narrowed channel and high velocity areas. In contrast to the small river, the large river had a mostly consistent flow regime throughout the domain. While the flow velocity did vary spatially in the large river, there were no areas of supercritical flow.

Transport simulations were performed using the steady-state velocity field from the hydrodynamic simulation. A constant sediment concentration of 3.75 mg/L was imposed at the upstream boundary, based on a representative value as mentioned earlier. A radionuclide injection point was chosen along a shore a few miles below the upstream boundary. The injection was made into a single cell, an area approximately 10 m by 10 m. The 10-day, 1,000 m^3 source term described in Section 2 was released from the shore in both river settings. Simulation output was saved at hourly intervals and later sampled at discrete locations near the release point and along the near and opposite shores. The simulation was started 2 days before the beginning of the 10-day release, which allowed the sediment transport to become steady state in the upper portions of the models. A 30-second computational time step was used for all of the river transport cases.

An important parameter for the transport simulations was the turbulent mixing coefficient. As with the hydrodynamic parameters, the turbulent mixing coefficient is usually determined through calibration and validation. In this case, an isotropic turbulent mixing coefficient, 0.186 m^2/s, validated for previous water-quality simulations in these settings, was chosen for all the river transport simulations. This value is near the lower end of some observed values in several rivers listed by Fischer et al. (1979). A second-order accurate advection scheme was used for all simulations: MUSCL for the large river and second-order upwind for the small river (as described by Darwish and Moukalled 1994).

The initial set of simulations continued for 3.5 days after the end of the 10-day release, which was enough time, in both rivers, for the principal pulse of released radionuclides to pass the 50-mi downstream sampling locations. Two transport simulations were performed for each river setting: one without sediment interaction (aqueous-only) and one with sediment transport and sediment-radionuclide interaction. All simulations account for radioactive decay under the assumption that radionuclides decay only after release into the freshwater systems (i.e., the specified source term activity is at release, not prior to release).

Sediment transport in the river scoping analyses was based on models and parameters from a previous assessment of similar river settings. For the small and large river settings, a 3.75 mg/L suspended sediment concentration was used with the following sediment properties:

- Median particle diameter between a fine sand and silt (d50): 0.003 cm
- Solids density: 2,650 kg/m^3
- Settling velocity: 0.000010 m/s
- Erodibility: 0.0
- Critical shear for erosion: 0.0073 kgf/m^2
- Critical shear for deposition: 0.0073 kgf/m^2

The modeling specification of the bed and suspended sediment is important for estimating radionuclide adsorption/desorption processes and their role in fate and transport. Consistent with the scoping nature of these analyses, the simulation of sediment fate and transport for the river settings of this study was kept simple. A single bed layer of sediment was uniformly initialized to a thickness of 0.1 ft (0.03048 m) with a porosity of 0.4. Simulated suspended sediment load was affected by local deposition, but the bed was not allowed to erode (i.e., erodibility was set to zero), in order to maintain a small bed layer throughout the river domains. This ensured that bed sediments would be available for interaction with dissolved radionuclides in the water column.

Partitioning coefficient (K_d) values from the literature are used to describe the radionuclide interaction with bed and suspended sediment particles (Table 3-1). Sorption and desorption between the bed and water column is governed by a rate that is driven by the deviation from equilibrated conditions defined by the radionuclide-specifc K_ds. The rate applies to the surface layer of the bed to a depth of one sediment grain diameter. The maximum (i.e., intrinsic) sorption/desorption rate in this study was 1.16×10^{-5} s^{-1}, which was used in previous work in these settings. Radionuclide exchange with organic matter is not considered in this scoping analysis, again, for simplicity.

4.5.3.1 Extended Large River Configurations

To examine the effects of 1) radionuclide-sediment interactions, 2) tributaries, and 3) impoundments over longer distances and durations, the original 2D large river domain was

extended to a dam 103 mi from the release point. This extension included two small tributaries that added a total of 18,000 cfs to the 100,000 cfs discharge. From this dam, two different configurations were simulated out to 293 mi from the release point: 1) unimpounded free-flowing river and 2) impounded river with three intervening dams (Figure 4-2)

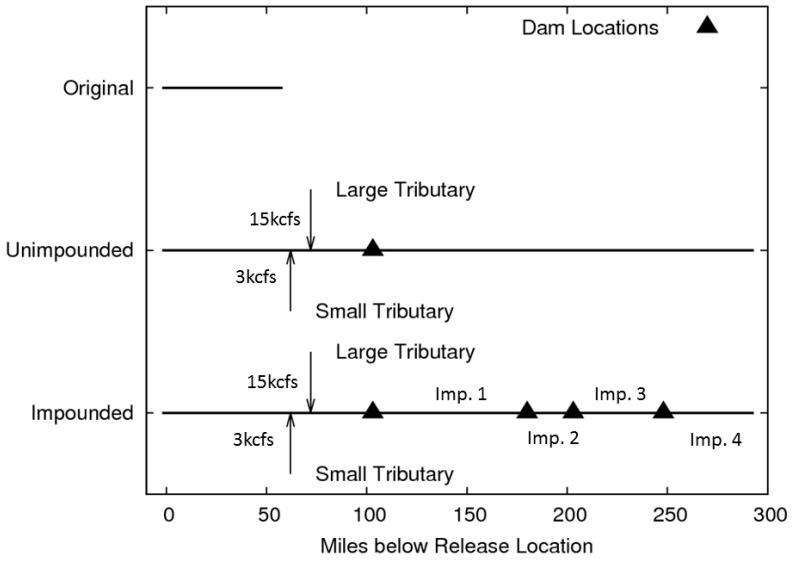

Figure 4-2. Configurations Used for Large River Cases. ***The lower river section was run both as a free-flowing river and as a series of impoundments.***

The bathymetry of the large river was adapted for unimpounded and impounded river scenarios. Characteristics of the river segments are given in Table 4-2. The numbering of the lower segments (e.g., Lower Imp. 1) is from upstream to downstream, and the lowest section (i.e., Lower Impoundment 4) does not terminate at a dam.

Eddy viscosity and turbulent mixing coefficient were the same as the original, 50-mi-long large river simulations.

Table 4-2. Characteristics of the Extended Large River

		Common Section	Lower River Scenarios				
			Unimpounded	Impounded			
Dimension	Units	Upper	Lower	Lower Imp. 1	Lower Imp. 2	Lower Imp. 3	Lower Imp. 4
Length	mi	103	190	77	23	45	45
Average depth	ft	19.7	9.5	35.5	30.7	33.3	18.0
Discharge	cfs	118,000	118,000	118,000	118,000	118,000	118,000
Susp sediment	kg/m^3	3.75E-3	3.34E-3	3.34E-3	2.61E-3	2.57E-3	2.44E-3
Mesh cells		784,800	439,383	99,430	62,281	155,916	114,985
Mesh resolution	ft	188	158	189	104	94	121
Transit time	hr	111	106	203	30	66	41

It should be noted that the average velocity for the unimpounded river segments is much larger than the impounded segments. The total travel time for the lower river was 106 hours for the unimpounded river, but 340 hours when simulated as a series of impoundments.

5. RADIONUCLIDE TRANSPORT MODELING RESULTS

5.1 Simulation Overview

5.1.1 Source Term

For all freshwater settings and scenarios in this study, aqueous and sorbed concentrations are simulated in space and time based on the release of 1 Bq of activity for each radionuclide (^{3}H, ^{90}Sr, ^{106}Ru, ^{125}Sb, ^{131}I, ^{134}Cs, ^{137}Cs, ^{144}Ce) with 1,000 m^3 of water over 10 days. These concentrations are reported in units of Bq/m^3 but could also be interpreted to be concentrations per Bq of activity released in the 10-day source term. For the linear partial differential equations and functions underlying the process models used in this study, this interpretation allows the reported radionuclide concentrations to be scaled for any activity release simply by multiplying by the intended activity release. For example, a 1 terabecquerel (TBq) ^{137}Cs release would result in concentrations 10^{12} times the reported ^{137}Cs concentrations. The scaling is valid when the advection, diffusion, decay and partitioning functions have linear dependence.

5.1.2 Sequence of Simulation Cases

Steady-state hydrodynamics are simulated first and saved. The resulting flow field is then used in radionuclide transport simulations using the source term described above. The base case for each of the three hydrologic settings is an aqueous-only simulation (i.e., without radionuclide-sediment interactions) focusing on the transport of each of the eight radionuclides in the 10-day release pulse. The base case targeted short-term simulations. In the lake setting, a 30-day period was simulated. In the river settings, the simulation period was 13.5 days (enough time for the primary pulse of released radionuclides to exit the domain).

A second set of analyses focused on continuing the lake and coupled radionuclide-sediment interaction river simulations out to one year. To ease the computational requirements for these simulations, the release was limited to the four radionuclides that represent the principal contributors to dose: ^{131}I, ^{134}Cs, ^{137}Cs, and ^{90}Sr. For the small and large river settings, water column activity concentrations were simulated with and without sediment-radionuclide interactions to identify the impact of sorption/desorption processes on the water column activity concentrations.

The third set of analyses examined the effect of impoundments on radionuclide transport by extending the one-year, large river simulation out to a total of 293 mi. In this case, the last 190 mi were modeled in two different configurations: 1) free-flowing unimpounded river and 2) impounded river with three intervening dams.

The complete results including ^{3}H, ^{106}Ru, ^{125}Sb, and ^{144}Ce in the initial base case simulations can be found in the Appendix B. In the case of the small and large river settings, the 13.5-day simulations were also used to examine the inclusion of radionuclide-sediment interactions. In all simulations, radionuclides decay according to the half-lives listed in Table 3-1.

5.2 Modeling Results

5.2.1 Small Lake/Reservoir

Unlike the advection-dominated river cases, radionuclide movement in the small lake setting is dispersion-dominated, which is a much slower process than advection. Figure 5-1 shows the

progress of the ^{137}Cs plume over the short-term simulation period (30 days). Because advection is minimal, the plume spreads from the release point in a nearly circular manner until it reaches the far shore, after which it can only spread toward the ends of the lake domain. Figure 5-2 to Figure 5-5 show relative concentration time series for ^{131}I, ^{144}Ce, ^{90}Sr, and ^{137}Cs, respectively, at the selected sample locations (Figure 4-1). These four radionuclides are shown because they are considered to represent a range of decay behavior. Figures B-1 through B-8 in Appendix B show similar figures for the eight radionuclides considered. Concentrations remain very high, compared to the river cases, near the release point over the entire simulation period. At the end of the 30-day simulation (20 days after the end of the radionuclide release), concentrations are still rising at all locations, except the release point and 1 mile upstream on the near shore.

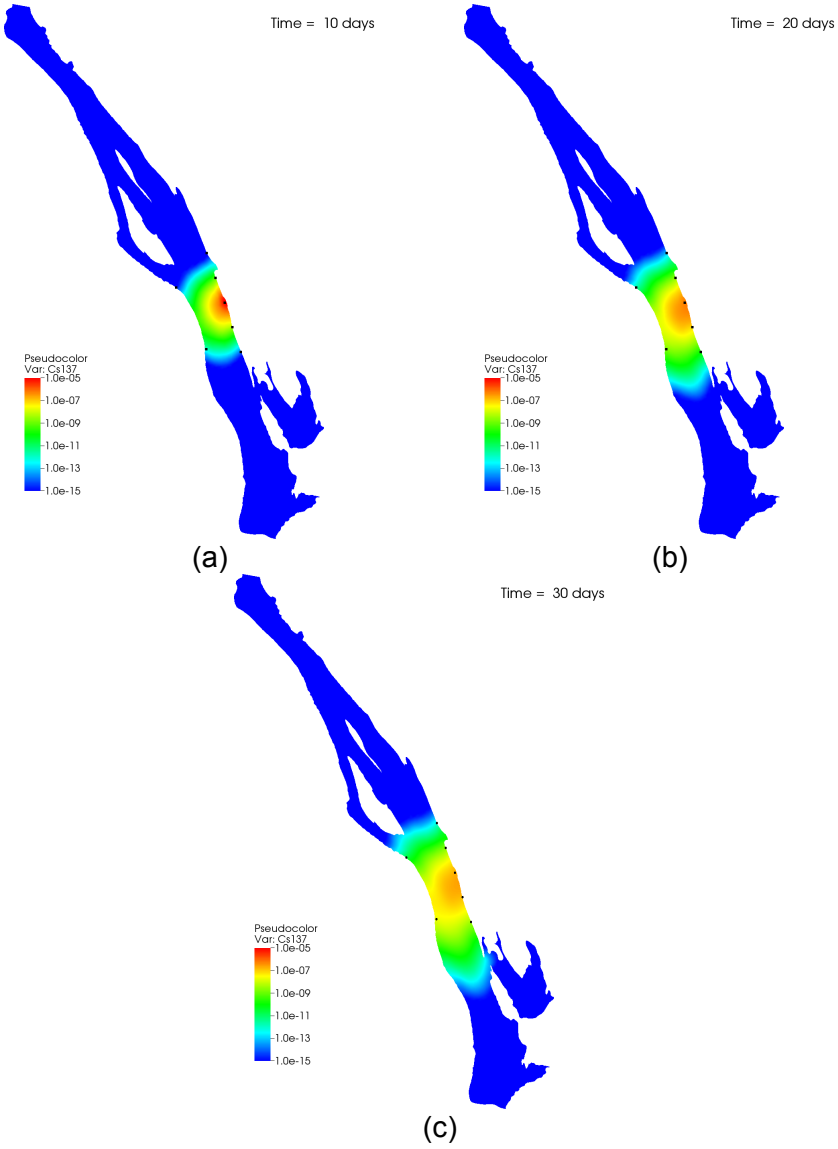

Figure 5-1. Simulated Near-Surface ^{137}Cs Concentrations, Bq/m^3 (a) 10 days, (b) 20 days, and (c) 30 Days after Start of Release in the Lake Scenario. *The black markers indicate sample locations.*

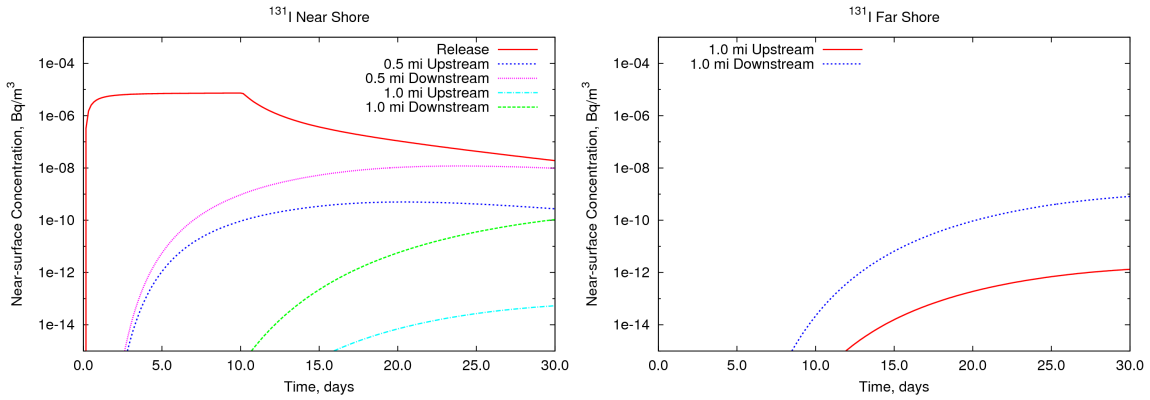

Figure 5-2. Simulated ^{131}I Activity Concentration History at the Near-Shore (left) and Far-Shore (right) Sample Locations in the Lake Scenario.

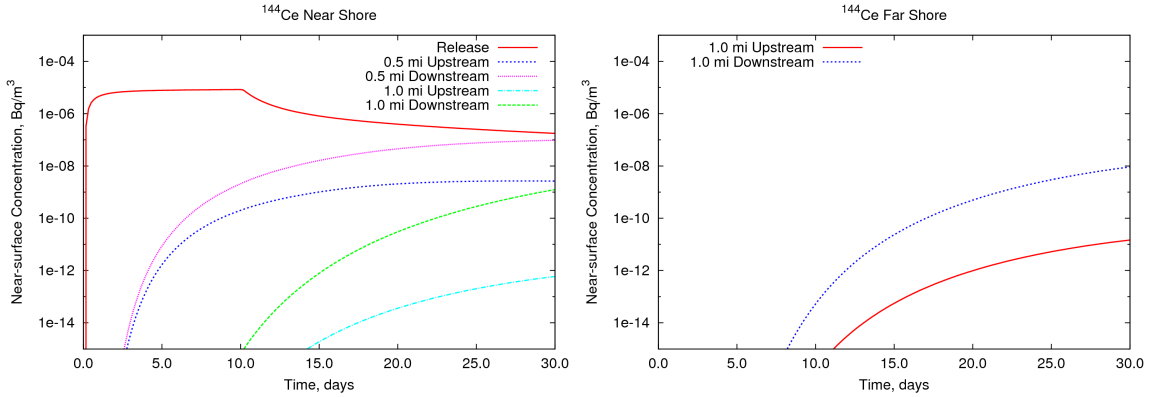

Figure 5-3. Simulated ^{144}Ce Activity Concentration History at the Near-Shore (left) and Far-Shore (right) Sample Locations in the Lake Scenario.

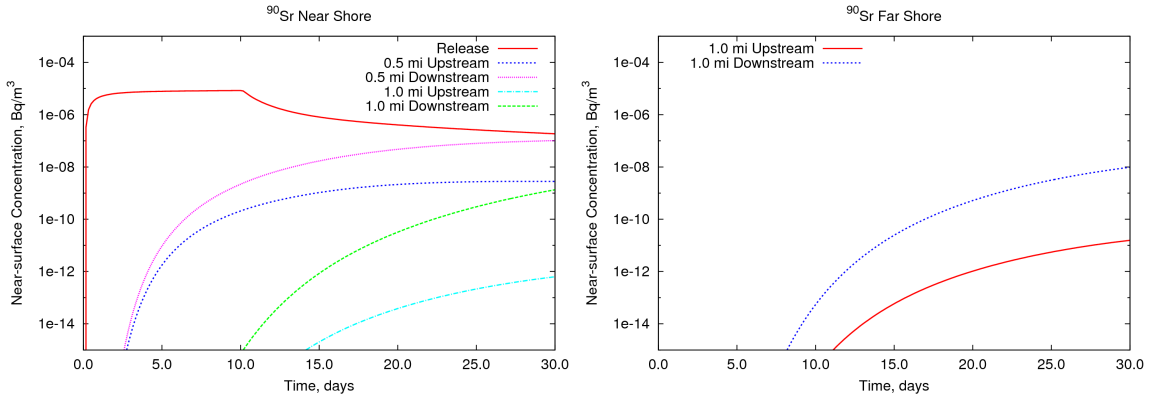

Figure 5-4. Simulated ^{90}Sr Activity Concentration History at the Near-Shore (left) and Far-Shore (right) Sample Locations in the Lake Scenario.

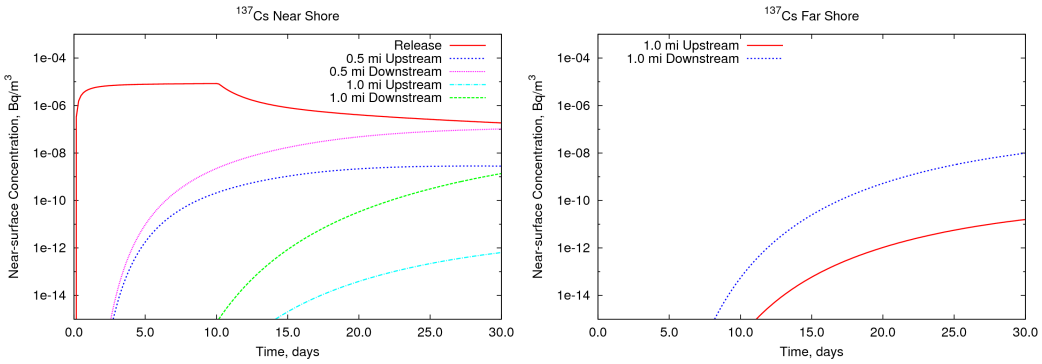

Figure 5-5. Simulated ^{137}Cs Activity Concentration History at the Near-Shore (left) and Far-Shore (right) Sample Locations in the Lake Scenario.

5.2.1.1 One-Year Simulations

For the lake simulations that were extended to one year, there were no changes in the lake boundary conditions and parameters. However, there were changes to the mesh resolution. Simulation of the four radionuclides, ^{134}Cs, ^{137}Cs, ^{131}I, and ^{90}Sr, for a full year with the original lake mesh resolution would have been computationally prohibitive. Consequently, a coarser mesh was developed. As with the original 100 ft resolution mesh, the interior of the lake shoreline was triangulated, but this time with a 400 ft horizontal resolution mesh. This triangular mesh was extruded in 3 ft vertical steps (versus 1 ft originally).

Figure 5-6 through Figure 5-9 show the simulated activities for the four radionuclides considered. Shorter half-lives result in earlier peaks at the seven monitoring locations. However, for a given radionuclide, the order of the peak occurrences at these locations is consistent. The earliest concentration peaks were at the 0.5-mi upstream and downstream locations on the near-shore. The latest peaks were at the far and near-shore locations 1 mi downstream with the latest peak (^{137}Cs and ^{90}Sr) at 69 days. ^{131}I activity decreases much quicker than the other radionuclides due to its short half-life. Even though it was small, advection had a marked effect on radionuclide transport. Concentrations at upstream locations were lower by 2 to 4 orders of magnitude than at the downstream locations.

Figure 5-10 shows plan views of the activity plume at several times during the simulated year. Even though it is small, advection has a significant effect on the overall movement of the plume. The plume extends about 1 mi upstream at most. The downstream edge of the plume reached the lake outlet by 90 days. Afterward, advection pushed the plume out without any additional upstream movement.

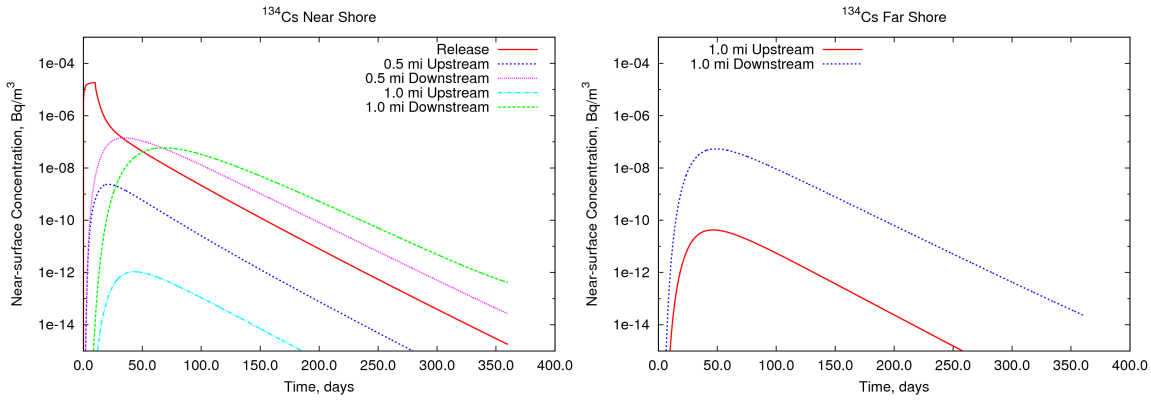

Figure 5-6. Lake ^{134}Cs Activity Over Time at Several Locations on the Same (left) And Opposite (right) Shore of the Release Location.

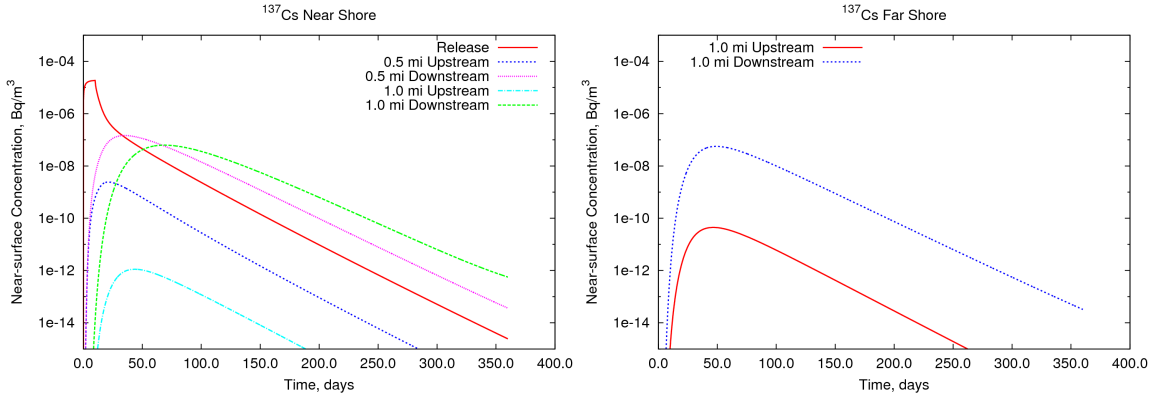

Figure 5-7. Lake ^{137}Cs Activity Over Time at Several Locations on the Same (left) and Opposite (right) Shore of the Release Location.

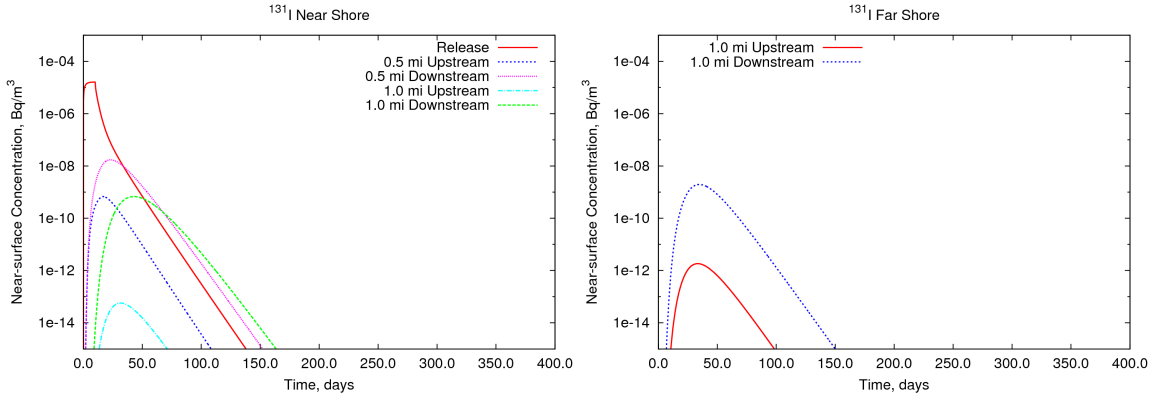

Figure 5-8. Lake ^{131}I Activity Over Time at Several Locations on the Same (left) and Opposite (right) Shore of the Release Location.

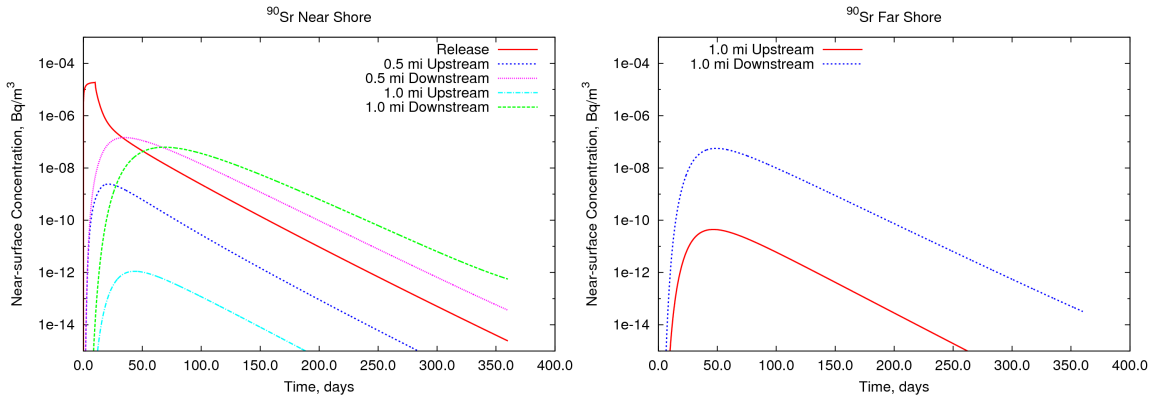

Figure 5-9. Lake ^{90}Sr Activity Over Time at Several Locations on the Same (left) and Opposite (right) Shore of the Release Location.

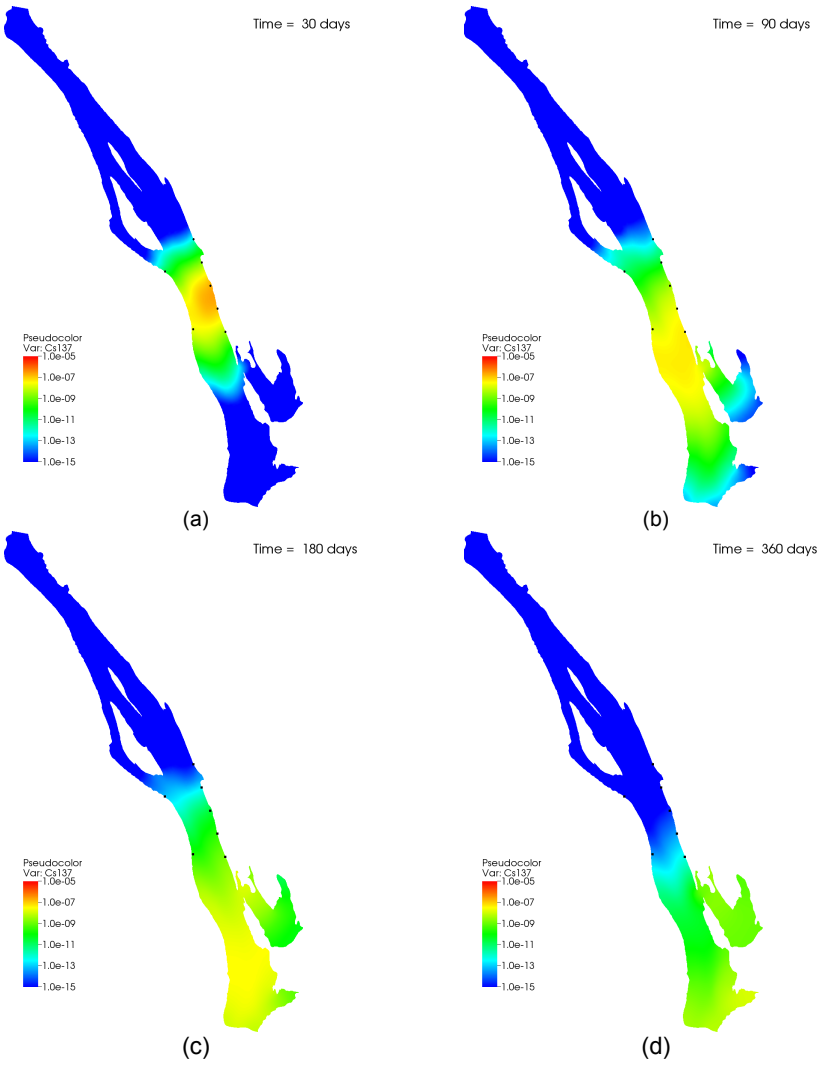

Figure 5-10. Simulated Lake Aqueous-Only, Near-Surface ^{137}Cs Concentrations, Bq/m^3 (a) 30 Days, (b) 90 Days, (c) 180 Days, and (d) 360 Days after Start of Release from the Lake One-Year Simulation. *The black markers indicate sample locations*.

5.2.1.2 Sensitivity Test for Turbulent Mixing Coefficient

The key parameter for the lake transport simulation was the turbulent mixing coefficient. The value chosen was in the range measured by Peeters et al. (1996) in smaller lakes, but near the minimum. The one-year lake simulation for ^{137}Cs was repeated with a turbulent mixing coefficient 5 times higher (0.2 m^2/s). This was near the upper end of the measurements made by Peeters et al. (1996).

Simulated time-dependent activity using the increased turbulent mixing coefficient is compared to the original simulation in Figure 5-11. With a higher mixing coefficient, concentrations at the sampling locations peak sooner and decrease much slower. The enhanced mixing peaks are higher than the original peaks for the upstream locations and lower than the original peaks for the downstream locations. This can be seen by comparing the simulated spatial activity distributions from the increased mixing coefficient simulation in Figure 5-12 with the original simulation results in Figure 5-10.

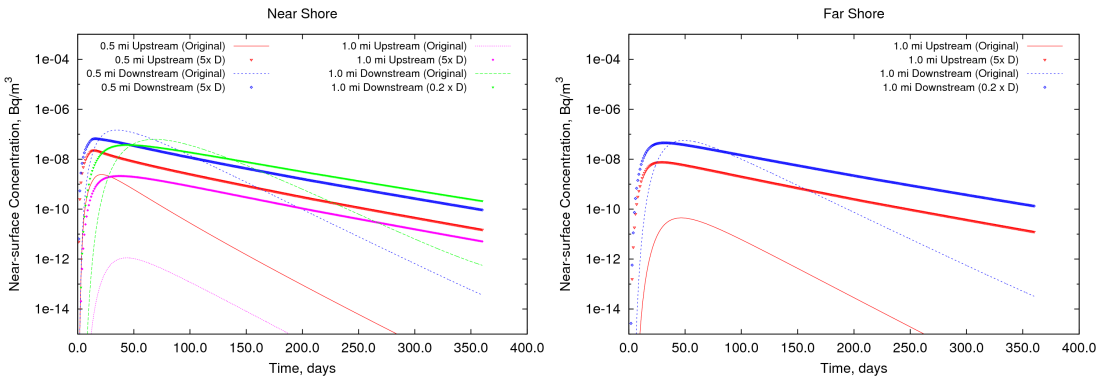

Figure 5-11. Comparison of Aqueous-Only ^{137}Cs Activity Concentrations Over Time for the Original and Increased Mixing Coefficient Lake Simulations at Locations along the Same (left) and Opposite (right) Shore as the Release.

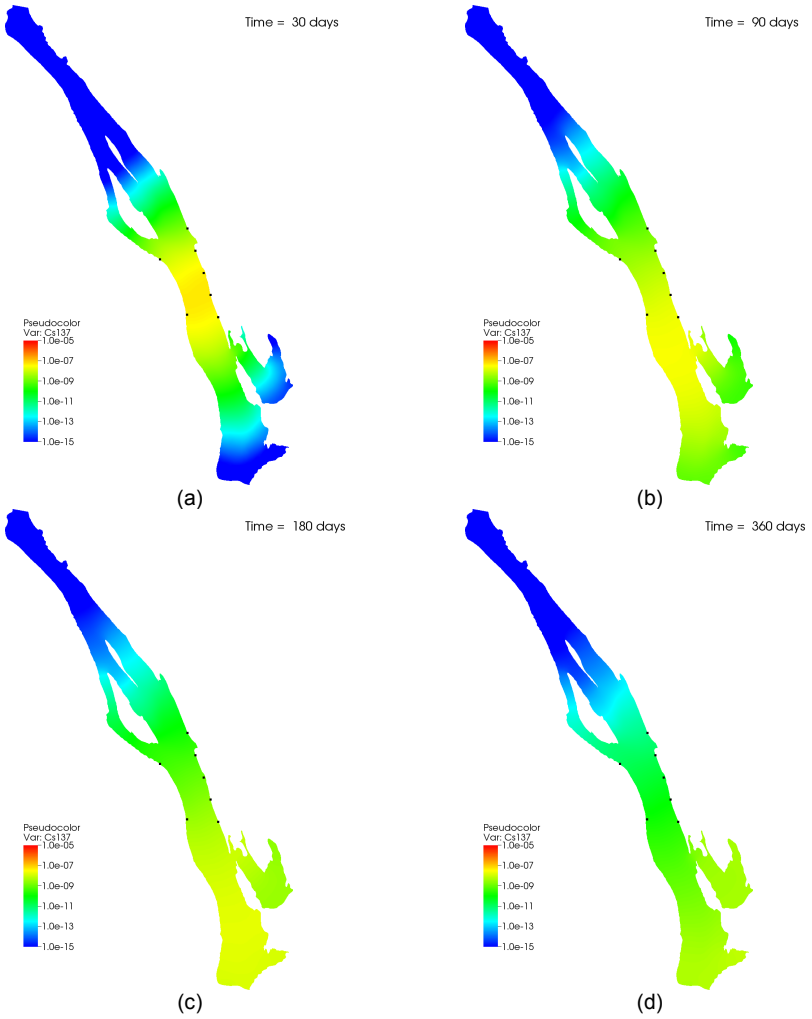

Figure 5-12. Simulated Lake Aqueous-Only, Near-Surface ^{137}Cs Activity Concentrations, Bq/m^3 (a) 30 Days, (b) 90 Days, (c) 180 Days, and (d) 360 Days after Start of Release From the Lake Increased Mixing Coefficient Simulation. *The black markers indicate sample locations. Compare to Figure 5-10.*

5.2.2 Small Discharge River

For a given radionuclide, the lower flow rate in the small river setting (5,000 cfs vs 100,000 cfs in the large river setting) results in water column concentrations ~20 times higher than in the large river simulations due to less dilution. In contrast to the large river, the activity plume in the small river setting mixes laterally quickly (Figure 5-13). Figure 5-14 to Figure 5-17 compare time series of ^{131}I, ^{90}Sr, ^{137}Cs, and ^{144}Ce activities, respectively, from the aqueous-only simulations. Note that in the interest of brevity, these four radionuclides are shown because they are considered to represent a range of sorption behavior. Similar figures for the eight radionuclides considered are shown in Figures B-14 through B-21 in Appendix B. The “average” line in those figures indicates what the concentration would be assuming complete mixing using the radionuclide release rate and river flow rate. The small river near-shore and far-shore concentrations converge to the fully mixed average concentration within 10 mi of the release. This is not only because of the smaller width and lower velocity of the small river case, but also from the additional mechanical mixing that occurs in the small river’s pool and riffle nature.

Aqueous water column activity concentrations from the sediment-inclusive simulations were only slightly lower than the respective aqueous-only simulations, except for ^{106}Ru and ^{144}Ce, which had the highest sediment sorption distribution coefficients (K_ds). Figure 5-18 compares the aqueous ^{144}Ce activity concentrations from the sediment-inclusive simulation to the aqueous-only simulation. Table 5-1 shows percent of released radionuclide activity remaining in the sediment bed 13.5 days after the start of the release for the entire model domains of both the small and large discharge river settings. The sediment retained substantial portions of ^{106}Ru and ^{144}Ce, lesser fractions of the Cs isotopes, and very little of the other radionuclides. Retention is based, in part, on the sediment sorption distribution coefficient, K_d, given in Table 3-1. Larger fractions of the released activity were left in the small river bed than in the large river simulation (Table 5-1). This is because the small river had significantly higher aqueous concentrations and longer contact time with the bed (i.e., lower average velocity), which resulted in much more activity sorbed to the bed sediments. Consequently, the post-pulse water column concentrations from bed desorption in the small river are commensurately higher.

Figure 5-13. Simulated Small River ^{137}Cs Water Column Concentrations (Bq/m^3) in the Aqueous-Only Simulation (top), Aqueous Phase in the Sediment-Inclusive Simulation (middle), and Suspended Sediment-Sorbed Phase in the Sediment-Inclusive Simulation (bottom). ***Flow is from right to left. Downstream blue-colored areas are inundated but not directly connected to the channel. The figures extend approximately 10 mi below the release location. Black markers indicate sample locations 2 and 10 mi downstream.***

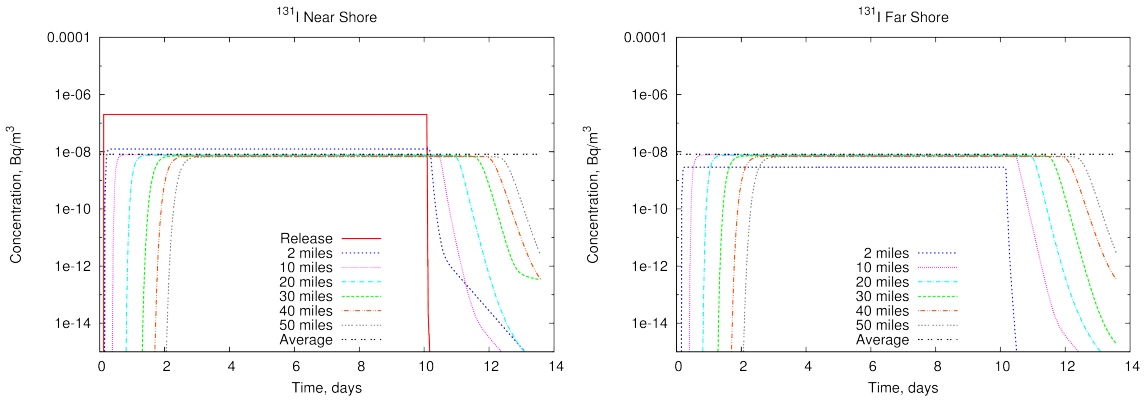

Figure 5-14. Simulated Small River Aqueous-Only ^{131}I Activity Over Time at Several Locations Along the Same Shore as the Release (left) and the Opposite Shore (right).

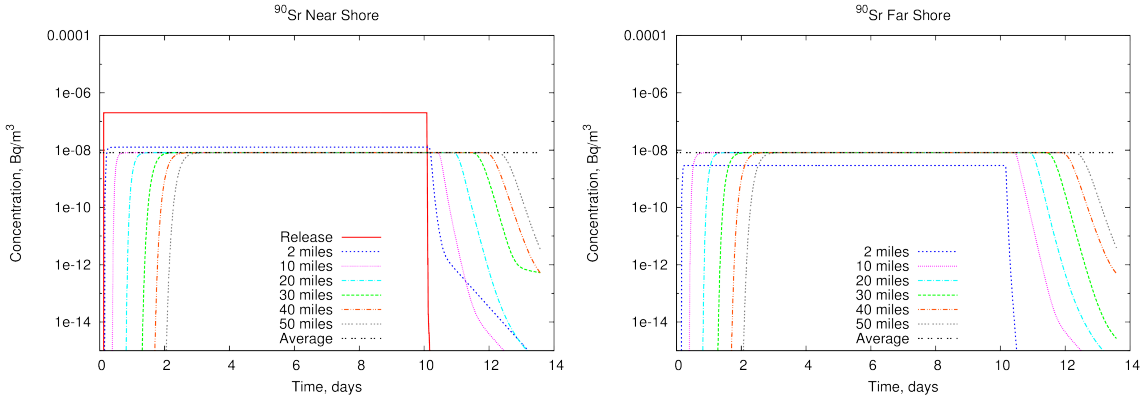

Figure 5-15. Simulated Small River Aqueous-Only ^{90}Sr Activity Over Time at Several Locations Along the Same Shore as the Release (left) and the Opposite Shore (right).

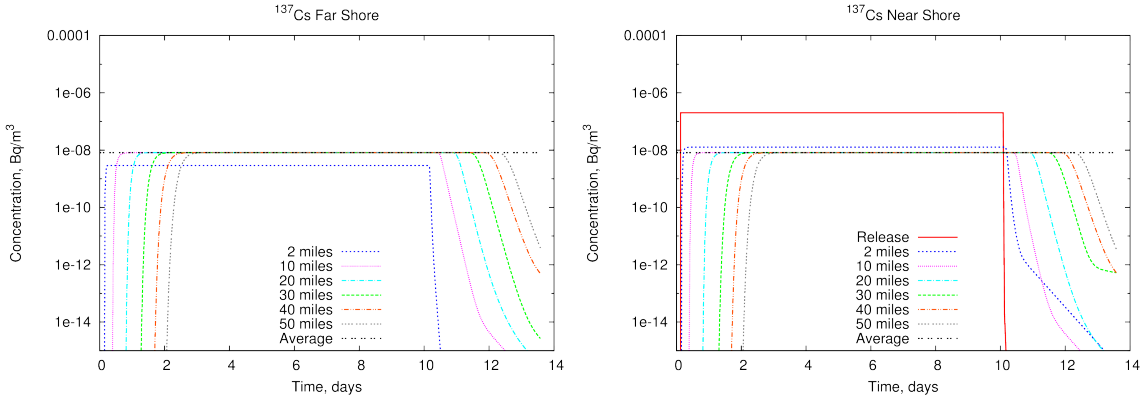

Figure 5-16. Simulated Small River Aqueous-Only ^{137}Cs Activity Over Time at Several Locations Along the Same Shore as the Release (left) and the Opposite Shore (right).

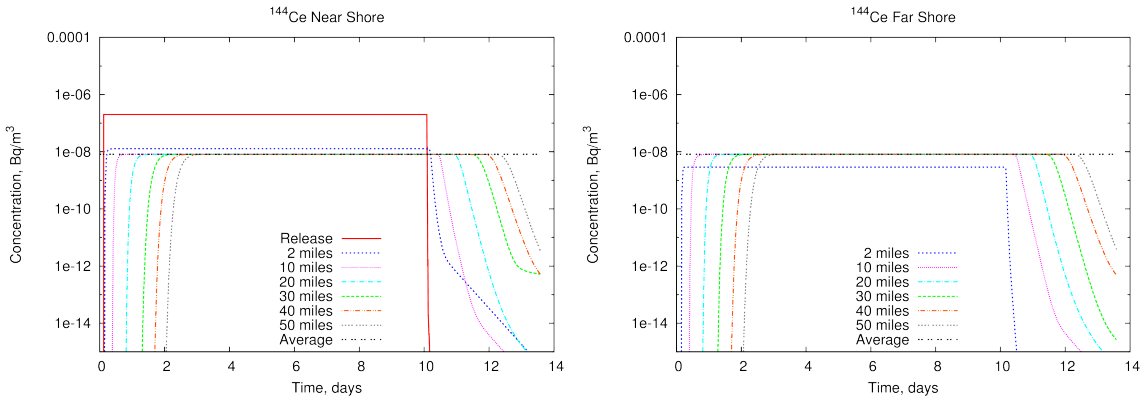

Figure 5-17. Simulated Small River Aqueous-Only ^{144}Ce Activity Over Time at Several Locations Along the Same Shore as the Release (left) and the Opposite Shore (right).

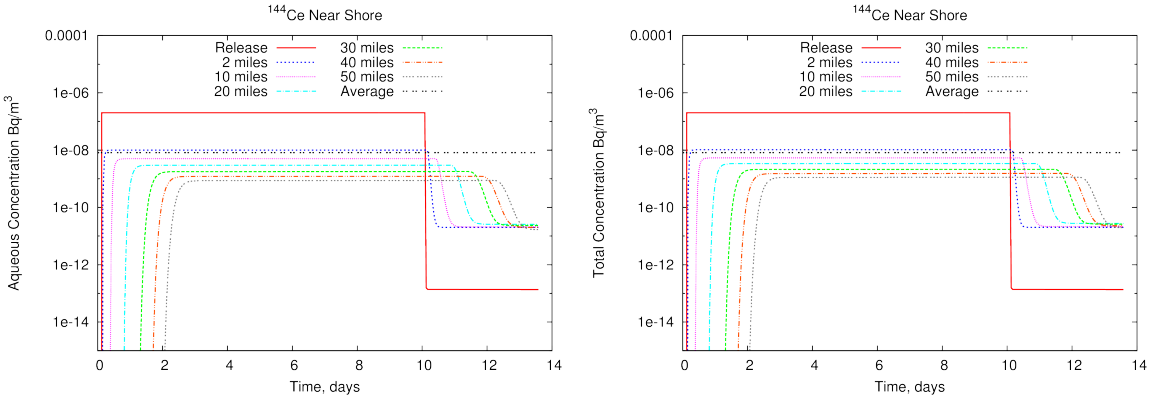

Figure 5-18. Time Series Small River ^{144}Ce Aqueous (left) and Total Aqueous and Suspended (right) Activity From the Sediment Simulation at Locations Along the Same Shore as the Release. *Compare with the results of the aqueous-only simulation (Figure 5-17).*

Table 5-1. Percent of Released Activity in the River Bed after 13.5 Days in the Small and Large Discharge River Settings

	Large River	Small River
Species	**% of Release**	**% of Release**
^{3}H	0	0
^{90}Sr	0.28	1.4
^{106}Ru	12	46
^{125}Sb	0.66	3.2
^{131}I	0.04	0.17
^{134}Cs	1.9	8.9
^{137}Cs	1.9	9.0
^{144}Ce	36	86

5.2.2.1 One-Year Simulations

To identify longer-term behaviors, the small discharge river simulations were extended in duration to one year. No changes were made in mesh, boundary conditions, or simulation parameters.

Figure 5-19 to Figure 5-22 show one-year time histories of water column activity for ^{134}Cs, ^{137}Cs, ^{131}I, and ^{90}Sr, respectively. Dissolved activities (aqueous phase) are in the top plot of each figure, the activities sorbed on the suspended sediment in the water column are in the middle plots, and the total of the two is shown in the bottom plots. During the passage of the pulse of released radionuclides, there was a large sorption of activity to the bed sediments. After the passage of the pulse of released radionuclides, the bed sediment-sorbed activity is slowly desorbed resulting in slightly elevated concentrations in the aqueous phase. Figure B-22 to Figure B-28, in Appendix B, show similar plots for the seven radionuclides considered for this case (tritium is assumed to not sorb). In general, there is a simple extension of the post-pulse radionuclide desorption from the bed sediments in the previous short duration simulations. The slowly decreasing post-pulse concentrations are controlled by the decay rate (i.e., half-life) and the radionuclide partitioning between the water column and the (bed) sediment (i.e., K_d). In particular, the ^{131}I activity concentrations rapidly decrease over the 45 half-lives in the one-year simulation. It also has the lowest K_d of the four simulated radionuclides, which means a smaller fraction is associated with the bed sediments. To a much lesser degree, the 2-year half-life for ^{134}Cs, results in a slightly faster rate of removal from the water column compared to ^{137}Cs.

Equilibrium is not reached in the post-pulse partitioning of radionuclides between the bed sediment and overlying water column (i.e., desorption is rate-limited). This means a parcel of water traveling downstream progressively accumulates more activity as it passes over continuously desorbing bed sediments. So while aqueous radionuclide concentrations at any given location are decreasing with time, the longitudinal distribution of water column concentrations at any instant of time is increasing with downstream distance. Figure 5-23 to Figure 5-26 show the time-dependent bed sediment-sorbed activity concentration for ^{134}Cs, ^{137}Cs, ^{131}I, and ^{90}Sr, respectively. Figure B-29 to Figure B-35, in Appendix B, show bed sediment-sorbed concentrations for the seven radionuclides considered for this case.

For ^{131}I, both water column (Figure 5-21, top) and bed (Figure 5-25), concentrations decrease quickly after passage of the release pulse. This is primarily due to decay. Figure 5-27 compares the history of ^{131}I and ^{134}Cs bed concentrations, the two shortest lived radionuclides. Blue lines have been added to the plots to show rates of decay. The reduction of bed ^{131}I can be almost entirely explained by decay, whereas ^{134}Cs activity falls at a much greater rate than its decay, indicating desorption plays a greater role.

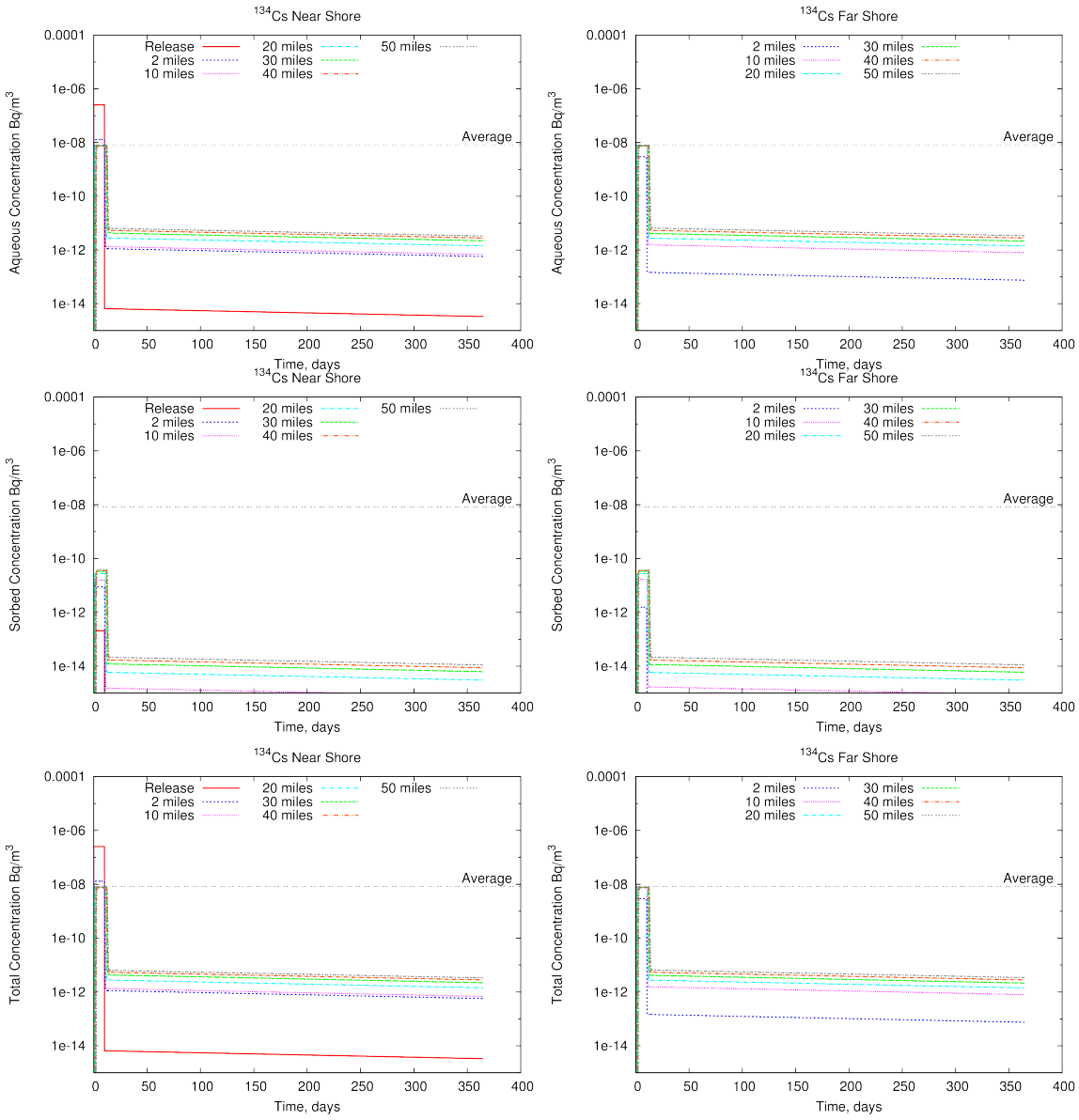

Figure 5-19. Small River Aqueous (top), Suspended Sediment-Sorbed (middle), and Total (bottom) ^{134}Cs Activity Over Time at Several Downstream Locations on the Same (left) and Opposite (right) Shore of the Release Point.

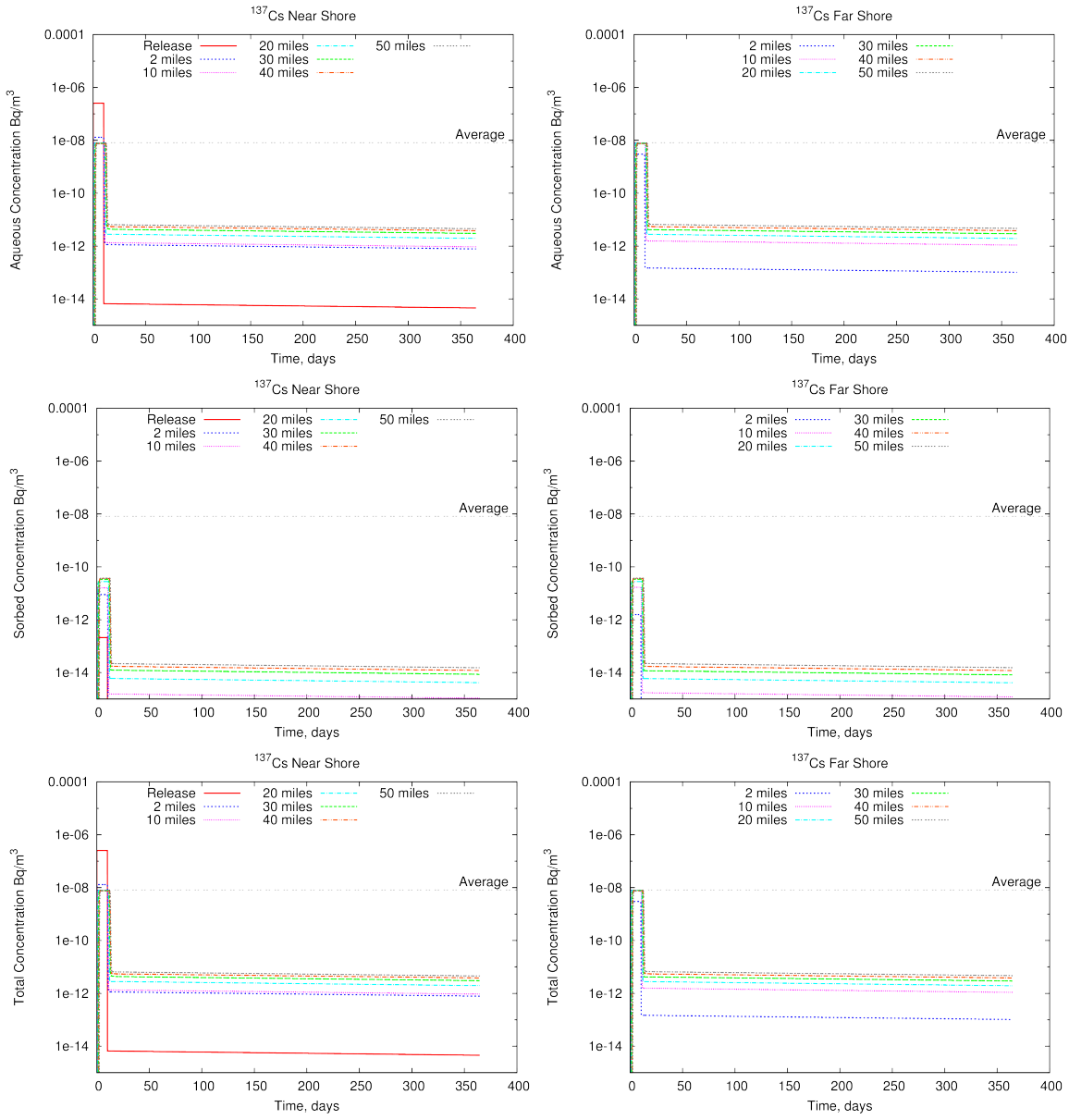

Figure 5-20. Small River Aqueous (top), Suspended Sediment-Sorbed (middle), and Total (bottom) ^{137}Cs Activity Over Time at Several Downstream Locations on the Same (left) and Opposite (right) Shore of the Release Point.

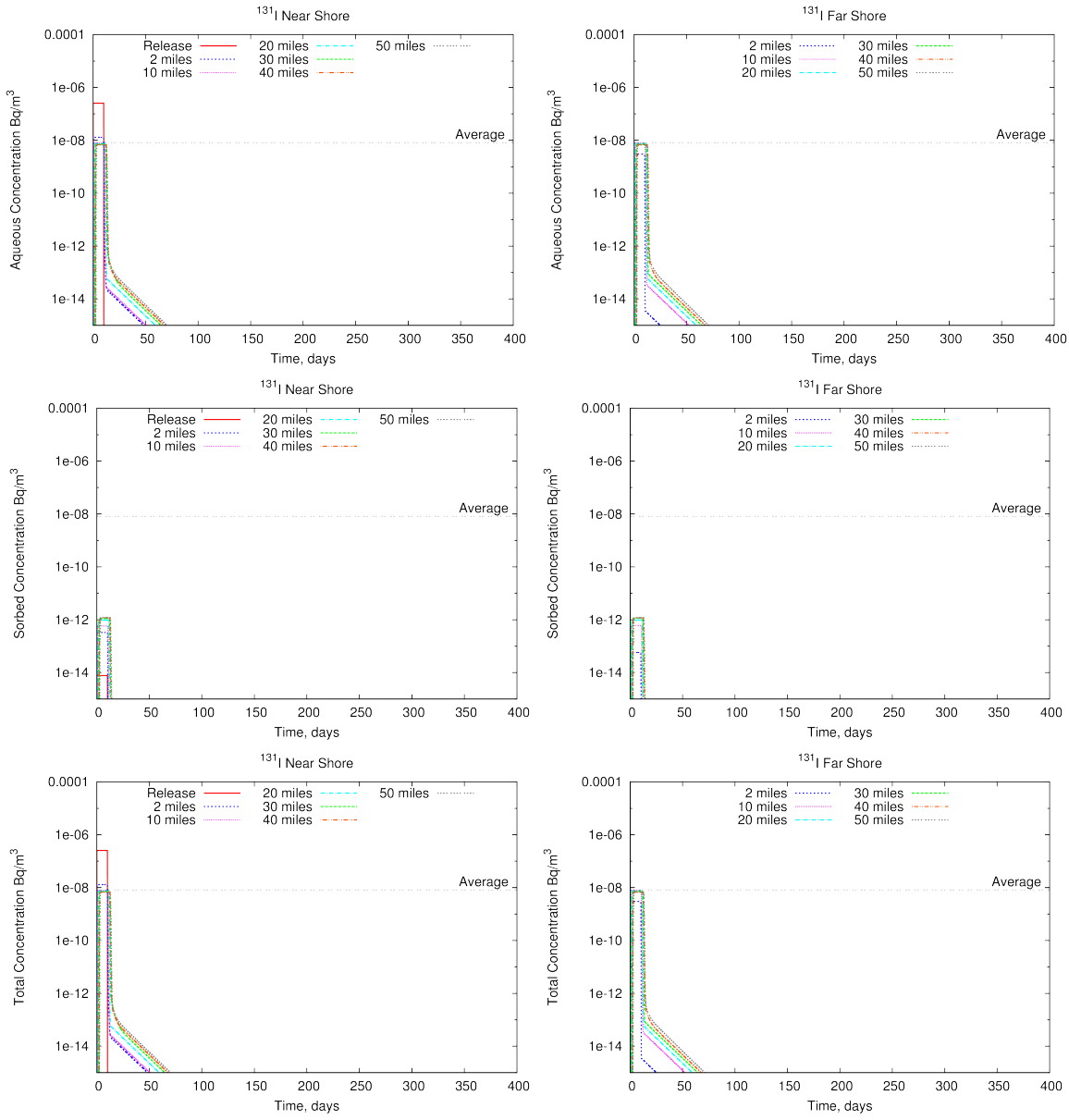

Figure 5-21. Small River Aqueous (top), Suspended Sediment-Sorbed (middle), and Total (bottom) ^{131}I Activity Over Time at Several Downstream Locations on the Same (left) and Opposite (right) Shore of the Release Point.

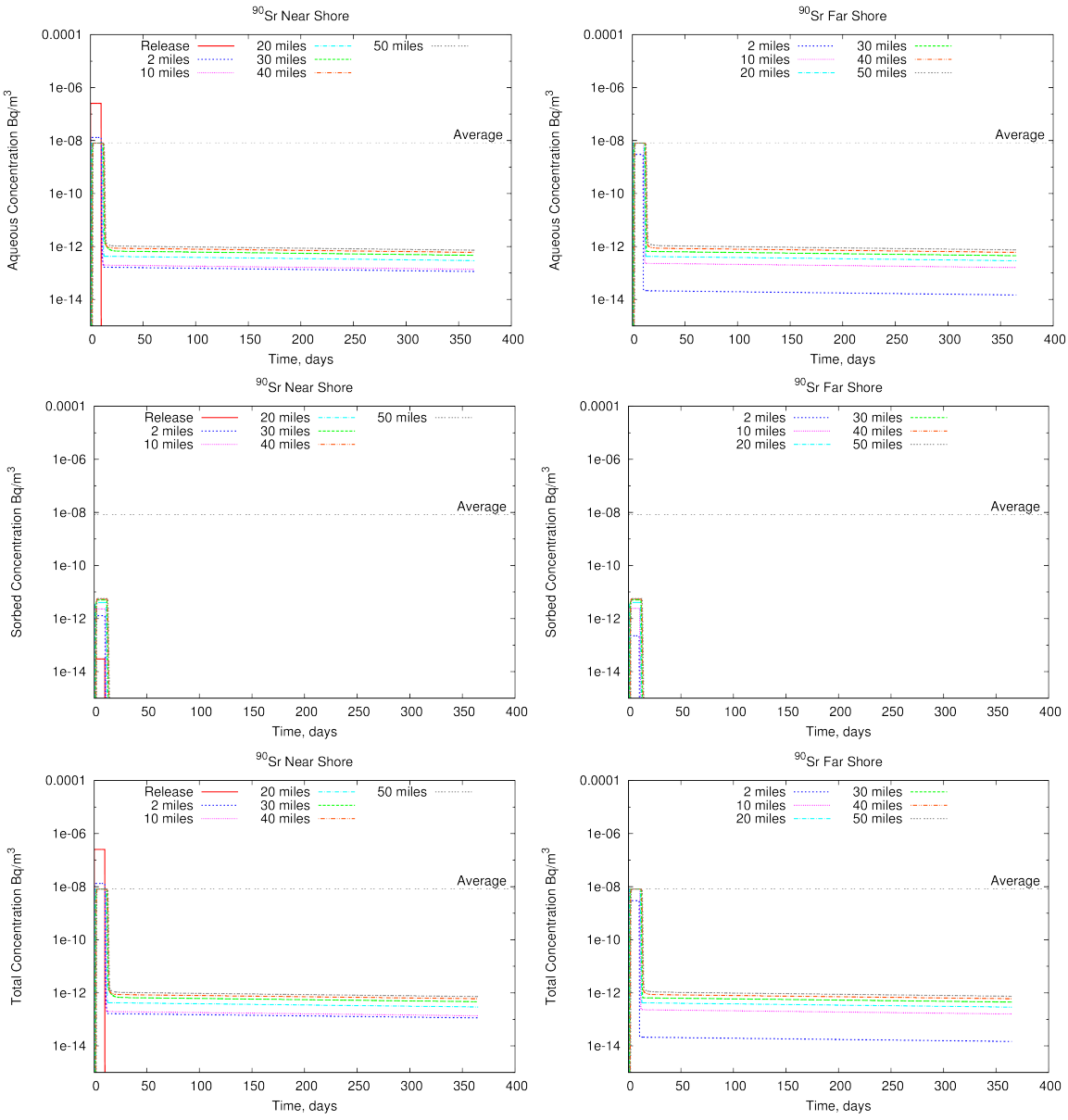

Figure 5-22. Small River Aqueous (top), Suspended Sediment-Sorbed (middle), and Total (bottom) ^{90}Sr Activity Over Time at Several Downstream Locations on the Same (left) and Opposite (right) Shore of the Release Point.

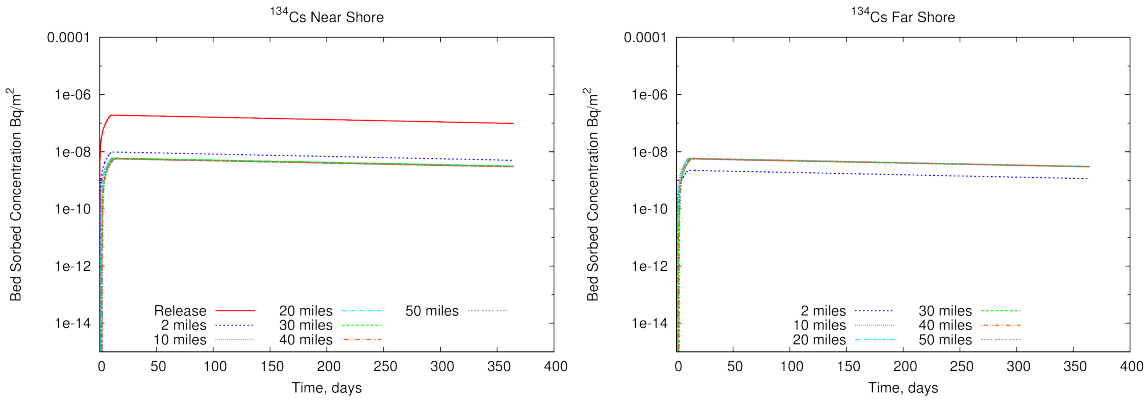

Figure 5-23. Small River Bed Sediment-Sorbed ^{134}Cs Activity Per Square Meter Over Time at Several Locations on the Same (left) and Opposite (right) Shore of the Release Location.

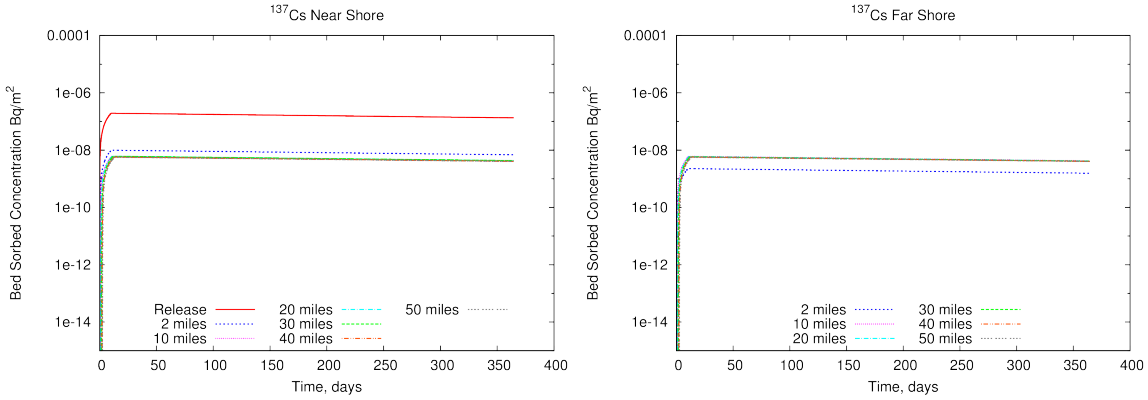

Figure 5-24. Small River Bed Sediment-Sorbed ^{137}Cs Activity Over Time at Several Locations on the Same (left) and Opposite (right) Shore of the Release Location.

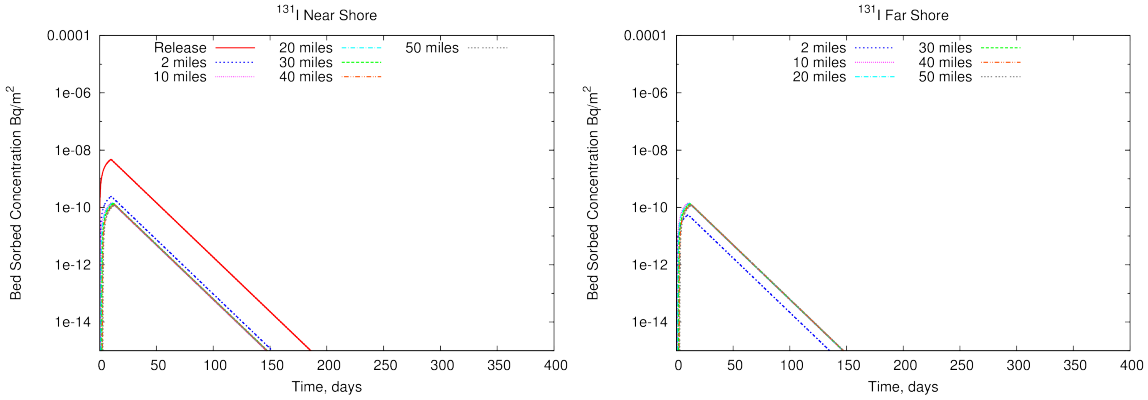

Figure 5-25. Small River Bed Sediment-Sorbed ^{131}I Activity Over Time at Several Locations on the Same (left) and Opposite (right) Shore of the Release Location.

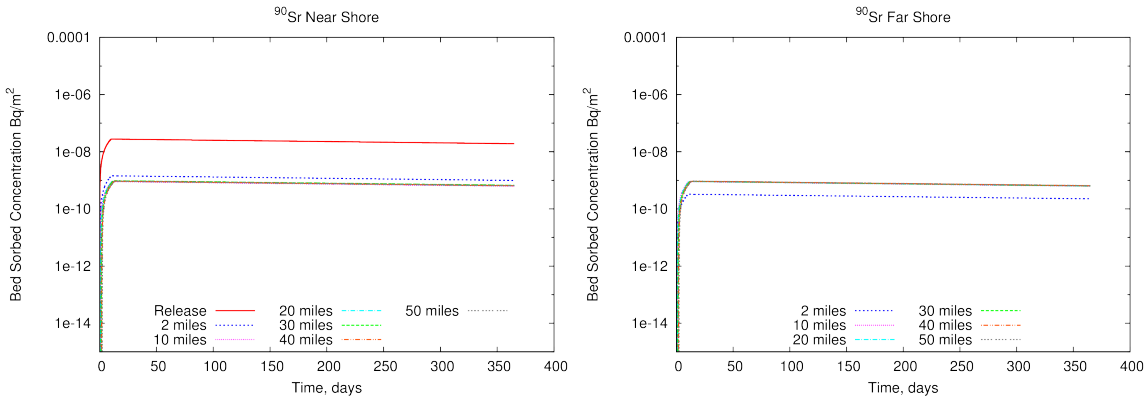

Figure 5-26. Small River Bed Sediment-Sorbed ^{90}Sr Activity Over Time at Several Locations on the Same (left) and Opposite (right) Shore of the Release Location.

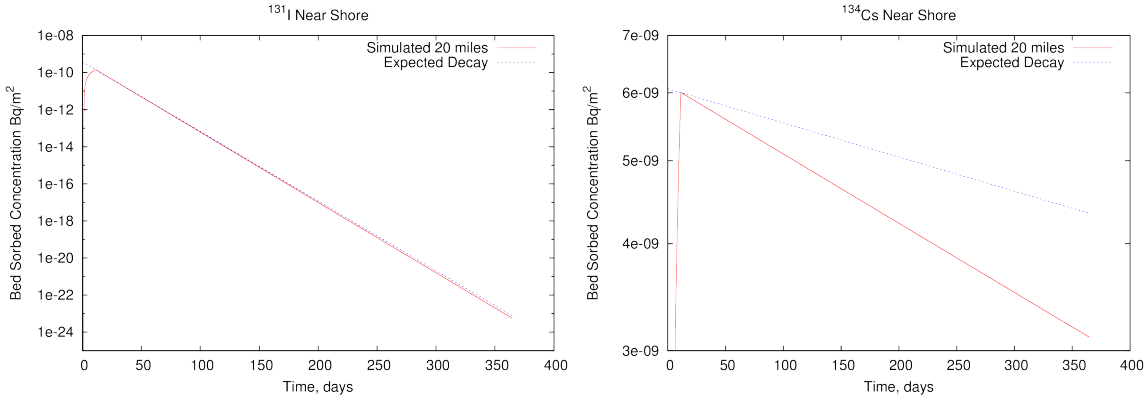

Figure 5-27. Small River Bed Sediment-Sorbed ^{131}I (left) and ^{137}Cs (right) 20 Mi Downstream of the Release Compared with the Decay Expected Starting with the Maximum Concentration.

5.2.3 Large Discharge River

In the large river base case simulations, the activity plume hugs the shore on which the release was made (Figure 5-28). There are orders of magnitude differences between the near-shore and far-shore concentrations for 10 mi downstream from the release point. Differences are still discernible 50 mi downstream from the release point.

Figure 5-29 to Figure 5-32 compare the 14-day time series of ^{131}I, ^{90}Sr, ^{137}Cs, and ^{144}Ce activities, respectively, from the aqueous-only simulations for near-shore and far-shore locations. Note that in the interest of brevity, these four radionuclides are shown because they are considered to represent a range of sorption and decay behavior. Figure B-44 to Figure B-51, in Appendix B, are similar figures for the eight radionuclides considered. The "average" line in those figures indicates what the activity concentration would be assuming complete mixing using the radionuclide release rate and river flow rate. The average is higher than any curves in the far-shore plots because it is an average of concentrations across the width of the river. As with the small river, concentrations in the pulse of released radionuclides flow downstream with very little dilution with distance. After the release is stopped, concentrations decrease rapidly and this profile of a rapid increase followed by near constant

concentrations and then a rapid decrease is maintained for miles. After the 10-day pulse passes through the system, aqueous concentrations decrease rapidly to a plateau ~3 orders of magnitude lower than peak concentrations followed by slower decline. These low, slowly diminishing radionuclide concentrations in the water column are the result of later arrivals from slower moving transport pathways.

When radionuclide-sediment interactions were included in the simulations, water column concentrations for most of the radionuclides were slightly lower than the aqueous-only base case simulation (c.f., the top two graphics in Figure 5-28). For the radionuclides with high affinity to sediment (i.e., high K_d values), ^{106}Ru and ^{144}Ce, water column concentrations were noticeably reduced downstream. In the coupled sediment and radionuclide transport simulation with ^{144}Ce, the downstream aqueous and total (aqueous plus suspended sediment-sorbed) water column ^{144}Ce activity concentrations (Figure 5-33) were noticeably lower than the ^{144}Ce activity concentrations in the aqueous-only base case simulation (Figure 5-32). This indicates significant ^{144}Ce sorption to the bed sediments. Figure B-52 to Figure B-58, in Appendix B, contain sets of 14-day plots showing aqueous concentrations, sorbed concentrations, and the aqueous plus suspended sediment-sorbed concentrations for each of the seven radionuclides considered (tritium is not included in these sorption cases).

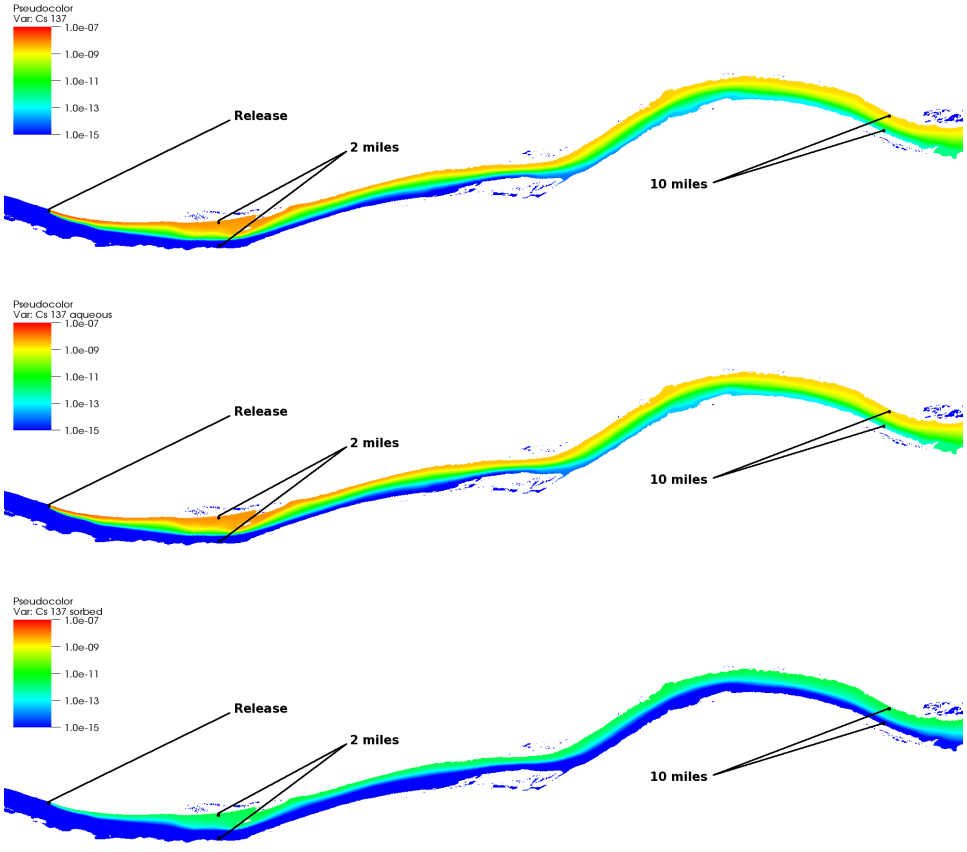

Figure 5-28. Simulated Large River ^{137}Cs Concentrations (Bq/m^3) in the Aqueous-Only Simulation (top), Aqueous Phase (middle) and Suspended Sediment Phase (bottom) in the Sediment Simulation. ***Flow is from left to right. The figures extend approximately 10 mi below the release location. Black markers indicate sample locations.***

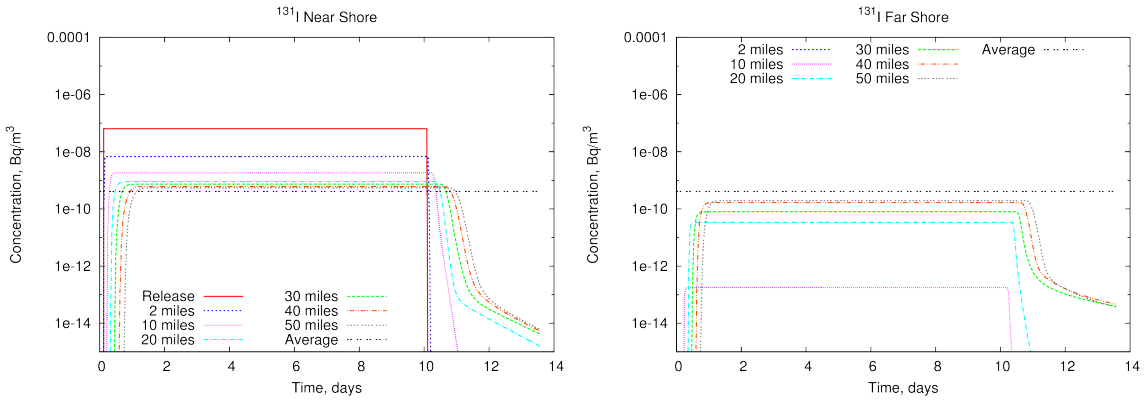

Figure 5-29. Simulated Large River Aqueous-Only ^{131}I Activity Over Time at Several Locations Along the Same Shore as the Release (left) and the Opposite Shore (right).

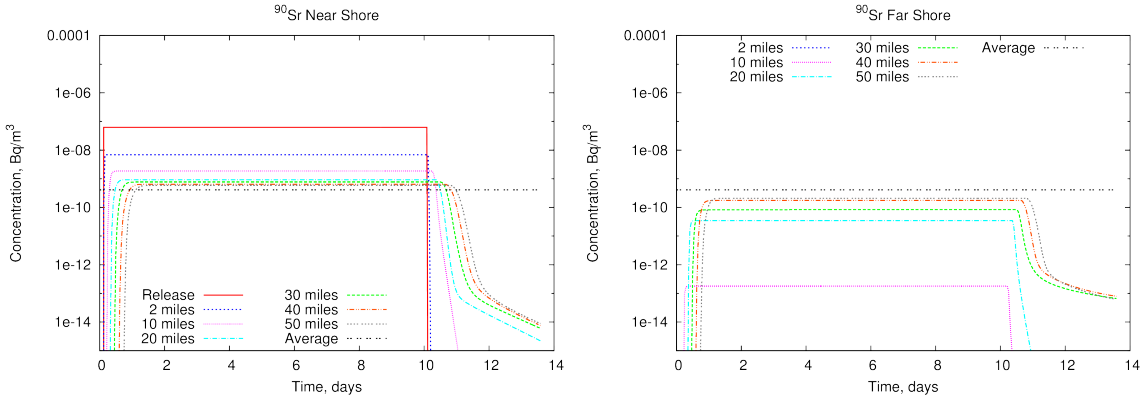

Figure 5-30. Simulated Large River Aqueous-Only ^{90}Sr Activity Over Time at Several Locations Along the Same Shore as the Release (left) and the Opposite Shore (right).

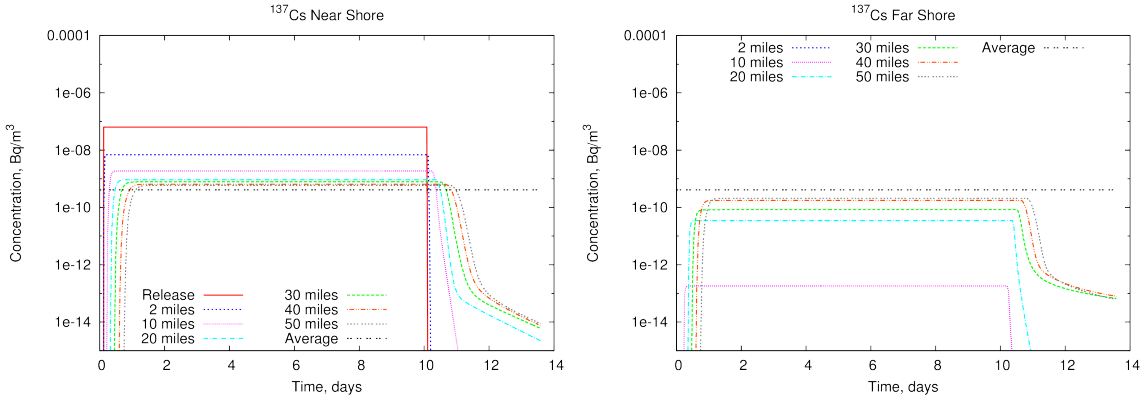

Figure 5-31. Simulated Large River Aqueous-Only ^{137}Cs Activity Over Time at Several Locations Along the Same Shore as the Release (left) and the Opposite Shore (right).

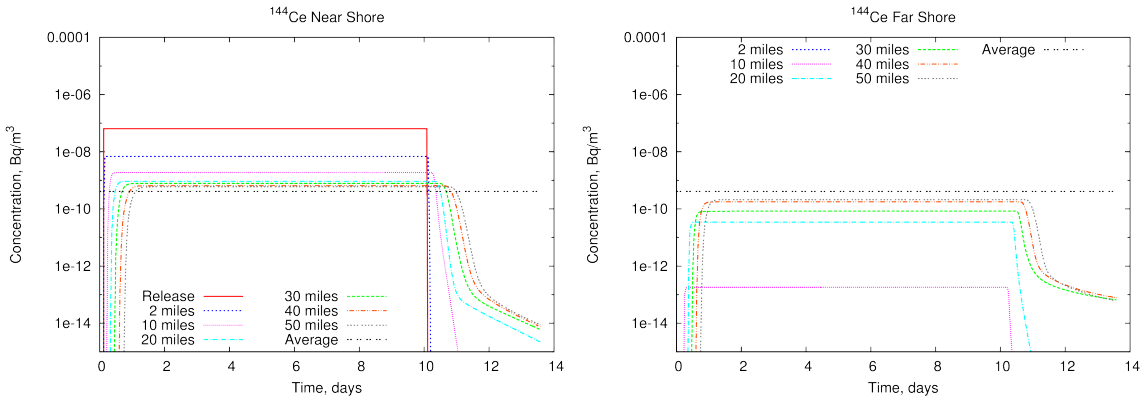

Figure 5-32. Simulated Large River Aqueous-Only ^{144}Ce Activity Over Time at Several Locations Along the Same Shore as the Release (left) and the Opposite Shore (right).

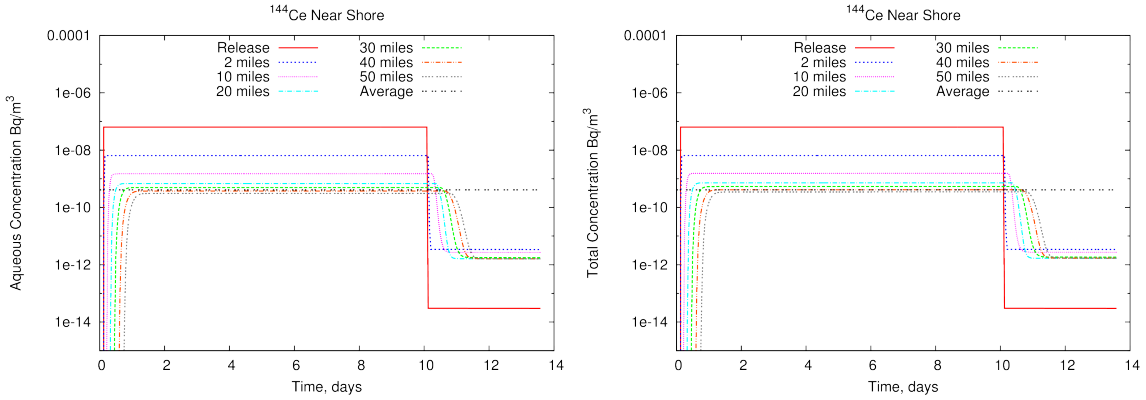

Figure 5-33. Time Series of Large River ^{144}Ce Aqueous (left) and Total Water Column (aqueous + sorbed to suspended sediment) (right) Activity from the Sediment Simulation Along the Same Shore as the Release. *Compare with the results of the aqueous-only simulation (Figure 5-32).*

5.2.3.1 One-Year Simulations with Extended Domain

To identify longer-term behaviors over longer distances, the MASS2 large river domains were extended 103 mi downstream from the release point, terminating at a dam. Simulations were lengthened to one year. The extended reach included 3,000 and 15,000 cfs contributions from two tributaries. Other than the extended mesh and tributary flows, no changes were made in the influent boundary conditions or parameters. The specification was summarized earlier in Table 4-2. Results are provided for the four radionuclides with the highest dose consequences: ^{131}I, ^{134}Cs, ^{137}Cs, and ^{90}Sr.

In these extended large river simulations, there are consistent patterns of concentration variation with time (Figure 5-34 to Figure 5-37, showing combined aqueous and suspended sediment activity concentrations in the water column) that are an extension of the previously identified behaviors: persistence of differences between near-shore and far-shore concentrations over 50 mi downstream and post-pulse concentrations that are non-zero but orders of magnitude lower than the 10-day pulse concentrations. The extended simulations also show 1) the slowing and spreading of the transported pulse when it encounters the lower-velocity impounded section, 2) the effect of tributaries on near-shore concentrations, 3) the

considerable effect of 45 half-lives of decay on the ^{131}I activity concentrations, and 4) the long tails of residual activity as radionuclides that partitioned to bed sediments during the passage of the 10-day pulse slowly desorb. These tails are a longer-term desorption effect with model-predicted concentrations orders of magnitude lower than the peak concentrations in the pulse of released radionuclides that slowly decrease over time. However, radionuclide activity concentrations increase slightly with distance downstream. This behavior is driven by disequilibrium between the radionuclide activity sorbed to the bed sediment, which was loaded during the passage of the radionuclide release pulse, and the radionuclide activity in the post-pulse water column, which is now much less contaminated. This leads to desorption from the contaminated bed sediments along the impacted length of the river. For the balance of the one-year simulation, the desorption rate was sufficiently low that the bed sediments and overlying water column never equilibrated. Consequently, a parcel of water traveling downstream progressively accumulates more activity as it passes over continuously desorbing bed sediments. So while aqueous radionuclide concentrations at any given location are decreasing with time, the tendency is for aqueous concentrations to increase with downstream distance at any given time (e.g., Figure 5-34).

The difference between near-shore and far-shore concentrations is highly dependent on proximity to the release location and the distance from release. The 2-mi far-shore sampling point has very low concentrations and the 10-mi far-shore point has peak pulse concentrations 5 orders of magnitudes less than the release location and very low concentrations in the water column post-pulse.

The 80-mi near-shore monitoring point has a consistent, but different shape than the other concentration curves. The 80-mi point is downstream of the large tributary and is subject to dilution from the tributary (Figure 5-38).

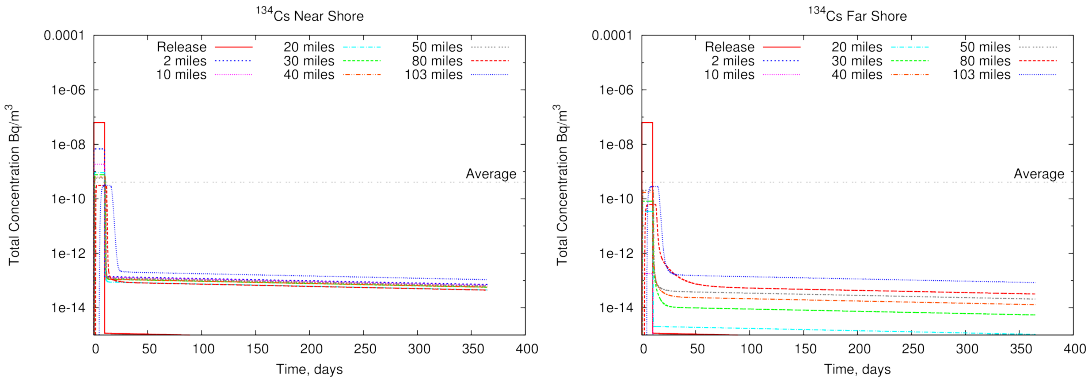

Figure 5-34. Near-Shore (left) and Far-Shore (right) ^{134}Cs Concentration in the Large River Over One Year.

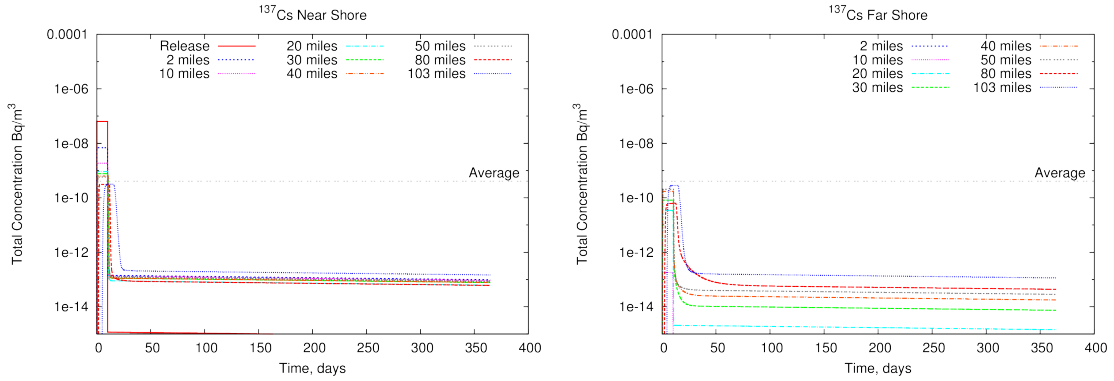

Figure 5-35. Near-Shore (left) and Far-Shore (right) ^{137}Cs Concentration in the Large River for One Year.

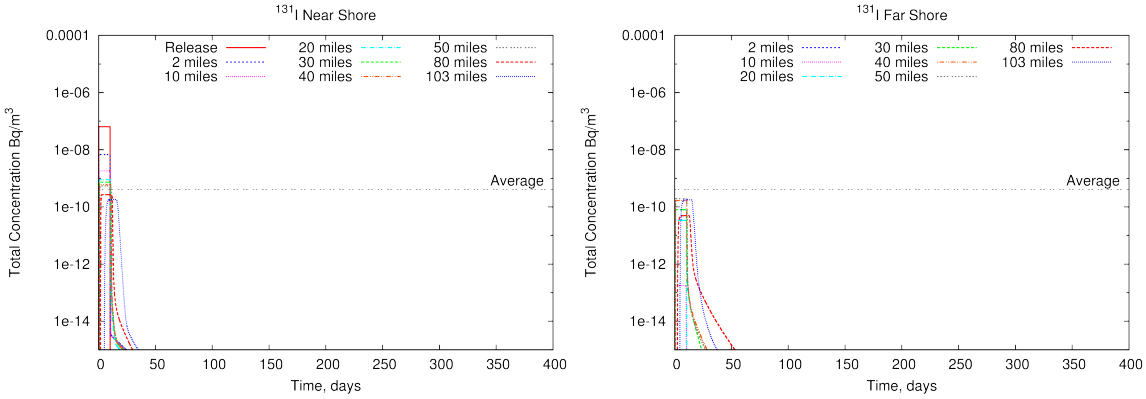

Figure 5-36. Near-Shore (left) and Far-Shore (right) ^{131}I Concentration in the Large River for One Year.

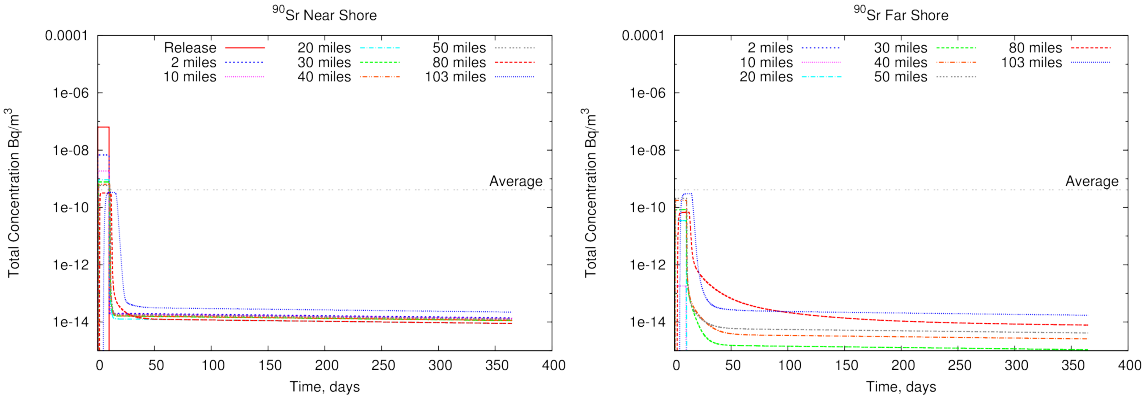

Figure 5-37. Near-Shore (left) and Far-Shore (right) ^{90}Sr Concentration in the Large River for One Year.

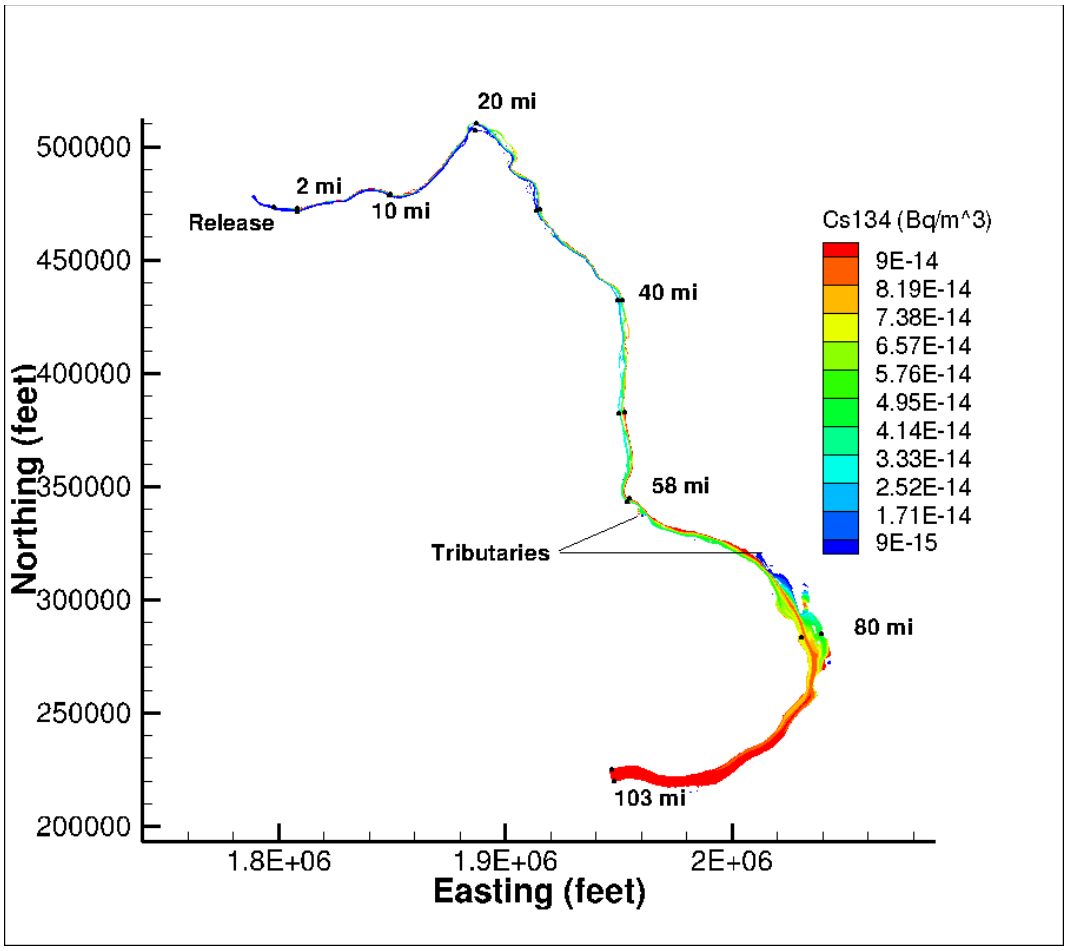

Figure 5-38. Aqueous Phase ^{134}Cs Concentration Increases with Downstream Location. ***This is from Day 138 after the end of the release period.***

5.2.3.2 Unimpounded and Impounded Large River Simulations

The output concentrations at mile 103 (downstream dam boundary) of the One-Year Extended Domain Large River simulations in the previous section were considered to be well mixed and then used as inputs to the two "lower river" configurations: free-flowing river and a river with a series of impoundments behind three intervening dams. The impoundment runs were done to assess the impact of dams on transported concentrations through space and time.

Plots of concentration as a function of time (relative to the start of the release) were created at various distances downstream from the release point. The lower river runs had monitoring locations from 104 to 293 mi from the release point. Table 5-2 details all of the sampling points.

Table 5-2. Monitoring Locations for the Extended Large River Simulations

Miles Downstream	Location
0	Release
2	Right and Left Banks
10	Right and Left Banks
20	Right and Left Banks
30	Right and Left Banks
40	Right and Left Banks
50	Right and Left Banks
80	Right and Left Banks
103	Above Dam 1
104	Below Dam 1
180	Dam 2
203	Dam 3
248	Dam 4
293	End

5.2.3.2.1. Unimpounded River

The unimpounded river model setting examines flow and contaminant transport assuming there are no dams below Dam 1, resulting in free flow from mile 104 to mile 293. Comparison of results for the impounded and unimpounded systems are shown in Figure 5-39 to Figure 5-42 for ^{134}Cs, ^{137}Cs, ^{131}I, and ^{90}Sr, respectively. The unimpounded river setting results in rapid travel as indicated by the narrowness of the release pulse in time-dependent plots at the monitoring locations (Figure 5-39 to Figure 5-42). There is also a general clustering of the arrival times of the pulse at different monitoring locations indicating short transit times. Similar to the previous results for the shorter 50-mi long river domain, there is a drop of several orders of magnitude in concentrations after the release pulse passes through. The post-pulse concentrations are controlled by the aqueous phase radionuclide concentration in the pulse, decay rate and sediment distribution coefficient. For example, the ^{131}I post-pulse activity concentrations in Figure 5-41 are dominated by rapid decay as a result of the 8-day half-life. At a given location over time, the other three radionuclides have long tails of slowly decreasing concentrations as desorption from the bed sediments is the principal longer-term source. As in the previous large river configurations, the post-pulse concentrations increase with downstream distance. This is principally because the desorption rate is sufficiently low that disequilibrium is maintained between the bed sediments and overlying water column. This allows a parcel of water traveling downstream to progressively accumulate desorbed activity.

5.2.3.2.2. Impounded River

In comparison to the unimpounded river, the results for the lower river with a series of impoundments are impacted by the deeper and wider wetted perimeter, which slows the average velocity of water flowing downstream, increases the contact time with the release pulse, and provides considerably more bed sediments for the radionuclides to interact with. This leads to a pattern of slower travel for the release pulse and increased concentrations for the desorption tail that increases with downstream distance (Figure 5-39 to Figure 5-42). Both

the impounded and unimpounded lower river configurations initially had a uniform 0.1 ft layer of sediment across the bottom.

The graphics shown here compare the modeled impounded to unimpounded concentrations over time at similar monitoring points starting at 104 miles from the release point. As expected, the 104-mile location (just below the upstream dam) was very similar between the impounded and unimpounded cases (the first 180 days are plotted to better show the differences in pulse shape). The first pool in the impounded configuration is the largest and has an average velocity that is less than half that of the other pools. The effect of the slower velocity is seen in the large temporal offset of the release pulse breakthroughs between the 104 and 180 mi monitoring locations, and the dilation in the duration of the pulses.

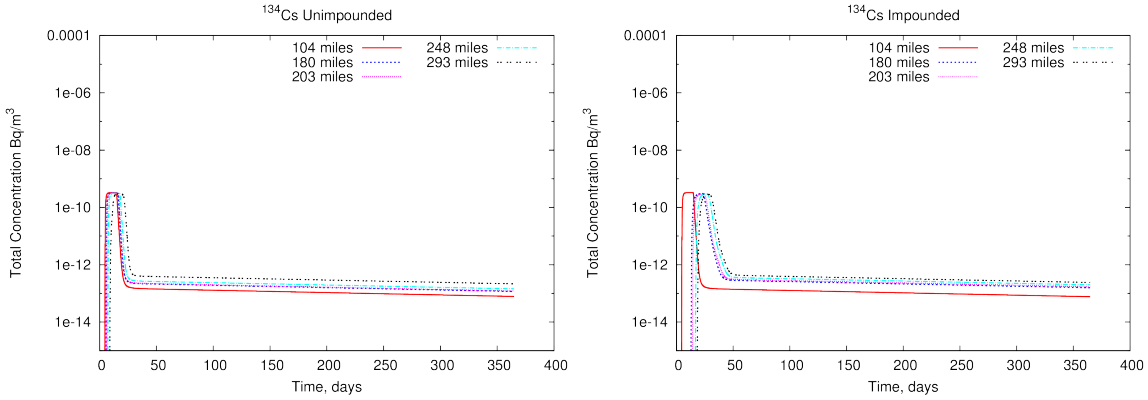

Figure 5-39. Unimpounded (left) and Impounded (right) Lower River Comparison for ^{134}Cs Total Water Column Concentrations at Lower River Locations.

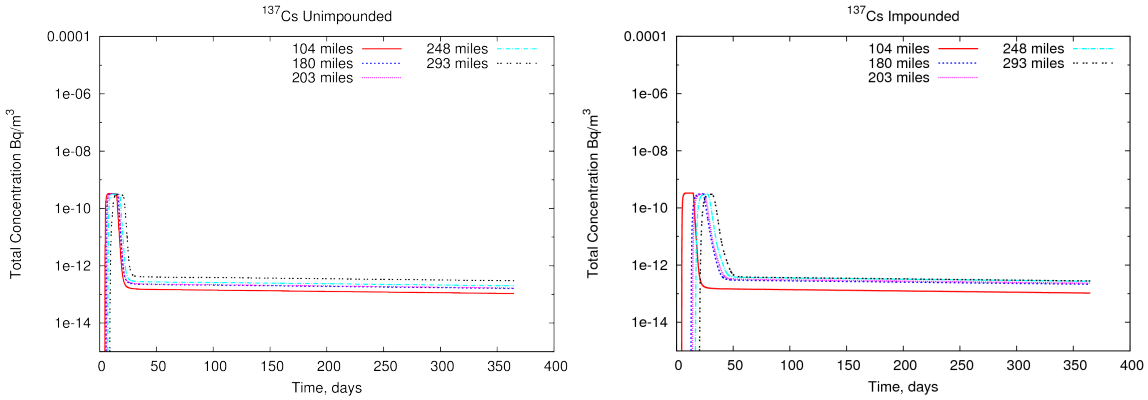

Figure 5-40. Unimpounded (left) and Impounded (right) Lower River Comparison for ^{137}Cs Total Water Column Concentrations at Lower River Locations.

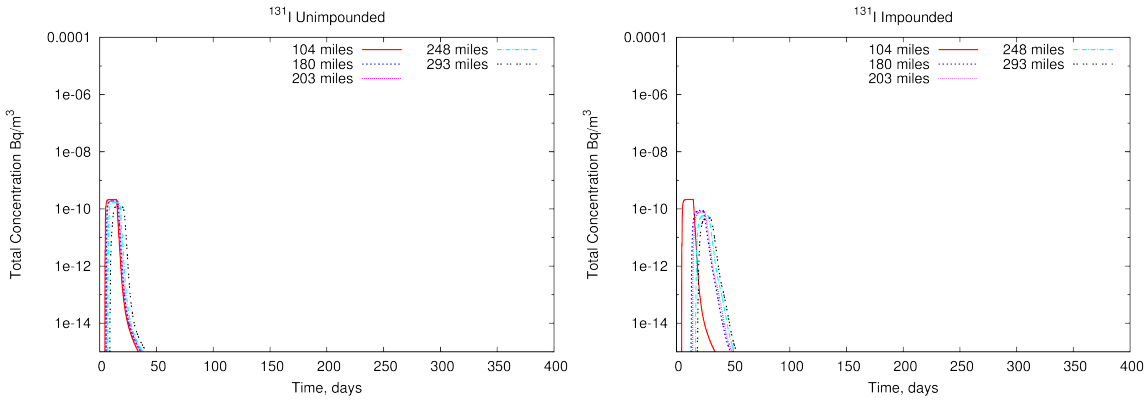

Figure 5-41. Unimpounded (left) and Impounded (right) Lower River Comparison for ^{131}I Total Water Column Concentrations at Lower River Locations.

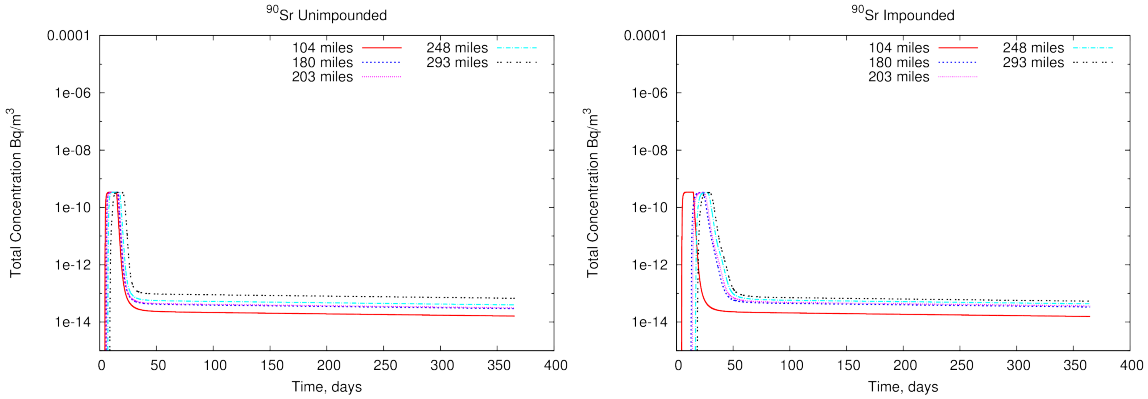

Figure 5-42. Unimpounded (left) and Impounded (right) Lower River Comparison for ^{90}Sr Total Water Column Concentrations at Lower River Locations.

5.2.3.3 Sensitivity Tests

The extended large river setting was used to conduct three sensitivity tests. The first sensitivity test addressed the linear scaling of simulated activity concentrations relative to the activity release. The second sensitivity test addressed the effect of a larger bed depth. The third sensitivity test addressed the effect of a larger suspended sediment load.

5.2.3.3.1. Reduced Activity Release

Simulated concentrations of a tracer scale linearly with tracer mass input. For example, concentrations simulated with a unit mass of input will be reduced by 50 percent if the input mass is reduced by 50 percent. This linearity holds even if the tracer decays. In the river settings, sorption to and desorption from suspended and bed sediments should also be linear. This test was carried out to verify that. In this case, the fate of ^{137}Cs and ^{131}I was simulated for 90 days, but the activity in the 10-day release was reduced by 3 orders of magnitude from the original simulations. Figure 5-43 and Figure 5-44 compare simulated concentrations of ^{137}Cs and ^{131}I, respectively, with those from the original simulation at two locations. As expected, the reduced concentration is 3 orders of magnitude less than that of the base case.

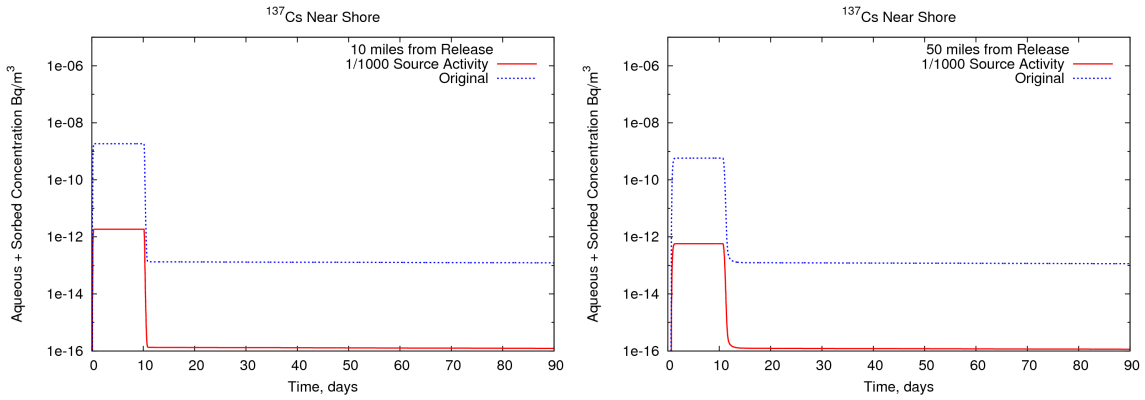

Figure 5-43. Comparison of Decreased Release and Original Simulated Large River ^{137}Cs Total Water Column Concentrations at 10 (left) and 50 (right) Mi from the Release.

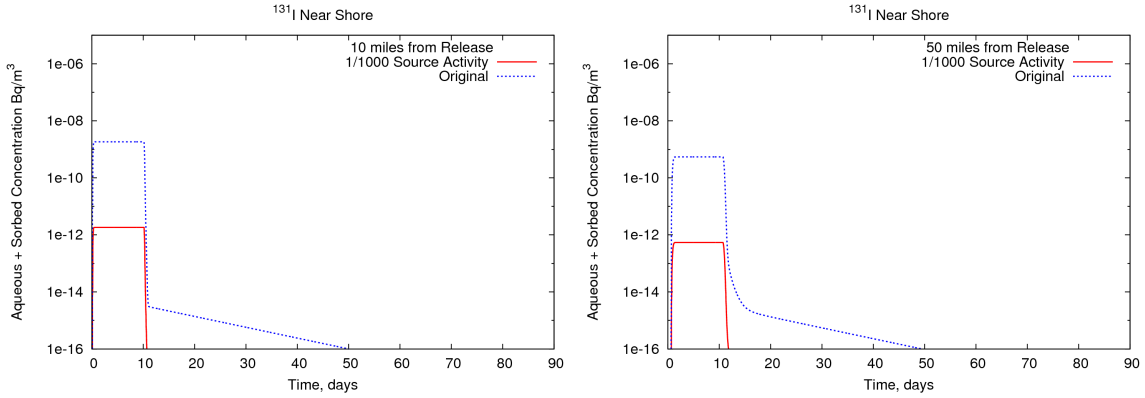

Figure 5-44. Comparison of Decreased Release and Original Simulated Large River ^{131}I Total Water Column Concentrations at 10 (left) and 50 (right) Mi from the Release.

5.2.3.3.2. Increased Bed Depth

The sorption to and desorption from the bed was shown to be very significant in the river settings simulations. A key parameter for that process is the bed depth. The original depth was arbitrarily chosen to be 0.1 ft. For this test, the uniform bed depth was increased to 0.2 ft to see how much of an effect such a change would have. The fate of ^{137}Cs and ^{131}I was simulated for one year, using the original release levels. Figure 5-45 and Figure 5-46 compare simulated water column and bed sediment-sorbed concentrations of ^{137}Cs with those from the original simulation at two locations. Increasing the bed depth by a factor of two results in a 4 percent increase in the amount of radionuclide sorbed to the bed sediments during the passage of the pulse of released radionuclides. Consequently, there is negligible impact on the aqueous pulse concentrations. Post-pulse water column concentrations, however, are about half of the base case. This is because a similar amount of bed-sorbed radionuclide is now associated with twice as much bed volume, which halves the bed concentration and the desorption rate.

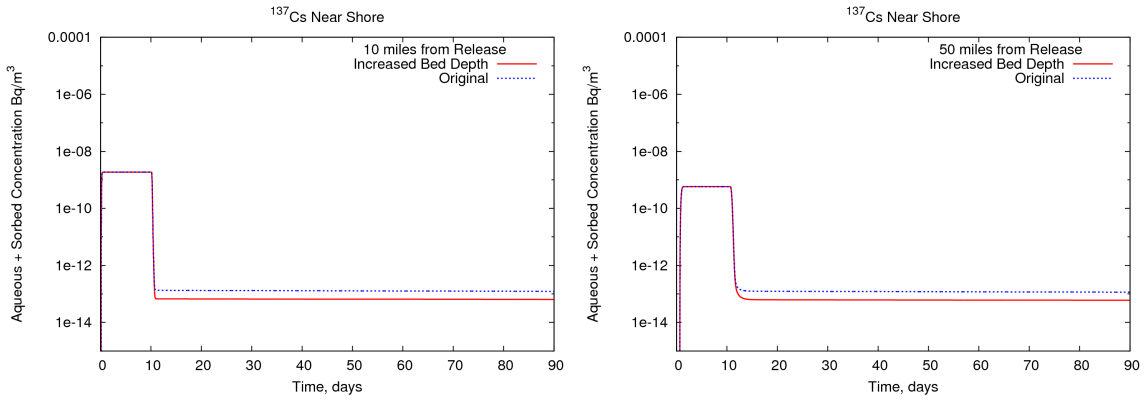

Figure 5-45. Comparison of Increased Bed and Original Simulated ^{137}Cs Total Activity Concentrations at 10 (left) and 50 (right) Mi from the Release.

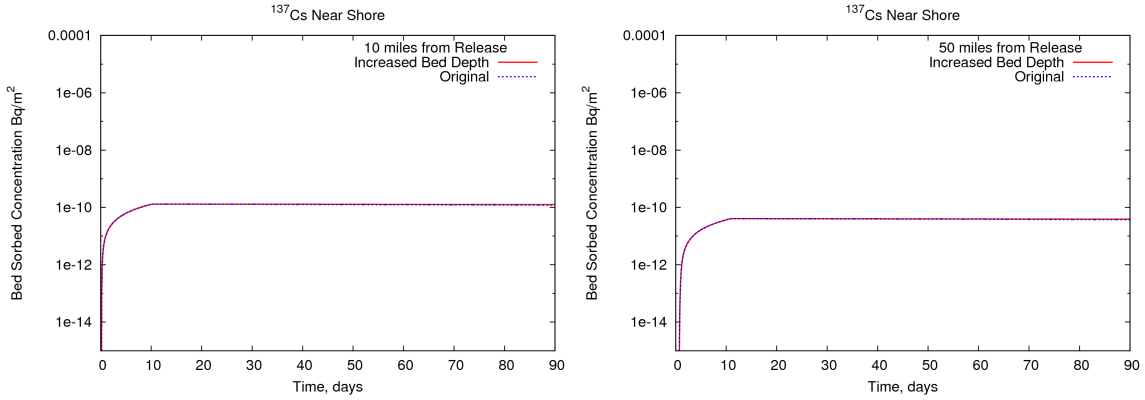

Figure 5-46. Comparison of Increased Bed and Original Simulated ^{137}Cs Bed-Sorbed Activity Concentrations at 10 (left) and 50 (right) Mi from the Release.

5.2.3.3.3. Increased Sediment Load

While typical for the two river settings, the suspended sediment load, 3.75 mg/l, is lower than many alluvial rivers. A one-year simulation of ^{137}Cs was carried out with the extended large river setting but with a suspended sediment load of 100 mg/l.

The increased sediment load had little effect on overall activities at locations above the dam. Concentrations of suspended sediment-sorbed radionuclide in the water column were increased by about 2 orders of magnitude (Figure 5-47, top). This, however, had very little effect on the total water column activity concentration (Figure 5-47, bottom) since the suspended sediment-sorbed concentrations were still about 2 orders of magnitude lower than the aqueous phase. In the dam forebay, 103 mi from the release, residual bed activity was noticeably higher. This indicates increased deposition of suspended sediment, with its sorbed activity, in the dam forebay as the release pulse passed (Figure 5-48). This leads to a small but noticeable increase in the longer-term post-pulse total radionuclide concentration in the water column in the forebay of the dam.

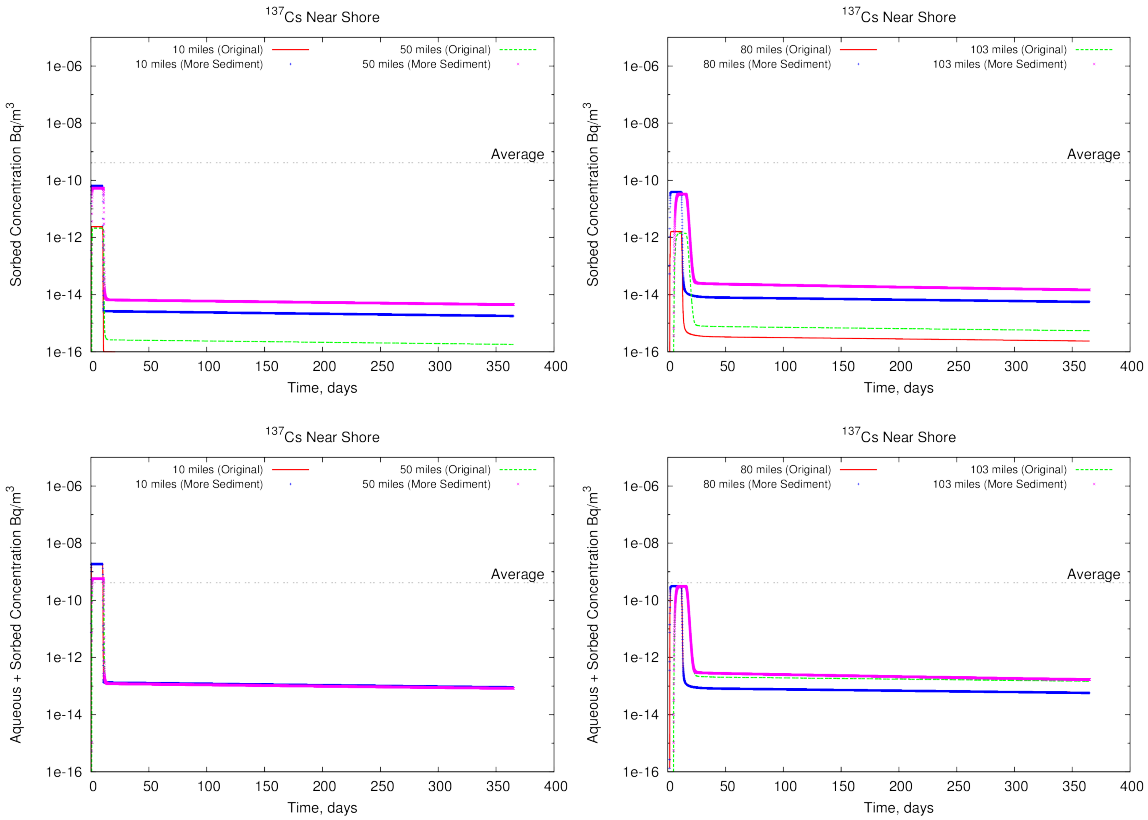

Figure 5-47. Comparison of Water Column Activity Concentration from the Original One-Year Large River and Increased Sediment Load Simulations. *Suspended sediment-sorbed phase (top) and total water column (bottom) ^{137}Cs activity concentrations at 10 and 50 (left) and 80 and 103 (right) mi from the release location are shown.*

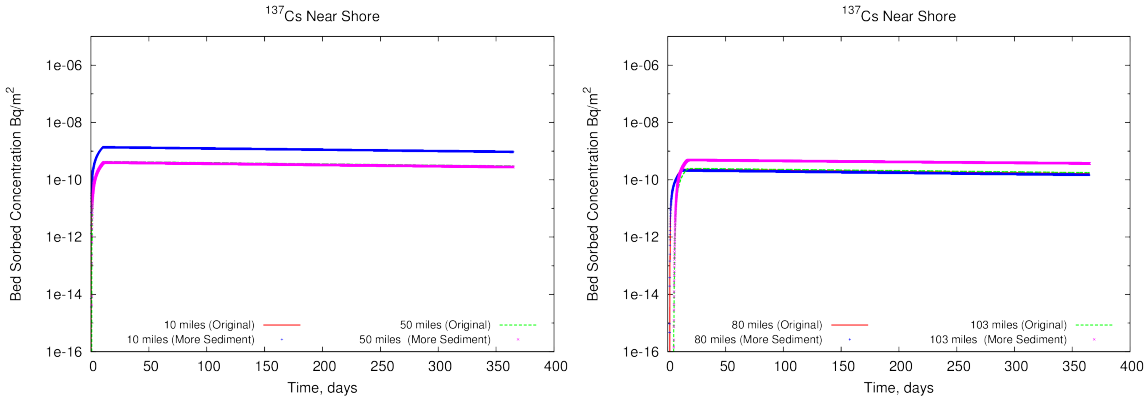

Figure 5-48. Comparison of Bed-Sorbed Activity from the Original One-Year Large River and Increased Sediment Load Simulation at 10 and 50 (left) and 80 and 103 (right) Mi Below the Release Location Are Shown.

5.3 Discussion

Of the three hypothetical hydrologic settings, the small lake scenario results in the highest radionuclide concentrations from the release of the radionuclide source term. Most of the large volume of water available for dilution is not accessed at early times because transport is essentially limited to dispersion, which is a relatively slow process. This allows high concentrations to persist well beyond the 10-day release period. Short-term peak ^{134}Cs and ^{137}Cs concentrations 0.5 mi from the release point on the near shore are at least 17 times higher than any downstream river sampling location. Far-shore lake concentrations are comparable to the peak river concentrations. Peak ^{131}I concentrations are also high for all sampling locations before decay significantly attenuates concentrations after 5 months. The small, seemingly negligible 100 cfs discharge has an important effect as the three locations with the highest concentration peaks are all downstream. The latest peak concentration arrivals occur at the two 1.0 mi downstream locations on the near-shore and far-shore. A sensitivity analysis with a turbulent mixing coefficient 5 times higher results in earlier peak concentrations that subsequently decrease at a much slower rate. The lake modeled is 11 mi long and 0.62 mi wide with an average depth of 24 ft; results would not be applicable to a large lake (e.g., one of the Great Lakes).

Model results show that while dilution occurs as the pulse of released radionuclides becomes fully mixed in both the large and small river settings, the concentration pulse is transported downstream largely intact with little dispersive attenuation of peak concentrations for the entire length of the river (up to 293 mi). The exceptions are for radionuclides with 1) short half-lives relative to the transit time (e.g., ^{131}I) and 2) high distribution coefficients (e.g., ^{144}Ce). After the passage of the pulse, aqueous concentrations plateau ~3 orders of magnitude lower than the peak pulse concentrations. These results will vary depending on characteristics of the river system (e.g., channel braiding or the number and size of tributaries), decay, and the sediment interactions with the radionuclide.

The lower river velocities in the impoundments behind the dams have the effect of lengthening the duration of the release pulse passing a given location. In the extended large river simulation, transit time over a 190-mi reach took 4.4 days without dams and 14.2 days with three intervening dams for the same flow rate. ^{131}I concentrations are sensitive to these differences in transit times because of the 8-day half-life, which results in higher downstream concentrations for the unimpounded scenario. This suggests that dams could be used to control water releases with the intent of providing more time for ^{131}I to decay.

Radionuclide sorption is most significant during the passage of the pulse of released radionuclides, effectively loading radionuclide activity onto the bed sediments. After the passage of the pulse, the significant decrease in water column concentrations favors desorption from the bed sediments, which becomes the principal source of activity in the water column and an important control on the duration and magnitude of post-pulse concentrations. The modeling indicates that post-pulse desorption will occur for the balance of the one-year simulation period along the entire length of the impacted riverbed. Over time, desorption decreases bed sediment-sorbed concentrations. One less obvious consequence of continuous desorption along the entire impacted length of the river is that radionuclide water column concentrations increase with downstream distance. In this case, water traveling downstream progressively accumulates radionuclide activity as it passes over desorbing bed sediments. This effect would continue as long as nonequlibrium desorption conditions persist.

5.3.1 Mixing and Transport

As shown in Figure 5-28, a key feature of the river transport is the downstream persistence of higher concentrations along the near-shore of the radionuclide release. There can be orders of magnitude differences in near-shore versus far-shore concentrations. In the case of the large river scenario, higher near-shore concentrations occur as far as 100 mi downstream, although most transverse mixing takes place in the first 50 mi. In the small river scenario, complete mixing across the channel occurs after 10 mi of transport. Tributaries in the extended large river scenario also impact shoreline concentrations by providing flows of uncontaminated water to the shore from which they entered the river. Longitudinal mixing increases with distance downstream, spreading the pulse along the axis of the river as it is transported downstream. This effect is amplified when the pulse enters dammed impoundments where velocities are slower (Figures 5-39 to 5-42). Pulse durations increased by a factor of 2 to 3 during downstream transport, depending on the modeled scenario.

The small river scenario has a flow rate (5,000 cfs) that is 20 times smaller than the large river scenario (100,000 cfs). The principal consequence of this difference in flow rates is that there will be 20 times less dilution when the initial release pulse is fully mixed from bank to bank. Thus, concentrations will be commensurately higher in the small river scenario. The small river also has a lower average velocity, which increases the residence time. These conditions, high radionuclide concentrations and longer residence times, contribute to higher amounts of radionuclides sorbed to sediment. Sorption to bed sediments is therefore higher in 1) the small than the large river and 2) the impounded than the unimpounded lower river.

5.3.2 Sediment-Radionuclide Interactions

In the model, the partitioning of radionuclide activity between aqueous and sediment-sorbed phases is based on a K_d model in which the equilibrium radionuclide concentration on the sediment is linearly proportional (based on K_d) to the aqueous concentration with no limit on the sorption capacity of the sediment. While sorption/desorption is instantaneous within the porewater of the sediment bed, the model uses a rate to control the sorption/desorption between the bed sediments and the water column. The highest rate will occur when the ratio of sediment-sorbed concentrations to aqueous water column concentrations differs the most from the K_d; conversely, the lowest rate will be zero when the ratio equals the K_d, which means that the sediment-sorbed and water column radionuclide concentrations are in equilibrium. In the model, the radionuclide-specific K_ds are from the literature and the sorption/desorption rate was developed for use in a previous sediment and radionuclide transport modeling application for a large river.

While sorption is an important process leading to elevated radionuclide concentrations in the bed sediment that could have longer-term effects, its impact on lowering aqueous concentrations in the release pulse is generally relatively small. High K_ds result in significant fractions of ^{144}Ce and ^{106}Ru sorbed to bed sediments, but the radionuclides expected to have the highest aqueous concentrations (i.e., ^{134}Cs, ^{131}I, ^{137}Cs, and ^{90}Sr in descending order) are only slightly lower in the water column than corresponding cases without sorption. For example, aqueous ^{134}Cs concentrations in the small river are 9 percent lower with adsorption than if no adsorption is included; ^{131}I is 0.34 percent lower. As a result, concentrations of sorbed radionuclides in the sediment bed are relatively constant along the length of the river; with slightly higher concentrations in areas of low velocity (e.g., dam embayments). After the passage of the pulse of released radionuclides, the bed sediment-sorbed radionuclide concentrations, which reflect loading during the pulse passage, are far from equilibrium with the

"cleaner" overlying aqueous radionuclide water column concentrations. This disequilibrium drives rate-limited desorption from the bed to the water column. Desorption from the bed sediments becomes a longer-term, widespread source, albeit with significantly lower water column concentrations than during the pulse.

For the balance of the one-year simulation after the passage of the release pulse, equilibrium is not reached in the partitioning of radionuclides between the bed sediment and overlying water column (i.e., desorption is rate-limited). As a result, radionuclides are continuously desorbing from the bed sediments along the entire downstream length of the river. This means a parcel of water traveling downstream progressively accumulates more activity as it passes over continuously desorbing bed sediments. So while aqueous radionuclide concentrations at any given location are decreasing with time, the tendency, as shown in Figure 5-40, is for aqueous concentrations to increase with downstream distance at any given time.

An important objective of this exploratory study is to provide information that can be used to decide whether further studies are needed to address the modeled radionuclide transport processes in more detail. Since each radionuclide was modeled under the same conditions with the same 1 Bq source term, radionuclide-specific behavior is differentiated only through the impact of decay and K_d. Consequently, the radionuclide transport scoping calculations can be viewed as a sensitivity analysis for a range of partitioning (including no sorption) and decay behavior. The general conclusion is that a fraction of the radionuclide activity in the 10-day pulse release will partition to the bed sediments and this will result in a chronic, distributed source to the water column via desorption. What is less certain is the magnitude of this effect. Thus, it is important to recognize the limitations of the sorption modeling approach used in this study.

Radionuclides partition to mineral and biological surfaces as a function of many factors including the availability, morphology, chemical composition, and charge of sorption sites, as well as the presence of competing, inhibiting, or complexing ions that alter reactivity with those sorption sites. The conditions controlling partitioning and rates are typically very site-specific with variation in space and time. For the 30-second temporal resolution in the model, sorption and desorption reaction rates are an appropriate consideration; however, these rates are not necessarily symmetric or fully reversible. For example, $^{137}Cs/^{134}Cs$ deposited in lakes from weapons test fallout and the Chernobyl accident were retained more strongly on sediment over periods on the scale of hundreds of days, reducing the desorption rate (Smith et al. 2000; Smith and Comans 1996). This effect may depend on how the contaminant was deposited. Experimental sorption/desorption studies of Cs on suspended river sediment indicated that retention increased by a factor of up to 16 when adsorption contact times were increased from 0.5 to 120 hours (Ciffroy et al. 2001). Enhanced retention of ^{137}Cs (but not ^{90}Sr) as the sediment/contaminant interaction ages is also observed in the Dnieper River system (IAEA 2006).

As a scoping study targeting generic freshwater settings, the sorption modeling does not consider these conditions. Instead, the modeling relies on literature values for radionuclide distribution coefficients (K_ds) that linearly relate aqueous and sediment-sorbed concentrations. The rate of partitioning is based on a maximum rate developed for a previous study that is scaled by the deviation of aqueous and sorbed radionuclide concentrations from equilibrium, which is defined by the K_d.

Over time Cs may become fixed to the sediment, essentially making it unavailable to the water column under normal chemical conditions. With the variability of K_d and the desorption rate, as

well as possible dependence on the source term, the chronic concentrations of radionuclides in the aqueous phase presented in this section must be considered estimates with substantial uncertainty. In particular, if the desorption rate of Cs decreases substantially over a time scale of days to months, the aqueous concentrations will be correspondingly lower. This could result in substantial reductions of the chronic concentrations of Cs radionuclides in the water column.

5.3.3 Fate of Contaminated Sediment

While the long-term fate of contaminated sediment is beyond the scope of this study, it should be mentioned briefly that there are several processes that impact the distribution of contaminated sediment. Over time, clean sediment is naturally supplied as it moves downstream from uncontaminated areas. This clean material can be deposited over contaminated layers of sediment, inhibiting interaction of contaminants with the water column. This is especially the case where flow rates are decreased (e.g., in dam forebays where sediment tends to accumulate). While the burial of contaminated sediment can potentially reduce the transport of contaminants, periodic high-flow events can scour that sediment from the bed, rapidly mixing it with clean sediment and redistributing it further downstream. If flooding occurs, the contaminated sediment may be deposited outside the normal course of the river.

5.3.4 Scaling

The space- and time-dependent aqueous and sorbed radionuclide concentrations scale linearly with their source term magnitude. This scaling applies to the transport and sediment-radionuclide interaction process models used in this study. The scaling is valid when the decay and partitioning functions are linearly dependent on concentrations. The scaling property allows quick estimates for releases that are smaller or larger than the modeled source term.

6. CONCLUSIONS

6.1 Summary

6.1.1 Objectives

This scoping study explores the potential behavior of contaminated water released directly to a freshwater body in a scenario similar to the 2011 Fukushima Daiichi (FD) accident, in which some contaminated building water leaked directly into the sea. The FD accident highlighted a scenario not currently addressed in the NRC's severe accident consequence analysis. Very large volumes of contaminated water were generated by emergency measures to cool the reactors and spent fuel pools. UNSCEAR (UN 2014) estimated that between late March and April 2011,15 to 30 PBq of ^{131}I, ^{134}Cs, and ^{137}Cs (many other radionuclides were present but not reported) were released into the ocean due to this accidental release.

A number of U.S. nuclear power plants are located on or very near lakes or rivers. In these settings, although highly unlikely, a FD-like release scenario could result in immediate impacts on freshwater bodies as well as longer lasting consequences. This study provides a scoping level assessment of the contaminant behavior resulting from a reactor accident in which contaminated water is generated and some of it is lost to a freshwater body. A key objective is to understand how advection, dilution/dispersion, decay, and sorption processes control the distribution of radionuclides in the context of freshwater settings and conditions.

The approach in this study differed from previous studies in the following ways:

- multidimensional surface water modeling was used to account for the 3D bathymetry and spatially varying flow fields;
- radionuclide sorption and desorption was addressed in the context of bed and suspended sediment in the model;
- a method was developed to calculate the aqueous radionuclide inventory from 1) an estimation of the reactor core inventory as a function of reactor type, metric tons of uranium fuel, and fuel burnup, and 2) the aqueous partitioning of the reactor core inventory based on measurements of radionuclide concentrations in building water from Three Mile Island Unit 2;
- an estimate of the fraction of the aqueous radionuclide inventory released from the FD nuclear power plant was shown to be consistent with estimates of the 2011 surface water release of radioactivity to the marine environment; and
- the source term for the radionuclide transport analyses was released directly to surface water bodies without transport through intervening subsurface media, which is consistent with the 2011 environmental monitoring of radioactivity from the FD nuclear power plant.

The scoping nature of the source term, freshwater settings, and conditions are primarily in the simplifying assumptions:

- limited number of surface water settings (i.e., three) to represent U.S. nuclear power plant sites (e.g., no marine or Great Lake settings);
- steady flow conditions;
- single sediment grain size with no erosion of bed sediments;

- single K_d for each radionuclide to describe sediment sorption and desorption with a single sorption/desorption rate;
- no wind or thermal stratification for the lake scenario; and
- four radionuclides (^{131}I, ^{134}Cs, ^{137}Cs, ^{90}Sr) to represent the inventory for the extended duration and extended river length simulations.

6.1.2 Modeling Quality Assurance

Each modeling component of this study has been tested and assessed for accuracy using observations, mass balance calculations, analytical solutions, or benchmarking. This includes 1) comparing the estimated aqueous radionuclide inventory against the Fukushima building water composition; 2) comparing the release fraction of the aqueous radionuclide inventory against estimates based on monitored radionuclide concentrations in the marine waters off the coast from FD, and 3) comparing the simulated river and lake radionuclide concentrations against analytical transport solutions. The latter are described in Appendix A.

6.2 Conclusions from Model Results

In the case of direct release to a water body, depending on the source term, the pulse of contaminated water can have very high concentrations of radionuclides. In free-flowing river reaches, the first arrival of a release to a downstream exposure location may occur after a few hours of transport, especially along the near shore of the release. The radionuclide concentrations in the release pulse will be diluted by several orders of magnitude once it is well mixed with river or lake water. Further mixing in the lake or transport downstream may lower peak concentrations; however, depending on the source term concentrations could still be sufficiently high to require emergency actions. In lakes, this condition could persist for some time.

As discussed in Section 5, a contaminant pulse released into a river system can move downstream as a relatively coherent pulse potentially for hundreds of miles. After the 10-day release of radionuclides attained a fully mixed concentration over the river cross-section, the steady flow conditions assumed in these scoping studies were able to transport the pulse intact for 293 mi despite longitudinal mixing and other attenuation processes. Consequently, it is important to recognize that monitoring and emergency actions may be needed for significant distances downstream.

Flow through many river systems is heavily regulated by dams. The principal effects of the impoundments behind dams are to 1) slow downriver transport of released radionuclides, 2) increase residence time, 3) increase bed sediment surface area available for sorption, and 4) increase deposition of suspended sediments with sorbed radionuclides. The transport of a radionuclide release pulse through a river system with impoundments may take many days if not months for large systems. This will influence the amount of time that monitoring and emergency actions may be needed. It also presents an opportunity to regulate flow to help minimize impacts.

Following passage of the release pulse in river systems, contaminant concentrations will decrease sharply. However, residual radionuclide activity retained on bed sediments will desorb at a slow rate, resulting in water concentrations that still may degrade water quality. In effect, these bed sediments become a distributed source of radionuclides in the river that will persist long after the initial release event. The modeling results presented in Section 5 depict the

transport of a unit activity release of radionuclides over 10 days followed by longer-term desorption of residual radioactivity from bed sediments into the overlying water column.

6.2.1 Transport

- Of the three hydrologic settings, the lake scenario results in the highest radionuclide concentrations. Most of the lake volume available for dilution is not accessed at early times because transport is essentially limited to dispersion. As a result, radionuclide concentrations remain high, likely for extended times.
- Once the release is fully mixed over the river cross-section, dilution from the ratio of river flow to volumetric release rate is 1×10^5 for the small river and 2×10^6 for the large river.
- In the river settings considered, the 10-day pulse of released activity remains largely intact for the entire length of the river, which for the extended large river model is 293 mi.
- A key feature of the river transport is the downstream persistence of higher concentrations along the near shore of the radionuclide release. There can be orders of magnitude differences in near-shore versus far-shore concentrations. In the case of the large river, transverse mixing is mostly complete after 50 mi of downstream transport. In the small river scenario, complete mixing across the channel occurs after 10 mi of transport.
- For the sediment-radionuclide interaction and transport process models used in this study, the simulated aqueous and sorbed radionuclide concentrations scale linearly with source term to three significant figures. This scaling property allows quick conversion of the presented concentrations, which are per Bq in the 10-day release, simply by multiplying by the desired source term radionuclide activity.

6.2.2 Transit Times

- Transit times for free-flowing river reaches can be quite fast. For a point 50 mi downstream from the source term release point, radionuclides first arrived after 17 hours for the large river and 25 hours for the small river. However, different river stages and different reaches could result in much slower or faster transport times.
- Dams can slow the transit time considerably. In the extended large river simulation, transit time over a 190-mi reach took 4.4 days without dams and 14.2 days with three intervening dams.

6.2.3 Sorption and Desorption

- Radionuclide sorption is most significant during the passage of the pulse of released activity due to the difference in concentration between the water column and the sediment bed, which drives adsorption to the bed sediment.
- After the passage of the pulse of released activity, desorption from the bed sediments becomes a longer-term, widespread source of radionuclides to the water column, albeit with significantly lower water column concentrations than the pulse.
- Sorption to suspended sediment accounts for a negligible fraction of the released radionuclides. While this is due, in part, to the relatively low 3.75 mg/L suspended sediment load in the baseline specification of the river scenarios, a 100 mg/L suspended sediment load sensitivity case did not alter this finding.
- Sorption to bed sediments is higher in 1) the small than the large river and 2) the impounded than the unimpounded lower river. In the small river, significantly higher water column

concentrations during the passage of the release pulse (due to less dilution) result in commensurately higher bed-sorbed concentrations. The impoundments behind the dams are wide and deep, providing a larger wetted surface area (i.e., more bed sediment) for sorption. In both cases, sorption is enhanced by comparatively longer residence times.

- Sorption onto bed sediments has only a small effect in lowering dissolved concentrations of ^{137}Cs, ^{134}Cs, ^{90}Sr, and ^{131}I in the pulse of released radionuclides. For example, aqueous ^{134}Cs and ^{137}Cs concentrations in the small river are 9 percent lower with adsorption than the aqueous-only case (no adsorption); ^{131}I is 0.34 percent lower. However, depending on the magnitude of activity released and radionuclide sorption properties, water column concentrations driven by longer-term post-pulse desorption from bed sediments could still require intervention.
- After the passage of the pulse of released activity, aqueous river concentrations increase with downstream distance from the release point for the remainder of the one-year simulation period. This is because the desorption rate from the bed sediments is sufficiently low that equilibrium between activity sorbed to the bed sediments and activity in the overlying water column is never attained during the simulation. This disequilibrium drives the continuous desorption of radionuclides from bed sediments along the entire downstream length of the river, resulting in a progressive accumulation of desorbed radionuclides as water travels downstream. This effect will depend on the magnitude of the source term, K_d values, and desorption rates.

6.3 Site-Specific Applications

Sensitivity analyses for modeling parameters in this scoping study can be used to inform follow-on modeling of more realistic sites and conditions. The relatively high radionuclide concentrations in the lake result largely from limited mixing that prevents most of the large volume from being accessed for dilution at early time. While common scenarios not addressed in this scoping study can accelerate dilution, the insight from the sensitivity analysis was that an intermediate increase in the turbulent mixing coefficient can result in similar, but earlier, peak concentrations and longer persistence of elevated concentrations. Generic distribution coefficients (i.e., K_ds) would not be expected to reproduce site-specific radionuclide sorption/desorption behavior, which is generally a function of the solid concentrations, solids geometry, bed configuration and conditions, mineralogical and organic matter character of the solids, and the geochemical conditions controlling the radionuclide speciation. The insight from the sensitivity analysis (Section 5.1.3.3.) was that changing the bed thickness can directly affect post-pulse water column concentrations (i.e., long-term desorption phase) even though there is no significant reduction of water column concentrations during the passage of the release pulse (i.e., short-term sorption phase).

This was an exploratory study that relied on previous studies for many parameters. While reasonable values were chosen, they are necessarily not specific to any site. The selection of a site and use of site- (and time-) specific values for parameters (e.g., river discharge rates, dispersion, transit times, and K_d values) will undoubtedly alter results in important ways. Characteristics of other rivers (e.g., more tributaries, more meanders, and more flow dynamics) and the use of river water may be different, altering the relative importance of certain features. For example, irrigation with river water is of particular interest to dose calculations for western sites, whereas its use may be quite limited in many eastern rivers.

Possible site-specific extensions to the scoping analyses that were performed could include the following:

- lake processes: wind-driven flow, thermal stratification, and radionuclide-sediment interactions;
- unsteady flow: flood and drought conditions, and event-based flow regimes (e.g., storms);
- sediment transport: multiple bed layers, multiple sediment sizes, erosion, and bedload transport; and
- radionuclide-sediment interactions: sorption to sediments moving very slowly as bedload in an alluvial river, nonuniform sediment distributions, desorption kinetics and hysteresis of adsorbed radionuclides (e.g., recalcitrant fractions), and multicomponent sorption controls (e.g., competitive sorption).

The scoping analyses also provide a framework for simpler modeling approaches that may be appropriate for site-specific analysis or emergency planning including the following:

- one dimensional river simulations where transverse and vertical mixing are sufficiently efficient;
- reduced inventory size: ^{131}I, ^{134}Cs, and ^{137}Cs for short-term analyses; ^{134}Cs and ^{137}Cs for long-term analyses; and
- scaling of the current results to calculate concentrations for larger/smaller releases and shorter/longer durations.

7. REFERENCES

Bailly du Bois, P., P. Laguionie, D. Boust, I. Korsakissok, D. Didier, and B. Fiévet. 2012. "Estimation of marine source-term following Fukushima Daiichi accident." *Journal of Environmental Radioactivity,* 114:2-9. Accessed October 14, 2016 at http://www.sciencedirect.com/science/article/pii/S0265931X1100289X.

Balay, S., S. Abhyankar, M.F. Adams, J. Brown, P. Brune, K. Buschelman, V. Eijkhout, W.D. Gropp, D. Kaushik, M.G. Knepley, L.C. McInnes, K. Rupp, B.F. Smith, and H. Zhang. 2014. "PETSc webpage." Accessed October 14, 2016 at http://www.mcs.anl.gov/petsc.

Buesseler, K. 2013. Fukushima – A View From the Ocean, Woods Hole Oceanographic Institution. Accessed October 14, 2016 at http://www.iscors.org/doc/ken-buesseler-9-18-13.pdf.

Caplow, T., P. Schlosser, and D. Ho. 2004. "Tracer Study of Mixing and Transport in the Upper Hudson River with Multiple Dams."*J. Environ. Eng.*, 10.1061/(ASCE)0733-9372(2004)130:12(1498), 1498-1506.

Casacuberta, N., P. Masqu, J. García-Orellana, R. García-Tenorio, K.O. Buesseler. 2013. "^{90}Sr and 89Sr in Seawater off Japan as a Consequence of the Fukushima Dai-ichi Nuclear Accident." *Biogeosciences*, 10:3649–3659. Accessed October 14, 2016 at www.biogeosciences.net/10/3649/2013/.

Charette, M.A., C.F. Breier, P.B. Henderson, S.M. Pike, I.I. Rypina, S.R. Jayne, K.O. Buesseler. 2013. "Radium-based estimates of cesium isotope transport and total direct ocean discharges from the Fukushima Nuclear Power Plant accident." *Biogeosciences*, 10:2159–2167. Accessed October 14, 2016 at www.biogeosciences.net/10/2159/2013/.

Chernobyl Forum. 2005. Chernobyl's Legacy: Health, Environmental and Socio-Economic Impacts and Recommendations to the Governments of Belarus, the Russian Federation and Ukraine. International Atomic Energy Agency, Vienna. Accessed October 14, 2016 at http://www.iaea.org/Publications/Booklets/Chernobyl/chernobyl.pdf

Chow, V.T. 1959. Open-Channel Hydraulics. McGraw-Hill, New York, 1959.

Ciffroy, P., J. Garnier, and M.K. Pham. 2001. "Kinetics of the adsorption and desorption of radionuclides of Co, Mn, Cs, Fe, Ag and Cd in freshwater systems: experimental and modelling approaches." *Journal of Environmental Radioactivity*, 55:71-91.

Darwish, M.S. and F. Moukalled. 2003. "TVD Schemes for Unstructured Grids." *International Journal of Heat and Mass Transfer,* 46:599–611.

Darwish, M.S. and F.H. Moukalled. 1994. "Normalized Variable and Space Formulation Methodology for High-Resolution Schemes." Numerical Heat Transfer Part B-Fundamentals 26(1):79–96.

Estournel, C., E. Bosc, M. Bocquet, C. Ulses, P. Marsaleix, V. Winiarek, I. Osvath, C. Nguyen, T. Duhaut, F. Lyard, H. Michaud, F. Auclair. 2012. "Assessment of the amount of cesium-137 released into the Pacific Ocean after the Fukushima accident and analysis of its dispersion in

Japanese coastal waters." *Journal of Geophysical Research*, Vol. 117, C11014, doi:10.1029/2012JC007933.

Ferziger, J.H. and M. Perić. 2002. Computational Methods for Fluid Dynamics, 3rd edition. Springer-Verlag.

Fischer, H., E.J. List, R. Koh, J. Imerger, and N. Brooks. 1979. Mixing in Inland and Coastal Waters. Academic Press, New York, New York.

García, M. 2008. *Sedimentation Engineering: Processes, Measurements, Modeling, and Practice*. Manuals of Practice 110. ASCE Publications. Accessed October 14, 2016 at http://www.asce.org/templates/publications-book-detail.aspx?id=8110.

Gudiksen, P.H., T.F. Harvey, R. Lange. 1989. "Chernobyl source term, atmospheric dispersion, and dose estimation." *Health Physics*, 57(5):697-706.

Hanrahan T.P. and M.C. Richmond. 2008. "Quantifying Large River Habitat Restoration Potential Through Hydrodynamic Modeling and Geomorphic Analysis." PNNL-SA-63862. Abstract submitted to National Conference on Ecosystem Restoration, Los Angeles, California.

Hidaka, A. and J. Ishikawa. 2014. "Quantities of I-131 and Cs-137 in accumulated water in the basements of reactor buildings in process of core cooling at Fukushima Daiichi nuclear power plants accident and its influence on late phase source terms." *Journal of Nuclear Science and Technology*, 51(4): 413-424. http://dx.doi.org/10.1080/00223131.2014.881725.

IAEA (International Atomic Energy Agency). 2006. Radiological Conditions in the Dneiper River Basin, IAEA Radiological Assessment Report Series Pub 1230.

Kawamura, H., T. Kobayashi, A. Furuno, T. In, Y. Ishikawa, T. Nakayama, S. Shima, T. Awaji. 2011. "Preliminary Numerical Experiments on Oceanic Dispersion of ^{131}I and ^{137}Cs Discharged into the Ocean because of the Fukushima Daiichi Nuclear Power Plant Disaster." *Journal of Nuclear Science and Technology*, 48(11):1349–1356. Accessed October 14, 2016 at http://www.tandfonline.com/toc/tnst20/48/11#.UnQ211OmZ3s.

Kincaid, C.T., P.W. Eslinger, W.E. Nichols, A.L. Bunn, R.W. Bryce, T.B. Miley, M.C. Richmond, S.F. Snyder, R.L. Aaberg. 2000. "System Assessment Capability (Revision 0); Assessment Description, Requirements, Software Design, and Test Plan." BHI-01365, Bechtel Hanford, Inc., Richland, Washington.

Krone, R.B. 1962. Flume Studies of the Transport of Sediment in Estuarial Shoaling Processes. Hydraulic Engineering and Sanitary Engineering Research Laboratory, University of California, Berkeley, California.

Martin, J.E., M.L. Carr, M.H. García. 2012. Handbook of environmental fluid dynamics: systems, pollution, modeling, and measurements, Vol 2, Chap. 16. Riverine Transport, Mixing, and Dispersion, CRC Press, Boca Raton, pp 215–228.

McIsaac, C.V. and D.G. Keefer. 1984. *TMI-2 Reactor Building Source Term Measurements: Surfaces and Basement Water and Sediment*. GEND-042: General Public Utilities, Electric Power Research Institute, U.S. Nuclear Regulatory Commission, U.S. Department of Energy.

Miyazawa, Y., Y. Masumoto, S.M. Varlamov, T. Miyama, M. Takigawa, M. Honda, T. Saino. 2013. "Inverse estimation of source parameters of oceanic radioactivity dispersion models associated with the Fukushima accident." *Biogeosciences*, 10:2349–2363, 2013. Accessed October 14, 2016 at www.biogeosciences.net/10/2349/2013.

MPI Forum. 2009. "MPI: A Message-Passing Interface Standard. Version 2.2." Accessed October 14, 2016 at http://www.mpi-forum.org.

Napier, B.A. 2014. "Joint U.S./Russian Studies of Population Exposures resulting from Nuclear Production Activities in the Southern Urals." *Health Physics* 106(2):294-304.

NEI (Nuclear Energy Institute). 2015. " Diverse And Flexible Coping Strategies (FLEX) Implementation Guide, NEI 12-06 [Rev 1]," Nuclear Energy Institute, Washington, D.C.

Nelson, J., R.W. Perkins, and W.L. Haushild. 1966. "Determination of Columbia River Flow Times Downstream from Pasco, Washington, Using Radioactive Tracers Introduced by the Hanford Reactors."*Water Resources Research*, 2(1):31-39.

Niehus, S.E., W.A. Perkins, and M.C. Richmond. 2014. Simulation of Columbia River Hydrodynamics and Water Temperature from 1917 through 2011 in the Hanford Reach (Final Report No. PNWD-3278). Battelle-Pacific Northwest Division, Richland, Washington.

Niemczyk, S.J., K.G. Adams, W.B. Murfin, L.T. Ritchie, E.W. Eppel, and J.D. Johnson. 1981. *The consequences from liquid pathways after a reactor meltdown accident*. NUREG/CR–1596. U.S. Nuclear Regulatory Commission, Washington, DC.

Nieplocha, J., R. Harrison, and R. Littlefield. 1996. "Global arrays: A nonuniform memory access programming model for high-performance computers." *The Journal of Supercomputing* 10(2):169–189.

Nieplocha, J., B. Palmer, V. Tipparaju, M. Krishnan, H. Trease, and E. Aprà. 2006. "Advances, applications and performance of the global arrays shared memory programming toolkit." *International Journal of High Performance Computing Applications* 20(2):203–231.

Oberlander, P.L., R.L. Skagge, and J.M. Shafer. 1985. *Mitigative Techniques for Ground-Water Contamination Associated With Severe Nuclear Accidents*. NUREG/CR–4251, U.S. Nuclear Regulatory Commission, Washington, DC.

Onishi, Y. and F.L. Thompson. 1984. *Mathematical Simulation of Sediment and Radionuclide Transport in Coastal Waters, Volume 1: Testing of the Sediment/Radionuclide Transport Model, FETRA*. PNL-5088-1, NUREG/CR–2424, Pacific Northwest Laboratory, Richland, Washington 99352. Prepared for the U.S. Nuclear Regulatory Commission.

Oostrom M., Y. Mehmani, P.D.J. Romero Gomez, Y. Tang, H. Liu, H. Yoon, Q. Kang, V. Joekar Niasar, M. Balhoff, T. Dewers, G.D. Tartakovsky, E.A.E. Leist, N.J. Hess, W.A. Perkins, C.L. Rakowski, M.C. Richmond, J.A. Serkowski, C.J. Werth, A.J. Valocchi, T.W. Wietsma, and C. Zhang. 2016. "Pore-scale and Continuum Simulations of Solute Transport Micromodel Benchmark Experiments." *Computational Geosciences* 20(4):857-879. doi:10.1007/s10596-014-9424-0

Partheniades, E. 1962. A Study of Erosion and Deposition of Cohesive Soils in Salt Water. PhD thesis, University of California, Berkeley, California.

Patankar, S.V. 1980. Numerical Heat Transfer and Fluid Flow. Hemisphere, Washington, DC.

Peeters, F., A. Wüest, G. Piepke, and D. M. Imboden. 1996. "Horizontal Mixing in Lakes." *Journal of Geophysical Research: Oceans* 101 (C8): 18361–75. doi:10.1029/96JC01145.

Perkins, W.A. and M.C. Richmond. 2004a. *MASS2, Modular Aquatic Simulation System in Two Dimensions, Theory and Numerical Methods*. PNNL-14820-1, Pacific Northwest National Laboratory, Richland, Washington.

Perkins, W.A. and M.C. Richmond. 2004b. *MASS2, Modular Aquatic Simulation System in Two Dimensions, User Guide and Reference*. PNNL-14820-2, Pacific Northwest National Laboratory, Richland, Washington 99352.

Perkins, W. A., M.C. Richmond, and G.A. McMichael. 2004. Two-Dimensional Modeling of Time-Varying Hydrodynamics and Juvenile Chinook Salmon Habitat in the Hanford Reach of the Columbia River. *In Critical Transitions in Water and Environmental Resources Management, Proceedings of the 2004 World Water and Environmental Resources Congress, June 27-July 1*, Salt Lake City, Utah. Reston, Virginia. https://doi.org/10.1061/40737(2004)180.

Pretzsch, G., V. Hannstein, M. Wehrfritz. Radioactive Inventory at the Fukushima NPP, Gesellschaft für Anlagen-und Reaktorsicherheit (GRS) mbH, Köln, Germany. https://inis.iaea.org/search/search.aspx?orig_q=RN:43127336.

Ramsdell Jr., J.V., C.E. Beyer, D.D. Lanning, U.P. Jenquin, R.A. Schwarz, D.L. Strenge, P.M. Daling, and R.T. Dahowski. 2001. E*nvironmental Effects of Extending Fuel Burnup Above 60 Gwd/MTU*. NUREG/CR–6703, U.S. Nuclear Regulatory Commission, Washington, D.C.

Richmond, M.C., W.A. Perkins, and T.D. Scheibe. 1999. Two-Dimensional Simulation of Hydrodynamics, Water Quality, and Fish Exposure in the Columbia/Snake River System. American Society of Civil Engineers. https://doi.org/10.1061/40440(1999)48.

Richmond, M.C., W.A. Perkins, and Y. Chien. 2000. Numerical Model Analysis of System-wide Dissolved Gas Abatement Alternatives. Report submitted to U.S. Army Corps of Engineers, Walla Walla District. PNWD-3245. Battelle Pacific Northwest Division, Richland, Washington.

Richmond, M.C., W.A. Perkins, T.D. Scheibe, A. Lambert, and B.D. Wood. 2013. "Flow and axial dispersion in a sinusoidal-walled tube: Effects of inertial and unsteady flows." *Advances in Water Resources* 62(B):215–226.

Rutherford, J.C. 1994. *River Mixing*, John Wiley and Sons, New York, USA, 347 pp.

Scheibe T.D., W.A. Perkins, M.C. Richmond, M.I. McKinley, P.D.J. Romero Gomez, M. Oostrom, T.W. Wietsma, J.A. Serkowski, and J.M. Zachara. 2015. "Pore-Scale and Multiscale Numerical Simulation of Flow and Transport in a Laboratory-Scale Column." *Water Resources Research* 51(2):1023-1035. doi:10.1002/2014WR015959.

Schnitzler, B.G., J.B. Briggs. 1985. *TMI-2 Isotope Inventory Calculations, EGG-PBS-6798, EG&G Idaho, Inc. Idaho Falls, Idaho*. Referenced in Wolf JR. TMI-2 Vessel Investigation

Project Integration Report, NUREG/CR–6197 Part 2. Idaho National Laboratory. Idaho Falls, Idaho.

Shi, J. 2014. Lecture Notes: Partial Differential Equations and Mathematical Biology. College of William and Mary. URL:http://www.resnet.wm.edu/~jxshix/math490/lecture-chap3.pdf (Accessed November 3, 2016).

Smith, J.T. and R.N.J. Comans. 1996. "Modeling the diffusive transport and remobilasation of 137Cs in sediments: The effects of sorption kinetics and reversibility." *Geochimica et Cosmochimica Acta*, 60(6):995-1004.

Smith, J.T., R.N.J. Comans, D.G. Ireland, L. Nolan, and J. Hilton. 2000. "Experimental and in situ study of radiocaesium transfer across the sediment-water interface and mobility in lake sediments." *Applied Geochemistry*, 15(6):833-848. http://dx.doi.org/10.1016/S0883-2927(99)00095-5.

Taylor, K.R., R.W. James Jr., and B.M. Helinsky. 1985. *Traveltime and Dispersion in the Potomac River, Cumberland, Maryland to Washington, D.C.* U.S. Geological Survey Water-Supply Paper 2257.

TEPCO. 2011a. The results of the measurement of puddle of water in the basement of the turbine building of Unit 2 of Fukushima Daiichi Nuclear Power Station(2nd release), Press Release (Mar 27, 2011). Accessed October 14, 2016 at http://www.tepco.co.jp/en/press/corp-com/release/11032714-e.html#top.

TEPCO. 2011b. Out flow of fluid containing radioactive materials to the ocean from areas near intake channel of Fukushima Daiichi Nuclear Power Station Unit 2, Press Release (Apr 05, 2011). Accessed October 14, 2016 at http://www.tepco.co.jp/en/press/corp-com/release/11040506-e.html.

TEMPO. 2012. Fukushima Nuclear Accident Analysis Report. 2012. Tokyo Electric Power Company, Inc. June 20, 2012. Accessed October 14, 2016 at http://www.tepco.co.jp/en/press/corp-com/release/betu12_e/images/120620e0104.pdf. Attachments located at http://www.tepco.co.jp/en/press/corp-com/release/2012/1205638_1870.html.

Tsumune, D., T. Tsubono, M. Aoyama; K. Hirose. 2012. Distribution of oceanic Cs-137 from the Fukushima Dai-ichi Nuclear Power Plant simulated numerically by a regional ocean model. *Journal of Environmental Radioactivity*. 111:100-108.

NRC (U.S. Nuclear Regulatory Commission). 1981. *Final programmatic environmental impact statement related to decontamination and disposal of radioactive wastes resulting from March 28, 1979, accident Three Mile Island Nuclear Station, Unit 2*, Docket no. 50-320, Metropolitan Edison Company, Jersey Central Power and Light Company, Pennsylvania Electric Company, U.S. Nuclear Regulatory Commission, Office Of Nuclear Reactor Regulation, Washington, D.C.

United Nations. 2014. Sources, Effects And Risks of Ionizing Radiation, UNSCEAR 2013 Report to the General Assembly with Scientific Annexes, United Nations Scientific Committee on the Effects of Atomic Radiation, New York.

USGS (United States Geological Survey). 1969. Travel of Solutes in the Lower Missouri River, USGS Hydrologic Investigations Atlas HA-332.

USGS (United States Geological Survey). 1976. Geological Survey Research 1976, Geological Survey Professional Paper 1000, U.S. Department of the Interior, Washington, D.C.

Van Genuchten, M. Th., F.J. Leij, T.H. Skaggs, N. Toride, S.A. Bradford, and E.M. Pontedeiro. 2013. "Exact Analytical Solutions for Contaminant Transport in Rivers 1. The Equilibrium Advection-Dispersion Equation." *Journal Hydrology and Hydromechanics*. 61(2):146-160. DOI 10.2478/johh-2013-0020.

Versteeg, H.K. and W. Malalasekera. 2007. An Introduction to Computational Fluid Dynamics, the Finite Volume Method, 2nd edition. Pearson Education Limited.

Walters, W.H., M.C. Richmond, B.G. Gilmore. 1996. "Title Reconstruction of Radioactive Contamination in the Columbia River." *Health Physics,* 71(4):556-567.

Wiley, J.B. 1997. *Traveltime and Dispersion Data, Including Associated Discharge and Water-Surface Elevation Data, for the Upper Ohio River, Pennsylvania, Ohio, and West Virginia; October through November 1991*. U.S. Geological Survey, Open-file Report 97-562.

Yang, X., T.D. Scheibe, M.C. Richmond, W.A. Perkins, S.J. Vogt, S.L. Codd, J.D. Seymour, and M.I. McKinley. 2013. "Direct numerical simulation of pore-scale flow in a bead pack: Comparison with magnetic resonance imaging observations." *Advances in Water Resources 54:228–241.*

Yang X., Y. Mehmani, W.A. Perkins, M. Schoenherr, A. Pasquali, C. Clark, K. Kim, M. Perego, M.L. Parks, M. Balhoff, M.C. Richmond, M. Geier, M. Krafczyk, L.S. Luo, A.M. Tartakovsky, C.L. Winter, and T.D. Scheibe. 2015. "Intercomparison of 3D Pore-scale Flow and Solute Transport Simulation Methods." *Advances in Water Resources*. doi:10.1016/j.advwatres.2015.09.015.

Yotsukura, N., H.B. Fischer, and W.W. Sayre. 1970. Measurement of Mixing Characteristics of the Missouri River Between Sioux City, Iowa and Plattsmouth, Nebraska, U.S. Geological Survey Water-Supply Paper 1899-G.

APPENDIX A

MODELING QUALITY ASSURANCE

APPENDIX A

MODELING QUALITY ASSURANCE

A.1 Lake Transport Modeling

A check of the Transient Energy Transport HYdrodynamics Simulator (TETHYS) code was made by comparing simulated concentrations to an analytic solution in a simple approximation of the lake setting. The lake was approximated as a semi-infinite rectangular domain of constant width and depth. The outline of this approximation is overlayed as a black rectangle on the lake setting (Figure A-1). A schematic of the simplified domain is shown in Figure A-2 and the nomenclature is defined in Table A-1. The lake has a nominal discharge of 100 cfs through an approximantely constant width section of the lake. The depth profile at the central transect is shown in Figure A-1b, from which an average depth of 7.8 m was calculated. A constant tracer mass flux was released over a 10-day period from the shoreline of the three-dimensional (3D) large lake model shown in Figure A-1a. Probes are located at radii of 0.5 mi and 1.0 mi to moniter the progression of the contaminant from the source location (Figure A-2). Other dimensions and parameters are shown in Table A-1.

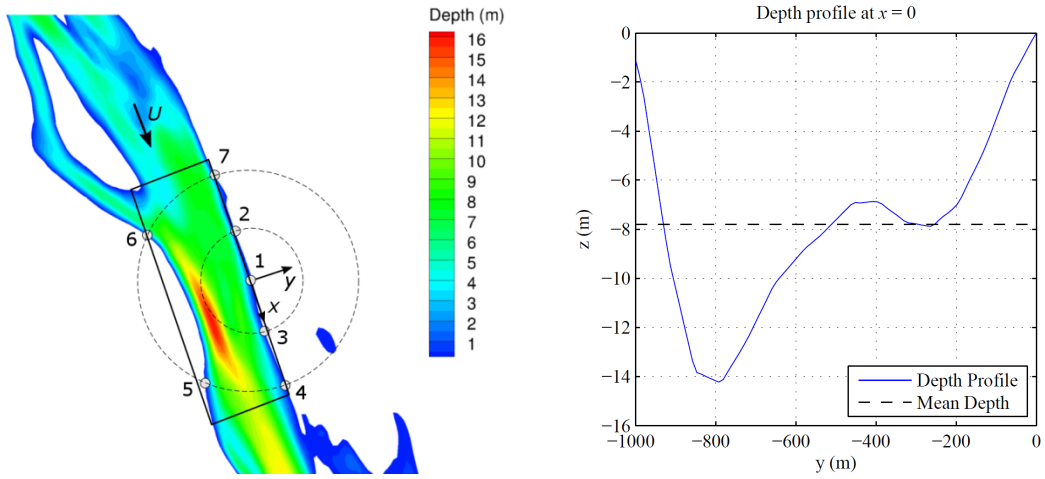

a b

Figure A-1. Domain of Simplified Two-Dimensional Model in the Context of the Large Lake Model and Depth Profile at x = 0

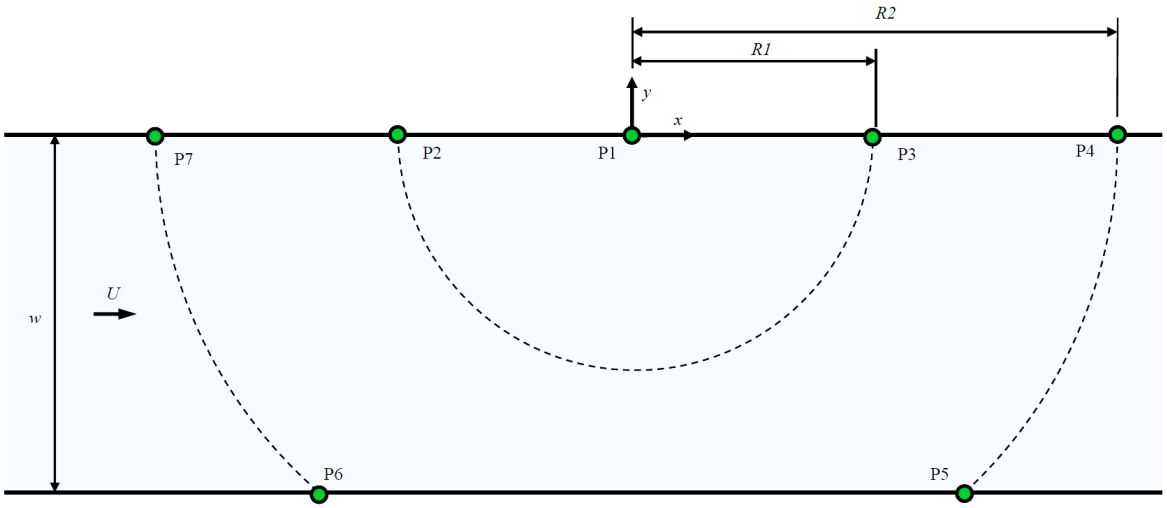

Figure A-2. Schematic and Notation of Two-Dimensional Approximation of Large Lake Model

Table A-1. Parameters of Simplified Analytical Model

Parameter	Nomenclature	Value	Unit
Lake discharge	$\dot{V}$	100	cfs
Mean flow velocity	*U*	3.5×10^{-4}	m/s
Lake width	*w*	1,000	m
Lake depth	*d*	7.8	m
Probe radius #1	*R1*	805	m
Probe radius #2	*R2*	1,609	m
Diffusivity constant	*D*	0.04	m^2/s
Tracer discharge rate	$\dot{m}$	1	g/s
Tracer discharge duration	t_r	10	days
Decay constant	*k*	0	1/s
Probe 1 Coordinates (Source)	*P1*	[0, 0, 0]	m
Probe 2 Coordinates	*P2*	[-805, 0, 0]	m
Probe 3 Coordinates	*P3*	[805, 0, 0]	m
Probe 4 Coordinates	*P4*	[1,609, 0, 0]	m
Probe 5 Coordinates	*P5*	[1,261, -1,000, 0]	m
Probe 6 Coordinates	*P6*	[-1,261, -1,000, 0]	m
Probe 7 Coordinates	*P7*	[-1,609, 0, 0]	m

The unbounded 3D analytical solution was derived from the integral formation of a time-dependent source term presented by Shi (2004):

$$C(x,y,z,t) = \gamma \int_0^t \frac{1}{(t-\tau)^{3/2}} \exp\left(-\frac{\alpha}{(t-\tau)} - \beta(t-\tau)\right) \mathrm{d}\tau$$

where

$$\gamma = \frac{\dot{m}}{8(\pi D)^{3/2}} \exp\left(\frac{xU}{2D}\right)$$

$$\alpha = \frac{x^2 + y^2 + z^2}{4D}$$

$$\beta = \frac{U^2}{4D} + k$$

and C is concentration, x, y, and z are spatial coordinates, and t is time. During continuous injection from $t = 0$ to $t = t_r$:

$$C_0(x,y,z,t) = \frac{\gamma\sqrt{\pi}}{2\sqrt{\alpha}}\left\{\exp\left(2\sqrt{\alpha\beta}\right)\operatorname{erfc}\left(\sqrt{\frac{\alpha}{t}} + \sqrt{\beta t}\right) + \exp\left(-2\sqrt{\alpha\beta}\right)\operatorname{erfc}\left(\sqrt{\frac{\alpha}{t}} - \sqrt{\beta t}\right)\right\}$$

The solution following the release period ($t > t_r$) is:

$$C_0(x,y,z,t) = \frac{\gamma\sqrt{\pi}}{2\sqrt{\alpha}}\left\{\exp\left(2\sqrt{\alpha\beta}\right)\left[\operatorname{erf}\left(\sqrt{\frac{\alpha}{(t-t_r)}} + \sqrt{\beta(t-t_r)}\right) - \operatorname{erf}\left(\sqrt{\frac{\alpha}{t}} + \sqrt{\beta t}\right)\right]\right.$$
$$\left. + \exp\left(-2\sqrt{\alpha\beta}\right)\left[\operatorname{erf}\left(\sqrt{\frac{\alpha}{(t-t_r)}} - \sqrt{\beta(t-t_r)}\right) - \operatorname{erf}\left(\sqrt{\frac{\alpha}{t}} - \sqrt{\beta t}\right)\right]\right\}$$

For the bounded case of the semi-infinite lake, the solution is reflected about the lake banks in the *y*-direction and the surface and lake-bed in the *z*-directions, such that the above equations become:

$$\alpha = \frac{x^2 + \left(y + 2n_y w\right)^2 + (z + 2n_z d)^2}{4D}$$

$$C(x,y,z,t) = \sum_{n_z=-\infty}^{\infty} \sum_{n_y=-\infty}^{\infty} 4C_0$$

For the geometry defined in Table A-1, this converges to a stable result when $-2 \leq n_y \leq 2$ and $-25 \leq n_z \leq 25$.

TETHYS was configured to simulate the domain of the analytic solution using the same parameters (Table A-1). Simulation results were sampled at the locations shown in Figure A-2 and the analytic solution was computed for the same locations. Simulation results were very close to the analytic solution (Figure A-3).

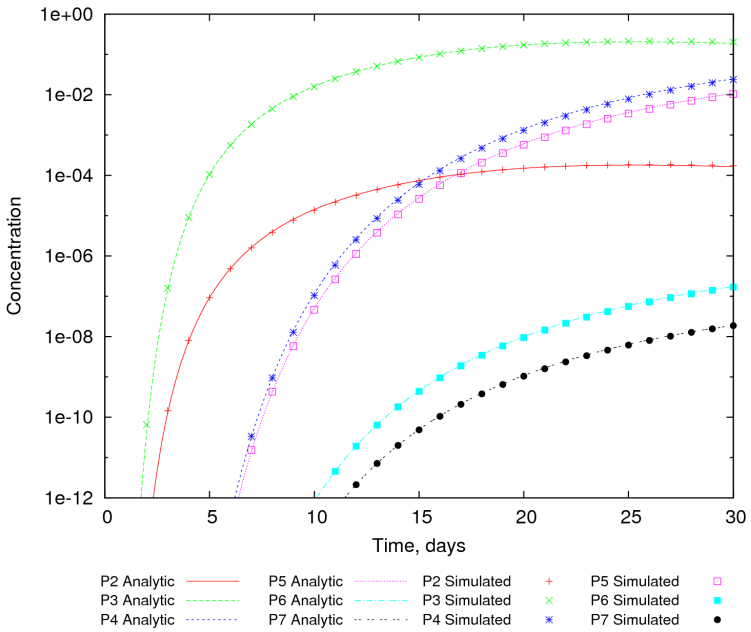

Figure A-3. Comparison of TETHYS Simulation Results with Analytic Solution

A.2 River Transport Modeling

In order to check the reasonability of the Modular Aquatic Simulation System in 2 Dimensions (MASS2) numerical solutions for the small and large river contaminant transport solutions, simple analytical solutions were computed based on an adaptation of the solution provided in van Genuchten et al. (2013). The van Genuchten analytic solution is based on the following assumptions:

- the longitudinal (*x*-direction) turbulent mixing is much less significant than the longitudinal advective transport;
- the transverse (*y*-direction) turbulent mixing coefficient has a constant value of ε_y;
- the contaminant is conservative;
- the contaminant flux is a constant and steady *F;*
- the point release of contamination occurs at *x=0, y=*y_0; and
- the river discharge is steady and has uniform flow depth H and water speed *u*, and width, *B*.

For the case where the shoreline boundaries are sufficiently distant from the release point, a simple unbounded solution can be used to compute the contaminant concentration $C_U(x,y)$ for positions laterally across the river and longitudinally downstream from the source, *x*.

$$C_U(x,y) = F \exp\left(\frac{-u\,(y-y_0)^2}{4x\varepsilon_y}\right)[2\,H\,\sqrt{\pi u \varepsilon_y x}]^{-1}$$

Superpositioning of reflected solutions for C_U accounts for the presence of the shoreline boundaries. This is necessary to obtain bounded solutions for the contaminant activities, $C_B(x,y)$. These solutions ensure that lateral diffusion does not occur laterally beyond the near and far shores. The number of reflected terms, *n*, is based on what is considered necessary to

develop a satisfactory solution respecting the solid boundaries of the shorelines. The literature suggests that *n* should be greater than four. All solutions presented here are based on *n* equal to 10. The modified solution accounting for boundary reflection is based on the summation of a series of unbounded solutions that are laterally offset from the position of the contaminant release. This is given by van Genuchten et al. (2013) below:

$$C_B\,(x,y) = C_U(x,y) + \sum_{k=1}^{n} C_U\big(x, kB - y0 + (-1)^k y\big) + C_U(x, -kB + y0 - (-1)^k y)$$

For this project, first-order decay needed to be included. This process was added to the unbounded contaminant equation based on first-order decay with a decay rate, r, where the downstream position x is a precise predictor of the elapsed time-of-travel of a parcel of contaminant released at x=0:

$$C_U(x,y) = F \exp\left(\frac{-u\,(y-y_0)^2}{4x\varepsilon_y}\right)[2\,H\,\sqrt{\pi u \varepsilon_y x}]^{-1} \exp(-r\frac{x}{u})$$

The analytical solution is based on a steady release. This differs from the 10-day release scenario that was evaluated using MASS2. While this prevents the analytical solution from capturing the initial rise and final decline of the contamination levels, it does allow for comparison to the peak concentrations that could be expected. It is also expected that the contaminant will attain a peak level of contaminant concentration and sustain that level for a duration lasting about as long as the release duration (i.e., 10 days).

A Matlab program was used to compute solutions to the above equation for domains approximating those simulated by MASS2 in the large and small discharge river cases. Dimensions of the two domains are listed in Table A-2. The actual flow depth and width varied widely in both river settings. Those listed in Table A-2 are estimates. Again, the domain assumed by the analytic solution is a rough approximation of the actual river setting. The source term and radionuclide-specific parameters used in the analytical transport solution are summarized in Table A-3.

Table A-2. Small and Large River Scenario Flow and Mixing Parameters Used in the Analytical Transport Solution

	Width *B*	Depth *H*	Discharge	Velocity *u*	Transverse turbulent mixing coefficient ε_y
River Case	**m**	**m**	**m^3/s,(cfs)**	**(m/s)**	**m^2/s**
Small	150	4.0	141.58 (5,000)	0.236	0.19
Large	550	7.0	2,831.68 (100,000)	0.736	0.19

Table A-3. Small and Large River Scenario Aqueous Radionuclide Inventory, Flux and Decay Characteristics and Parameters Used in the Analytical Transport Solution.

Case	Radionuclide	Decay coefficient, r[(a)]	Water Volume Released	Release Duration	Release Rate, F	Fully Mixed Activity, Small River	Fully Mixed Activity, Large River
		1/days	m^3	days	Bq/s	Bq/m^3	Bq/m^3
1	^{144}Ce	0	1,000	10	868,056	6131	307
2	^{134}Cs	0	1,000	10	13,020,833,333	91,965,267	4,598,263
3	^{137}Cs	0	1,000	10	8,391,203,704	59,266,505	2,963,325
4	^{3}H	0	1,000	10	49,189,815	347,424	17,371
5	^{131}I	0.09495	1,000	10	12,731,481,481	NA	NA
6	^{106}Ru	0	1,000	10	2,314,815	16,349	817
7	^{125}Sb	0	1,000	10	3,472,222	24,524	1,226
8	^{90}Sr	0	1,000	10	240,162,037	1,696,248	84,812

(a) Decay rates are internally converted from d^{-1} to s^{-1} in the analytical solution calculation.

Comparisons of simulated small river peak activity values with those from the analytic solution are shown in Figure A-4 through Figure A-11. MASS2 compare closely for the longer lived radionuclides. Complete lateral mixing is achieved within the upper 10 mi of the 50 river mi considered; that is, the near and far bank concentrations are nearly equal to each other and the simply calculated fully mixed activity levels expected for each long-lived radionuclide treated as conservative. For the decaying radionuclide (^{131}I, Figure A-8), the complete lateral mixing occurs for both numerical and analytic models as it does for the long-lived radionuclides. However, the numerical model shows a trend of less decay than the analytical and what would be indicated by a simple calculation of fully mixed but decayed activity as estimated from the time-of-travel to each downstream location.

Comparisons of simulated large river peak activity values with those from the analytic solution are shown in Figure A-12 through Figure A-19. When compared with the small river, the large river is wider and has a higher velocity. Complete transverse mixing is not achieved within the 50 river mi considered; that is, the near and far bank concentration are unequal to each other but approach the simply calculated, fully mixed activity levels expected for each isotope. Within the upper 10 mi, the numerical model shows slightly less lateral mixing than the analytic model. However, both models show increased and very comparable levels of lateral mixing at distances of 20 mi and greater.

The quality of the comparison is good for the large and small rivers for all radionuclides treated as conservative; all solutions seem to be converging to the expected fully mixed activity levels. This also holds true for the large river ^{131}I case, where the swift currents reduced travel times and therefore diminishes the impact of ^{131}I decay. In the small river ^{131}I case, where travel time is longer, there is a larger level difference between the analytical solutions and the MASS2 solution. All MASS2 and analytical solution comparisons show agreement that is better (and most often much better) than order of magnitude. There is no indication that the MASS2 model is producing results that are inconsistent with expectations for conservative transport cases.

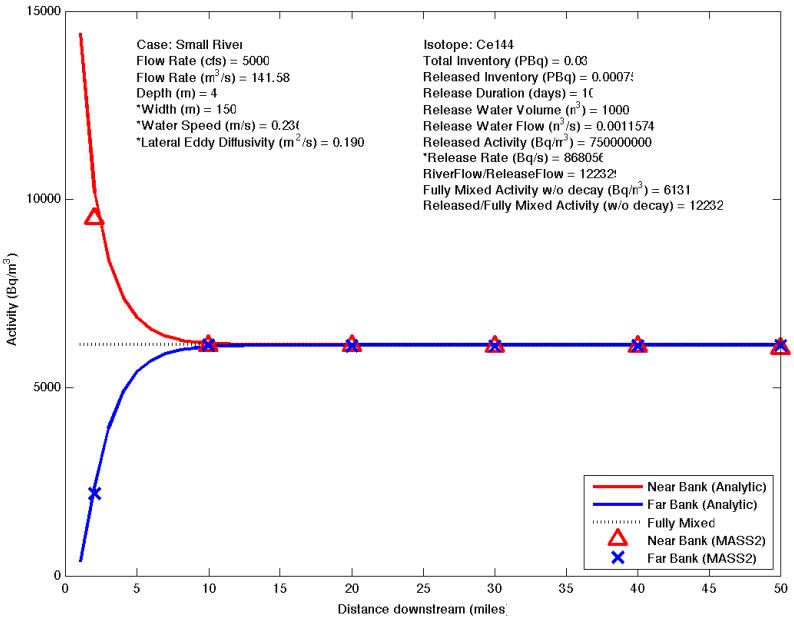

Figure A-4. MASS2 and Analytical Solution Longitudinal Small River Solutions for Estimated ^{144}Ce Activity at Near and Far Banks.

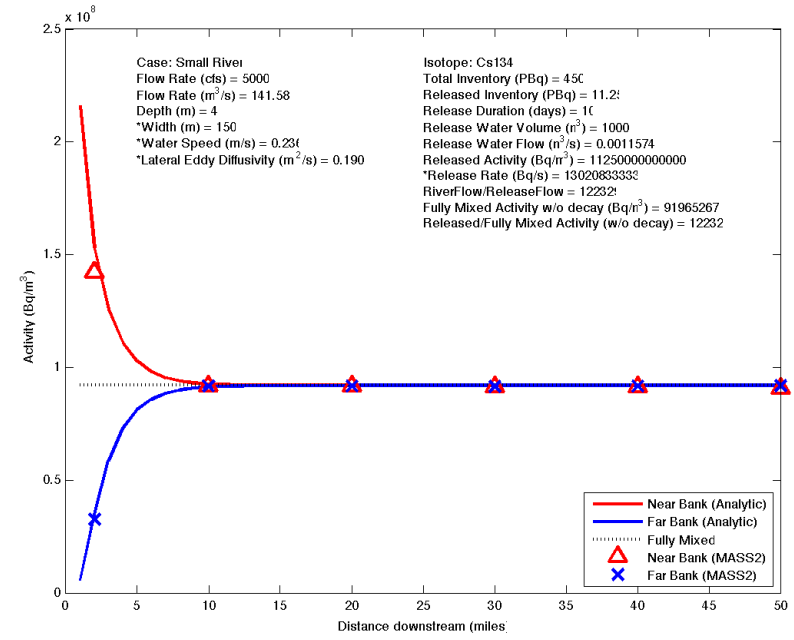

Figure A-5. MASS2 And Analytical Solution Longitudinal Small River Solutions for Estimated ^{134}Cs Activity at Near and Far Banks.

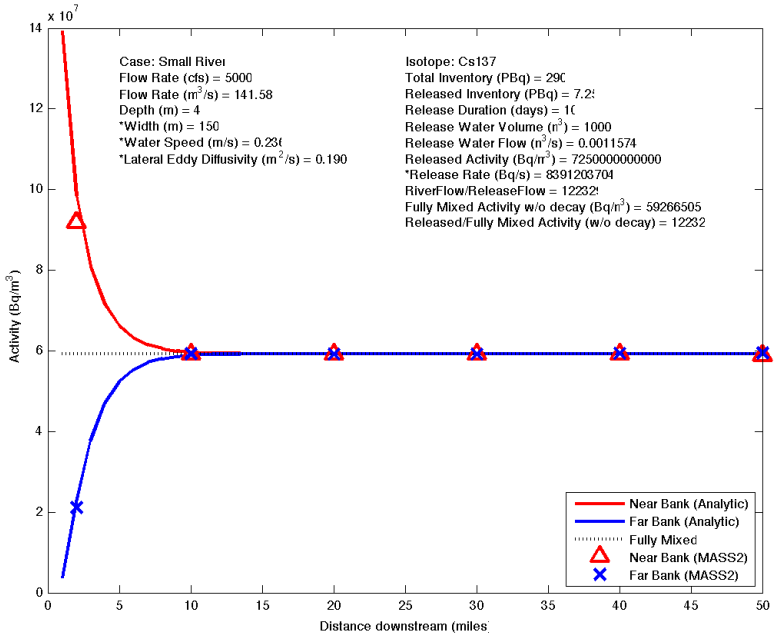

Figure A-6. MASS2 And Analytical Solution Longitudinal Small River Solutions for Estimated ^{137}Cs Activity at Near and Far Banks.

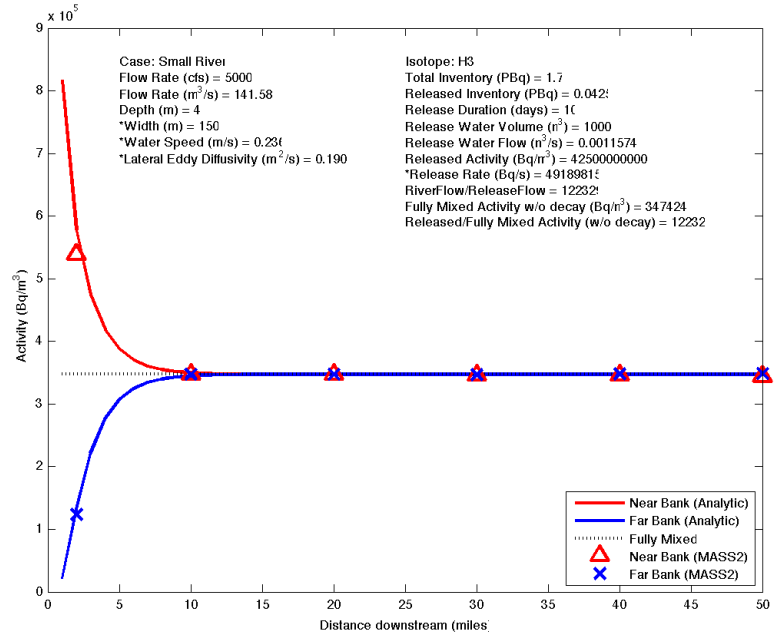

Figure A-7. MASS2 and Analytical Solution Longitudinal Small River Solutions for Estimated ^{3}H Activity at Near and Far Banks.

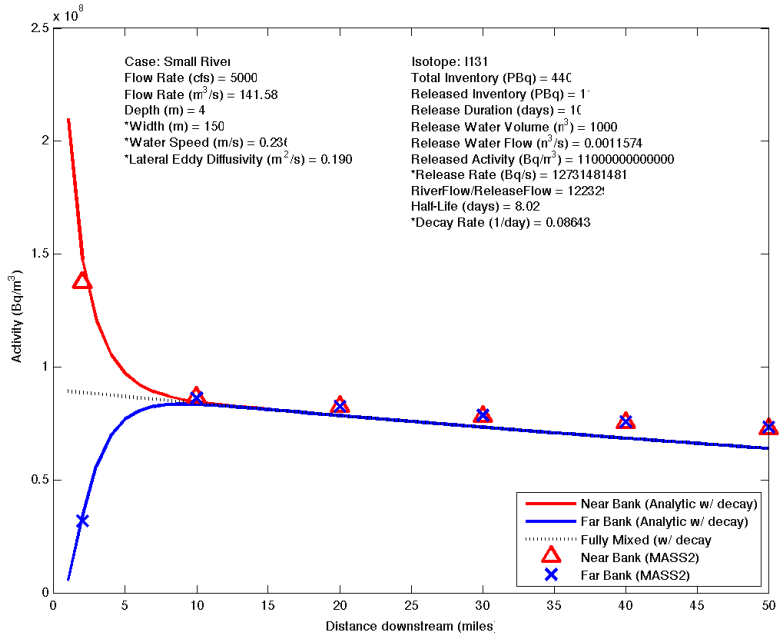

Figure A-8. MASS2 and Analytical Solution Longitudinal Small River Solutions for Estimated ^{131}I Activity at Near and Far Banks.

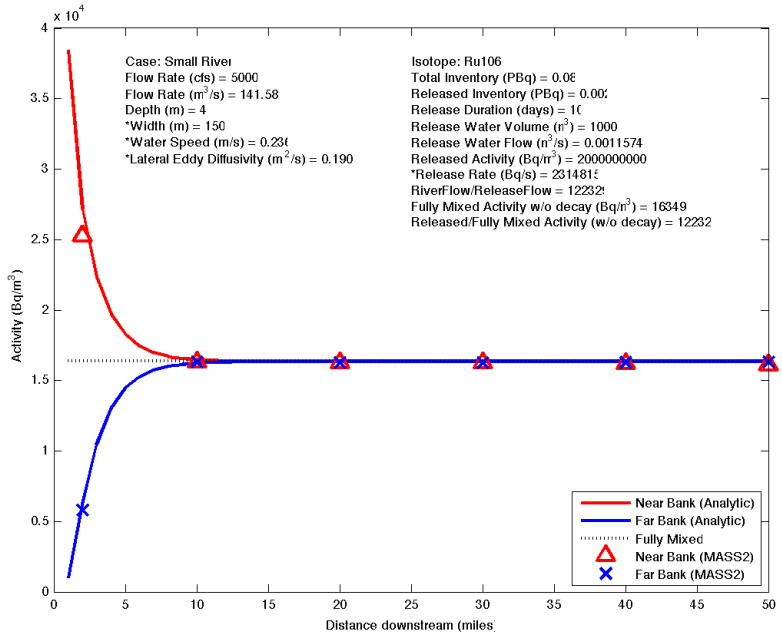

Figure A-9. MASS2 and Analytical Solution Longitudinal Small River Solutions for Estimated ^{106}Ru Activity at Near and Far Banks.

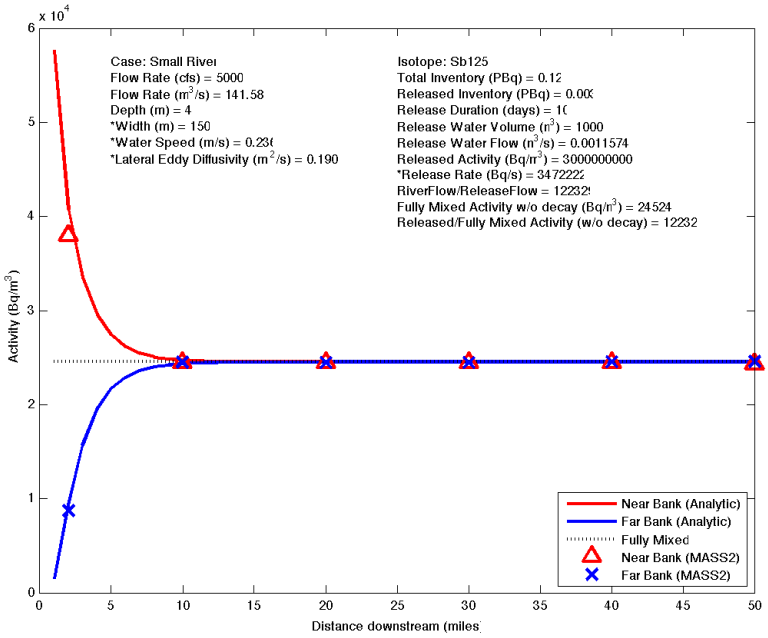

Figure A-10. MASS2 and Analytical Solution Longitudinal Small River Solutions for Estimated ^{125}Sb Activity at Near and Far Banks.

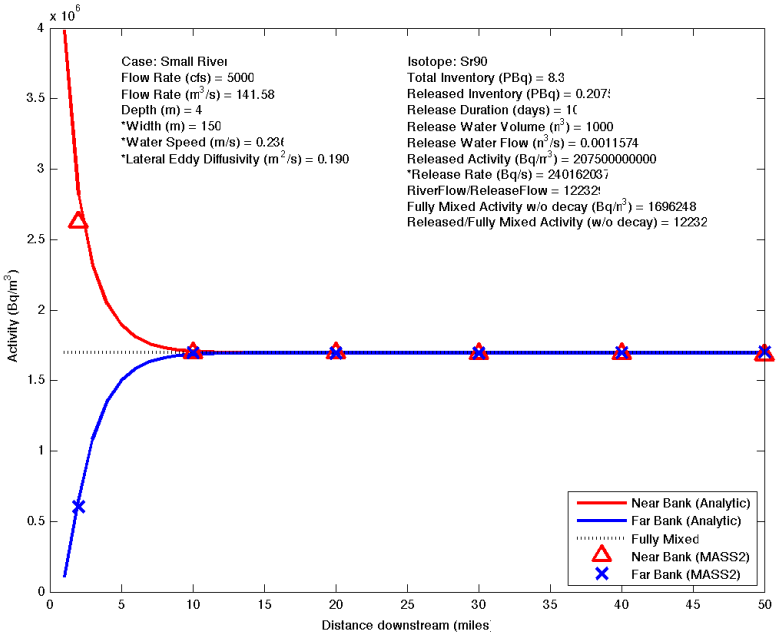

Figure A-11. MASS2 and Analytical Solution Longitudinal Small River Solutions for Estimated ^{90}Sr Activity at Near and Far Banks.

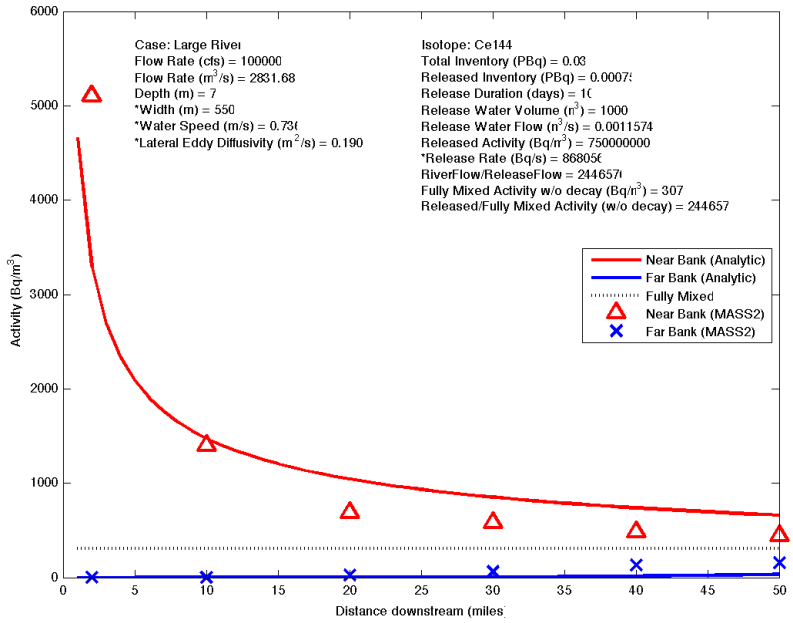

Figure A-12. MASS2 and Analytical Solution Longitudinal Large River Solutions for Estimated ^{144}Ce Activity at Near and Far Banks.

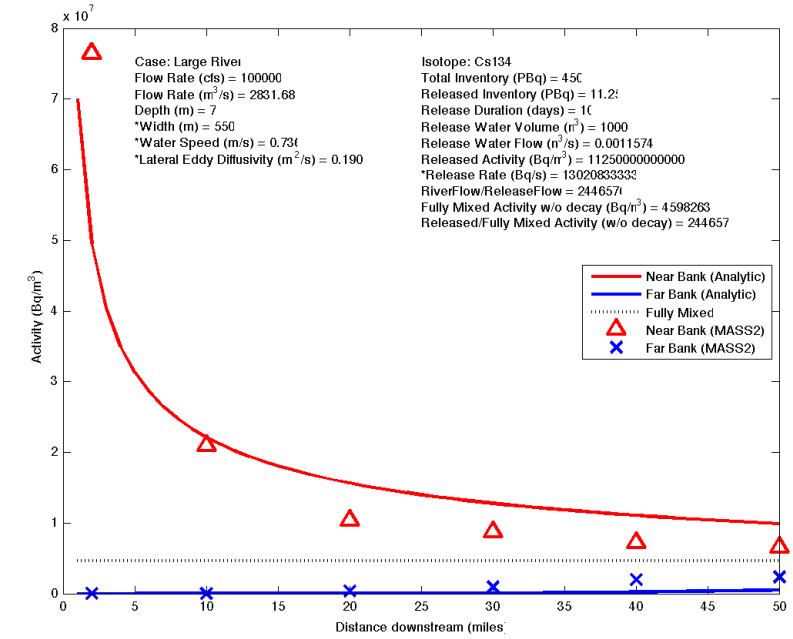

Figure A-13. MASS2 and Analytical Solution Longitudinal Large River Solutions for Estimated ^{134}Cs Activity at Near and Far Banks.

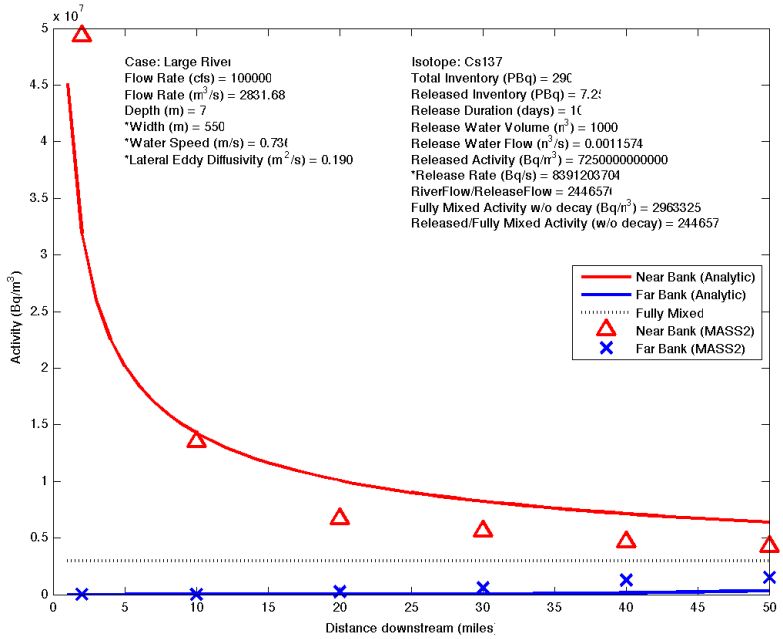

Figure A-14. MASS2 and Analytical Solution Longitudinal Large River Solutions for Estimated ^{137}Cs Activity at Near and Far Banks.

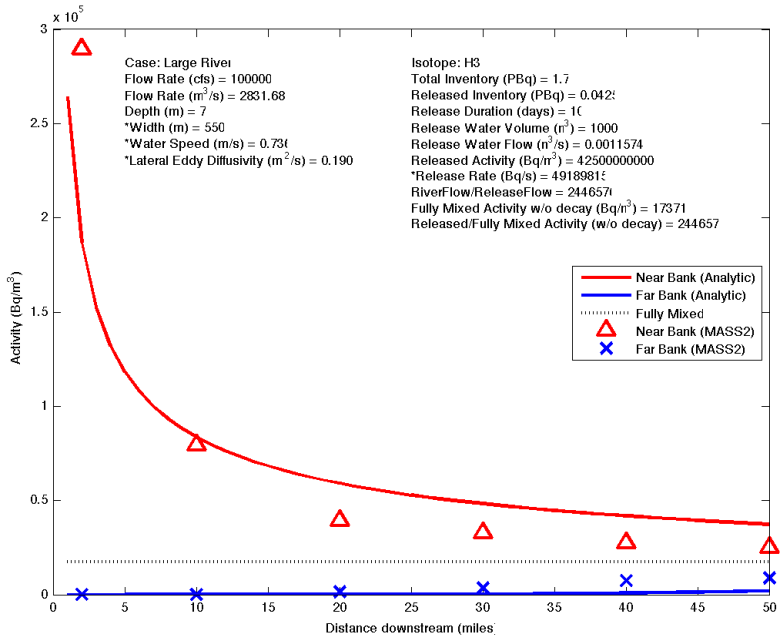

Figure A-15. MASS2 and Analytical Solution Longitudinal Large River Solutions for Estimated ^{3}H Activity at Near and Far Banks.

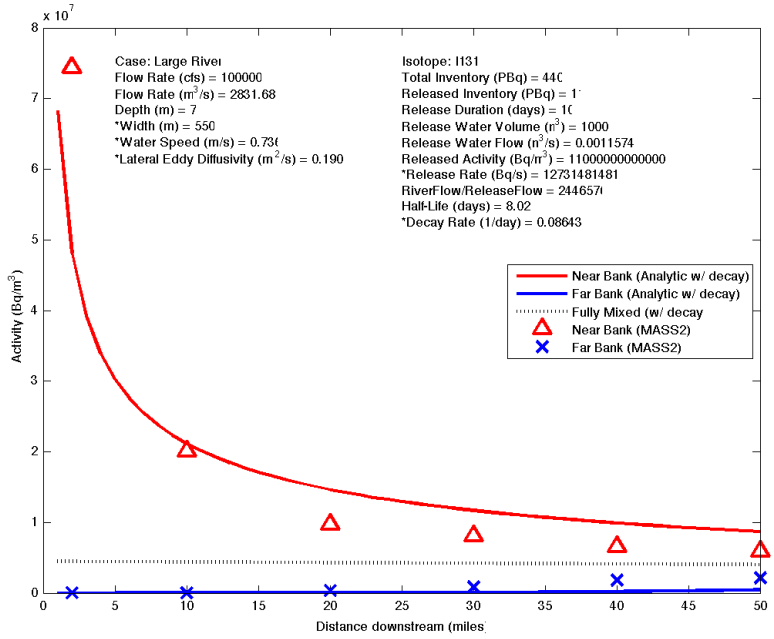

Figure A-16. MASS2 and Analytical Solution Longitudinal Large River Solutions for Estimated ^{131}I Activity at Near and Far Banks.

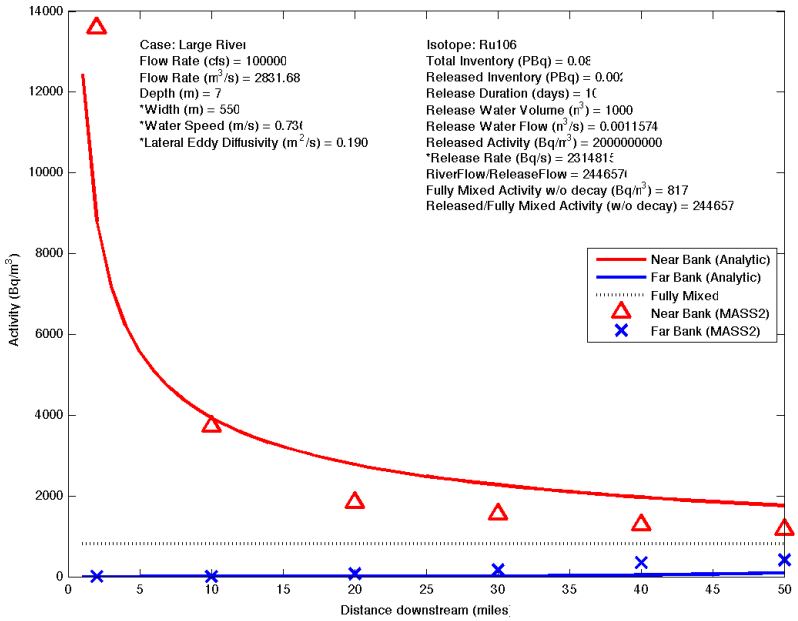

Figure A-17. MASS2 and Analytical Solution Longitudinal Large River Solutions for Estimated ^{106}Ru Activity at Near and Far Banks.

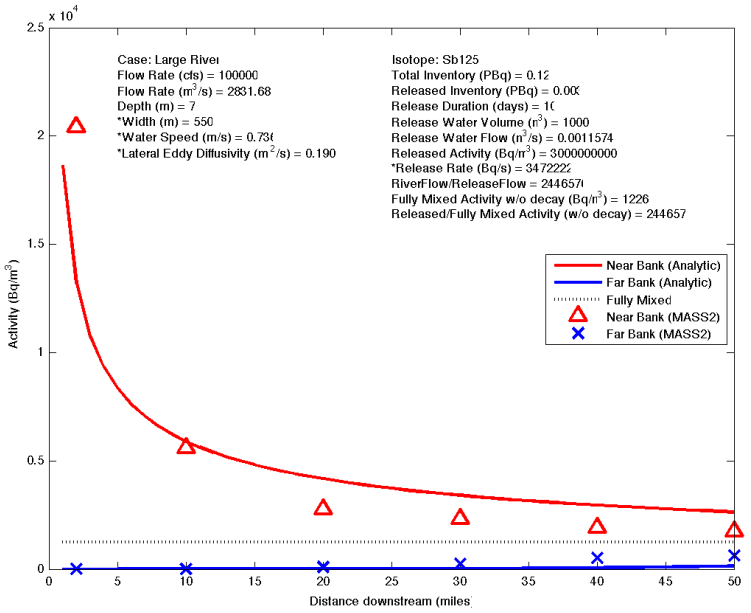

Figure A-18. MASS2 and Analytical Solution Longitudinal Large River Solutions for Estimated ^{125}Sb Activity at Near and Far Banks.

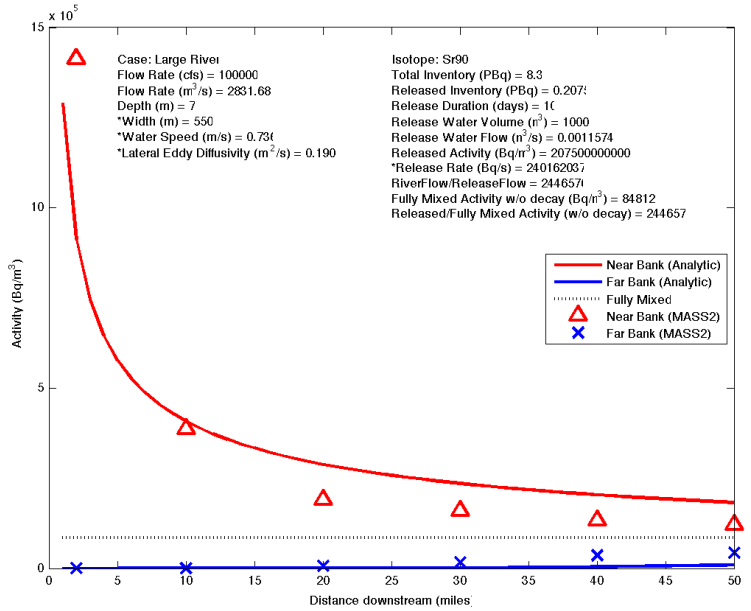

Figure A-19. MASS2 and Analytical Solution Longitudinal Large River Solutions for Estimated ^{90}Sr Activity at Near and Far Banks.

A.3 Source Term Details

A.3.1 Reactor Fuel Content for PWR and BWR of Various Burnups

This appendix lists core-average radionuclide inventories calculated by ORIGEN-ARP as a function of peak rod burnup for 60 radionuclides developed by Ramsdell et al. (2001). Table A-4 contains the inventories for PWR fuel, and Table A-5 contains the inventories for BWR fuel.

Table A-4. PWR Core-Averaged Inventory of Radionuclides as a Function of Burnup (Bq/MTU) (from NUREG/CR–6703)

Nuclide	Peak Rod Burnup. GWd/MTU												
	22	24	25	42	43	46	48	50	60	62	65	70	75
H-3	1.16E+13	1.27E+13	1.32E+13	2.16E+13	2.21E+13	2.35E+13	2.45E+13	2.54E+13	3.00E+13	3.09E+13	3.22E+13	3.44E+13	3.66E+13
Co-58	3.55E+14	3.59E+14	3.61E+14	3.92E+14	3.92E+14	3.96E+14	4.00E+14	4.03E+14	4.14E+14	4.18E+14	4.18E+14	4.26E+14	4.29E+14
Co-60	1.80E+14	1.95E+14	2.02E+14	3.26E+14	3.33E+14	3.54E+14	3.68E+14	3.81E+14	4.51E+14	4.66E+14	4.85E+14	5.18E+14	5.51E+14
Kr-85m	8.33E+15	8.18E+15	8.07E+15	6.92E+15	6.88E+15	6.70E+15	6.51E+15	6.40E+15	5.85E+15	5.74E+15	5.55E+15	5.33E+15	5.07E+15
Kr-85	2.62E+14	2.81E+14	2.90E+14	4.29E+14	4.37E+14	4.55E+14	4.70E+14	4.81E+14	5.33E+14	5.44E+14	5.59E+14	5.77E+14	5.96E+14
Kr-87	1.68E+16	1.65E+16	1.63E+16	1.39E+16	1.38E+16	1.34E+16	1.31E+16	1.28E+16	1.17E+16	1.14E+16	1.10E+16	1.05E+16	1.00E+16
Kr-88	2.36E+16	2.31E+16	2.28E+16	1.93E+16	1.91E+16	1.85E+16	1.80E+16	1.76E+16	1.60E+16	1.56E+16	1.51E+16	1.43E+16	1.36E+16
Rb-86	2.66E+13	2.94E+13	3.08E+13	5.74E+13	5.92E+13	6.44E+13	6.77E+13	7.14E+13	8.92E+13	9.25E+13	9.81E+13	1.07E+14	1.17E+14
Sr-89	3.30E+16	3.23E+16	3.20E+16	2.68E+16	2.66E+16	2.57E+16	2.51E+16	2.45E+16	2.19E+16	2.14E+16	2.07E+16	1.95E+16	1.84E+16
Sr-90	2.27E+15	2.44E+15	2.53E+15	3.81E+15	3.89E+15	4.07E+15	4.18E+15	4.33E+15	4.85E+15	4.96E+15	5.11E+15	5.33E+15	5.51E+15
Sr-91	4.03E+16	3.96E+16	3.92E+16	3.37E+16	3.36E+16	3.26E+16	3.18E+16	3.13E+16	2.86E+16	2.80E+16	2.72E+16	2.61E+16	2.49E+16
Sr-92	4.18E+16	4.11E+16	4.07E+16	3.59E+16	3.58E+16	3.49E+16	3.42E+16	3.37E+16	3.14E+16	3.08E+16	3.01E+16	2.91E+16	2.80E+16
Y-90	2.37E+15	2.55E+15	2.64E+15	3.99E+15	4.06E+15	4.25E+15	4.40E+15	4.51E+15	5.11E+15	5.22E+15	5.37E+15	5.60E+15	5.82E+15
Y-91	4.18E+16	4.07E+16	4.03E+16	3.49E+16	3.46E+16	3.36E+16	3.29E+16	3.23E+16	2.95E+16	2.89E+16	2.81E+16	2.69E+16	2.56E+16
Y-92	3.28E+12	3.35E+12	3.37E+12	3.96E+12	4.03E+12	4.14E+12	4.18E+12	4.26E+12	4.59E+12	4.63E+12	4.74E+12	4.92E+12	5.03E+12
Y-93	3.12E+16	3.08E+16	3.05E+16	2.76E+16	2.75E+16	2.69E+16	2.65E+16	2.62E+16	2.48E+16	2.44E+16	2.40E+16	2.34E+16	2.27E+16
Zr-95	5.24E+16	5.21E+16	5.17E+16	4.85E+16	4.86E+16	4.78E+16	4.75E+16	4.71E+16	4.54E+16	4.50E+16	4.43E+16	4.37E+16	4.30E+16
Zr-97	4.86E+16	4.83E+16	4.83E+16	4.67E+16	4.71E+16	4.68E+16	4.65E+16	4.65E+16	4.59E+16	4.56E+16	4.52E+16	4.53E+16	4.46E+16
Nb-95	5.28E+16	5.24E+16	5.21E+16	4.89E+16	4.86E+16	4.83E+16	4.79E+16	4.72E+16	4.55E+16	4.55E+16	4.48E+16	4.41E+16	4.31E+16
Mo-99	5.29E+16	5.29E+16	5.25E+16	5.18E+16	5.22E+16	5.22E+16	5.18E+16	5.18E+16	5.14E+16	5.14E+16	5.14E+16	5.11E+16	5.11E+16
Tc-99m	4.66E+16	4.66E+16	4.66E+16	4.63E+16	4.63E+16	4.63E+16	4.59E+16	4.59E+16	4.59E+16	4.59E+16	4.55E+16	4.55E+16	4.55E+16
Ru-103	3.81E+16	3.89E+16	3.92E+16	4.37E+16	4.40E+16	4.48E+16	4.51E+16	4.59E+16	4.81E+16	4.85E+16	4.88E+16	5.00E+16	5.07E+16
Ru-105	2.25E+16	2.33E+16	2.37E+16	2.96E+16	3.01E+16	3.12E+16	3.17E+16	3.24E+16	3.55E+16	3.59E+16	3.68E+16	3.81E+16	3.92E+16
Ru-106	9.36E+15	1.02E+16	1.07E+16	1.75E+16	1.78E+16	1.89E+16	1.96E+16	2.04E+16	2.37E+16	2.44E+16	2.53E+16	2.68E+16	2.82E+16
Rh-105	2.14E+16	2.23E+16	2.26E+16	2.80E+16	2.85E+16	2.94E+16	2.99E+16	3.06E+16	3.32E+16	3.36E+16	3.43E+16	3.55E+16	3.64E+16
Sb-125	2.05E+13	2.21E+13	2.28E+13	3.50E+13	3.57E+13	3.77E+13	3.89E+13	4.03E+13	4.63E+13	4.77E+13	4.96E+13	5.22E+13	5.51E+13
Sb-127	1.98E+15	2.03E+15	2.05E+15	2.36E+15	2.38E+15	2.43E+15	2.45E+15	2.49E+15	2.64E+15	2.66E+15	2.70E+15	2.76E+15	2.80E+15
Te-127m	3.21E+14	3.32E+14	3.36E+14	3.96E+14	4.00E+14	4.11E+14	4.14E+14	4.22E+14	4.48E+14	4.55E+14	4.63E+14	4.74E+14	4.81E+14
Te-127	1.95E+15	2.00E+15	2.02E+15	2.33E+15	2.36E+15	2.41E+15	2.43E+15	2.47E+15	2.62E+15	2.64E+15	2.68E+15	2.74E+15	2.78E+15
Te-129m	1.57E+15	1.59E+15	1.59E+15	1.70E+15	1.71E+15	1.73E+15	1.74E+15	1.75E+15	1.79E+15	1.80E+15	1.81E+15	1.83E+15	1.84E+15
Te-129	7.81E+15	7.92E+15	7.92E+15	8.40E+15	8.44E+15	8.51E+15	8.55E+15	8.58E+15	8.84E+15	8.84E+15	8.88E+15	8.99E+15	9.03E+15
Te-131n1	4.85E+15	4.92E+15	4.96E+15	5.40E+15	5.48E+15	5.55E+15	5.55E+15	5.62E+15	5.85E+15	5.85E+15	5.88E+15	5.99E+15	6.03E+15
Te-132	3.96E+16	3.96E+16	3.96E+16	3.96E+16	4.00E+16	4.00E+16	3.96E+16	4.00E+16	4.00E+16	3.96E+16	3.96E+16	4.00E+16	3.96E+16
I-131	2.73E+16	2.73E+16	2.74E+16	2.77E+16	2.78E+16	2.78E+16	2.78E+16	2.79E+16	2.79E+16	2.80E+16	2.80E+16	2.80E+16	2.80E+16
I-132	4.00E+16	4.03E+16	4.03E+16	4.03E+16	4.07E+16	4.07E+16	4.03E+16	4.07E+16	4.07E+16	4.07E+16	4.07E+16	4.07E+16	4.07E+16
I-133	5.81E+16	5.81E+16	5.81E+16	5.70E+16	5.74E+16	5.70E+16	5.70E+16	5.70E+16	5.66E+16	5.62E+16	5.62E+16	5.59E+16	5.55E+16
I-134	6.55E+16	6.51E+16	6.51E+16	6.33E+16	6.33E+16	6.33E+16	6.25E+16	6.25E+16	6.18E+16	6.14E+16	6.14E+16	6.11E+16	6.03E+16
I-135	5.51E+16	5.51E+16	5.48E+16	5.44E+16	5.48E+16	5.44E+16	5.44E+16	5.44E+16	5.40E+16	5.40E+16	5.40E+16	5.37E+16	5.37E+16

Table A-4. (contd)

Nuclide	Peak Rod Burnup. GWd/MTU												
	22	24	25	42	43	46	48	50	60	62	65	70	75
Xe-133	5.81E+16	5.81E+16	5.81E+16	5.74E+16	5.74E+16	5.74E+16	5.70E+16	5.70E+16	5.66E+16	5.66E+16	5.62E+16	5.62E+16	5.59E+16
Xe-135	2.39E+16	2.38E+16	2.36E+16	2.06E+16	2.05E+16	2.01E+16	1.97E+16	1.95E+16	1.77E+16	1.74E+16	1.71E+16	1.65E+16	1.62E+16
Cs-134	2.13E+15	2.49E+15	2.68E+15	6.40E+15	6.66E+15	7.40E+15	7.96E+15	8.47E+15	1.11E+16	1.17E+16	1.25E+16	1.39E+16	1.54E+16
Cs-136	9.88E+14	1.08E+15	1.13E+15	2.02E+15	2.08E+15	2.25E+15	2.36E+15	2.48E+15	3.11E+15	3.23E+15	3.43E+15	3.77E+15	4.07E+15
Cs-137	2.68E+15	2.92E+15	3.04E+15	5.00E+15	5.11E+15	5.44E+15	5.70E+15	5.92E+15	6.99E+15	7.22E+15	7.55E+15	8.07E+15	9.58E+15
Ba-139	5.25E+16	5.25E+16	5.22E+16	5.03E+16	5.03E+16	5.03E+16	4.96E+16	4.96E+16	4.88E+16	4.85E+16	4.85E+16	4.81E+16	4.74E+16
Ba-140	5.25E+16	5.22E+16	5.22E+16	5.07E+16	5.07E+16	5.03E+16	5.00E+16	5.00E+16	4.92E+16	4.88E+16	4.85E+16	4.81E+16	4.77E+16
La-140	5.33E+16	5.33E+16	5.29E+16	5.22E+16	5.25E+16	5.22E+16	5.18E+16	5.18E+16	5.18E+16	5.14E+16	5.14E+16	5.14E+16	5.11E+16
La-141	4.81E+16	4.81E+16	4.77E+16	4.59E+16	4.63E+16	4.59E+16	4.55E+16	4.51E+16	4.44E+16	4.40E+16	4.40E+16	4.37E+16	4.29E+16
La-142	4.74E+16	4.74E+16	4.70E+16	4.48E+16	4.51E+16	4.48E+16	4.40E+16	4.40E+16	4.33E+16	4.29E+16	4.26E+16	4.22E+16	4.14E+16
Ce-141	4.85E+16	4.85E+16	4.81E+16	4.66E+16	4.66E+16	4.63E+16	4.59E+16	4.59E+16	4.48E+16	4.48E+16	4.44E+16	4.40E+16	4.37E+16
Ce-143	4.63E+16	4.59E+16	4.59E+16	4.29E+16	4.29E+16	4.26E+16	4.22E+16	4.18E+16	4.07E+16	4.03E+16	4.00E+16	3.92E+16	3.89E+16
Ce-144	3.74E+16	3.81E+16	3.85E+16	4.00E+16	3.96E+16	3.96E+16	3.92E+16	3.92E+16	3.81E+16	3.77E+16	3.74E+16	3.67E+16	3.60E+16
Pr-143	4.55E+16	4.51E+16	4.51E+16	4.22E+16	4.22E+16	4.14E+16	4.14E+16	4.11E+16	3.96E+16	3.96E+16	3.92E+16	3.85E+16	3.81E+16
Nd-147	1.91E+16	1.91E+16	1.91E+16	1.87E+16	1.88E+16	1.87E+16	1.86E+16	1.86E+16	1.85E+16	1.84E+16	1.84E+16	1.83E+16	1.82E+16
Np-239	4.48E+17	4.55E+17	4.59E+17	5.37E+17	5.44E+17	5.59E+17	5.62E+17	5.74E+17	6.18E+17	6.25E+17	6.40E+17	6.59E+17	6.73E+17
Pu-238	2.82E+13	3.52E+13	3.89E+13	1.42E+14	1.50E+14	1.76E+14	1.95E+14	2.14E+14	3.17E+14	3.39E+14	3.70E+14	4.26E+14	4.81E+14
Pu-239	1.17E+13	1.21E+13	1.23E+13	1.41E+13	1.41E+13	1.42E+13	1.42E+13	1.42E+13	1.41E+13	1.41E+13	1.40E+13	1.39E+13	1.39E+13
Pu-240	9.10E+12	1.00E+13	1.05E+13	1.91E+13	1.95E+13	2.06E+13	2.13E+13	2.20E+13	2.55E+13	2.60E+13	2.66E+13	2.75E+13	2.79E+13
Pu-241	2.80E+15	3.22E+15	3.42E+15	5.66E+15	5.81E+15	6.18E+15	6.44E+15	6.66E+15	7.18E+15	7.29E+15	7.47E+15	7.70E+15	7.99E+15
Am-241	2.31E+12	2.87E+12	3.16E+12	8.29E+12	8.55E+12	9.29E+12	9.73E+12	1.02E+13	1.16E+13	1.18E+13	1.20E+13	1.23E+13	1.25E+13
Am-242	7.77E+14	9.81E+14	1.08E+15	3.20E+15	3.34E+15	3.74E+15	3.96E+15	4.22E+15	5.25E+15	5.40E+15	5.66E+15	5.99E+15	6.29E+15
Cm-242	3.05E+14	4.07E+14	4.63E+14	1.93E+15	2.03E+15	2.32E+15	2.52E+15	2.72E+15	3.66E+15	3.81E+15	4.03E+15	4.37E+15	4.66E+15
Cm-244	4.11E+12	6.40E+12	7.84E+12	9.99E+13	1.11E+14	1.51E+14	1.83E+14	2.19E+14	4.66E+14	5.33E+14	6.44E+14	8.55E+14	1.11E+15

Table A-5. BWR Core-Averaged Inventory of Radionuclides as a Function of Burnup (Bq/MTU) (from NUREG.CR-6703)

	Peak Rod Burnup, GWd/MTU												
Nuclide	22	24	25	42	43	46	48	50	60	62	65	70	75
H-3	1.15E+13	1.24E+13	1.30E+13	2.10E+13	2.14E+13	2.28E+13	2.36E+13	2.45E+13	2.88E+13	2.96E+13	3.08E+13	3.28E+13	3.47E+13
Co-58	3.13E+14	3.11E+14	3.12E+14	3.40E+14	3.42E+14	3.39E+14	3.41E+14	3.44E+14	3.59E+14	3.61E+14	3.65E+14	3.69E+14	3.74E+14
Co-60	1.65E+14	1.78E+14	1.85E+14	2.92E+14	2.98E+14	3.16E+14	3.28E+14	3.40E+14	4.00E+14	4.11E+14	4.29E+14	4.59E+14	4.88E+14
Kr-85m	6.51E+15	6.51E+15	6.44E+15	5.48E+15	5.44E+15	5.33E+15	5.22E+15	5.11E+15	4.63E+15	4.10E+15	4.40E+15	4.18E+15	3.96E+15
Kr-85	2.57E+14	2.75E+14	2.85E+14	4.14E+14	4.22E+14	4.40E+14	4.51E+14	4.63E+14	5.11E+14	5.18E+14	5.29E+14	5.44E+14	5.59E+14
Kr-87	1.32E+16	1.32E+16	1.30E+16	1.10E+16	1.09E+16	1.07E+16	1.04E+16	1.02E+16	9.18E+15	8.95E+15	8.70E+15	8.25E+15	7.77E+15
Kr-88	1.85E+16	1.84E+16	1.82E+16	1.52E+16	1.51E+16	1.48E+16	1.44E+16	1.41E+16	1.26E+16	1.22E+16	1.19E+16	1.12E+16	1.05E+16
Rb-86	2.33E+13	2.51E+13	2.63E+13	4.96E+13	5.14E+13	5.40E+13	5.74E+13	6.03E+13	7.73E+13	8.07E+13	8.58E+13	9.40E+13	1.02E+14
Sr-89	2.58E+16	2.54E+16	2.52E+16	2.11E+16	2.08E+16	2.02E+16	1.98E+16	1.94E+16	1.72E+16	1.68E+16	1.62E+16	1.52E+16	1.42E+16
Sr-90	2.25E+15	2.42E+15	2.50E+15	3.77E+15	3.85E+15	4.03E+15	4.14E+15	4.26E+15	4.77E+15	4.88E+15	5.00E+15	5.22E+15	5.40E+15
Sr-91	3.17E+16	3.17E+16	3.13E+16	2.66E+16	2.65E+16	2.60E+16	2.55E+16	2.48E+16	2.26E+16	2.21E+16	2.15E+16	2.05E+16	1.94E+16
Sr-92	3.29E+16	3.28E+16	3.25E+16	2.83E+16	2.82E+16	2.78E+16	2.73E+16	2.67E+16	2.47E+16	2.42E+16	2.37E+16	2.29E+16	2.18E+16
Y-90	2.34E+15	2.50E+15	2.60E+15	3.90E+15	3.98E+15	4.16E+15	4.31E+15	4.42E+15	4.98E+15	5.09E+15	5.24E+15	5.47E+15	5.66E+15
Y-91	3.25E+16	3.21E+16	3.19E+16	2.73E+16	2.71E+16	2.64E+16	2.59E+16	2.55E+16	2.31E+16	2.26E+16	2.20E+16	2.09E+16	1.99E+16
Y-92	3.31E+16	3.31E+16	3.28E+16	2.85E+16	2.84E+16	2.79E+16	2.75E+16	2.69E+16	2.49E+16	2.44E+16	2.39E+16	2.30E+16	2.19E+16
Y-93	2.45E+16	2.45E+16	2.43E+16	2.17E+16	2.16E+16	2.14E+16	2.11E+16	2.07E+16	1.95E+16	1.92E+16	1.89E+16	1.84E+16	1.77E+16
Zr-95	4.12E+16	4.08E+16	4.08E+16	3.80E+16	3.80E+16	3.75E+16	3.73E+16	3.70E+16	3.56E+16	3.53E+16	3.49E+16	3.43E+16	3.35E+16
Zr-97	3.83E+16	3.84E+16	3.83E+16	3.71E+16	3.71E+16	3.71E+16	3.69E+16	3.66E+16	3.62E+16	3.60E+16	3.59E+16	3.57E+16	3.52E+16
Nb-95	4.16E+16	4.12E+16	4.08E+16	3.84E+16	3.80E+16	3.77E+16	3.75E+16	3.72E+16	3.58E+16	3.55E+16	3.51E+16	3.45E+16	3.39E+16
Mo-99	4.14E+16	4.18E+16	4.18E+16	4.11E+16	4.11E+16	4.11E+16	4.11E+16	4.07E+16	4.07E+16	4.03E+16	4.03E+16	4.03E+16	4.00E+16
Tc-99m	3.67E+16	3.70E+16	3.69E+16	3.63E+16	3.64E+16	3.66E+16	3.64E+16	3.62E+16	3.61E+16	3.60E+10	3.60E+16	3.60E+16	3.56E+16
Ru-103	3.02E+16	3.05E+16	3.07E+16	3.43E+16	3.46E+16	3.51E+16	3.56E+16	3.59E+16	3.77E+16	3.81E+16	3.85E+16	3.92E+16	4.00E+16
Ru-105	1.77E+16	1.82E+16	1.84E+16	2.32E+16	2.35E+16	2.44E+16	2.48E+16	2.52E+16	2.78E+16	2.82E+16	2.90E+16	3.00E+16	3.07E+16
Ru-106	8.36E+15	9.03E+15	9.36E+15	1.45E+16	1.48E+16	1.57E+16	1.62E+16	1.68E+16	1.94E+16	1.99E+16	2.06E+16	2.18E+16	2.29E+16
Rh-105	1.71E+16	1.75E+16	1.77E+16	2.22E+16	2.25E+16	2.33E+16	2.36E+16	2.40E+16	2.63E+16	2.66E+16	2.73E+16	2.82E+16	2.89E+16
Sb-125	1.78E+14	1.92E+14	1.99E+14	3.05E+14	3.10E+14	3.26E+14	3.37E+14	3.47E+14	3.95E+14	4.04E+14	4.16E+14	4.37E+14	4.58E+14
Sb-127	1.55E+15	1.58E+15	1.59E+15	1.84E+15	1.86E+15	1.90E+15	1.93E+15	1.94E+15	2.07E+15	2.08E+15	2.12E+15	2.17E+15	2.19E+15
Te-127m	2.57E+14	2.64E+14	2.68E+14	3.13E+14	3.15E+14	3.23E+14	3.28E+14	3.32E+14	3.53E+14	3.57E+14	3.63E+14	3.70E+14	3.81E+14

Table A-5. (contd)

Nuclide	Peak Rod Burnup, GWd/MTU												
	22	24	25	42	43	46	48	50	60	62	65	70	75
Te-127	1.53E+15	1.56E+15	1.58E+15	1.82E+15	1.84E+15	1.89E+15	1.91E+15	1.93E+15	2.05E+15	2.07E+15	2.11E+15	2.15E+15	2.18E+15
Te-129m	1.24E+15	1.24E+15	1.25E+15	1.34E+15	1.34E+15	1.35E+15	1.36E+15	1.37E+15	1.41E+15	1.41E+15	1.42E+15	1.44E+15	1.44E+15
Te-129	6.14E+15	6.22E+15	6.25E+15	6.59E+15	6.62E+15	6.70E+15	6.73E+15	6.73E+15	6.92E+15	6.92E+15	6.99E+15	7.07E+15	7.07E+15
Te-131mn	3.81E+15	3.85E+15	3.89E+15	4.26E+15	4.26E+15	4.37E+15	4.37E+15	4.40E+15	4.55E+15	4.59E+15	4.63E+15	4.70E+15	4.70E+15
Te-132	3.11E+16	3.13E+16	3.13E+16	3.12E+16	3.13E+16	3.14E+16	3.14E+16	3.12E+16	3.13E+16	3.12E+16	3.13E+16	3.13E+16	3.09E+16
I-131	2.15E+16	2.14E+16	2.15E+16	2.18E+16	2.18E+16	2.18E+16	2.18E+16	2.18E+16	2.19E+16	2.19E+16	2.19E+16	2.19E+16	2.19E+16
I-132	3.15E+16	3.17E+16	3.17E+16	3.17E+16	3.19E+16	3.20E+16	3.20E+16	3.18E+16	3.20E+16	3.19E+16	3.19E+16	3.20E+16	3.16E+16
I-133	4.59E+16	4.59E+16	4.59E+16	4.48E+16	4.51E+16	4.51E+16	4.51E+16	4.48E+16	4.44E+16	4.40E+16	4.40E+16	4.40E+16	4.33E+16
I-134	5.14E+16	5.14E+16	5.14E+16	4.96E+16	5.00E+16	5.00E+16	4.96E+16	4.92E+16	4.85E+16	4.81E+16	4.81E+16	4.77E+16	4.70E+16
I-135	4.33E+16	4.37E+16	4.33E+16	4.29E+16	4.29E+18	4.29E+16	4.29E+16	4.26E+16	4.26E+16	4.22E+16	4.26E+16	4.22E+16	4.18E+16
Xe-133	4.59E+16	4.40E+16	4.44E+16	4.51E+16	4.51E+16	4.33E+16	4.37E+16	4.48E+16	4.37E+16	4.44E+16	4.44E+16	4.44E+16	4.37E+16
Xc-135	2.21E+16	2.12E+16	2.11E+16	1.87E+16	1.86E+16	1.78E+16	1.74E+16	1.71E+16	1.58E+16	1.55E+16	1.52E+16	1.46E+16	1.42E+16
Cs-134	2.13E+15	2.44E+15	2.60E+15	5.99E+15	6.22E+15	6.88E+15	7.29E+15	7.77E+15	1.01E+16	1.07E+16	1.14E+16	1.26E+16	1.39E+16
Cs-136	9.58E+14	1.03E+15	1.07E+15	1.92E+15	1.98E+15	2.10E+15	2.22E+15	2.33E+15	2.95E+15	3.06E+15	3.26E+15	3.56E+15	3.89E+15
Cs-137	2.67E+15	2.90E+15	3.02E+15	4.96E+15	5.07E+15	5.40E+15	5.59E+15	5.81E+15	6.88E+15	7.07E+15	7.40E+15	7.88E+15	8.40E+15
Ba-139	4.14E+16	4.14E+16	4.14E+16	3.96E+16	3.96E+16	3.96E+16	3.96E+16	3.92E+16	3.85E+16	3.81E+16	3.81E+16	3.77E+16	3.70E+16
Ba-140	4.11E+16	4.14E+16	4.14E+16	3.96E+16	3.96E+16	3.96E+16	3.96E+16	3.92E+16	3.85E+16	3.85E+16	3.81E+16	3.77E+16	3.74E+16
La-140	4.18E+16	4.40E+16	4.29E+16	4.11E+16	4.11E+16	4.33E+16	4.22E+16	4.07E+16	4.11E+16	4.03E+16	4.07E+16	4.07E+16	4.00E+16
La-141	3.77E+16	3.81E+16	3.77E+16	3.62E+16	3.62E+16	3.62E+16	3.60E+16	3.56E+16	3.50E+16	3.47E+16	3.46E+16	3.42E+16	3.36E+16
La-142	3.74E+16	3.74E+16	3.74E+16	3.54E+16	3.53E+16	3.53E+16	3.51E+16	3.47E+16	3.39E+16	3.36E+16	3.34E+16	3.30E+16	3.23E+16
Ce-141	3.81E+16	3.81E+16	3.81E+16	3.65E+16	3.65E+16	3.63E+16	3.62E+16	3.60E+16	3.52E+16	3.50E+16	3.49E+16	3.45E+16	3.40E+16
Ce-143	3.64E+16	3.65E+16	3.63E+16	3.39E+16	3.39E+16	3.37E+16	3.34E+16	3.30E+16	3.20E+16	3.16E+16	3.14E+16	3.09E+16	3.02E+16
Ce-144	3.14E+16	3.18E+16	3.19E+16	3.16E+16	3.15E+16	3.12E+16	3.10E+16	3.08E+16	2.97E+16	2.95E+16	2.91E+16	2.86E+16	2.80E+16
Pr-143	3.58E+16	3.53E+16	3.52E+16	3.33E+16	3.31E+16	3.26E+16	3.24E+16	3.24E+16	3.11E+16	3.11E+16	3.07E+16	3.02E+16	3.00E+16
Nd-147	1.51E+16	1.51E+16	1.51E+16	1.47E+16	1.48E+16	1.48E+16	1.47E+16	1.47E+16	1.46E+16	1.45E+16	1.45E+16	1.44E+16	1.42E+16
Np-239	3.49E+17	3.50E+17	3.53E+17	4.14E+17	4.18E+17	4.22E+17	4.33E+17	4.40E+17	4.81E+17	4.88E+17	5.00E+17	5.18E+17	5.25E+17
Pu-238	3.10E+13	3.85E+13	4.26E+13	1.51E+14	1.59E+14	1.86E+14	2.05E+14	2.25E+14	3.31E+14	3.53E+14	3.85E+14	4.40E+14	4.92E+16
Pu-239	1.15E+13	1.19E+13	1.21E+13	1.34E+13	1.34E+13	1.34E+13	1.34E+13	1.34E+13	1.31E+13	1.31E+13	1.30E+13	1.28E+13	1.28E+13
Pu-240	9.18E+12	1.04E+13	1.10E+13	1.97E+13	2.01E+13	2.14E+13	2.23E+13	2.32E+13	2.65E+13	2.69E+13	2.76E+13	2.86E+13	2.89E+13

Table A-5. (contd)

Pu-241	2.81E+15	3.04E+15	3.16E+15	5.44E+15	5.59E+15	5.85E+15	5.92E+15	6.03E+15	6.70E+15	6.81E+15	6.96E+15	7.10E+15	7.36E+15
Am-241	2.94E+12	3.66E+12	4.03E+12	9.62E+12	9.95E+12	1.09E+13	1.14E+13	1.19E+13	1.33E+13	1.34E+13	1.36E+13	1.37E+13	1.38E+13
Am-242	8.07E+14	9.88E+14	1.09E+15	3.06E+15	3.20E+15	3.56E+15	3.81E+15	4.03E+15	5.03E+15	5.18E+15	5.40E+15	5.66E+15	5.85E+15
Cm-242	3.63E+14	4.77E+14	5.40E+14	1.97E+15	2.06E+15	2.36E+15	2.56E+15	2.76E+15	3.65E+15	3.81E+15	4.00E+15	4.26E+15	4.48E+15
Cm-244	4.88E+12	7.55E+12	9.25E+12	1.09E+14	1.21E+14	1.62E+14	1.94E+14	2.30E+14	4.85E+14	5.51E+14	6.62E+14	8.70E+14	1.13E+15

APPENDIX B

DETAILED FLOW AND TRANSPORT MODELING RESULTS

APPENDIX B

DETAILED FLOW AND TRANSPORT MODELING RESULTS

B.1 Lake Transport Results

B.1.1 Lake Short-Term Simulations

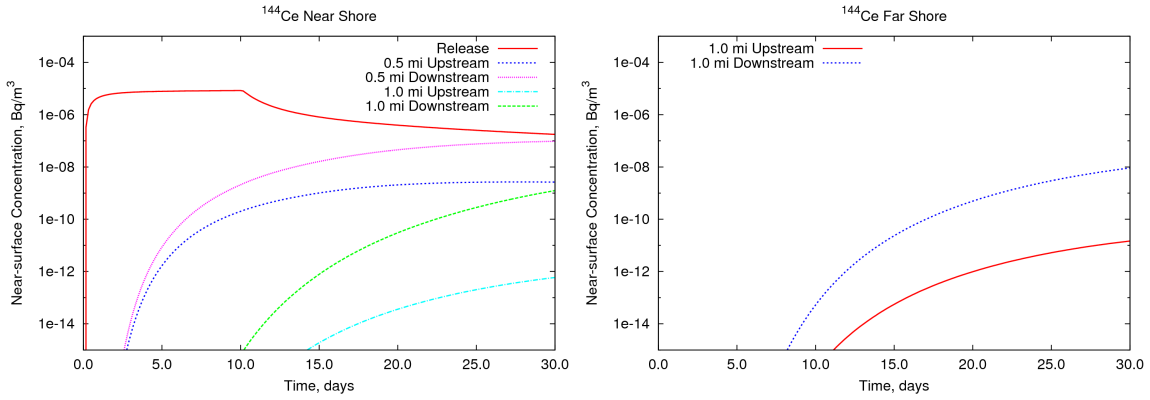

Figure B-1. Simulated lake aqueous-only ^{144}Ce activity over time at several locations along the same shore as the release (left) and the opposite shore (right).

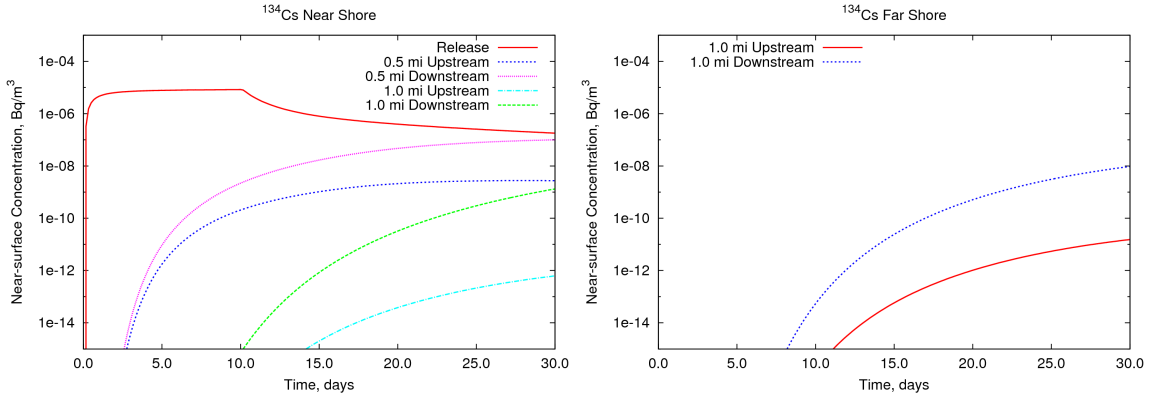

Figure B-2. Simulated lake aqueous-only ^{134}Cs activity over time at several locations along the same shore as the release (left) and the opposite shore (right).

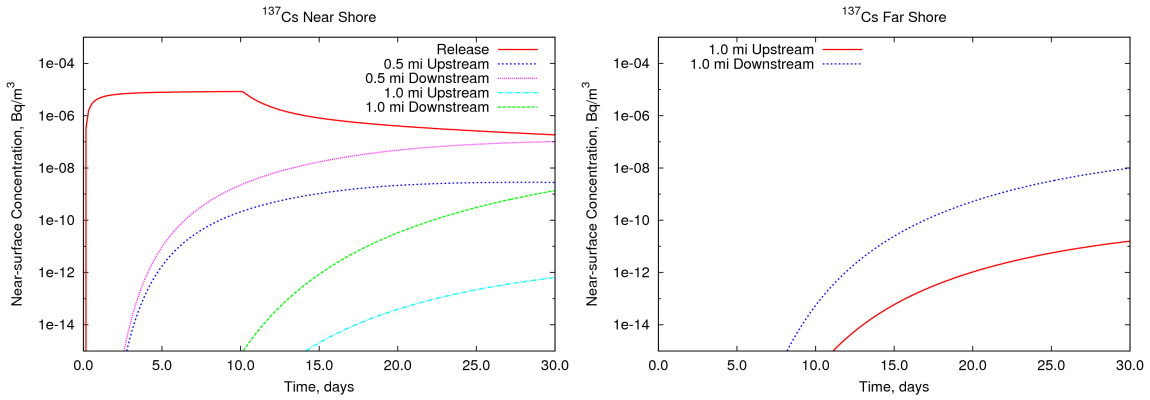

Figure B-3. Simulated lake aqueous-only ^{137}Cs activity over time at several locations along the same shore as the release (left) and the opposite shore (right).

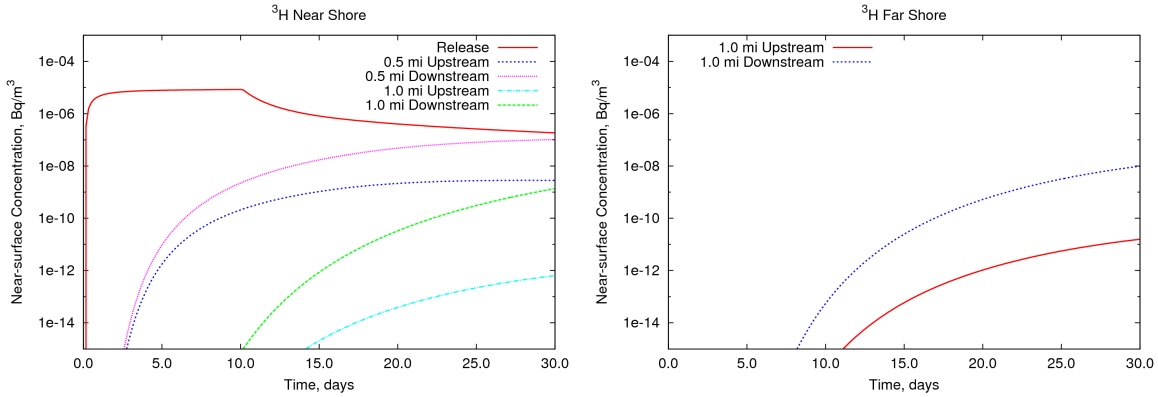

Figure B-4. Simulated lake aqueous-only ^{3}H activity over time at several locations along the same shore as the release (left) and the opposite shore (right).

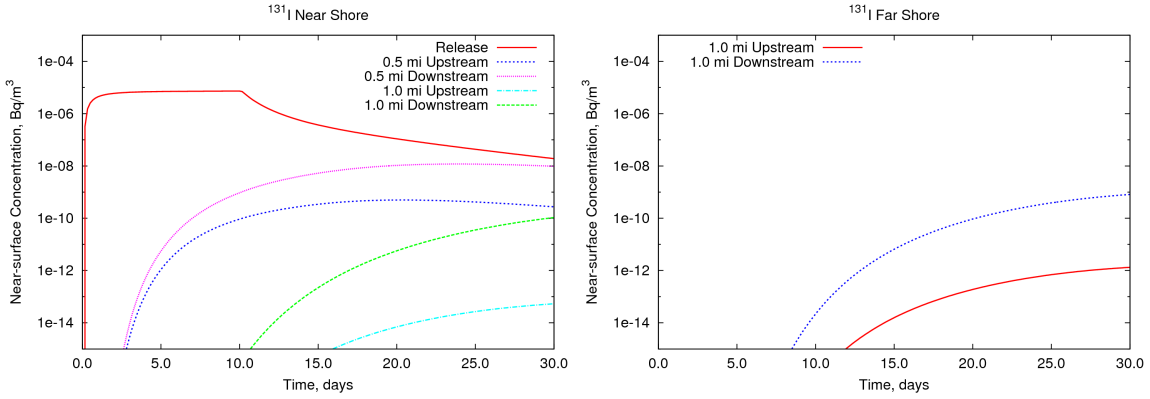

3

Figure B-5. Simulated lake aqueous-only ^{131}I activity over time at several locations along the same shore as the release (left) and the opposite shore (right).

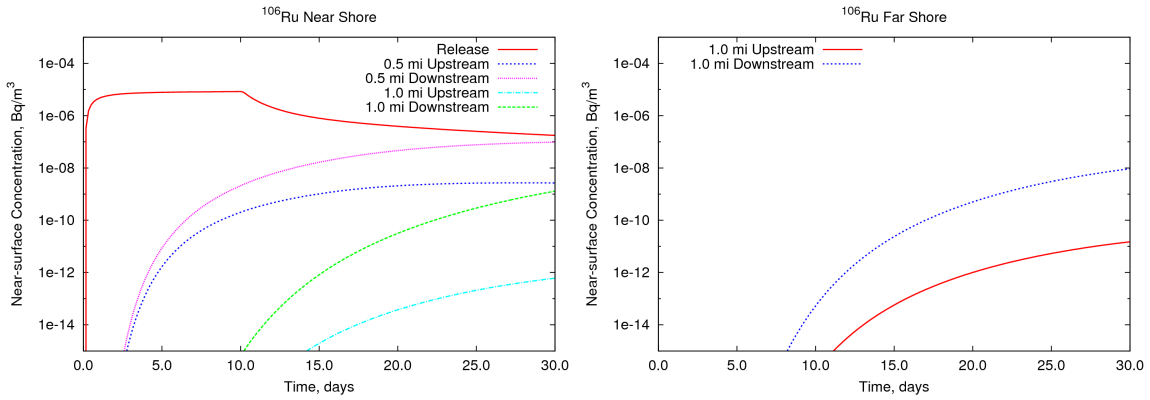

Figure B-6. Simulated lake aqueous-only ^{106}Ru activity over time at several locations along the same shore as the release (left) and the opposite shore (right).

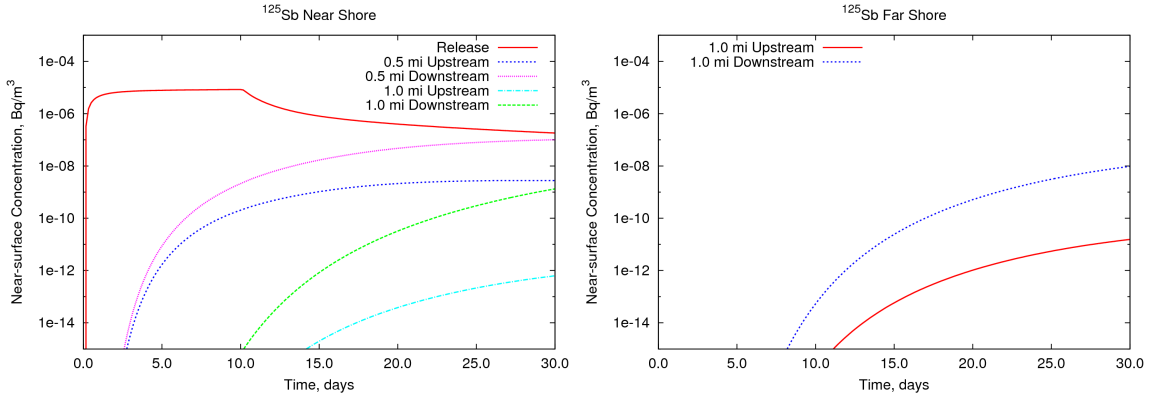

Figure B-7. Simulated lake aqueous-only ^{125}Sb activity over time at several locations along the same shore as the release (left) and the opposite shore (right).

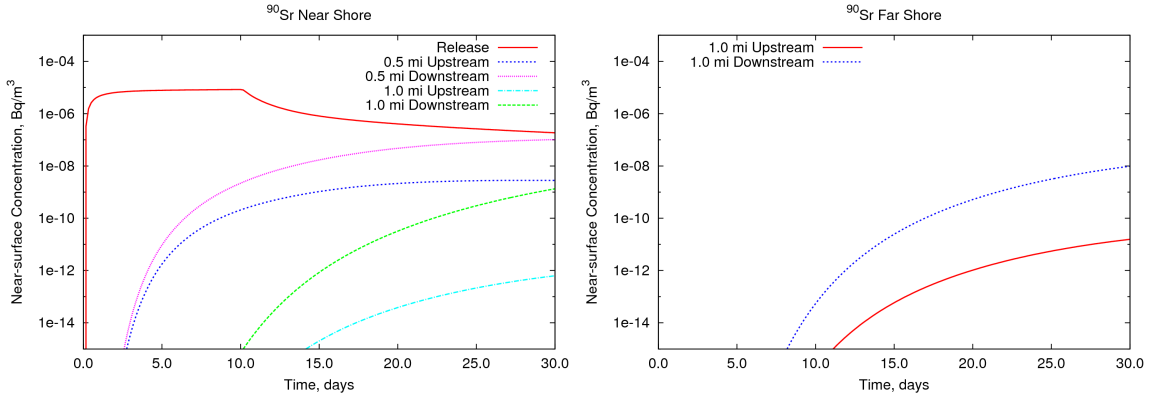

Figure B-8. Simulated lake aqueous-only ^{90}Sr activity over time at several locations along the same shore as the release (left) and the opposite shore (right).

B.1.2 One Year

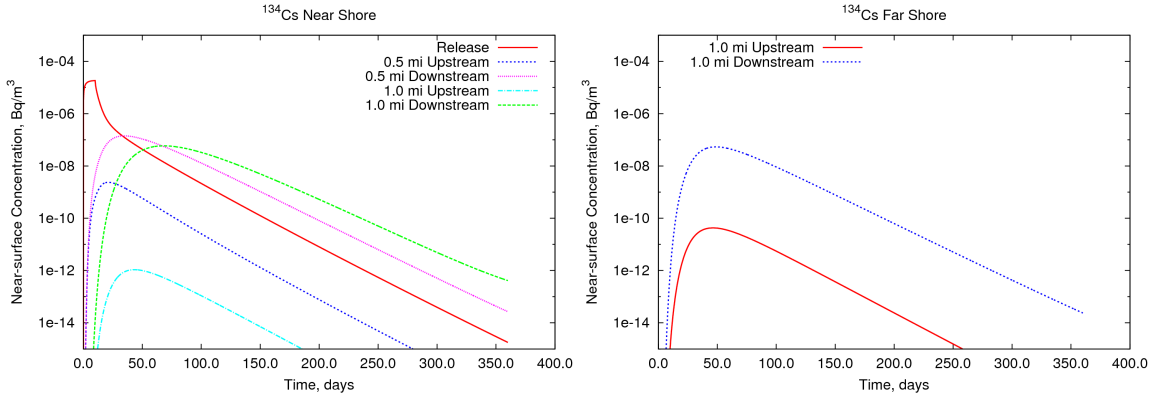

Figure B-9. Simulated lake aqueous-only ^{134}Cs activity over a full year at several locations along the same shore as the release (left) and the opposite shore (right).

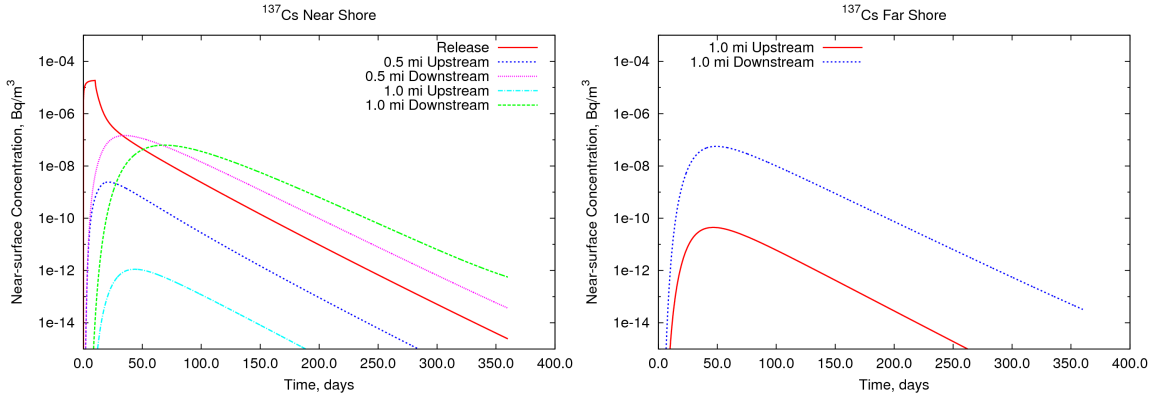

Figure B-10. Simulated lake aqueous-only ^{137}Cs activity over a full year at several locations along the same shore as the release (left) and the opposite shore (right).

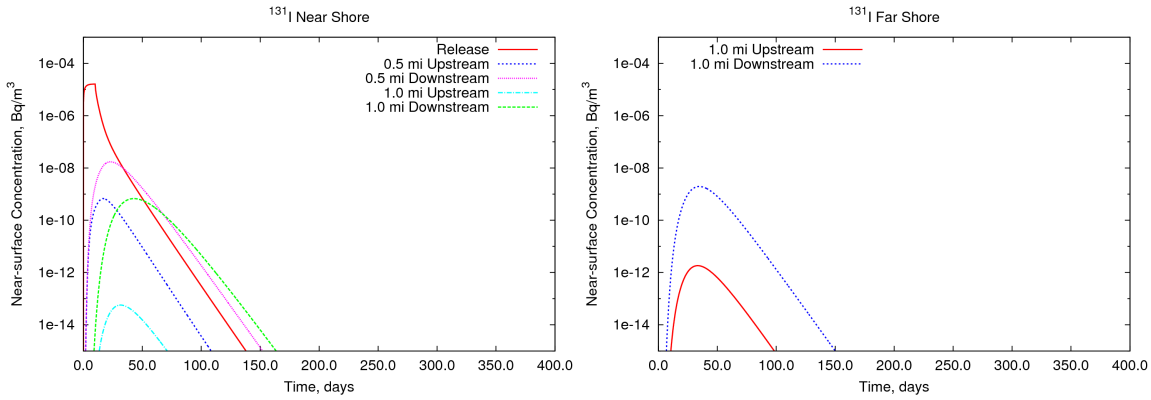

Figure B-11. Simulated lake aqueous-only ^{131}I activity over a full year at several locations along the same shore as the release (left) and the opposite shore (right).

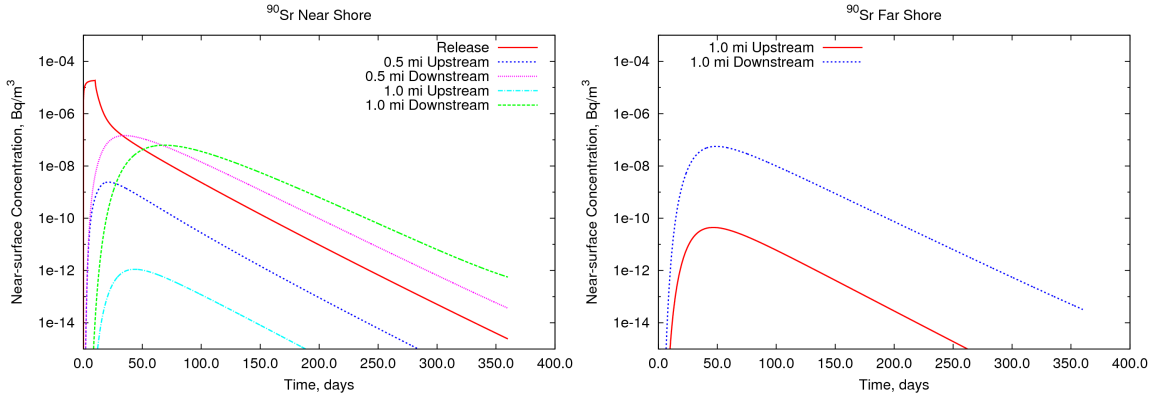

Figure B-12. Simulated lake aqueous-only ^{90}Sr activity over a full year at several locations along the same shore as the release (left) and the opposite shore (right).

B.1.3 Sensitivity

B.1.3.1 Increased Mixing Coefficient

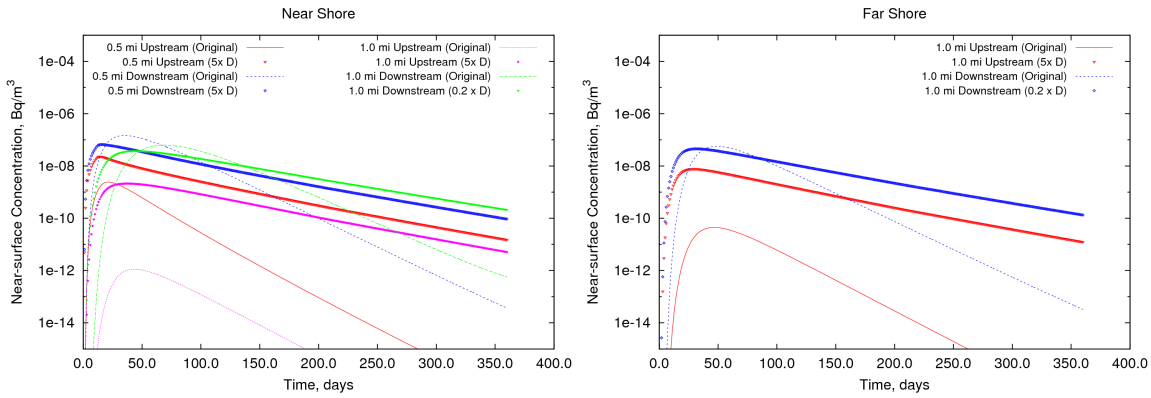

Figure B-13. Comparision of lake aqueous-only ^{137}Cs activity concentrations from the one-year and increased mixing coefficient simulations at locations along the same (left) and opposite (right) shore as the release

B.2 Small River

B.2.1 Aqueous Only

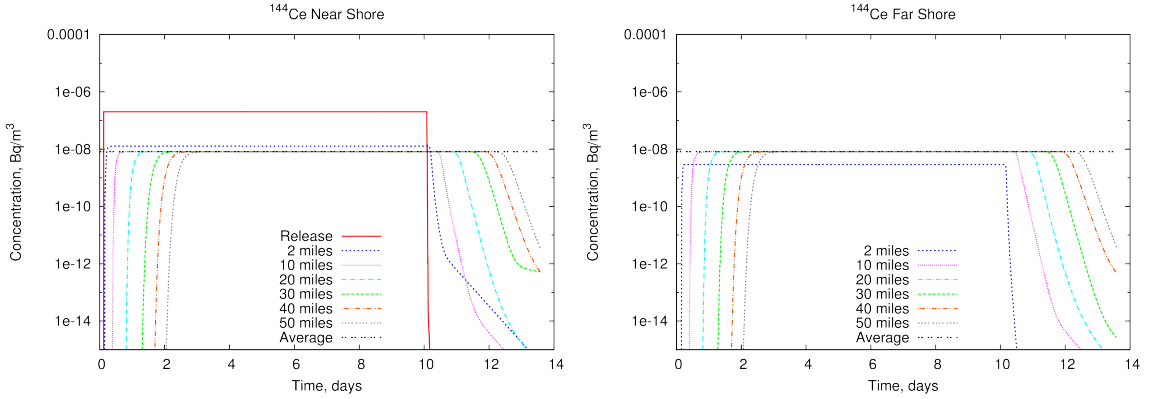

Figure B-14. Simulated small river aqueous-only ^{144}Ce activity over time at several locations along the same shore as the release (left) and the opposite shore (right).

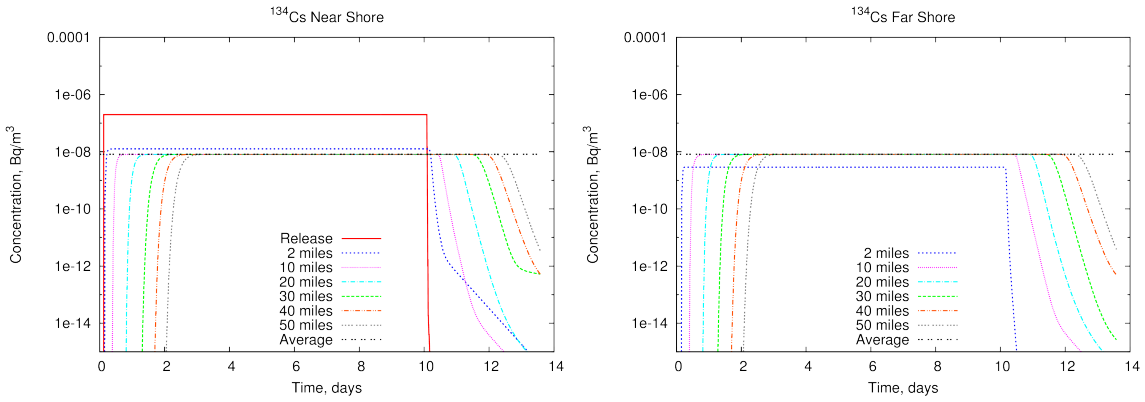

Figure B-15. Simulated small river aqueous-only ^{134}Cs activity over time at several locations along the same shore as the release (left) and the opposite shore (right).

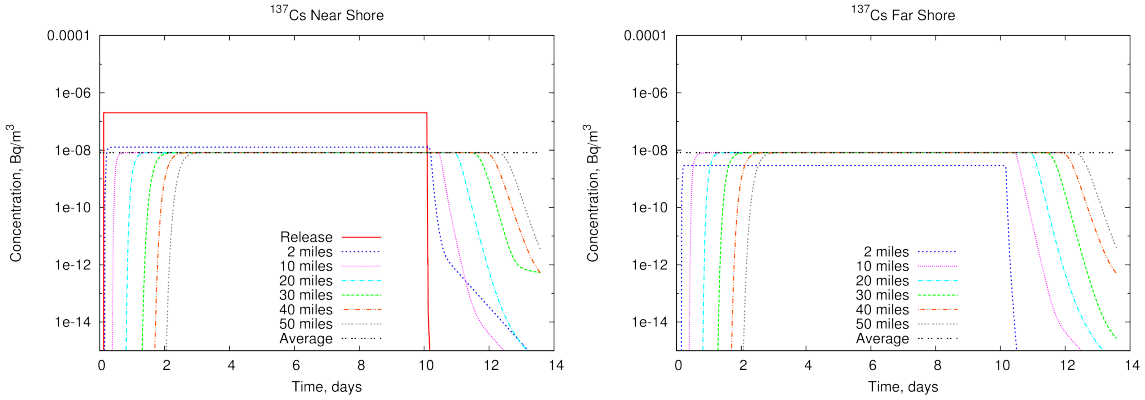

Figure B-16. Simulated small river aqueous-only ^{137}Cs activity over time at several locations along the same shore as the release (left) and the opposite shore (right).

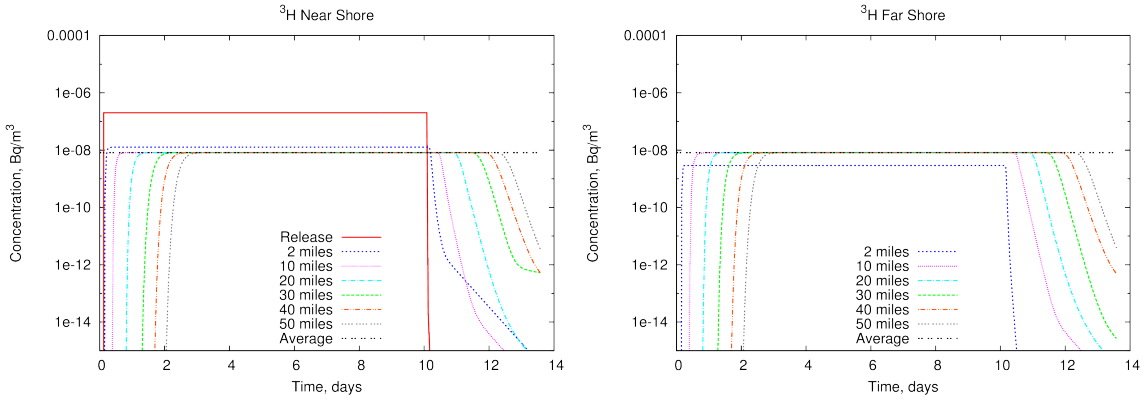

Figure B-17. Simulated small river aqueous-only ^{3}H activity over time at several locations along the same shore as the release (left) and the opposite shore (right).

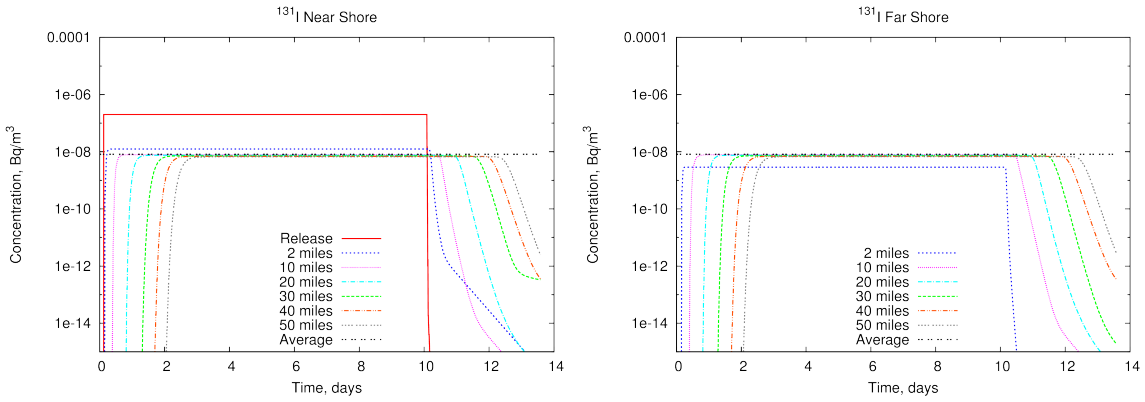

Figure B-18. Simulated small river aqueous-only ^{131}I activity over time at several locations along the same shore as the release (left) and the opposite shore (right).

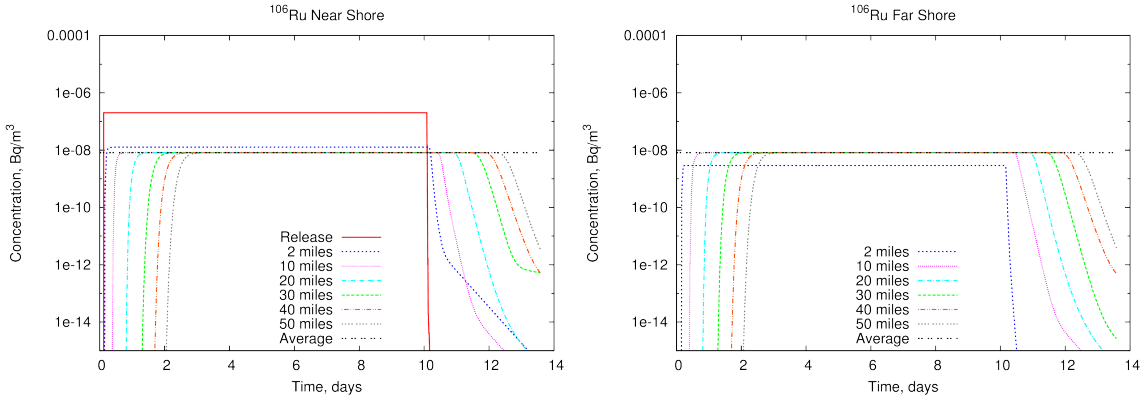

Figure B-19. Simulated small river aqueous-only ^{106}Ru activity over time at several locations along the same shore as the release (left) and the opposite shore (right).

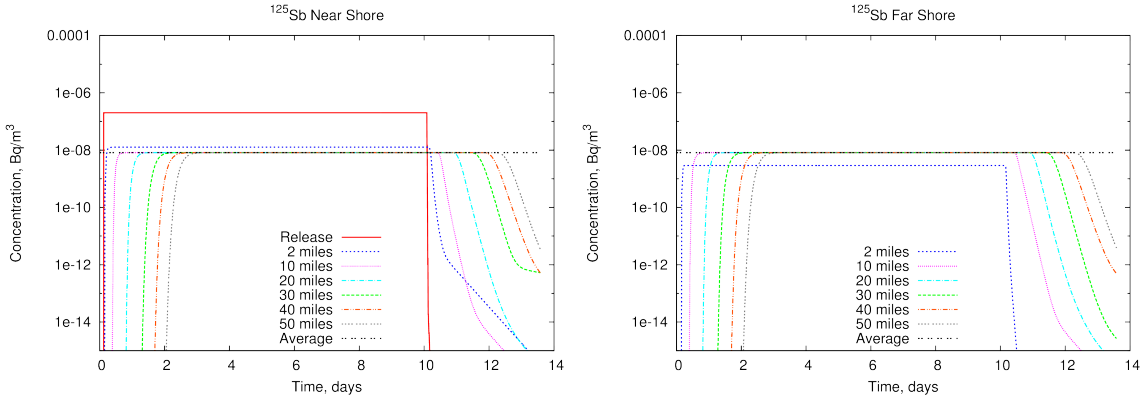

Figure B-20. Simulated small river aqueous-only ^{125}Sb activity over time at several locations along the same shore as the release (left) and the opposite shore (right).

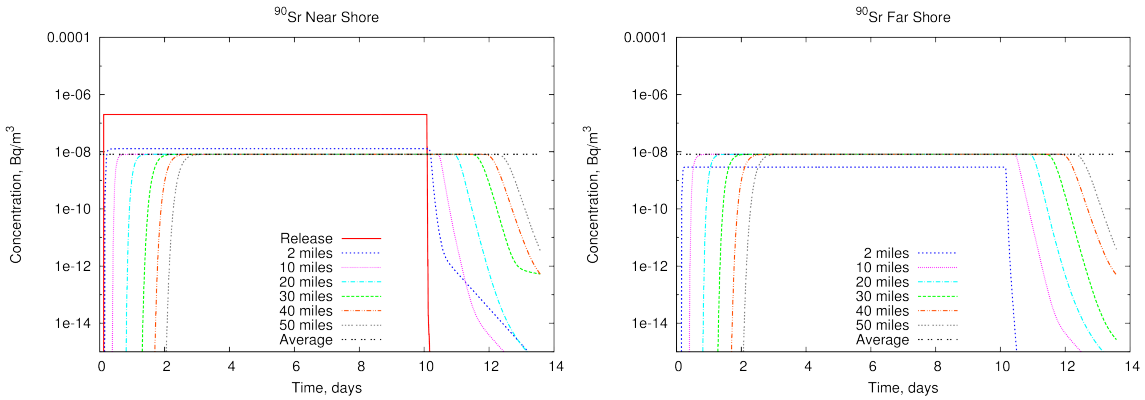

Figure B-21. Simulated small river aqueous-only ^{90}Sr activity over time at several locations along the same shore as the release (left) and the opposite shore (right).

B.2.2 Small River with Sediment

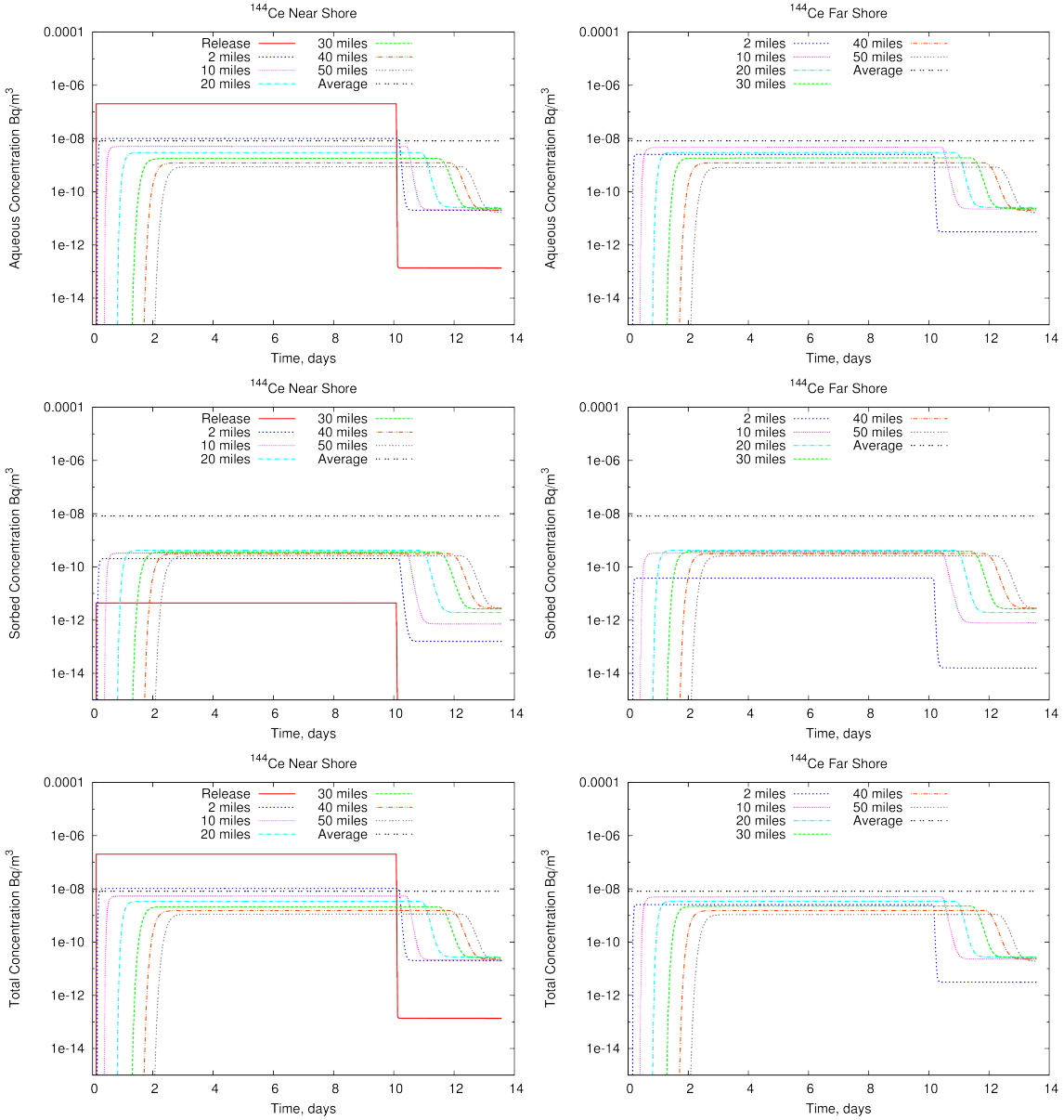

Figure B-22. Simulated small river aqueous (top), sorbed (middle), and total (bottom) ^{144}Ce activity over time at several locations along the same shore as the release (left) and the opposite shore (right).

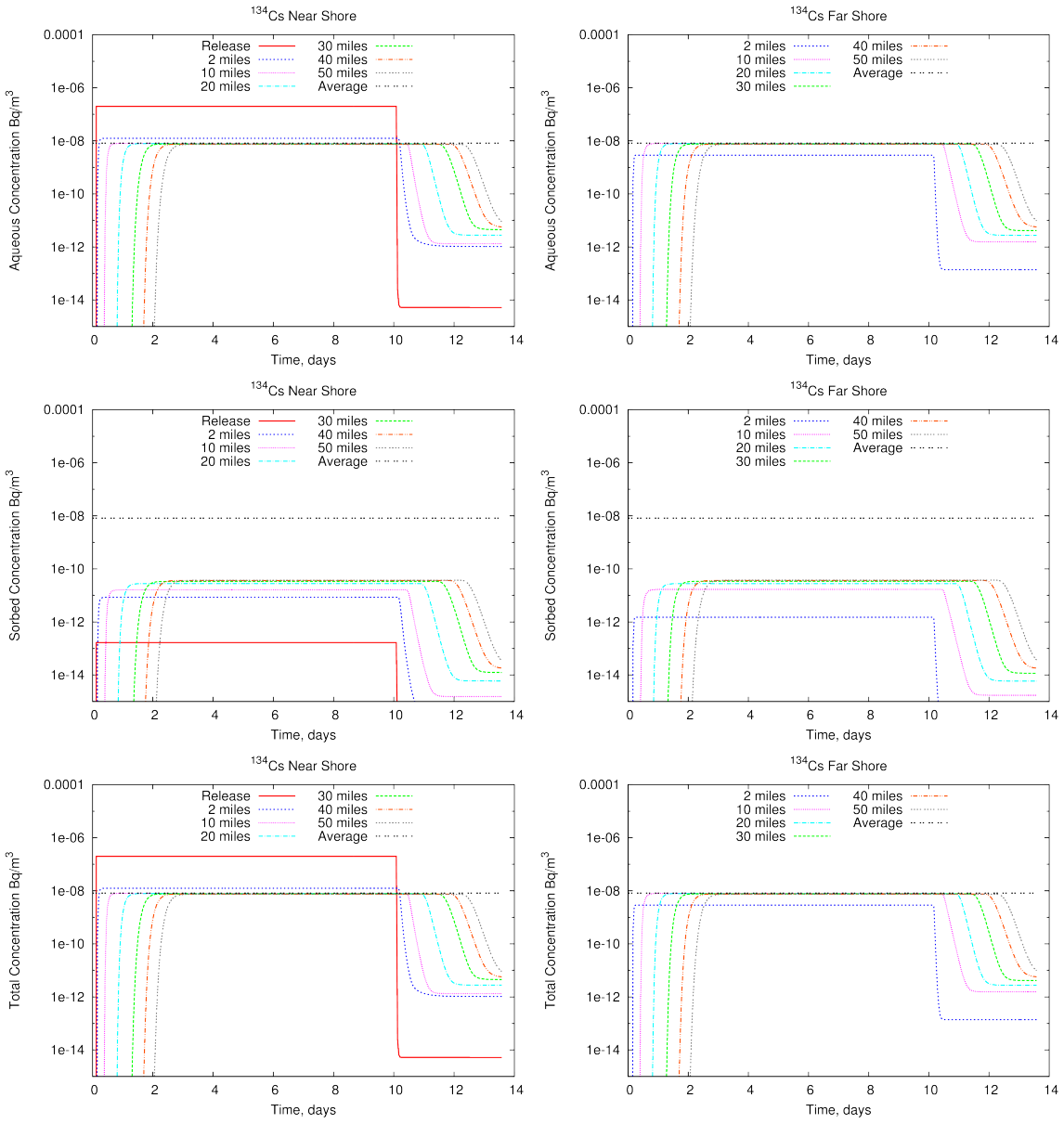

Figure B-23. Simulated small river aqueous (top), sorbed (middle), and total (bottom) ^{134}Cs activity over time at several locations along the same shore as the release (left) and the opposite shore (right).

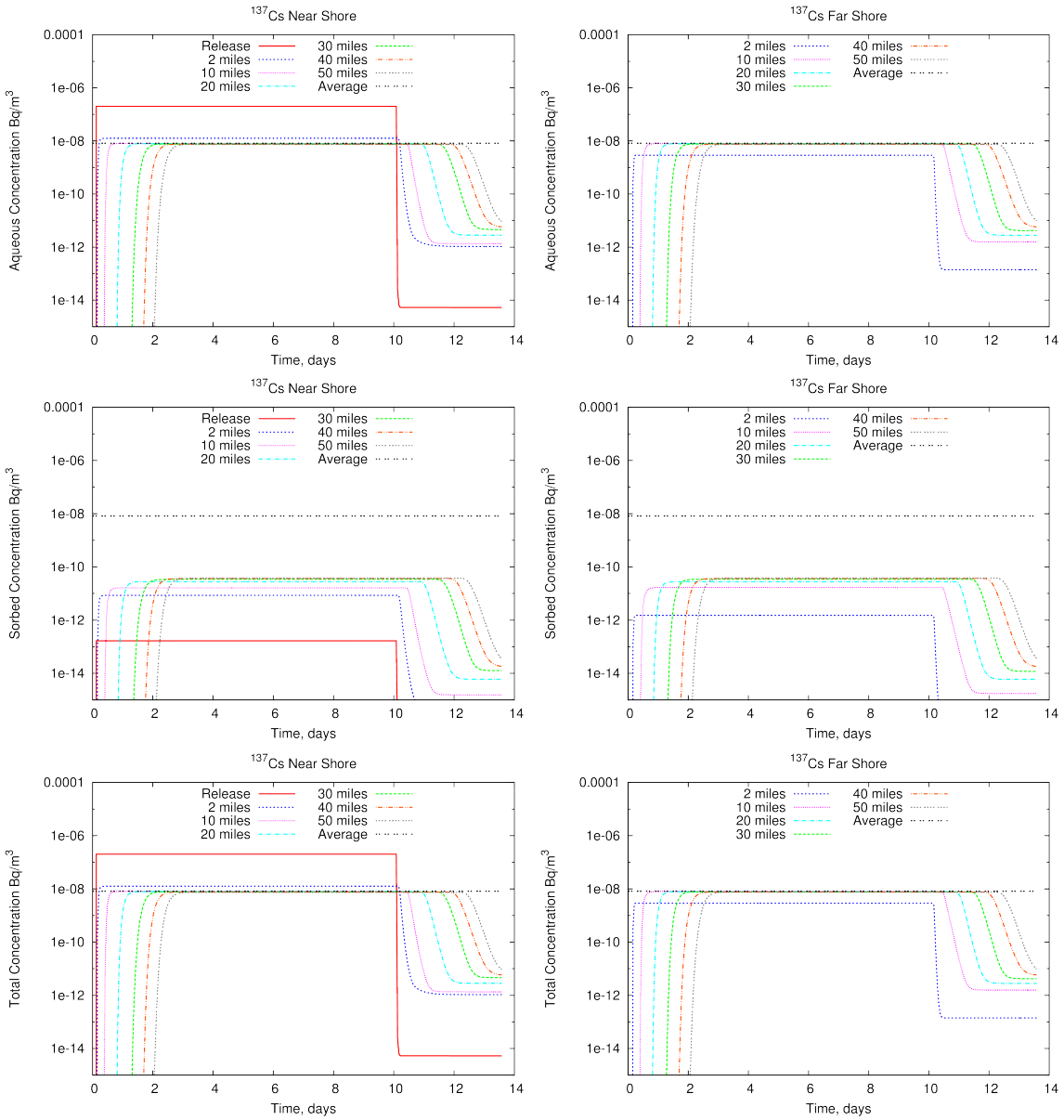

Figure B-24. Simulated small river aqueous (top), sorbed (middle), and total (bottom) ^{137}Cs activity over time at several locations along the same shore as the release (left) and the opposite shore (right).

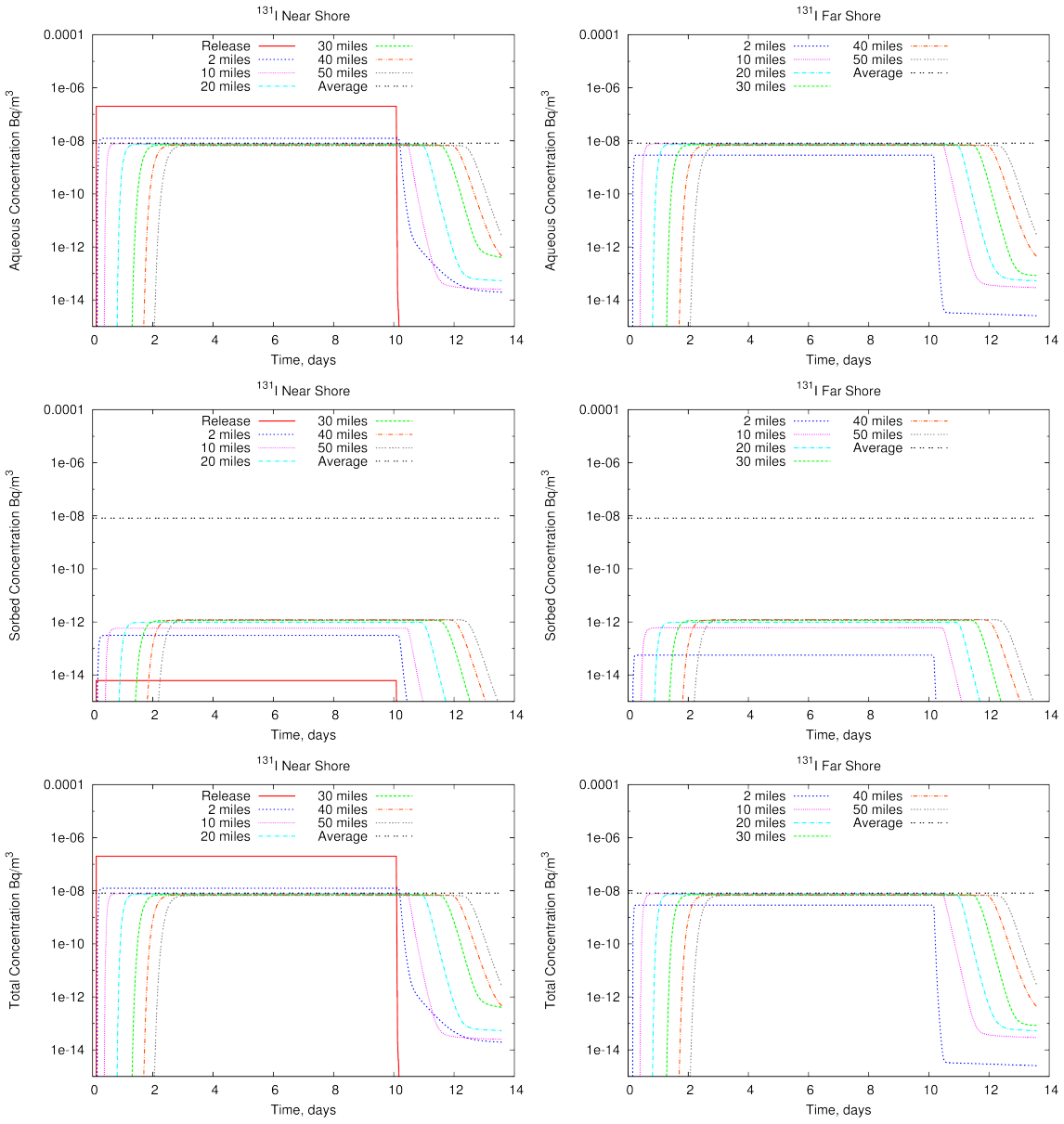

Figure B-25. Simulated small river aqueous (top), sorbed (middle), and total (bottom) ^{131}I activity over time at several locations along the same shore as the release (left) and the opposite shore (right).

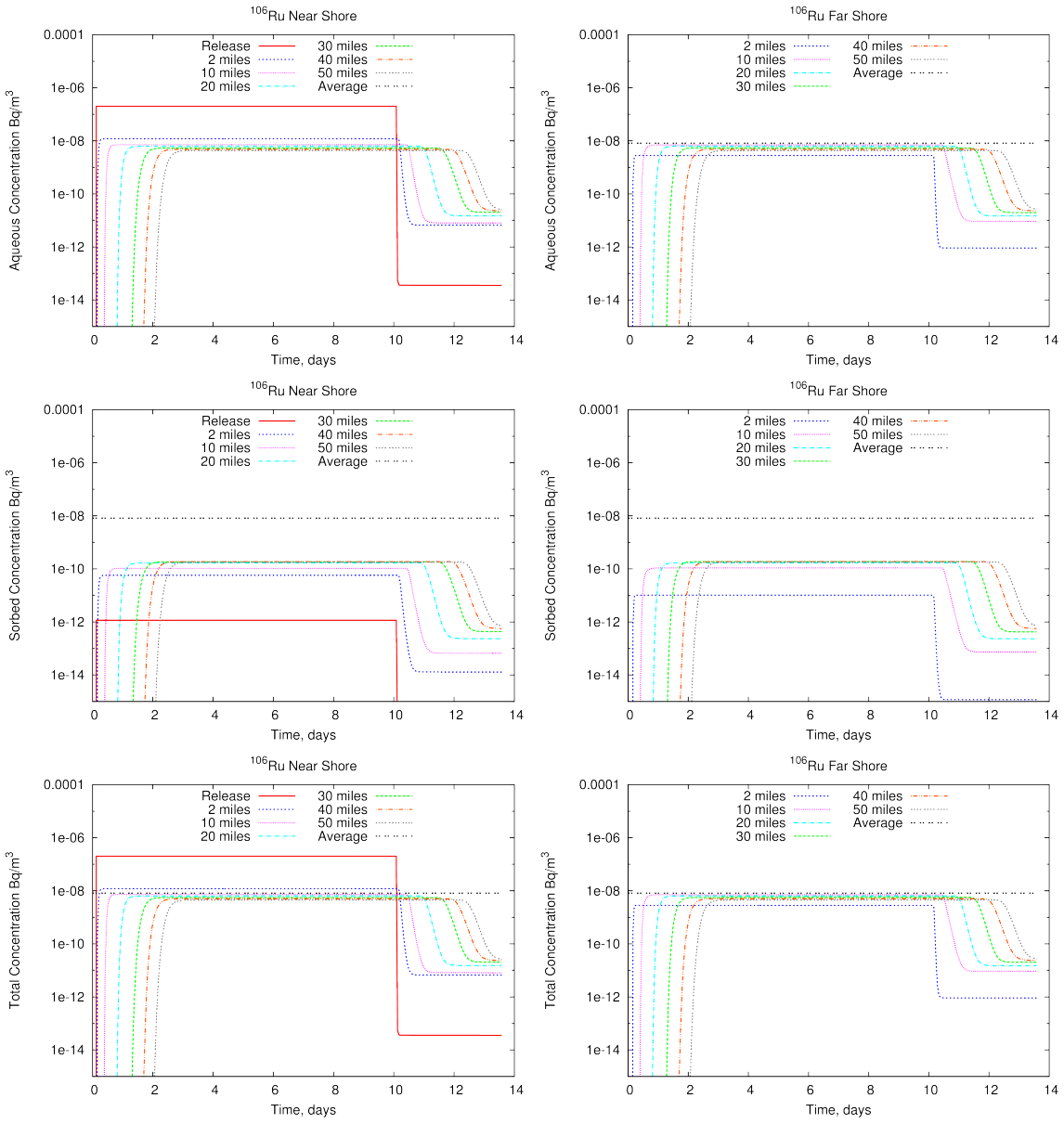

Figure B-26. Simulated small river aqueous (top), sorbed (middle), and total (bottom) ^{106}Ru activity over time at several locations along the same shore as the release (left) and the opposite shore (right).

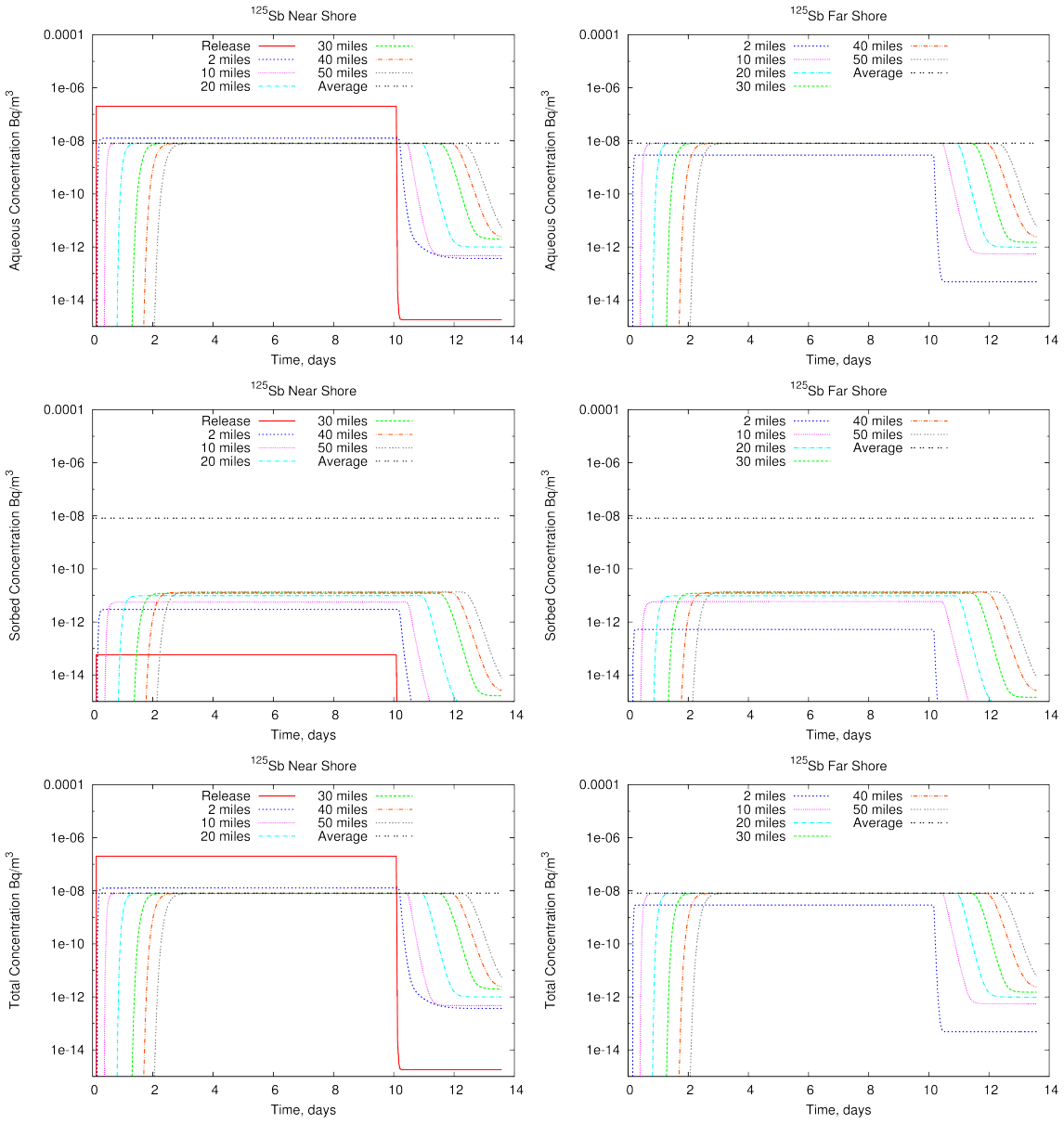

Figure B-27. Simulated small river aqueous (top), sorbed (middle), and total (bottom) ^{125}Sb activity over time at several locations along the same shore as the release (left) and the opposite shore (right).

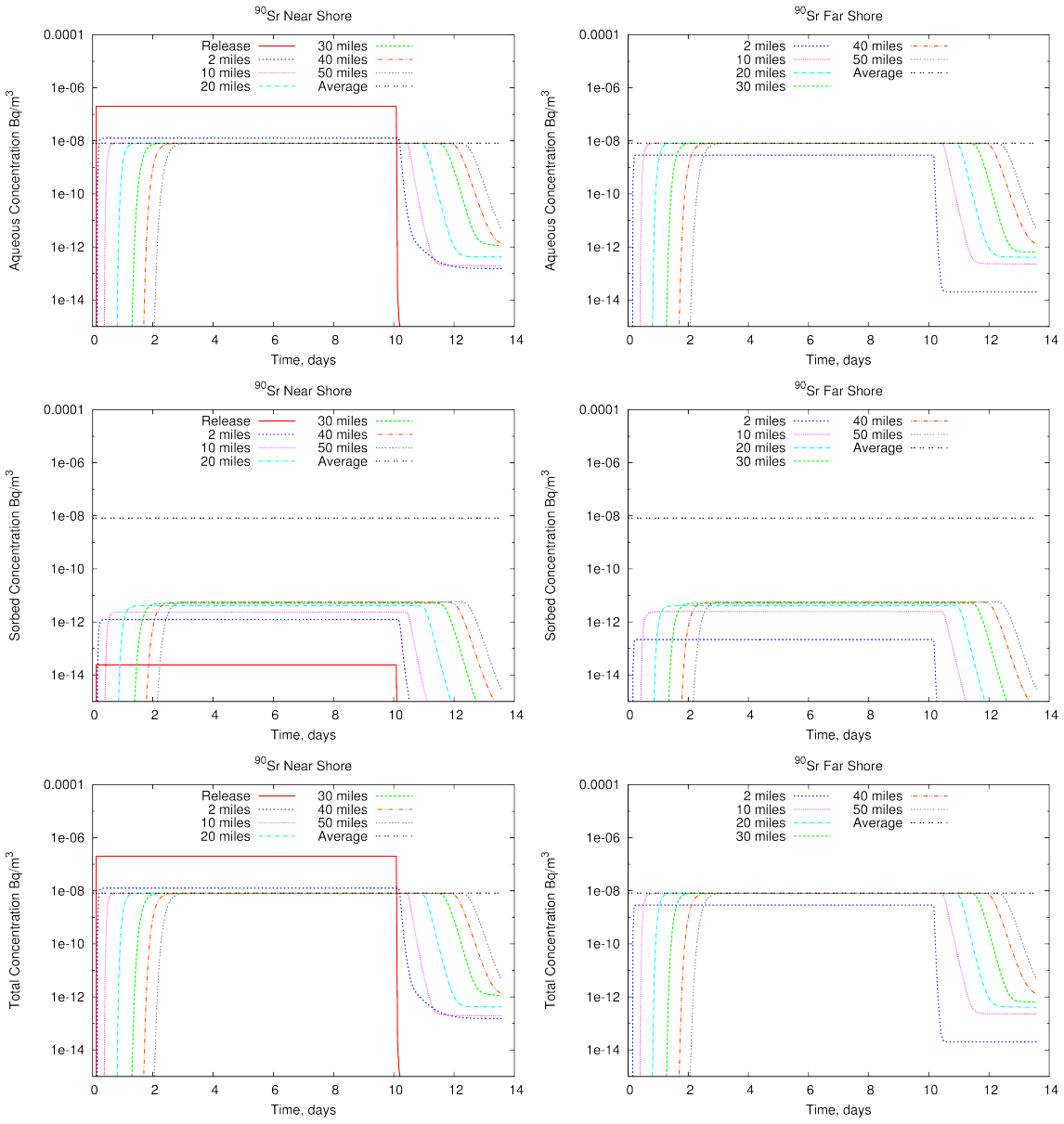

Figure B-28. Simulated small river aqueous (top), sorbed (middle), and total (bottom) ^{90}Sr activity over time at several locations along the same shore as the release (left) and the opposite shore (right).

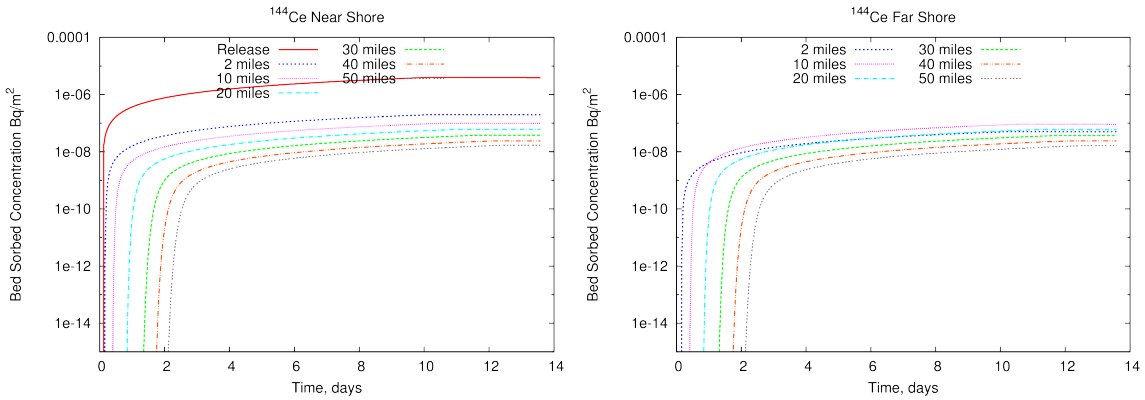

Figure B-29. Simulated small river bed-sorbed ^{144}Ce activity over time at several locations along the same shore as the release (left) and the opposite shore (right).

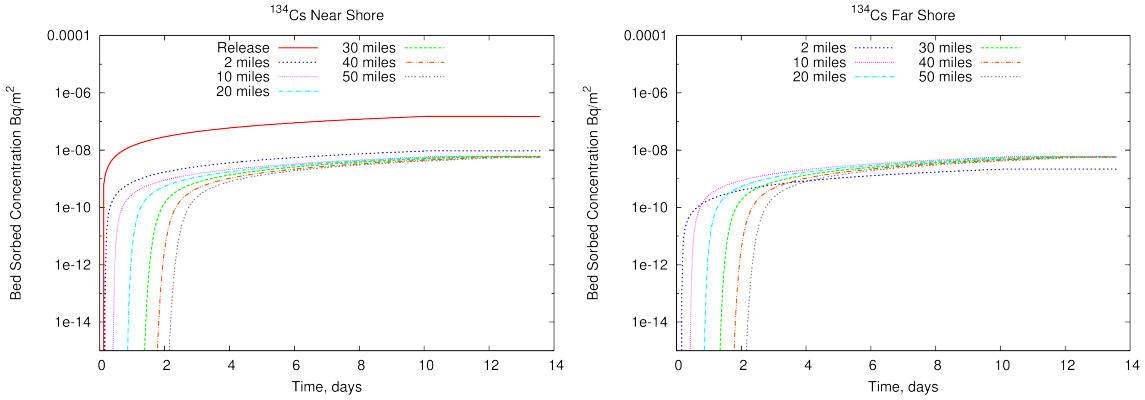

Figure B-30. Simulated small river bed-sorbed ^{134}Cs activity over time at several locations along the same shore as the release (left) and the opposite shore (right).

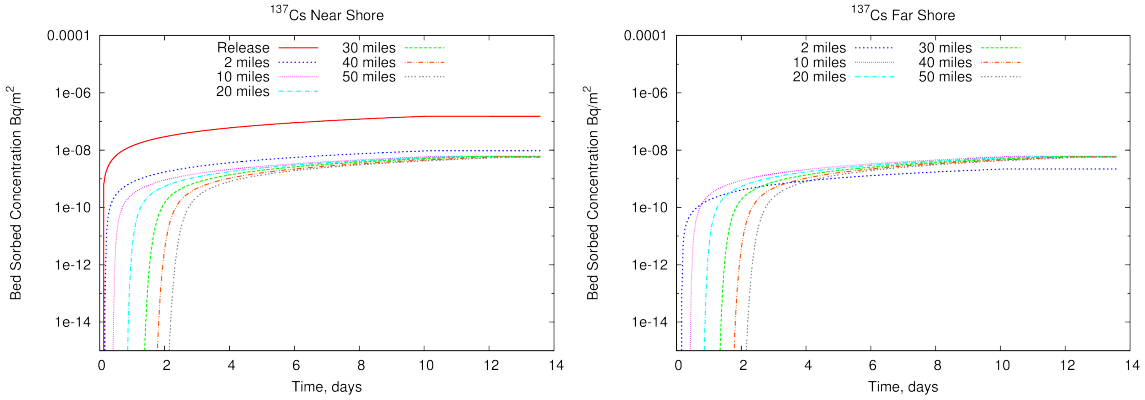

Figure B-31. Simulated small river bed-sorbed ^{137}Cs activity over time at several locations along the same shore as the release (left) and the opposite shore (right).

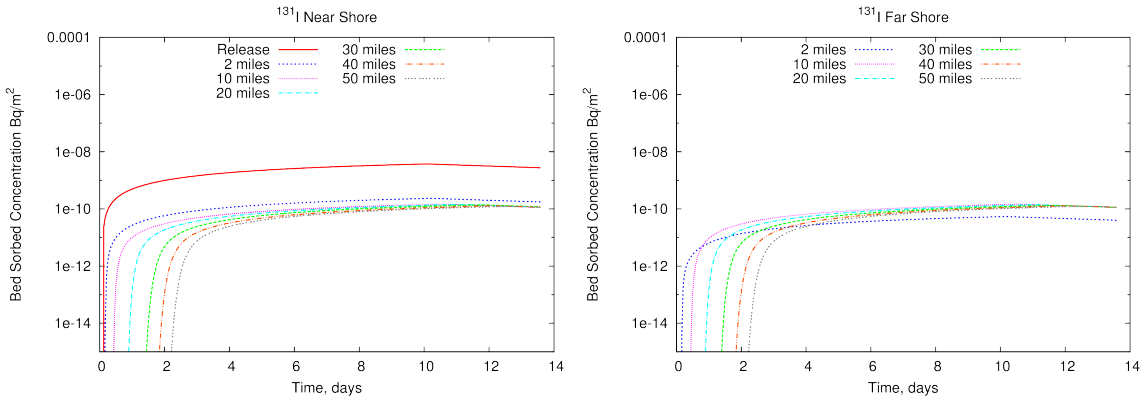

Figure B-32. Simulated small river bed-sorbed ^{131}I activity over time at several locations along the same shore as the release (left) and the opposite shore (right).

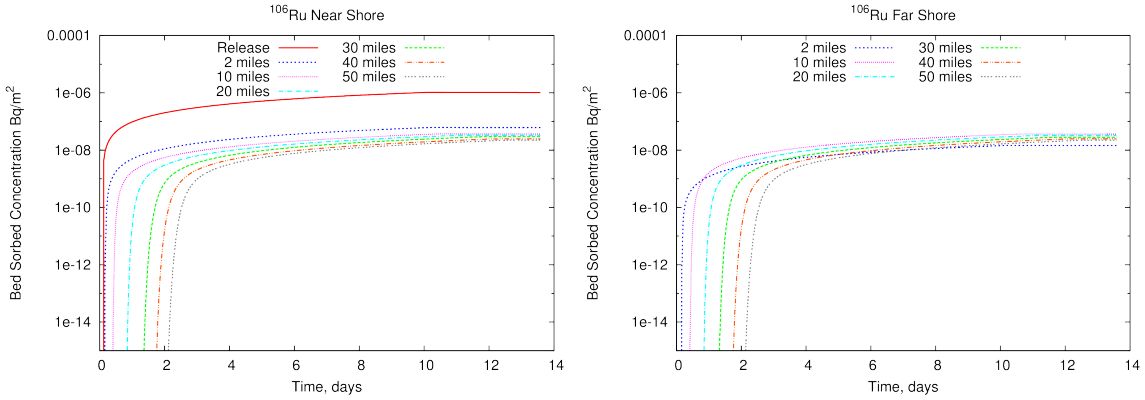

Figure B-33. Simulated small river bed-sorbed ^{106}Ru activity over time at several locations along the same shore as the release (left) and the opposite shore (right).

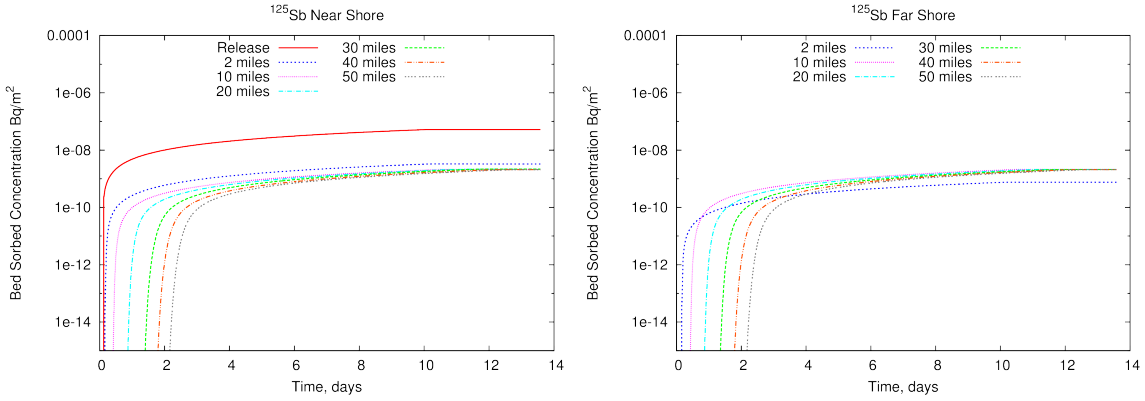

Figure B-34. Simulated small river bed-sorbed ^{125}Sb activity over time at several locations along the same shore as the release (left) and the opposite shore (right).

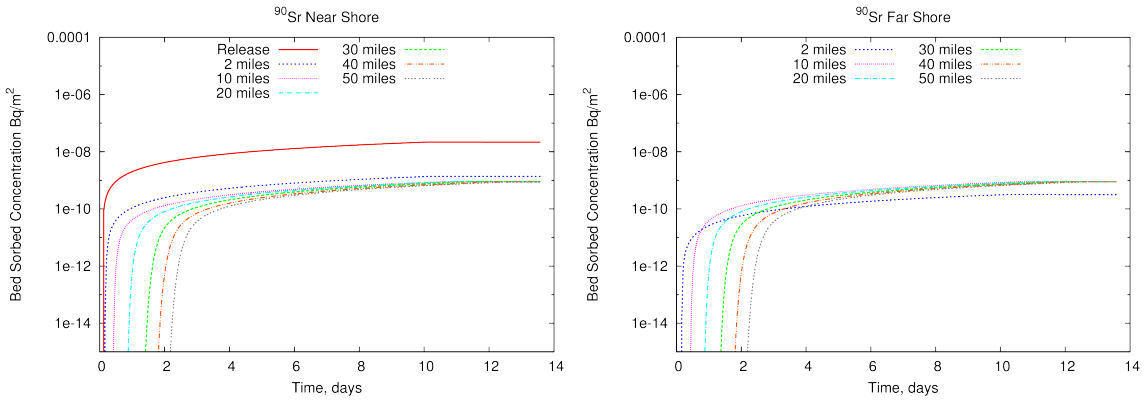

Figure B-35. Simulated small river bed-sorbed ^{90}Sr activity over time at several locations along the same shore as the release (left) and the opposite shore (right).

B.2.3 One Year

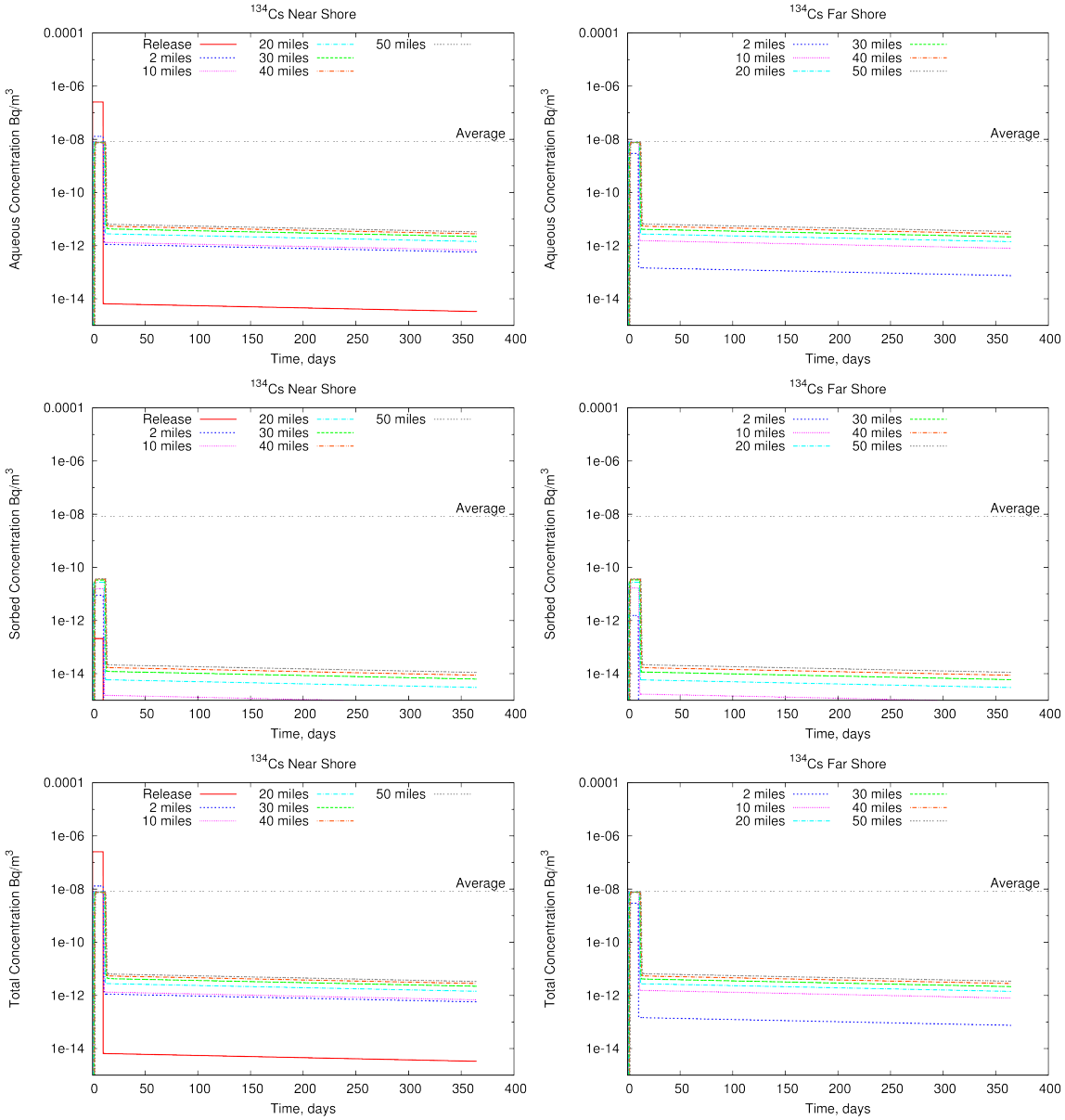

Figure B-36. Small river total suspended (top), particulate (middle), and total (bottom) ^{134}Cs activity over time at several locations on the same (left) and opposite (right) shore of the release location.

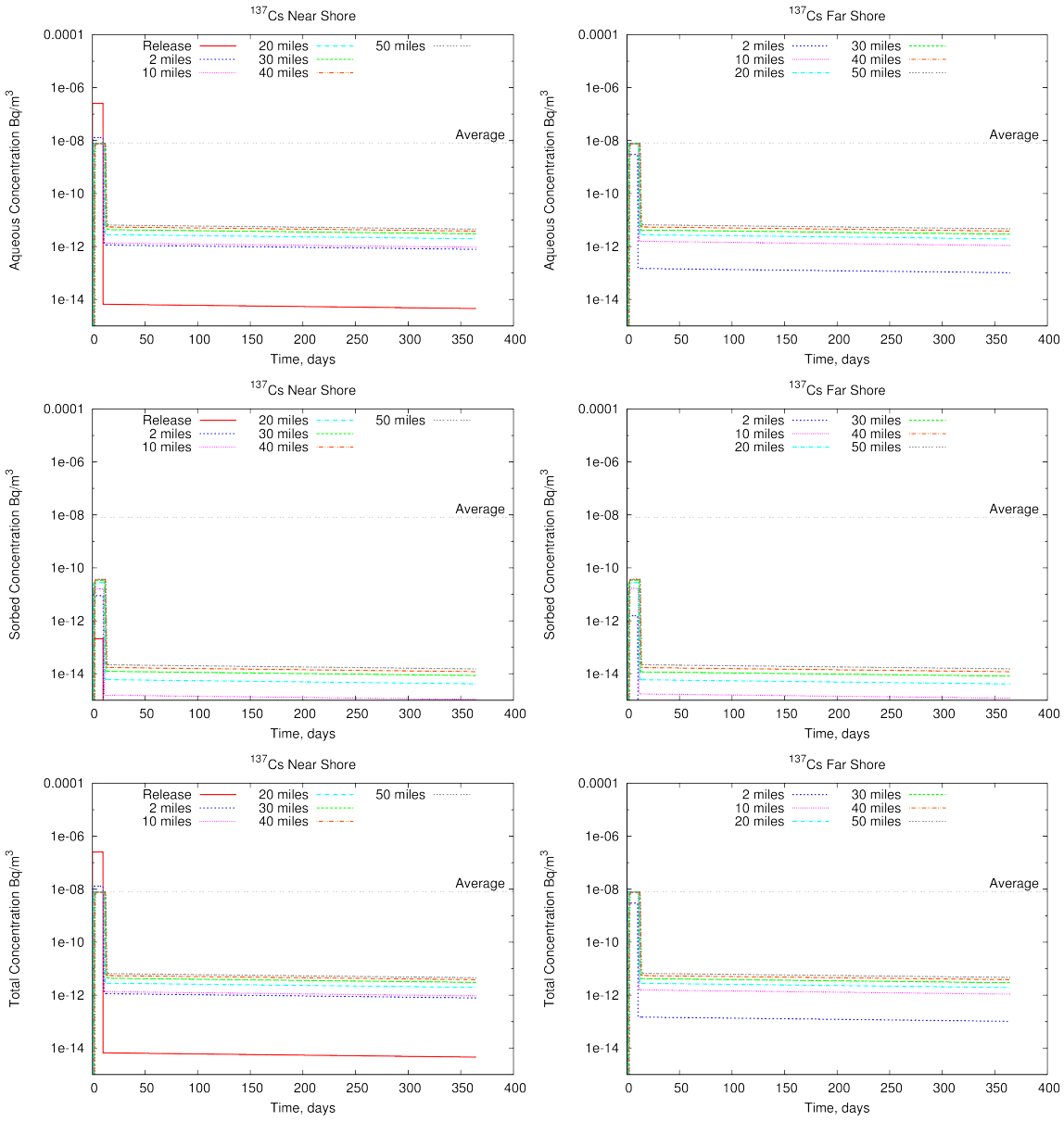

Figure B-37. Small river total suspended (top), particulate (middle), and total (bottom) ^{137}Cs activity over time at several locations on the same (left) and opposite (right) shore of the release location.

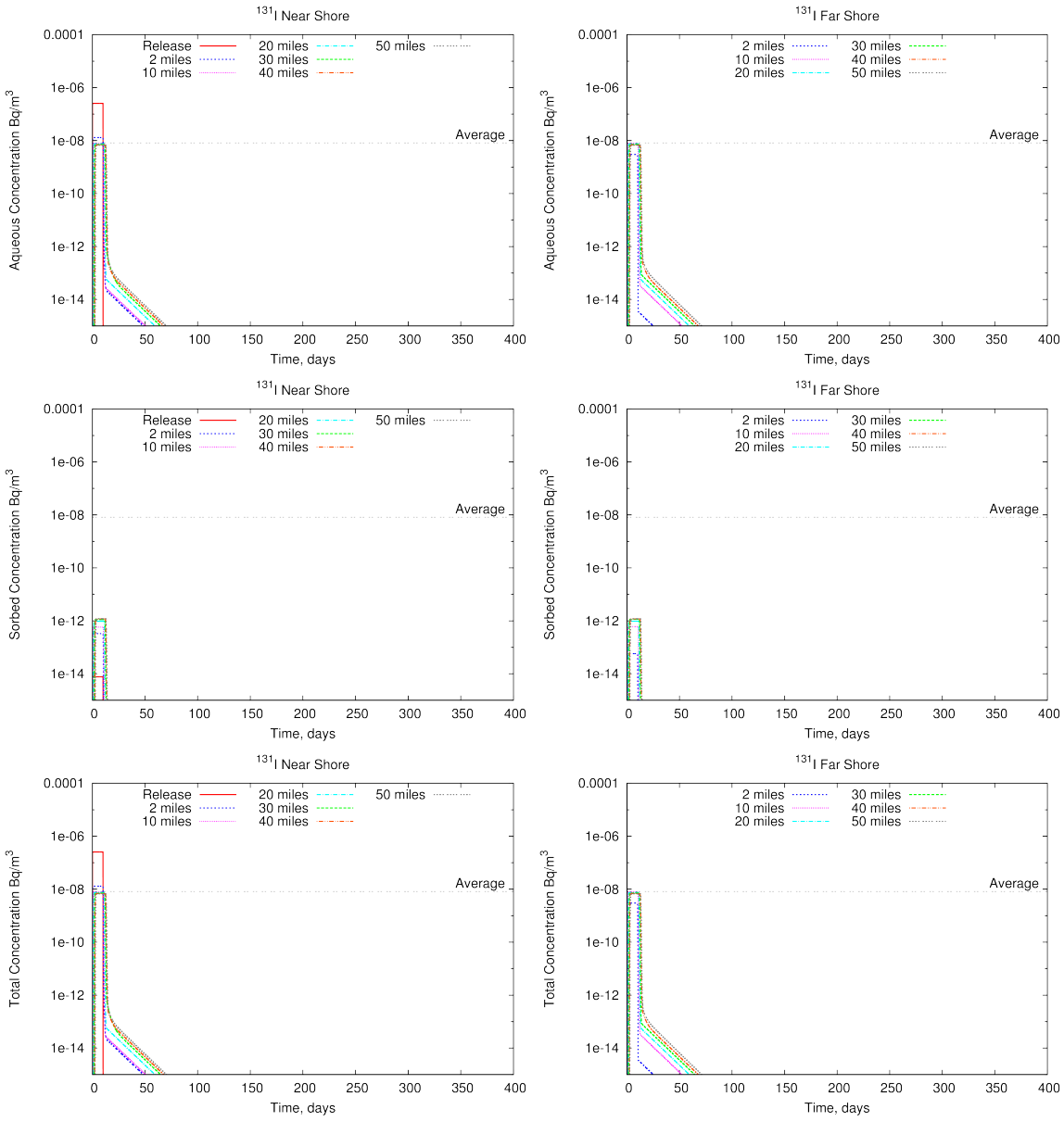

Figure B-38. Small river total suspended (top), particulate (middle), and total (bottom) ^{131}I activity over time at several locations on the same (left) and opposite (right) of the release location.

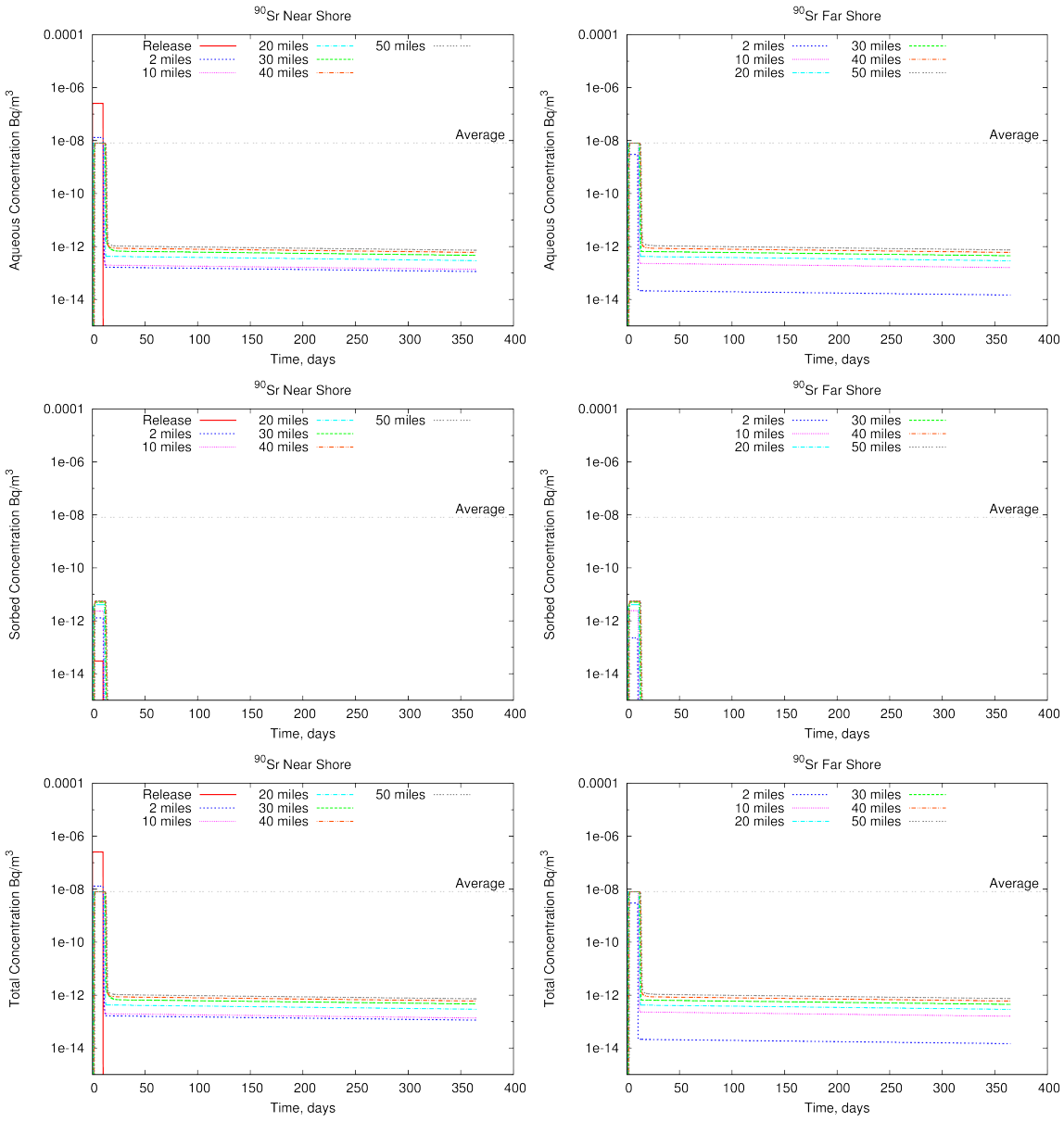

Figure B-39. Small river total suspended (top), particulate (middle), and total (bottom) ^{90}Sr activity over time at several locations on the same (left) and opposite (right) of the release location.

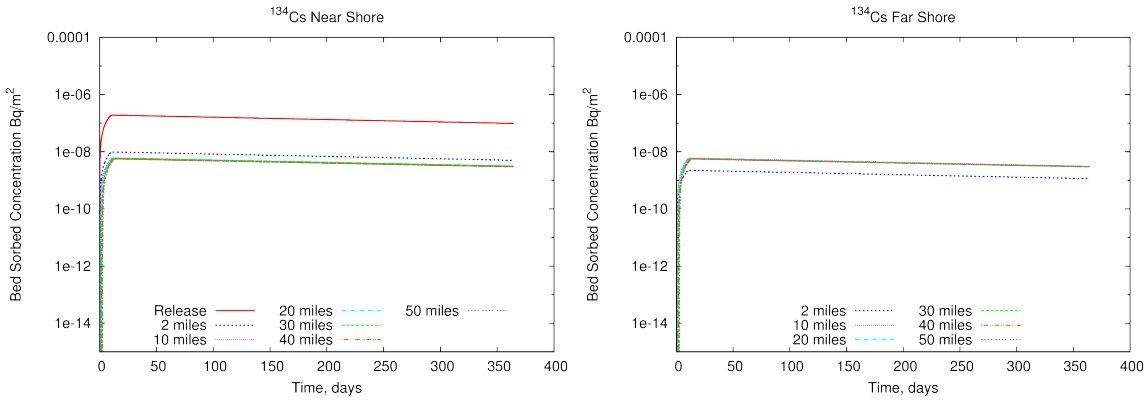

Figure B-40. Small river bed-sorbed ^{134}Cs activity over time at several locations on the same (left) and opposite (right) shore of the release location.

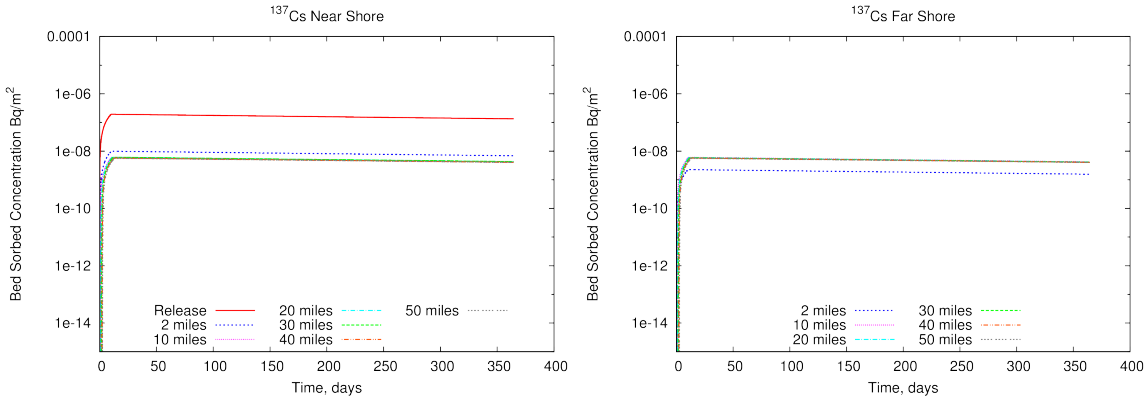

Figure B-41. Small river bed-sorbed ^{137}Cs activity over time at several locations on the same (left) and opposite (right) shore of the release location.

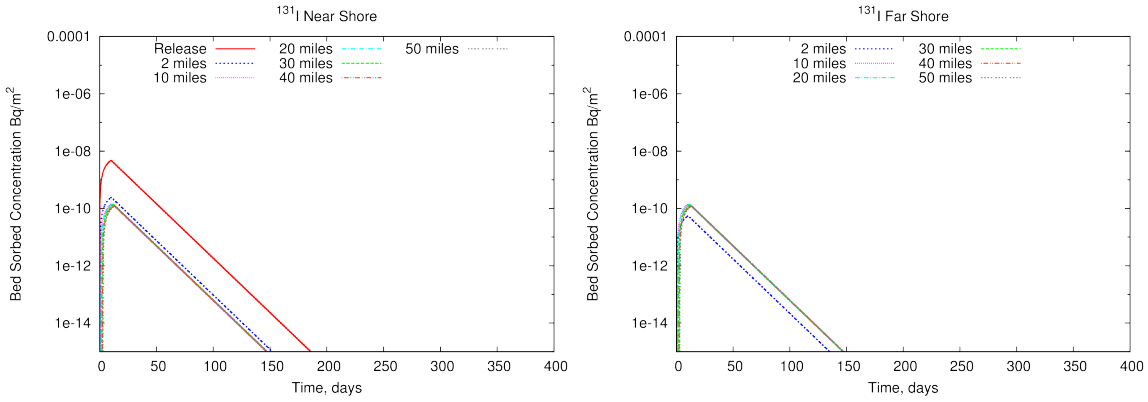

Figure B-42. Small river bed-sorbed ^{131}I activity over time at several locations on the same (left) and opposite (right) of the release location.

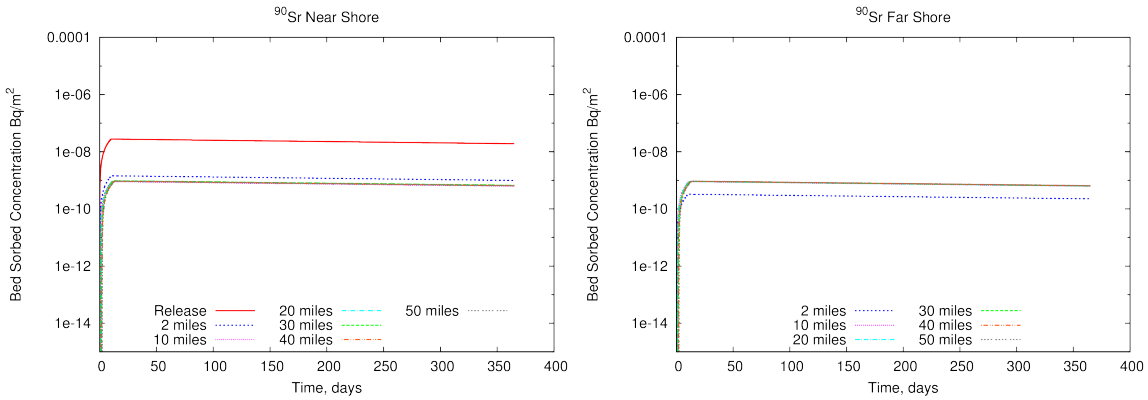

Figure B-43. Small river bed-sorbed ^{90}Sr activity over time at several locations on the same (left) and opposite (right) of the release location.

B.3 Large River

B.3.1 Large River Aqueous Only (Short-term)

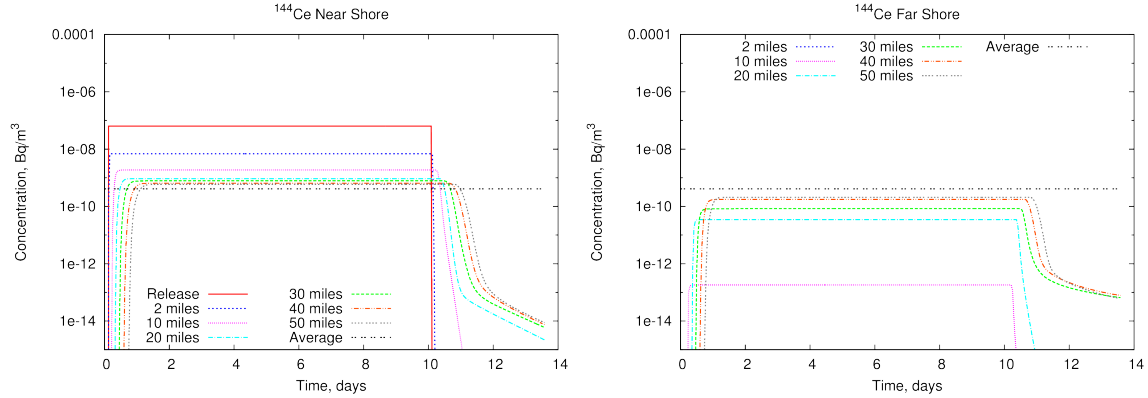

Figure B-44. Simulated large river aqueous-only ^{144}Ce activity over time at several locations along the same shore as the release (left) and the opposite shore (right).

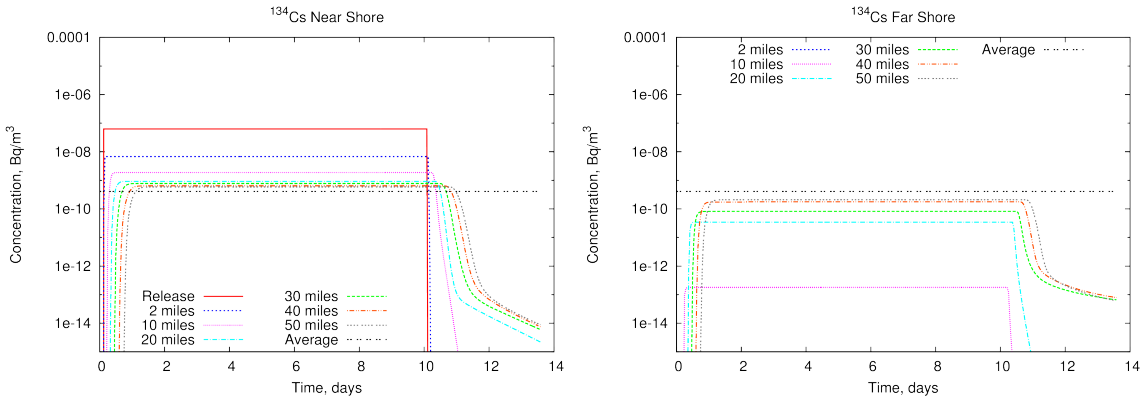

Figure B-45. Simulated large river aqueous-only ^{134}Cs activity over time at several locations along the same shore as the release (left) and the opposite shore (right).

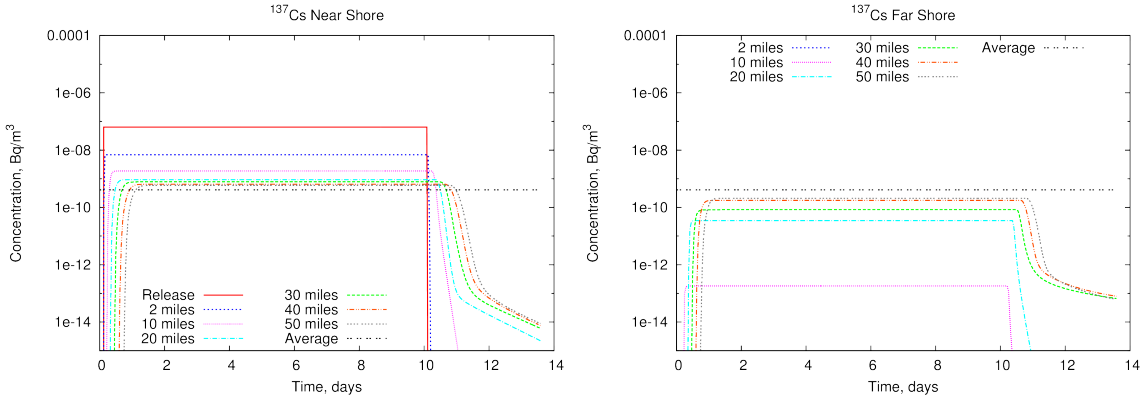

Figure B-46. Simulated large river aqueous-only ^{137}Cs activity over time at several locations along the same shore as the release (left) and the opposite shore (right).

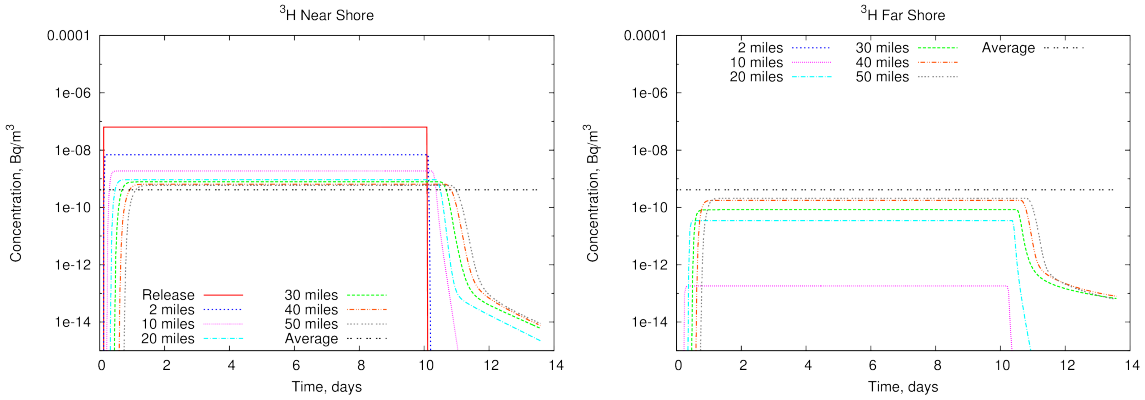

Figure B-47. Simulated large river aqueous-only ^{3}H activity over time at several locations along the same shore as the release (left) and the opposite shore (right).

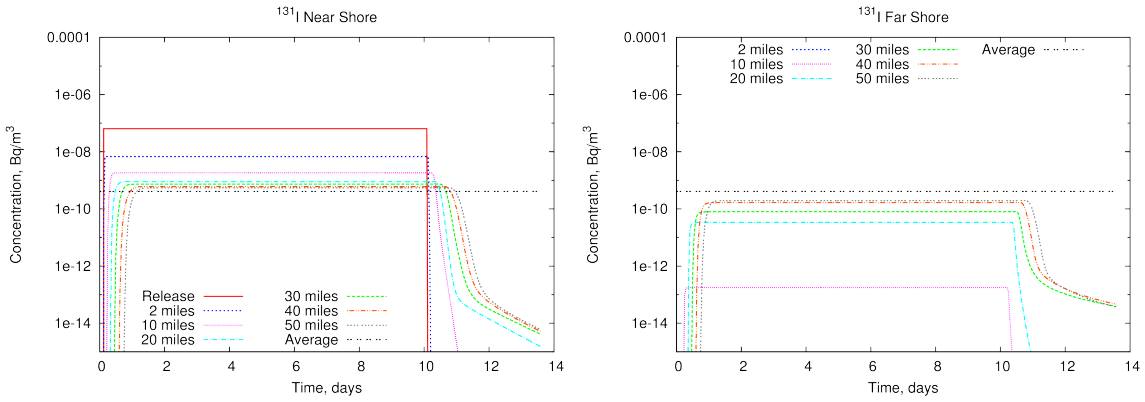

Figure B-48. Simulated large river aqueous-only ^{131}I activity over time at several locations along the same shore as the release (left) and the opposite shore (right).

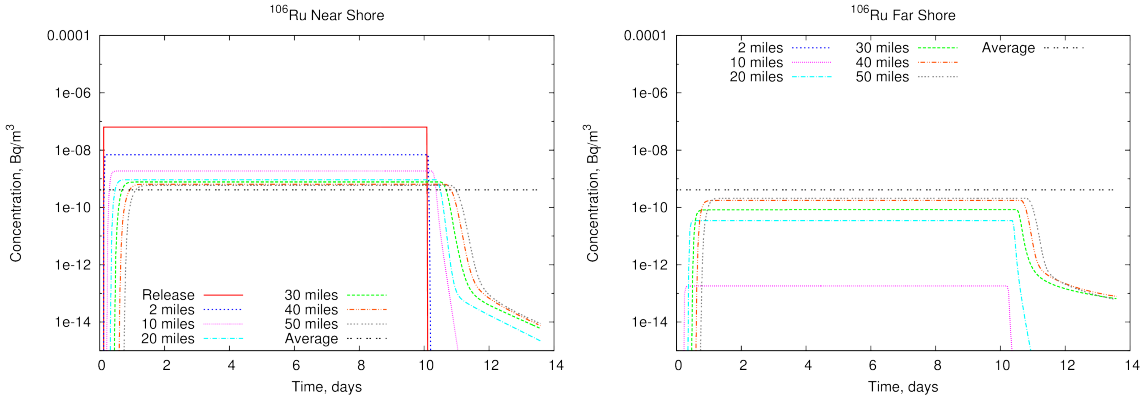

Figure B-49. Simulated large river aqueous-only ^{106}Ru activity over time at several locations along the same shore as the release (left) and the opposite shore (right).

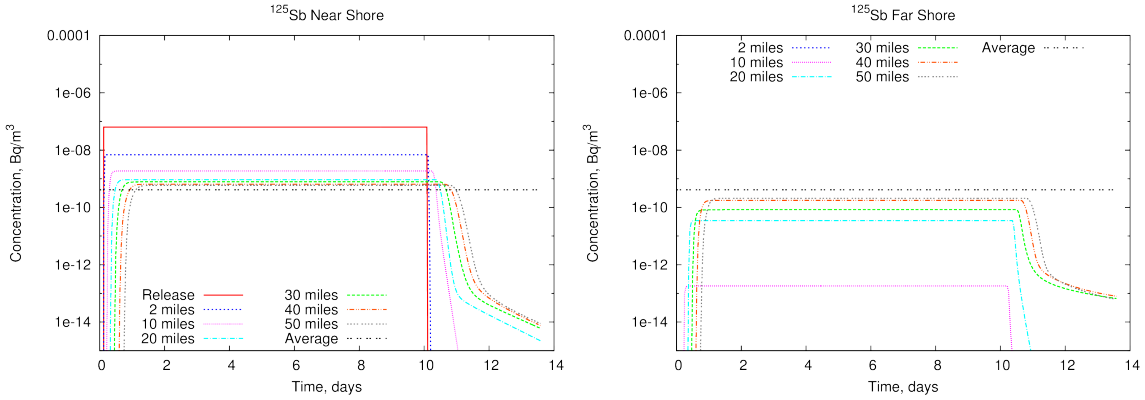

Figure B-50. Simulated large river aqueous-only ^{125}Sb activity over time at several locations along the same shore as the release (left) and the opposite shore (right).

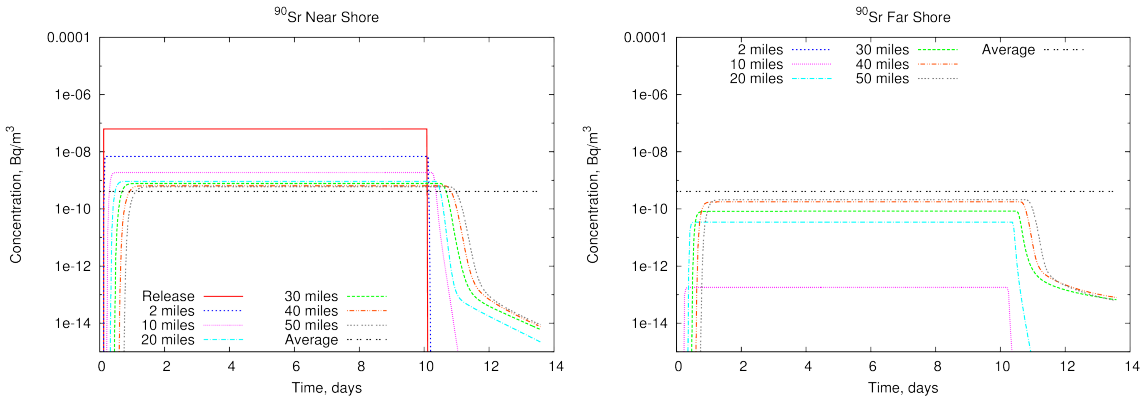

Figure B-51. Simulated large river aqueous-only ^{90}Sr activity over time at several locations along the same shore as the release (left) and the opposite shore (right).

B.3.2 Large River with Sediment (Short-term)

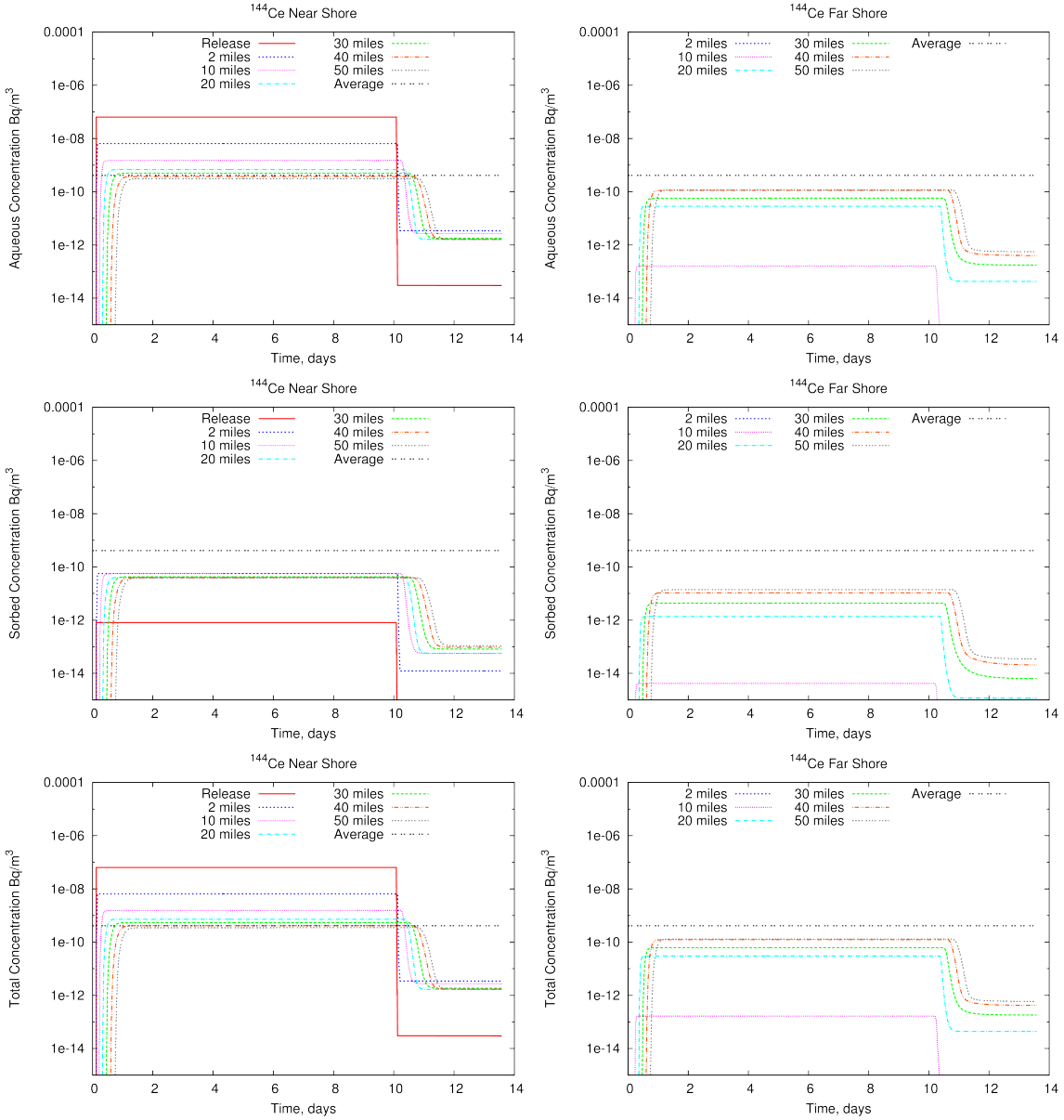

Figure B-52. Simulated large river aqueous (top), sorbed (middle), and total (bottom) ^{144}Ce activity over time at several locations along the same shore as the release (left) and the opposite shore (right).

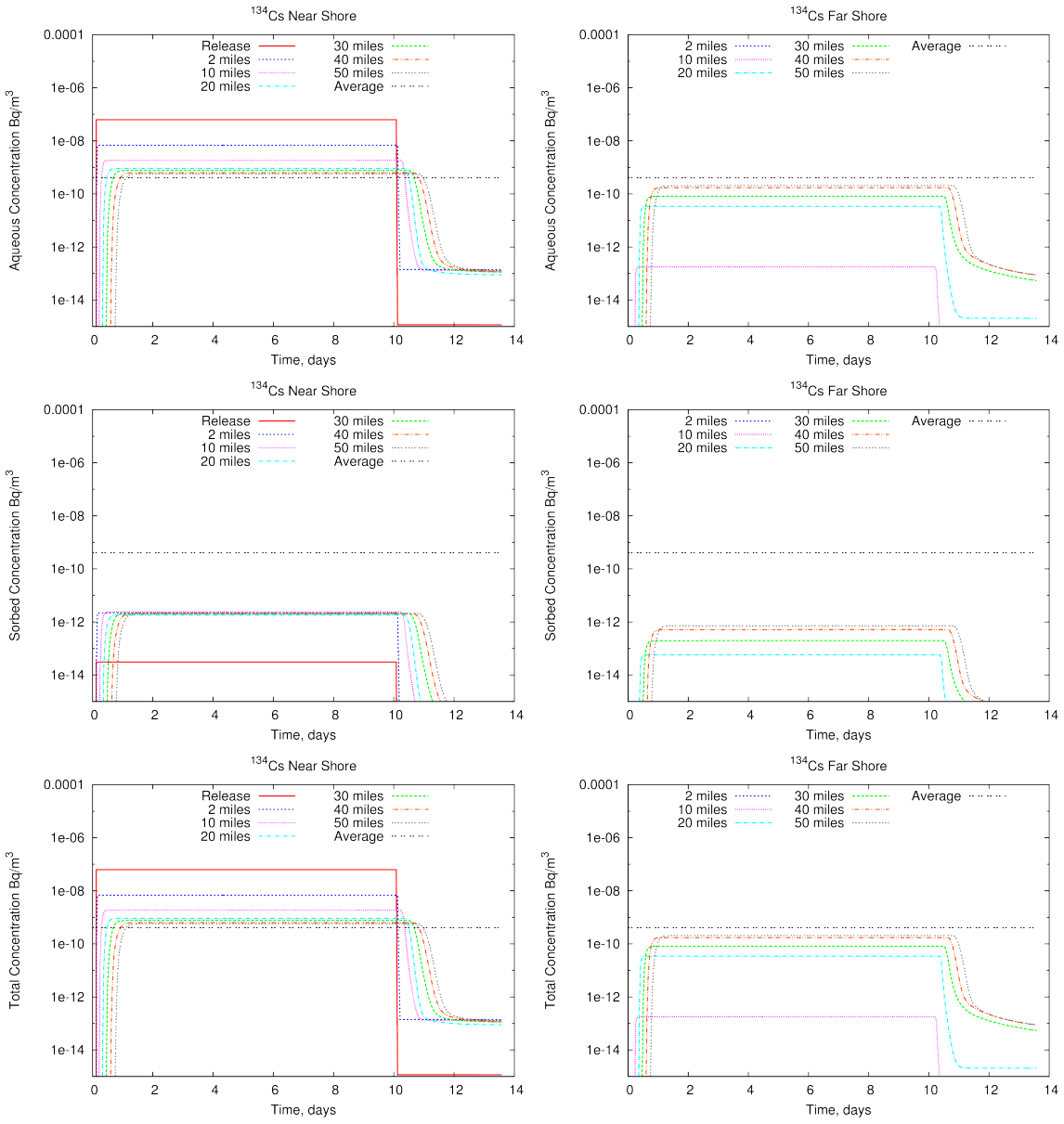

Figure B-53. Simulated large river aqueous (top), sorbed (middle), and total (bottom) ^{134}Cs activity over time at several locations along the same shore as the release (left) and the opposite shore (right).

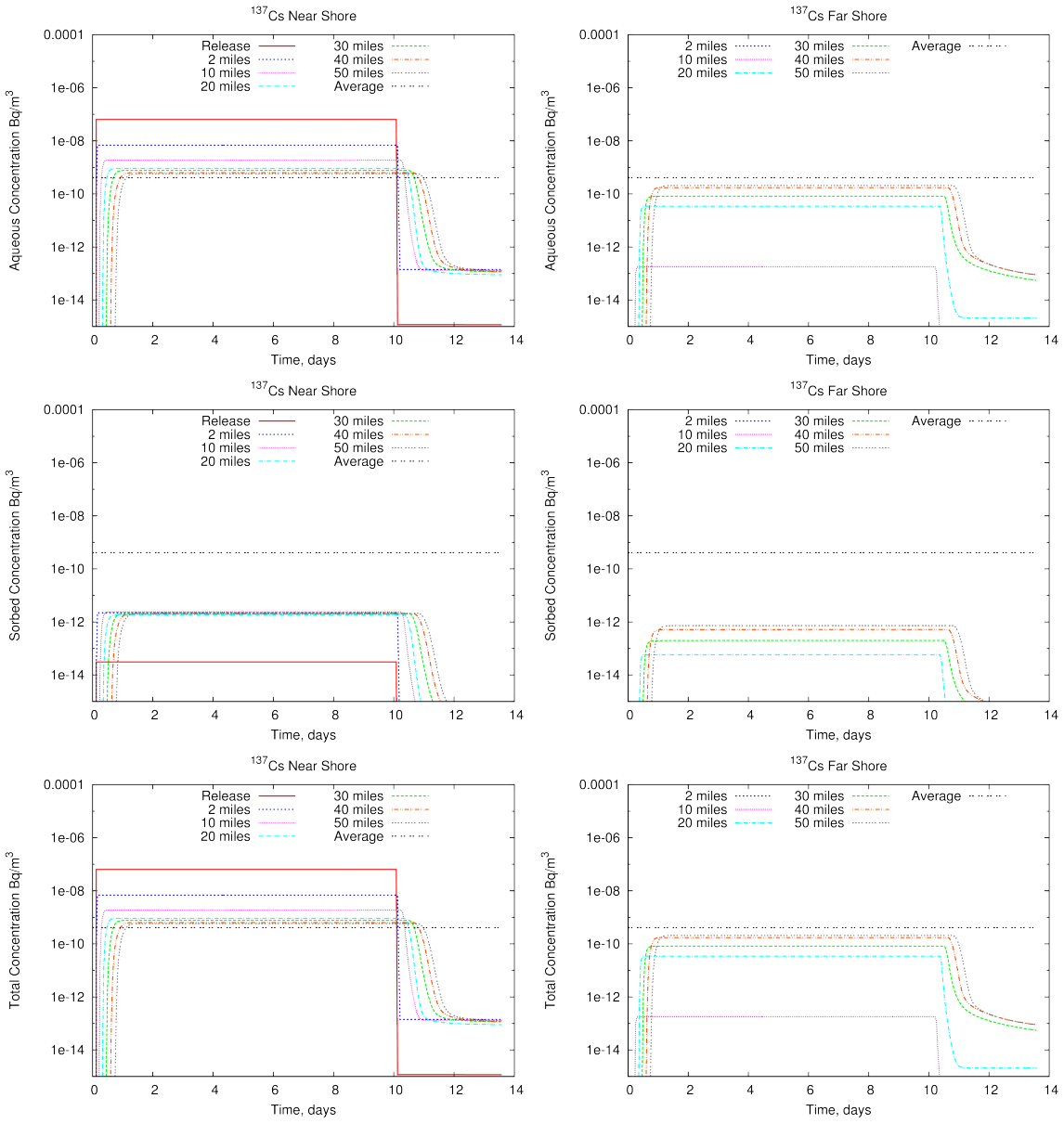

Figure B-54. Simulated large river aqueous (top), sorbed (middle), and total (bottom) ^{137}Cs activity over time at several locations along the same shore as the release (left) and the opposite shore (right).

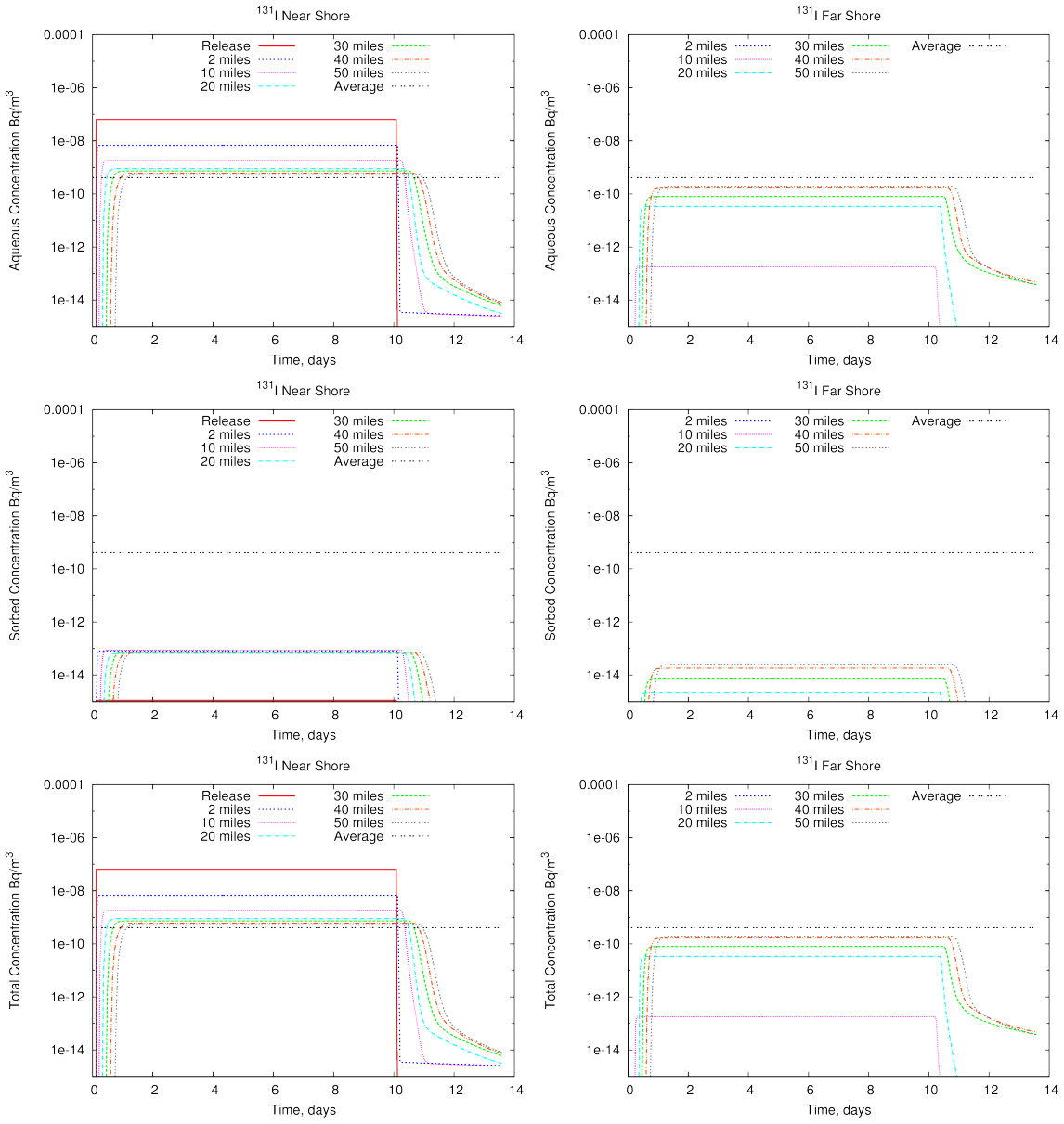

Figure B-55. Simulated large river aqueous (top), sorbed (middle), and total (bottom) ^{131}I activity over time at several locations along the same shore as the release (left) and the opposite shore (right).

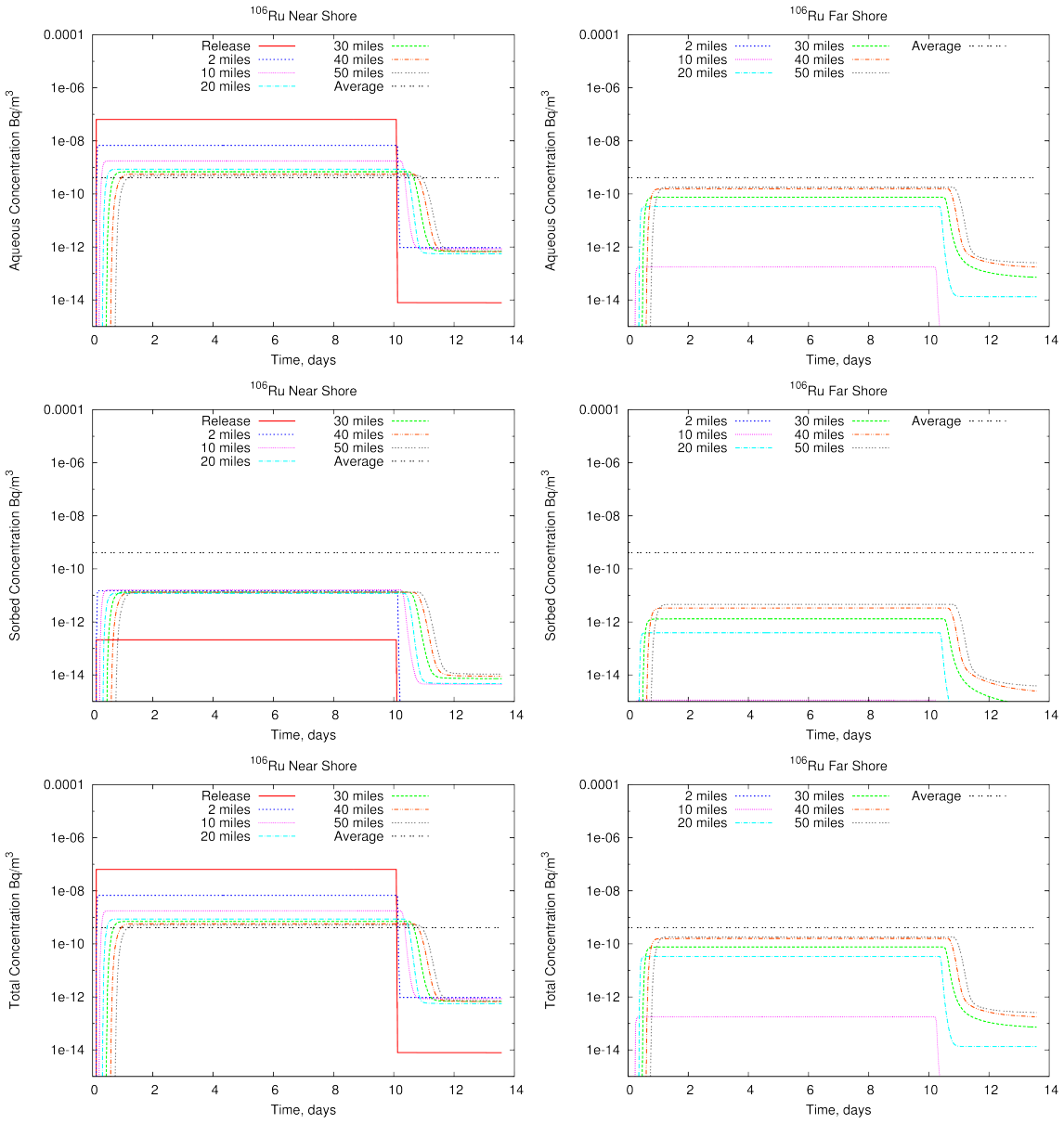

Figure B-56. Simulated large river aqueous (top), sorbed (middle), and total (bottom) ^{106}Ru activity over time at several locations along the same shore as the release (left) and the opposite shore (right).

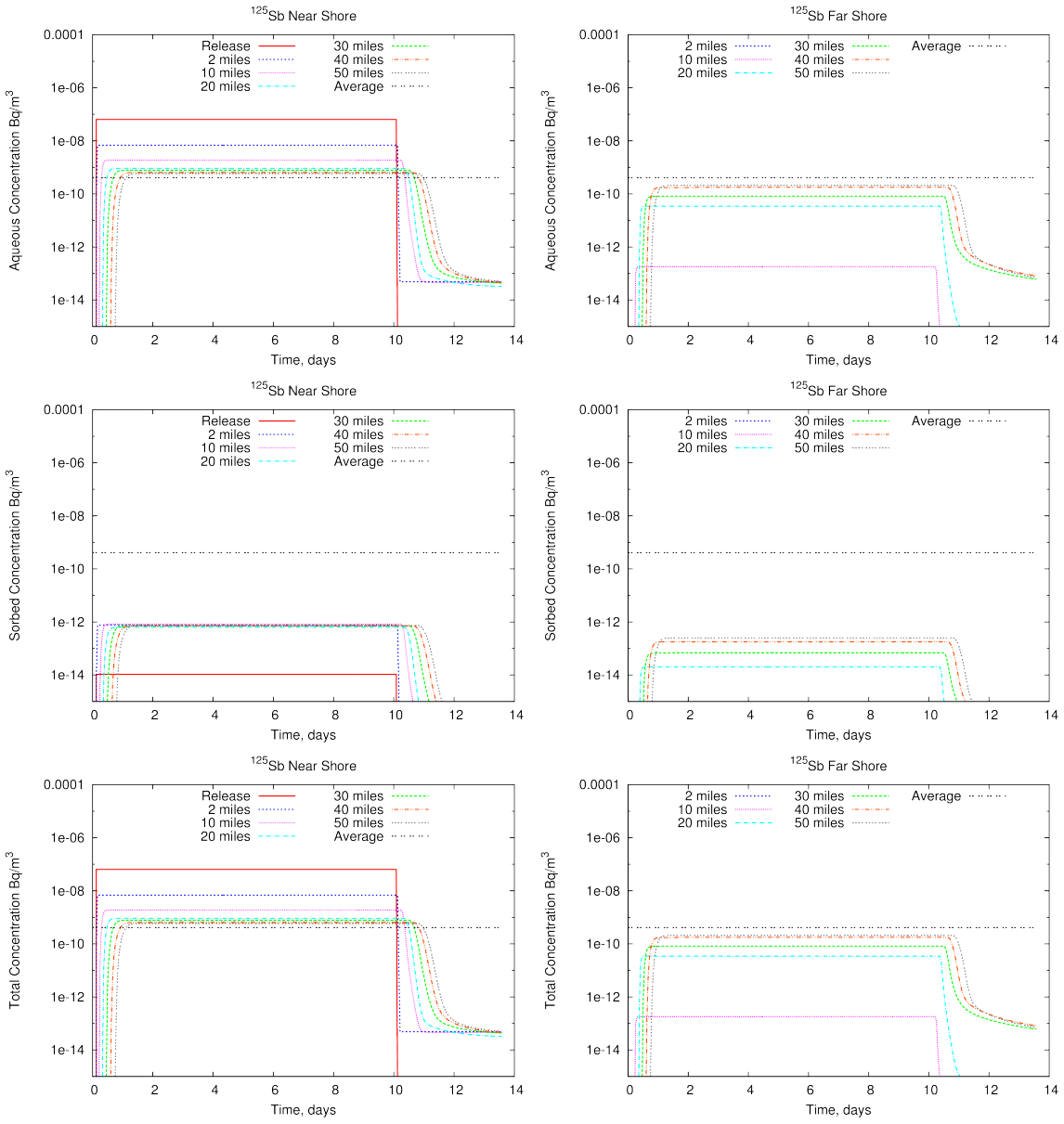

Figure B-57. Simulated large river aqueous (top), sorbed (middle), and total (bottom) ^{125}Sb activity over time at several locations along the same shore as the release (left) and the opposite shore (right).

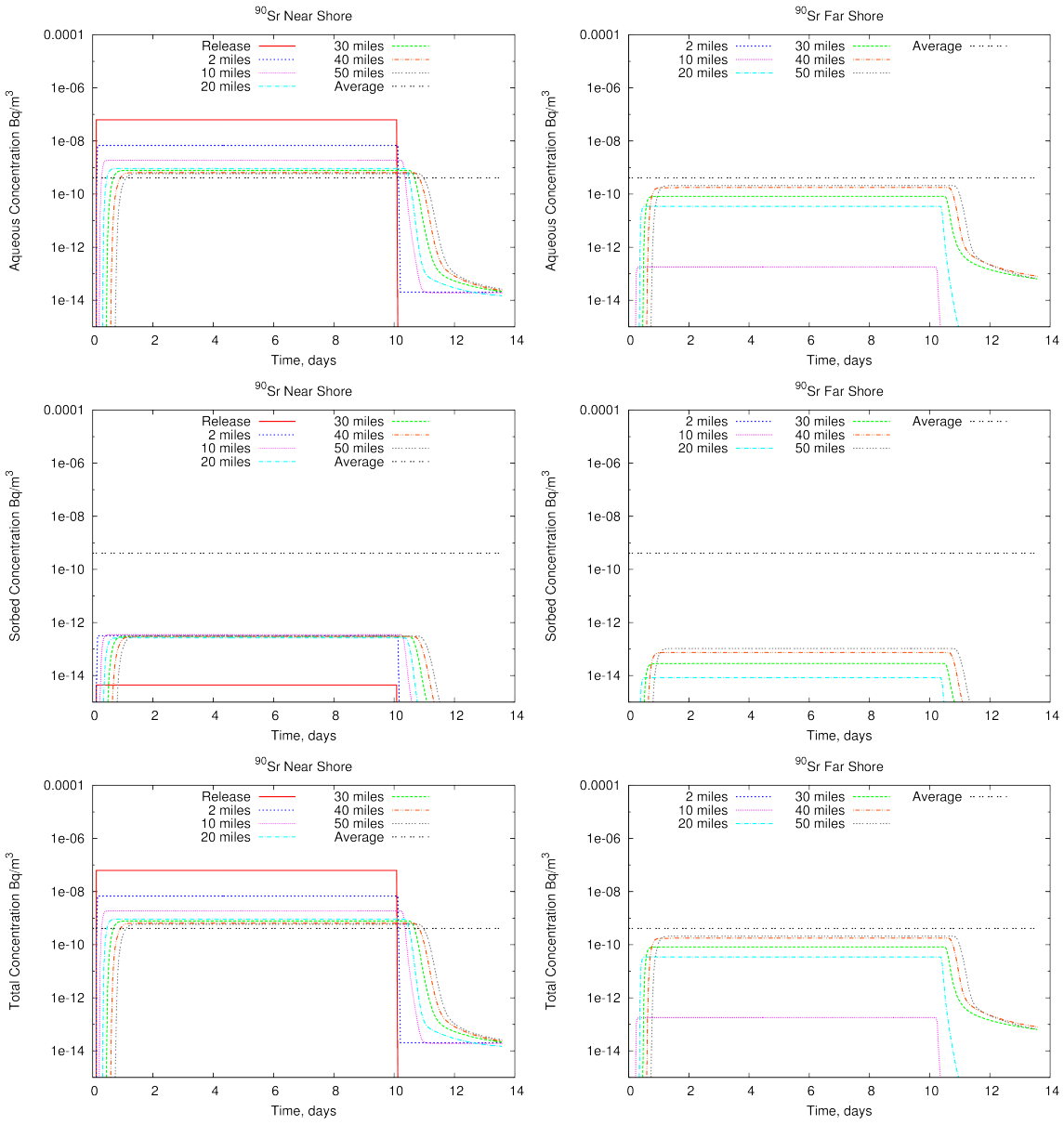

Figure B-58. Simulated large river aqueous (top), sorbed (middle), and total (bottom) ^{90}Sr activity over time at several locations along the same shore as the release (left) and the opposite shore (right).

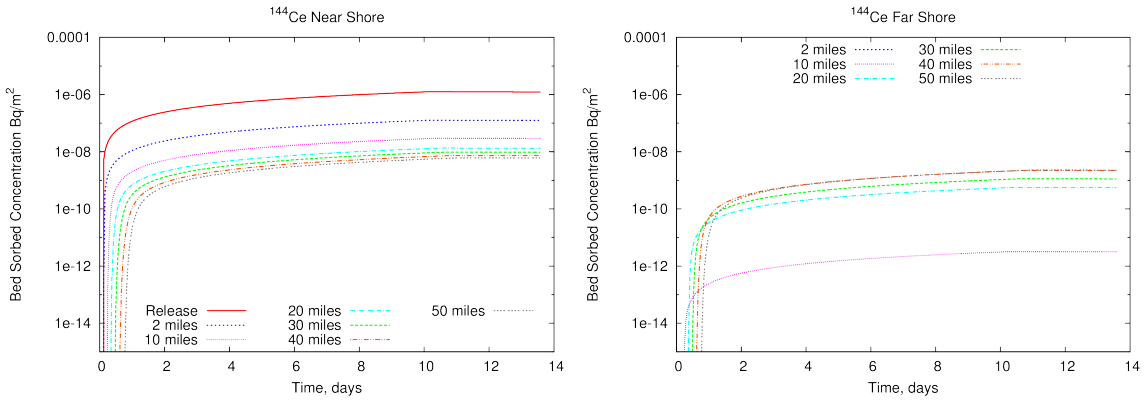

Figure B-59. Simulated large river bed-sorbed ^{144}Ce activity over time at several locations along the same shore as the release (left) and the opposite shore (right).

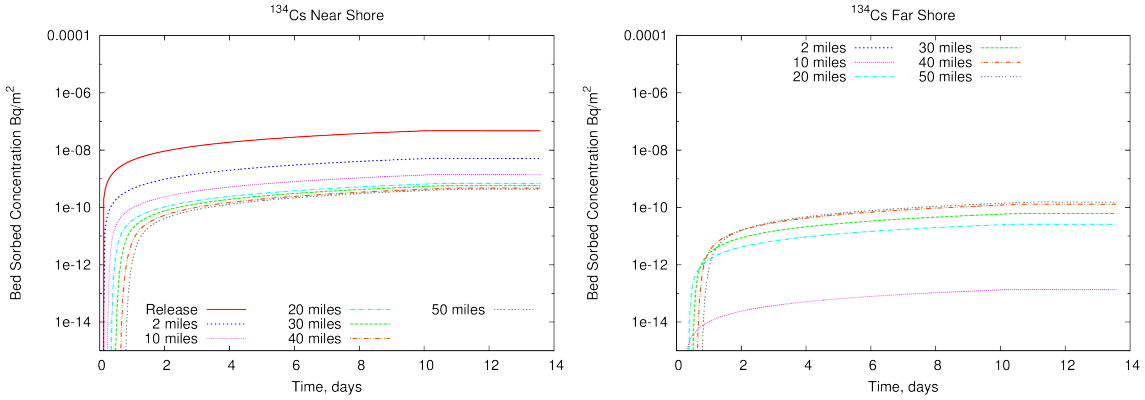

Figure B-60. Simulated large river bed-sorbed ^{134}Cs activity over time at several locations along the same shore as the release (left) and the opposite shore (right).

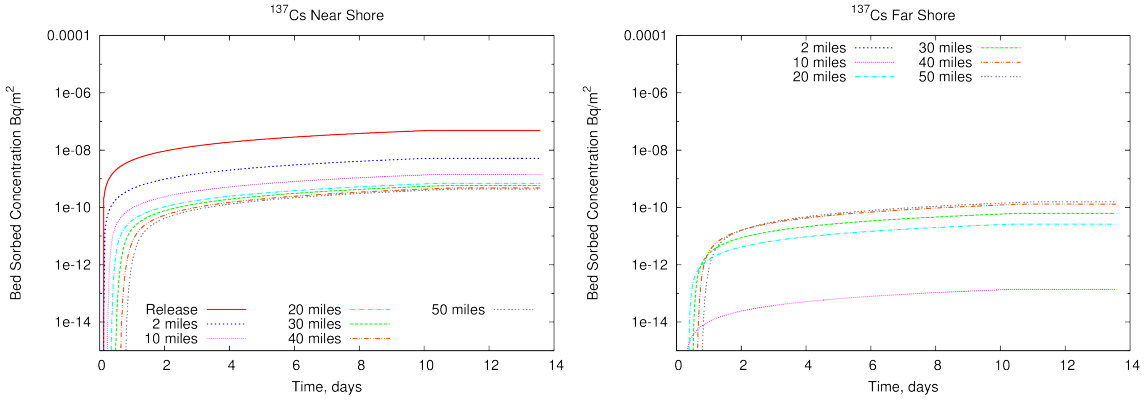

Figure B-61. Simulated large river bed-sorbed ^{137}Cs activity over time at several locations along the same shore as the release (left) and the opposite shore (right).

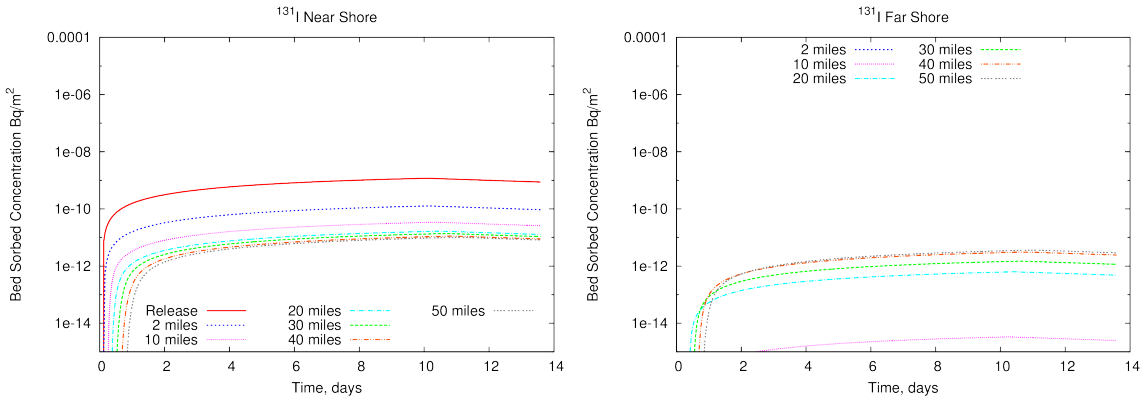

Figure B-62. Simulated large river bed-sorbed ^{131}I activity over time at several locations along the same shore as the release (left) and the opposite shore (right).

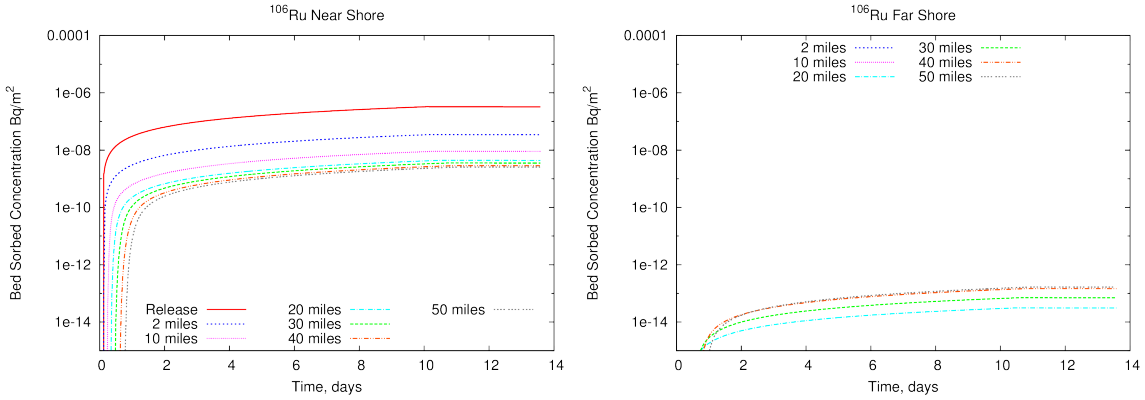

Figure B-63. Simulated large river bed-sorbed ^{106}Ru activity over time at several locations along the same shore as the release (left) and the opposite shore (right).

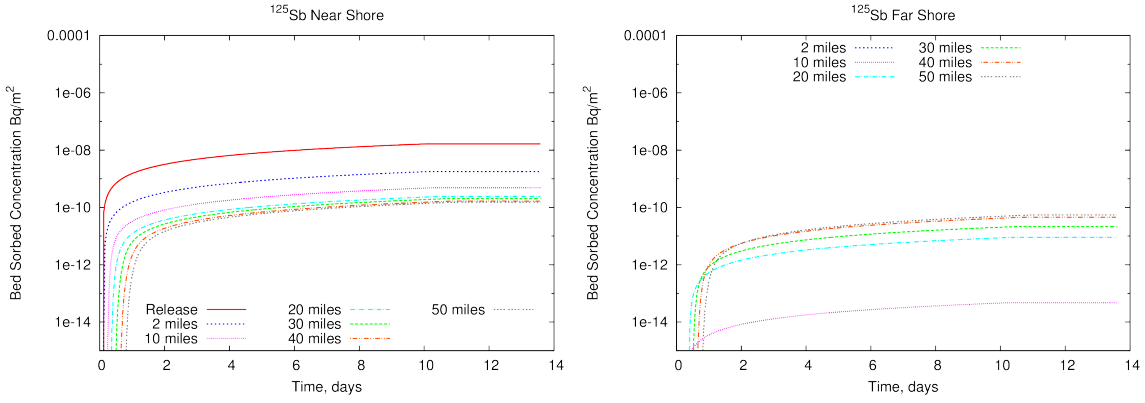

Figure B-64. Simulated large river bed-sorbed ^{125}Sb activity over time at several locations along the same shore as the release (left) and the opposite shore (right).

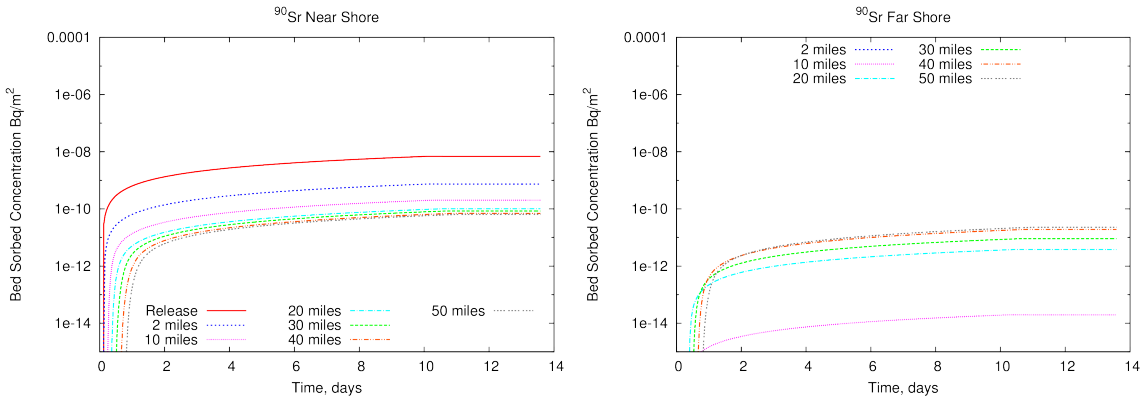

Figure B-65. Simulated large river bed-sorbed ^{90}Sr activity over time at several locations along the same shore as the release (left) and the opposite shore (right).

B.3.3 One-year Extended Domain

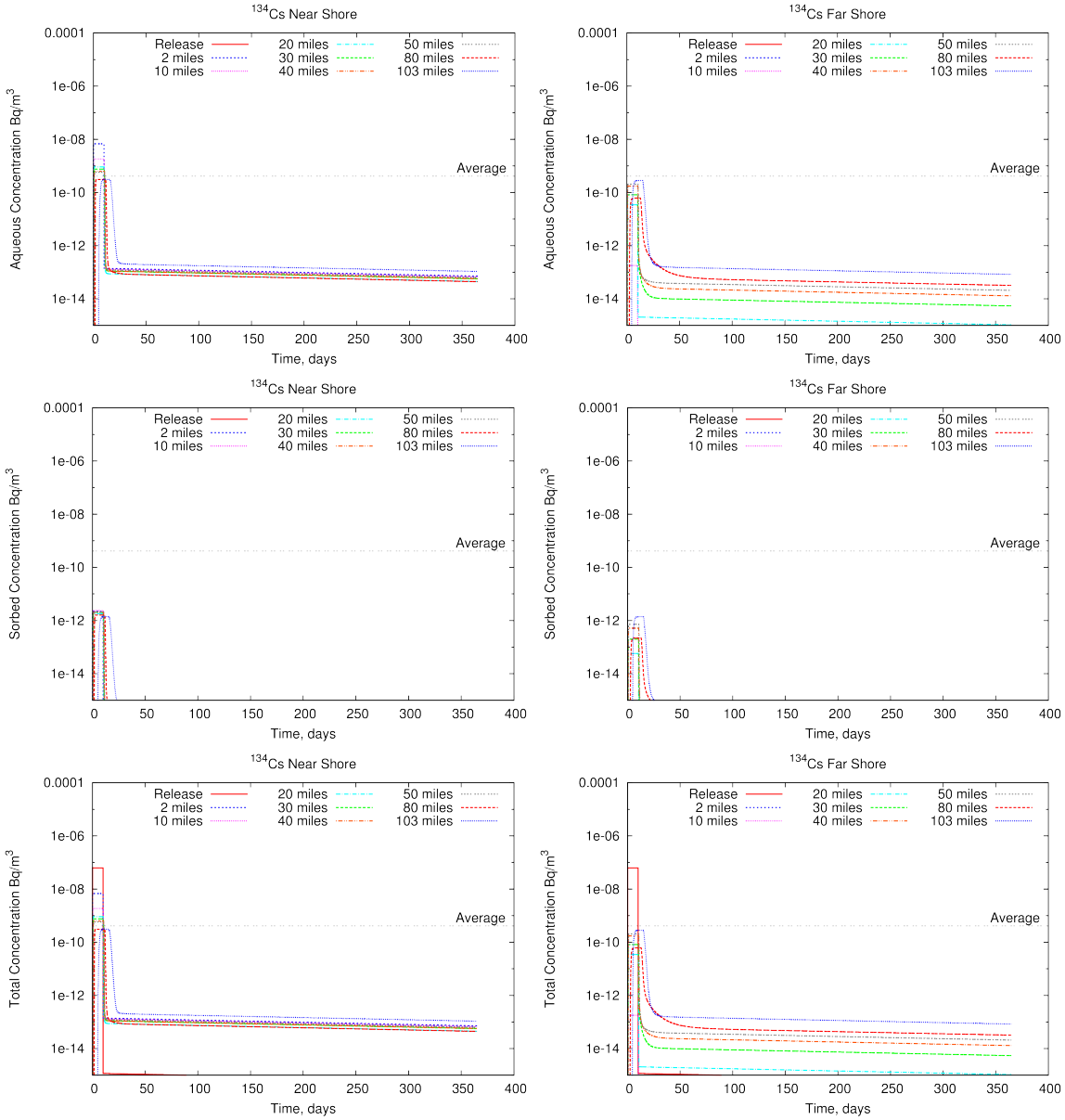

Figure B-66. Simulated extended large river aqueous (top), sorbed (middle), and total (bottom) ^{134}Cs activity over a full year at several locations along the same shore as the release (left) and the opposite shore (right).

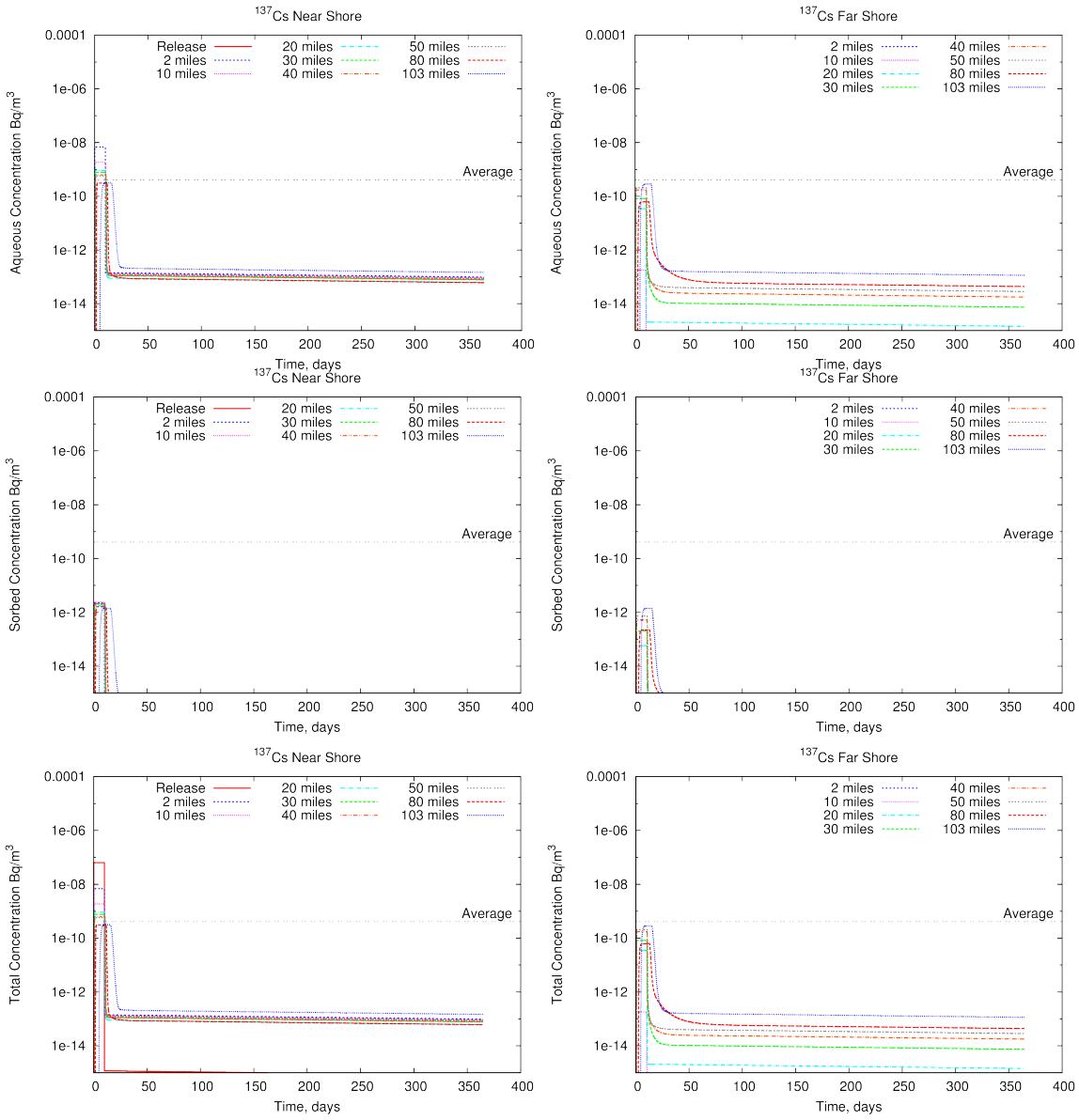

Figure B-67. Simulated extended large river aqueous (top), sorbed (middle), and total (bottom) ^{137}Cs activity over a full year at several locations along the same shore as the release (left) and the opposite shore (right).

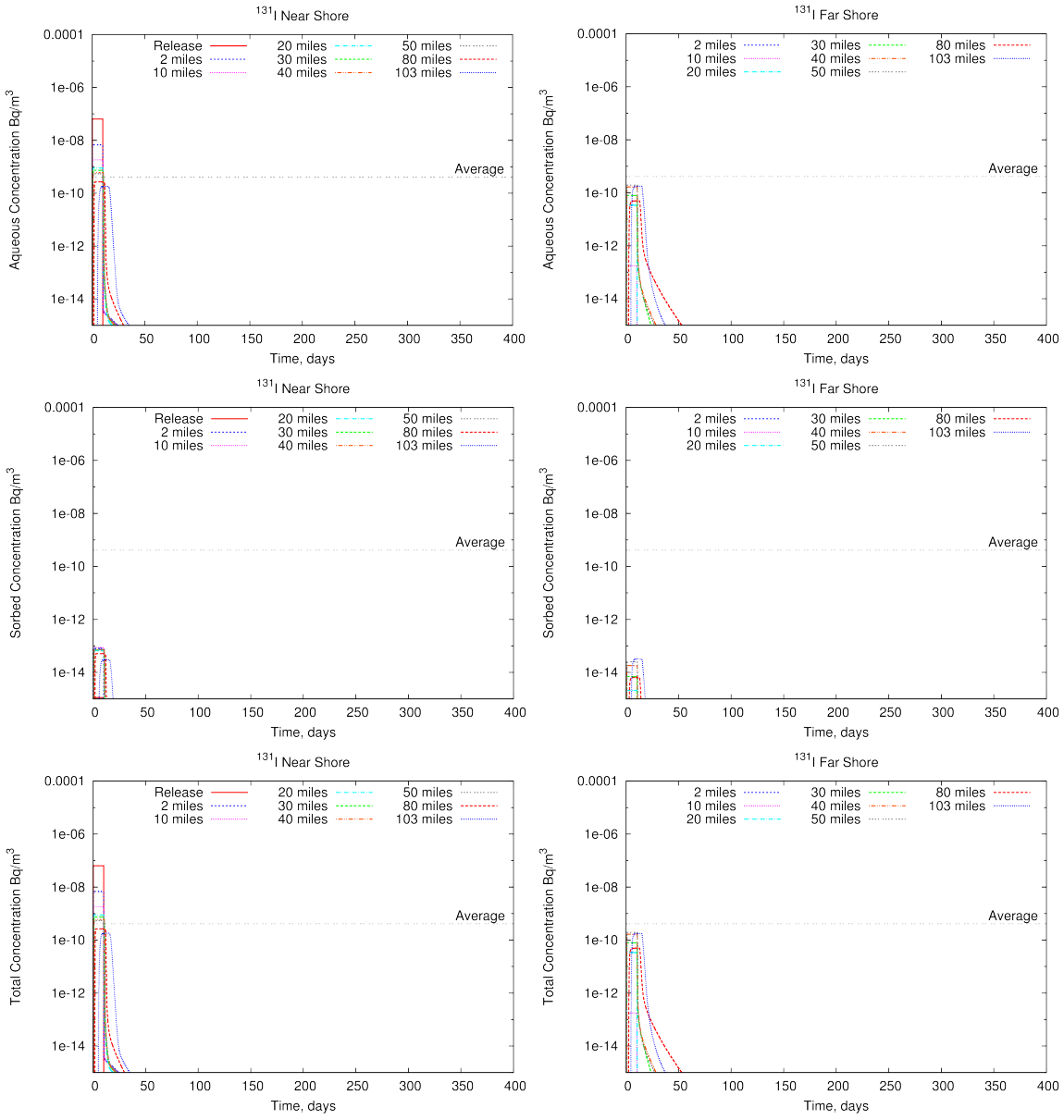

Figure B-68. Simulated extended large river aqueous (top), sorbed (middle), and total (bottom) ^{131}I activity over a full year at several locations along the same shore as the release (left) and the opposite shore (right).

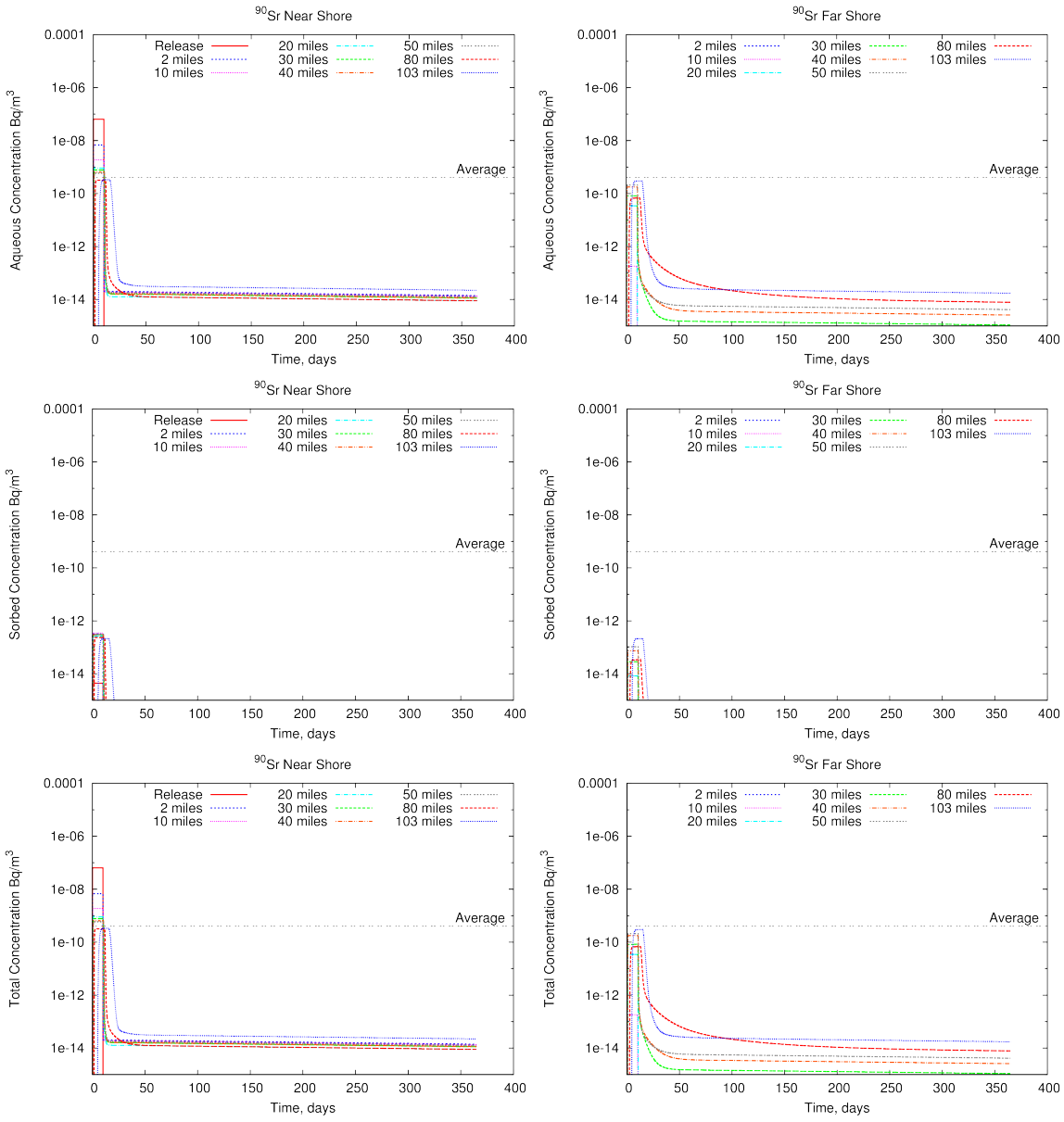

Figure B-69. Simulated extended large river aqueous (top), sorbed (middle), and total (bottom) ^{90}Sr activity over a full year at several locations along the same shore as the release (left) and the opposite shore (right).

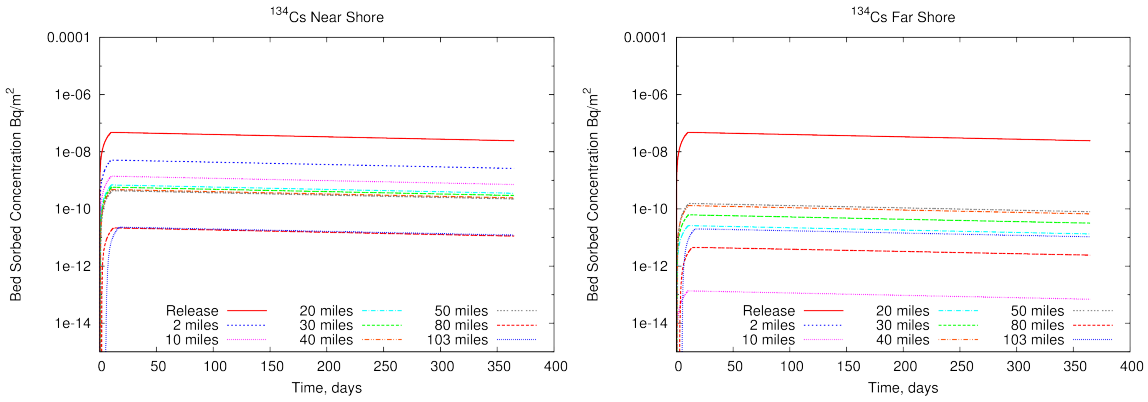

Figure B-70. Simulated extended large river bed-sorbed ^{134}Cs activity over a full year at several locations along the same shore as the release (left) and the opposite shore (right).

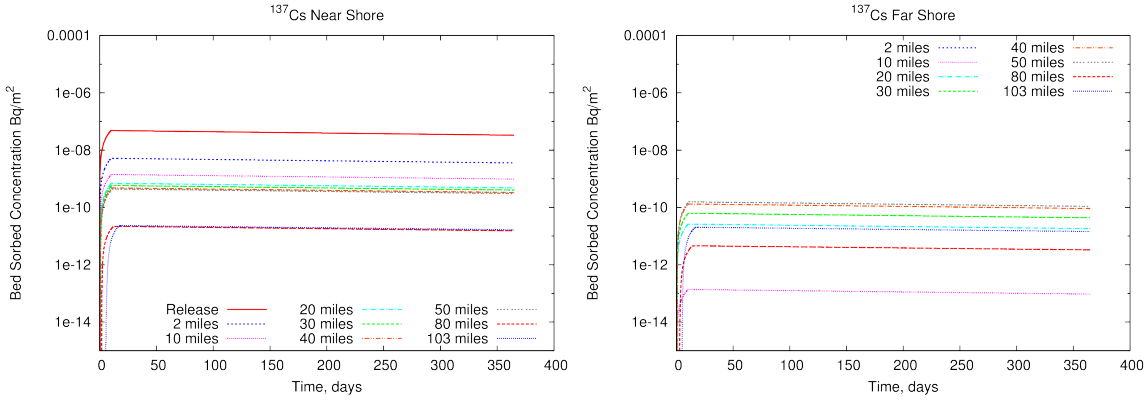

Figure B-71. Simulated extended large river bed-sorbed ^{137}Cs activity over a full year at several locations along the same shore as the release (left) and the opposite shore (right).

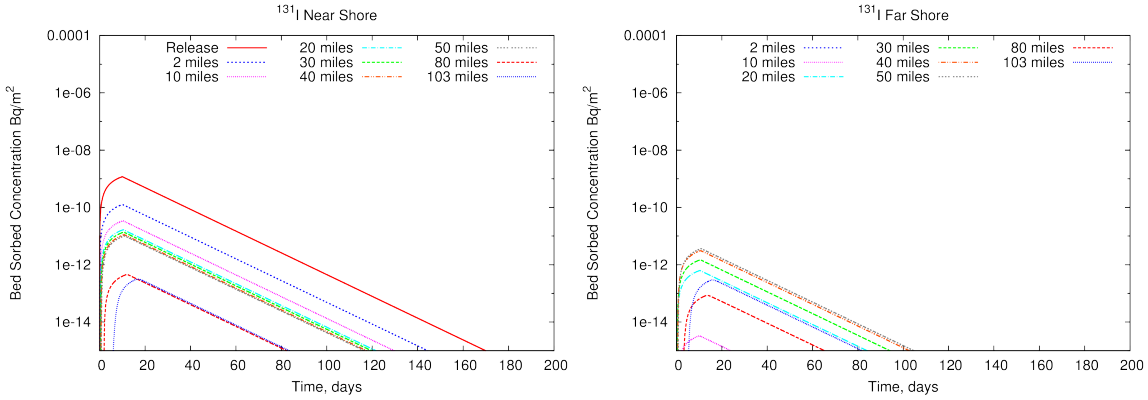

Figure B-72. Simulated extended large river bed-sorbed ^{131}I activity over a full year at several locations along the same shore as the release (left) and the opposite shore (right).

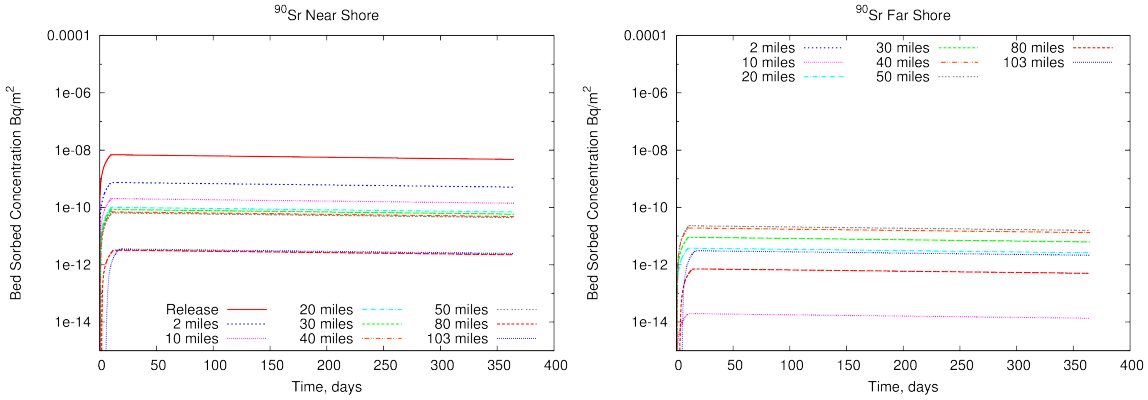

Figure B-73. Simulated extended large river bed-sorbed ^{90}Sr activity over a full year at several locations along the same shore as the release (left) and the opposite shore (right).

B.3.3.1 Unimpounded

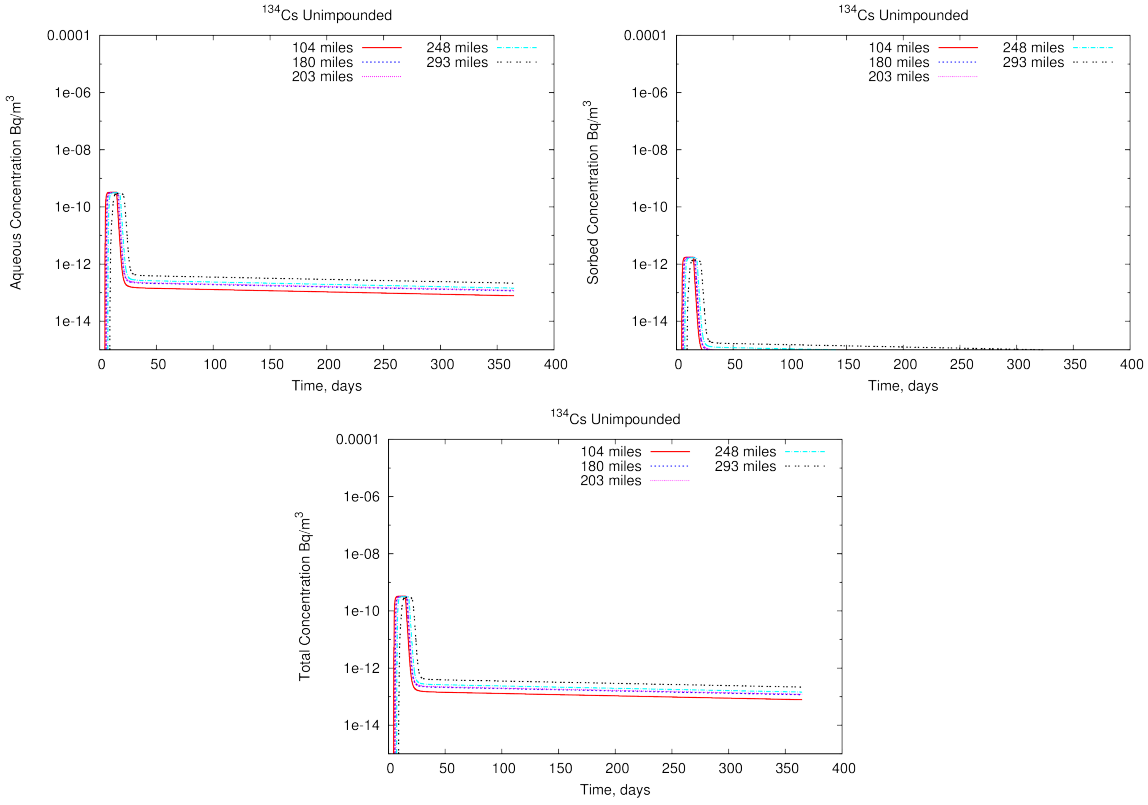

Figure B-74. Simulated unimpounded large river aqueous (top left), sorbed (top right), and total (bottom) ^{134}Cs activity over a full year at several locations.

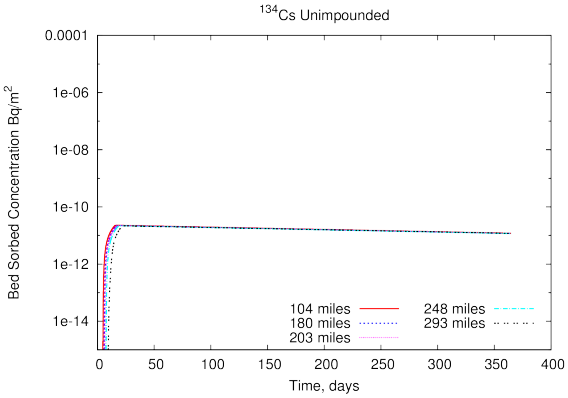

Figure B-75. Simulated unimpounded large river bed-sorbed ^{134}Cs activity over a full year at several locations.

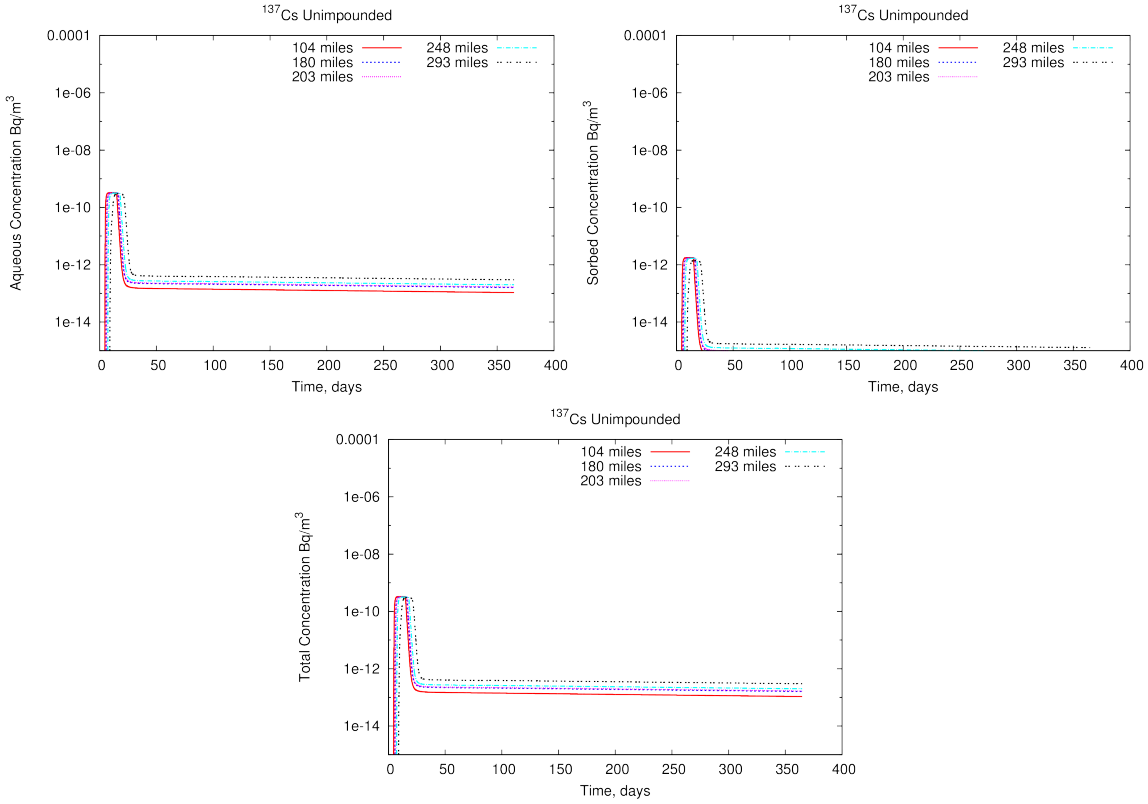

Figure B-76. Simulated unimpounded large river aqueous (top left), sorbed (top right), and total (bottom) ^{137}Cs activity over a full year at several locations.

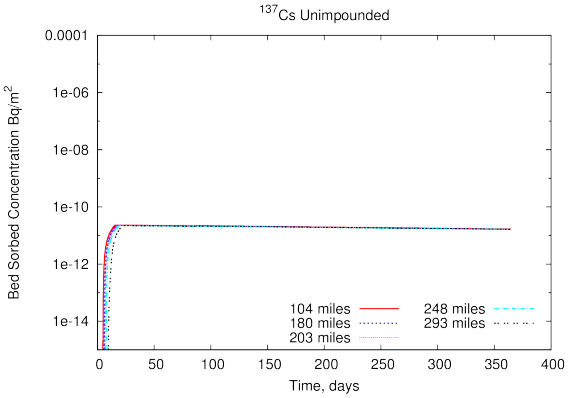

Figure B-77. Simulated unimpounded large river bed-sorbed ^{137}Cs activity over a full year at several locations.

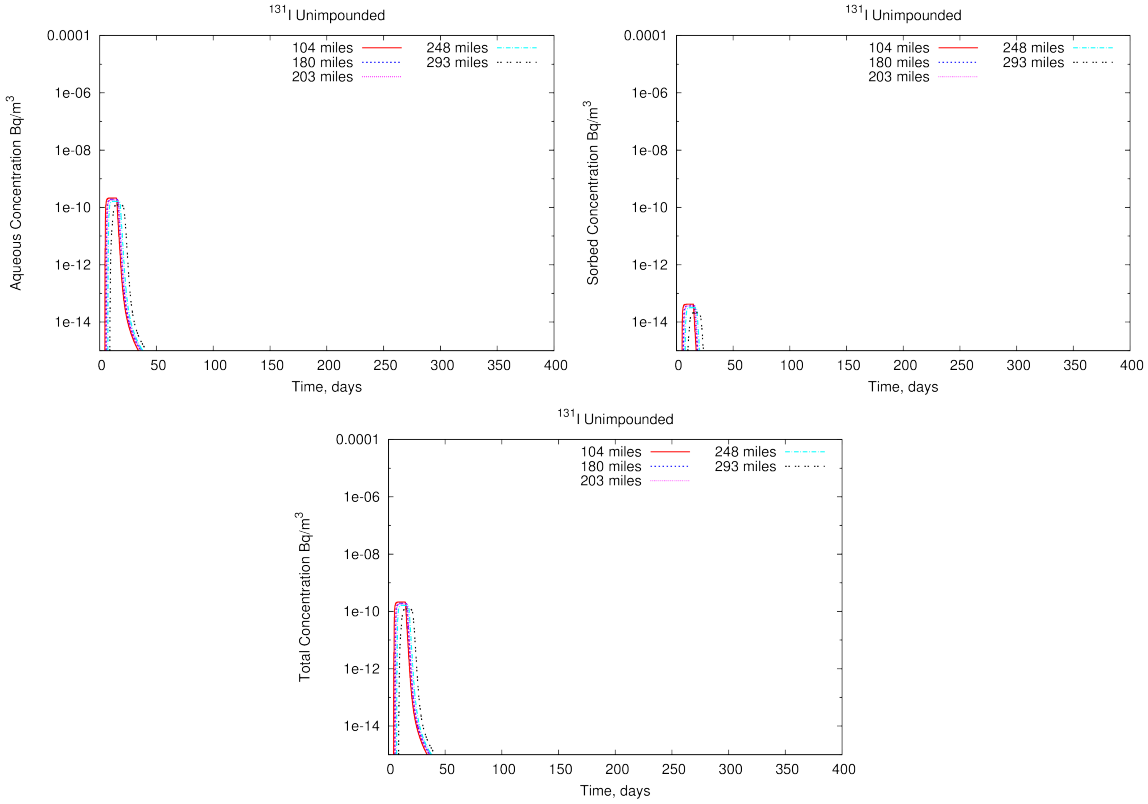

Figure B-78. Simulated unimpounded large river aqueous (top left), sorbed (top right), and total (bottom) ^{131}I activity over a full year at several locations.

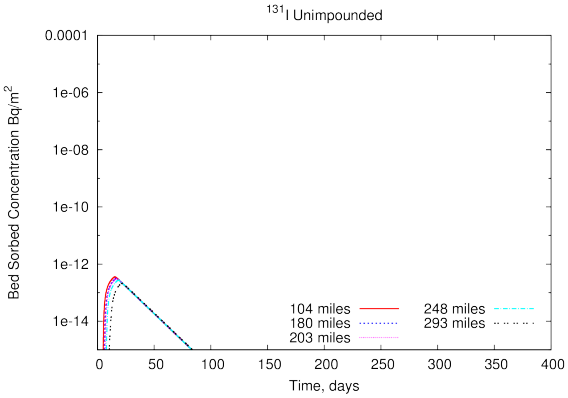

Figure B-79. Simulated unimpounded large river bed-sorbed ^{131}I activity over a full year at several locations.

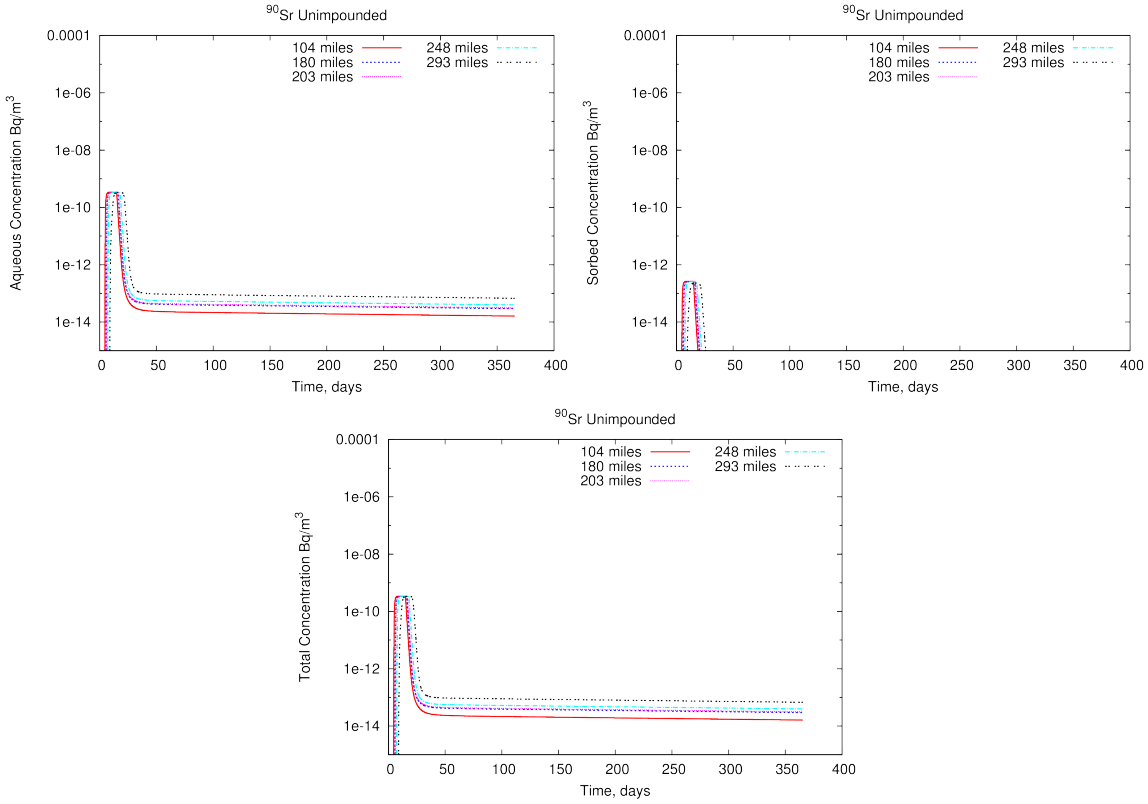

Figure B-80. Simulated unimpounded large river aqueous (top left), sorbed (top right), and total (bottom) ^{90}Sr activity over a full year at several locations along the same shore as the release (left) and the opposite shore (right).

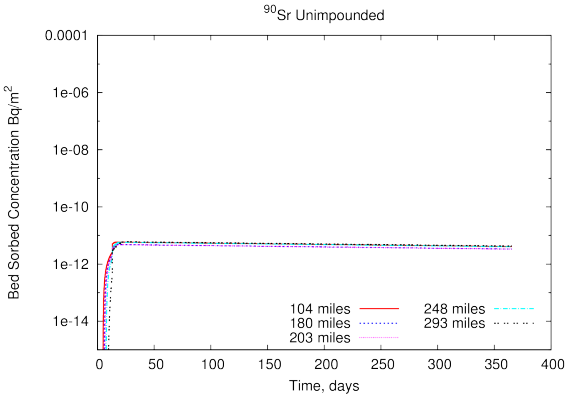

Figure B-81. Simulated unimpounded large river bed-sorbed ^{90}Sr activity over a full year at several locations.

B.3.3.2 Impounded

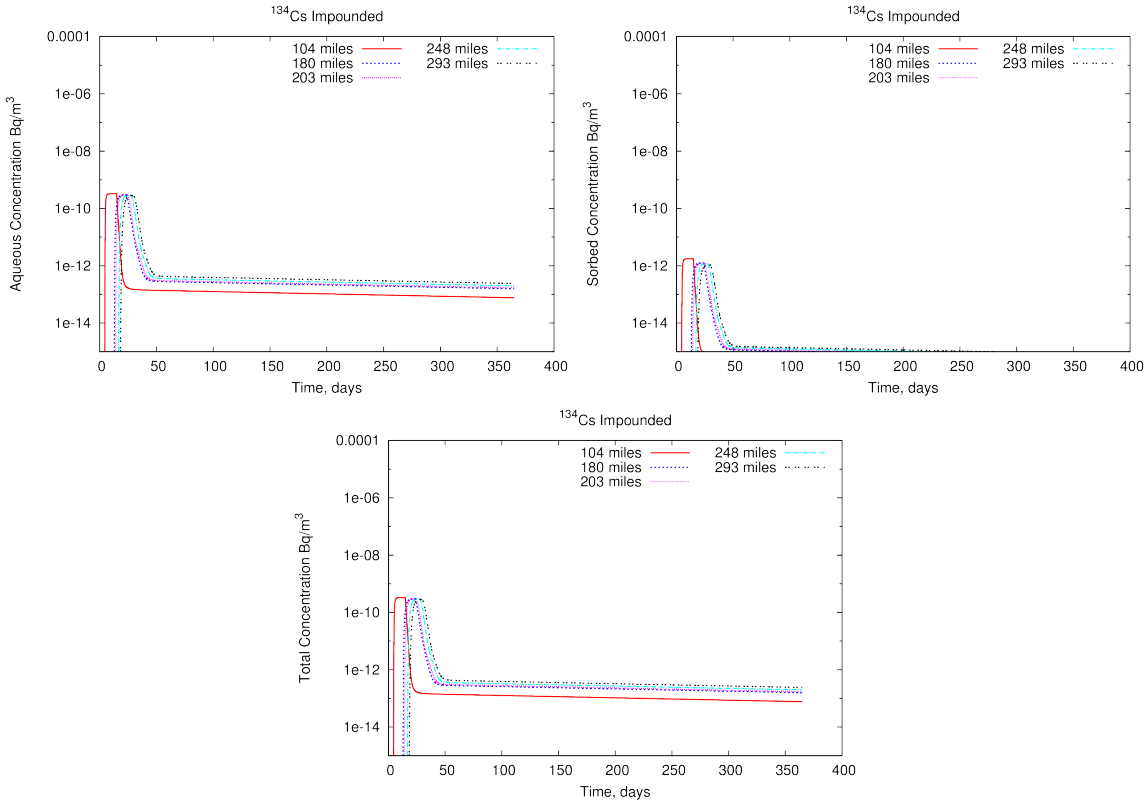

Figure B-82. Simulated impounded large river aqueous (top left), sorbed (top right), and total (bottom) ^{134}Cs activity over a full year at several locations along the same shore as the release (left) and the opposite shore (right).

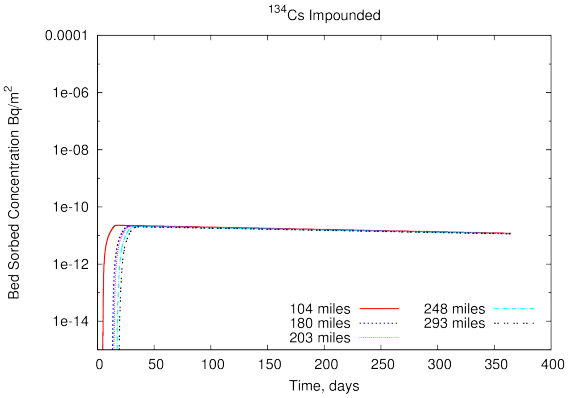

Figure B-83. Simulated impounded large river bed-sorbed ^{134}Cs activity over a full year at several locations.

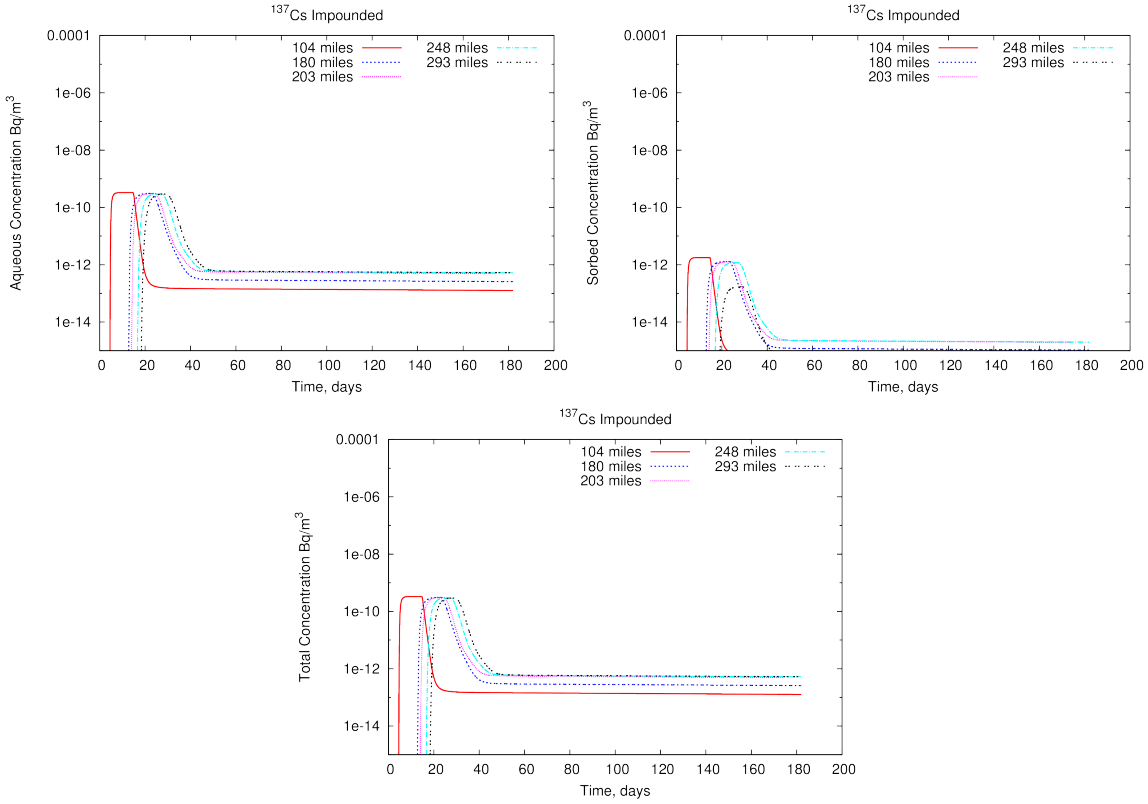

Figure B-84. Simulated impounded large river aqueous (top left), sorbed (top right), and total (bottom) ^{137}Cs activity over a full year at several locations.

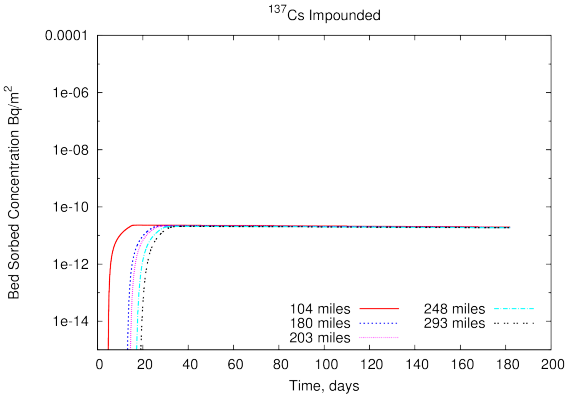

Figure B-85. Simulated impounded large river bed-sorbed ^{137}Cs activity over a full year at several locations.

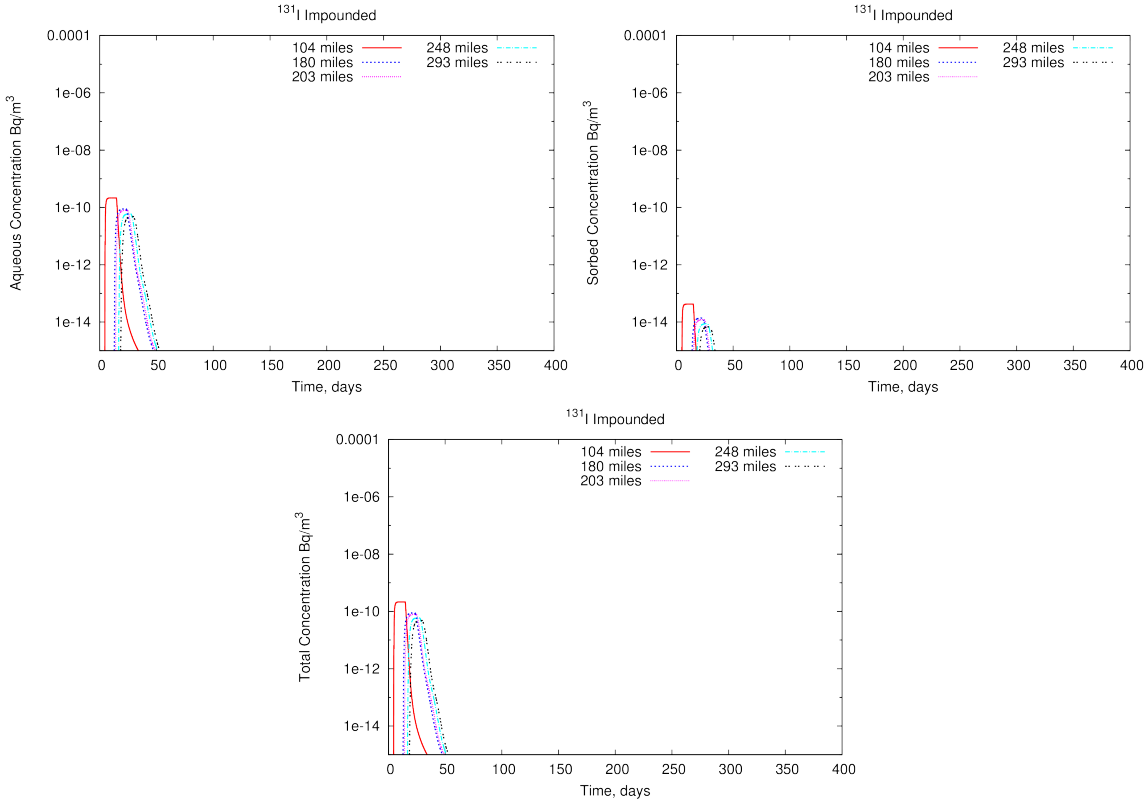

Figure B-86. Simulated impounded large river aqueous (top left), sorbed (top right), and total (bottom) ^{131}I activity over a full year at several locations.

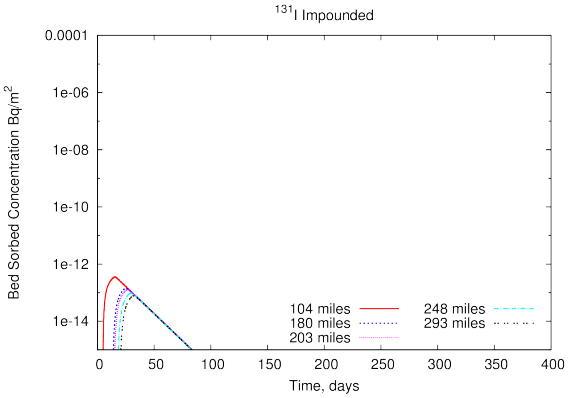

Figure B-87. Simulated impounded large river bed-sorbed ^{131}I activity over a full year at several locations.

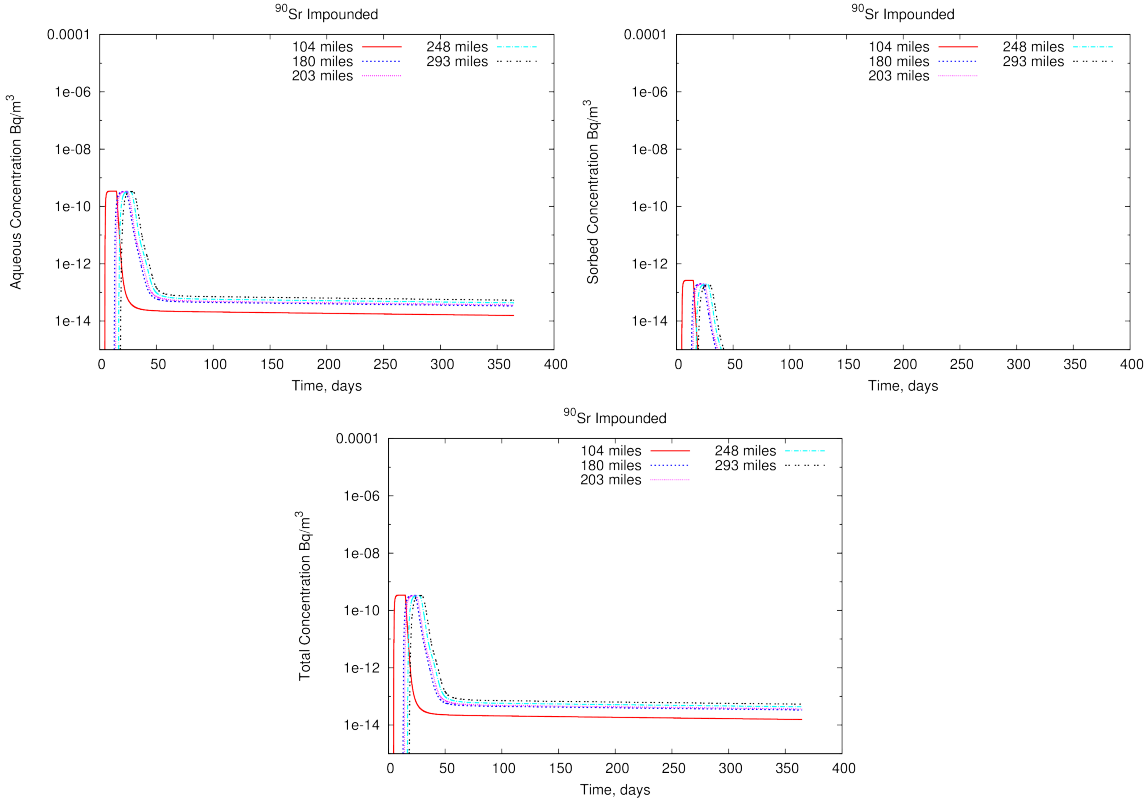

Figure B-88. Simulated impounded large river aqueous (top left), sorbed (top right), and total (bottom) ^{90}Sr activity over a full year at several locations.

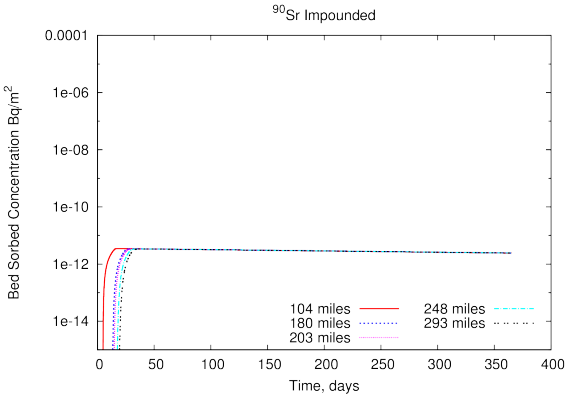

Figure B-89. Simulated impounded large river bed-sorbed ^{90}Sr activity over a full year at several locations.

B.3.4 Sensitivity Tests

B.3.4.1 Decreased Radionuclide Release

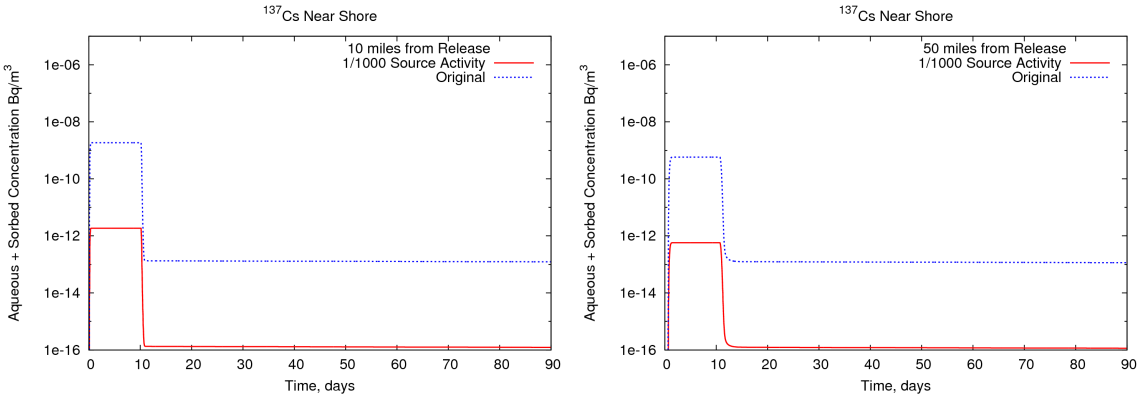

Figure B-90. Comparison of decreased release and original simulated large river ^{137}Cs activity concentrations at 10 (left) and 50 (right) miles from the release.

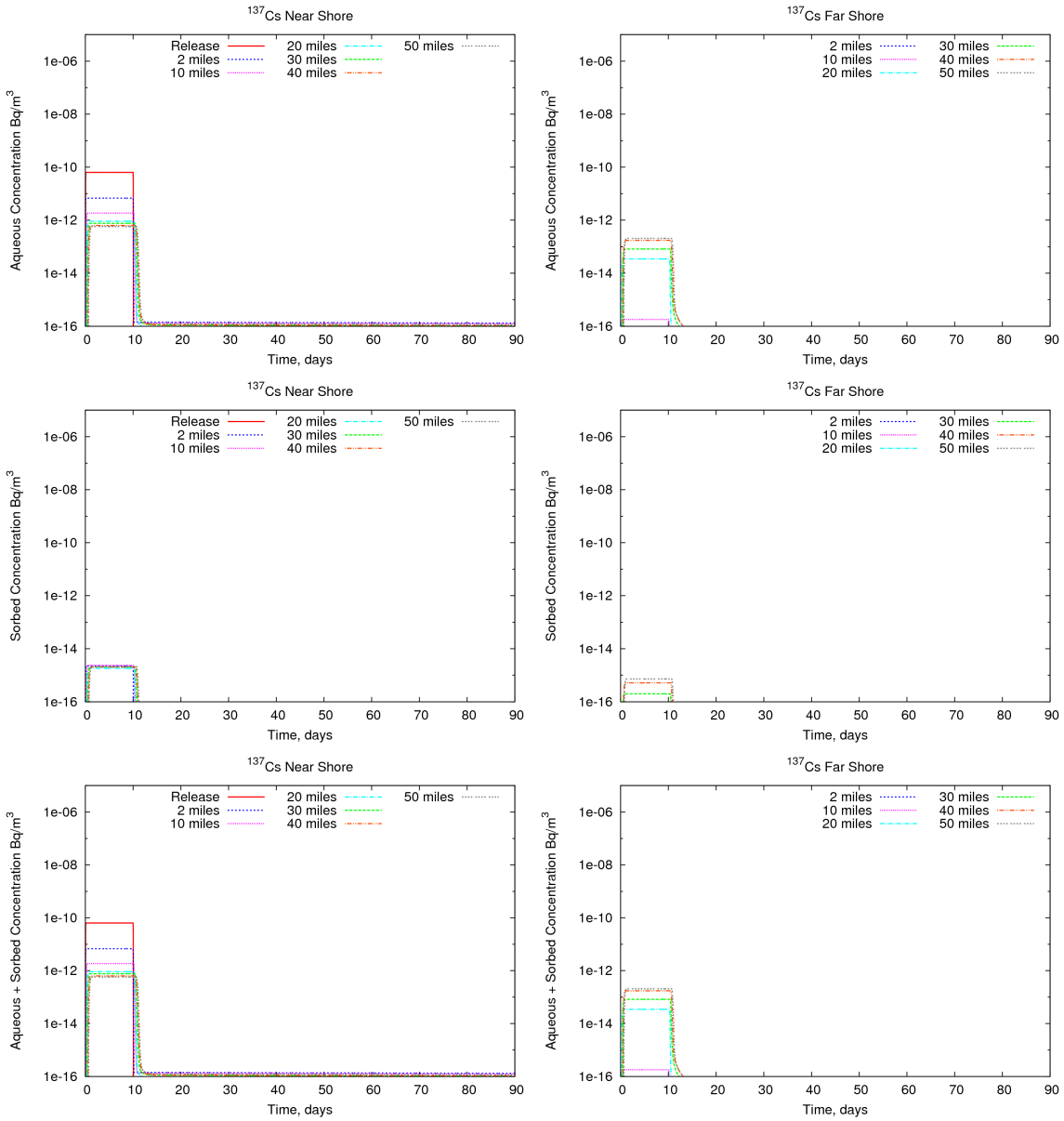

Figure B-91. Simulated decreased release large river aqueous (top), sorbed (middle), and total (bottom) ^{137}Cs activity over a full year at several locations along the same shore as the release (left) and the opposite shore (right).

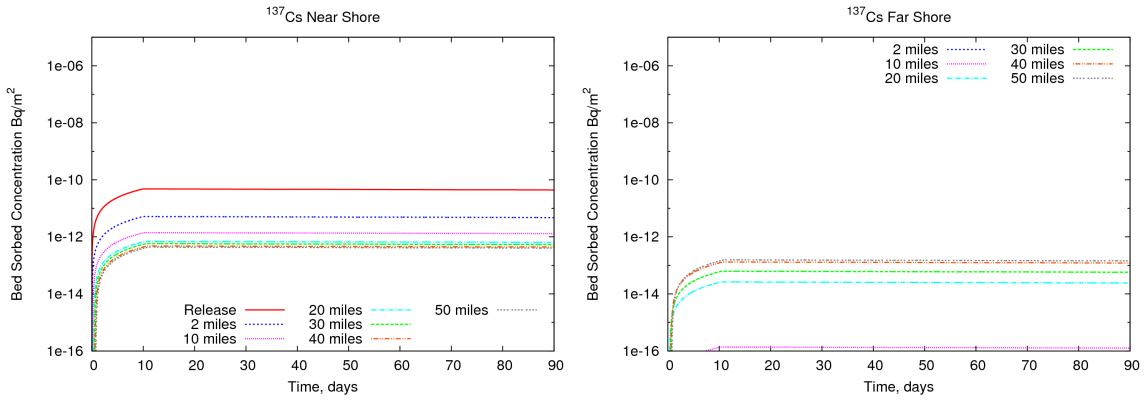

Figure B-92. Simulated decreased release large river bed-sorbed ^{137}Cs activity over a full year at several locations along the same shore as the release (left) and the opposite shore (right).

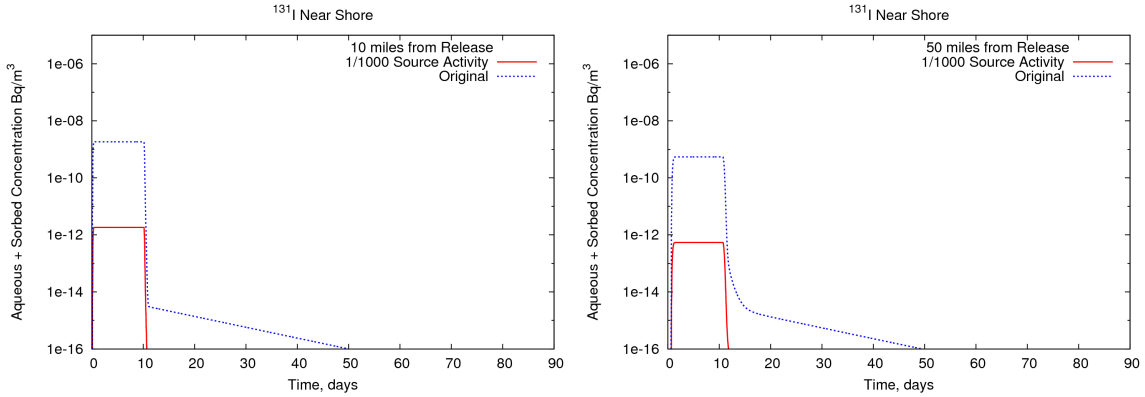

Figure B-93. Comparison of decreased release and original simulated ^{131}I activity concentrations at 10 (left) and 50 (right) miles from the release.

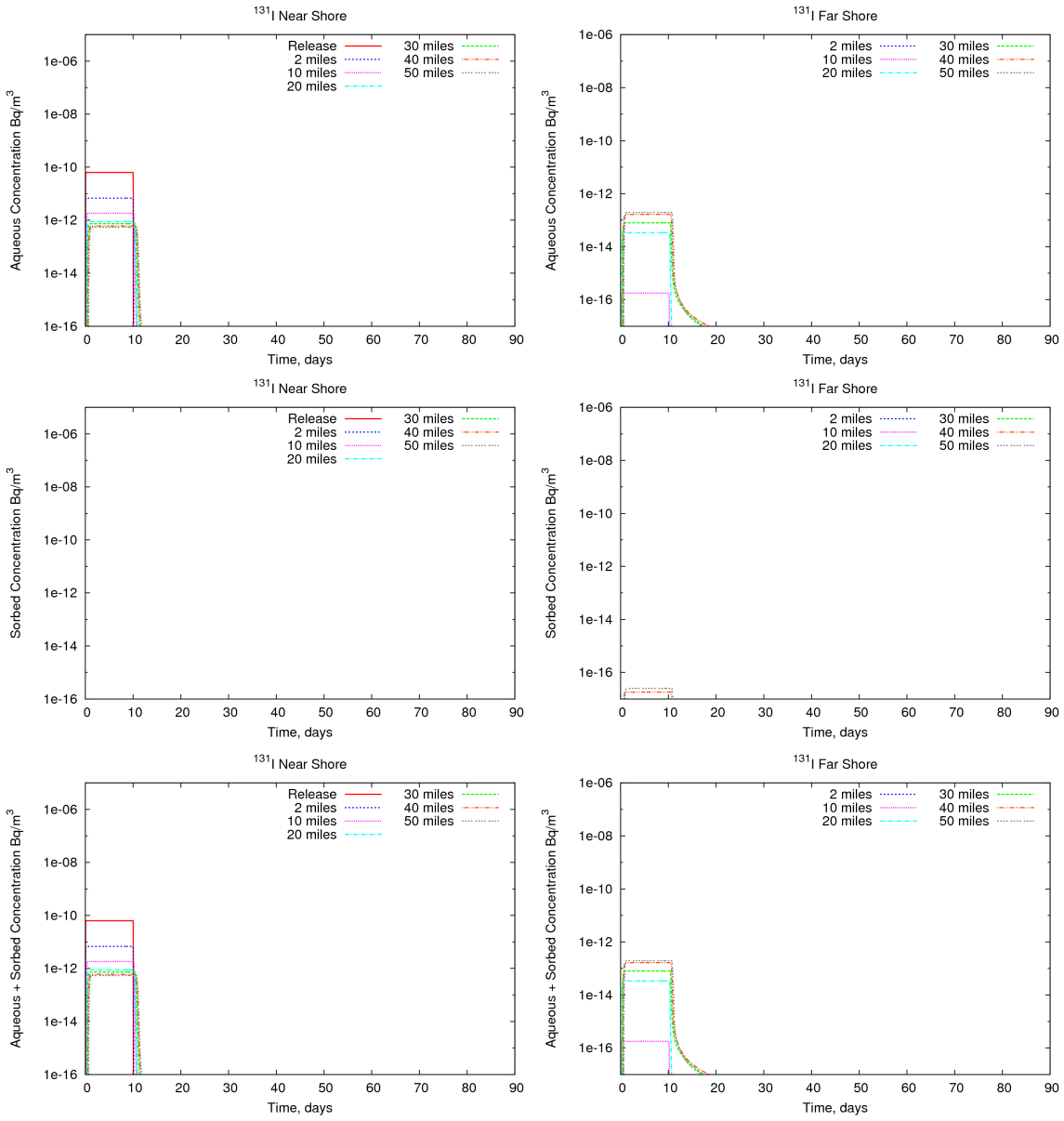

Figure B-94. Simulated decreased release large river aqueous (top), sorbed (middle), and total (bottom) ^{131}I activity over a full year at several locations along the same shore as the release (left) and the opposite shore (right).

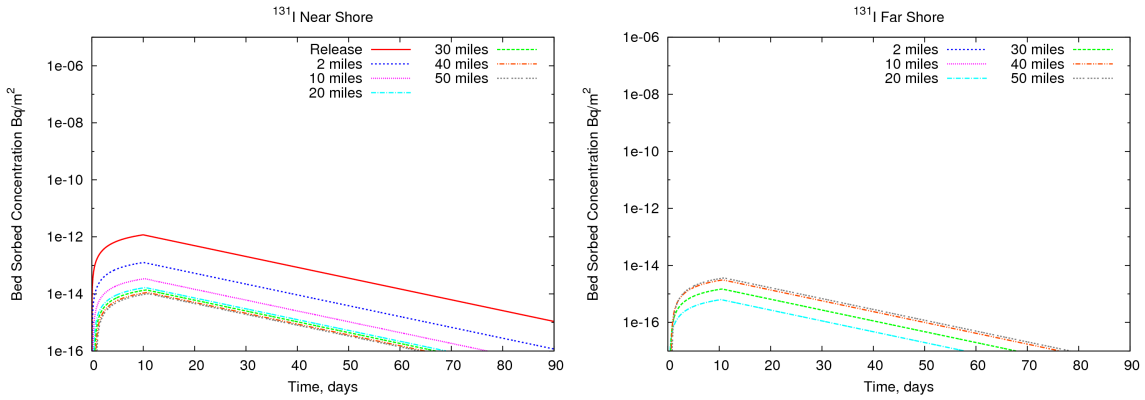

Figure B-95. Simulated decreased release large river bed-sorbed ^{131}I activity over a full year at several locations along the same shore as the release (left) and the opposite shore (right).

B.3.4.2 Increased Bed Depth

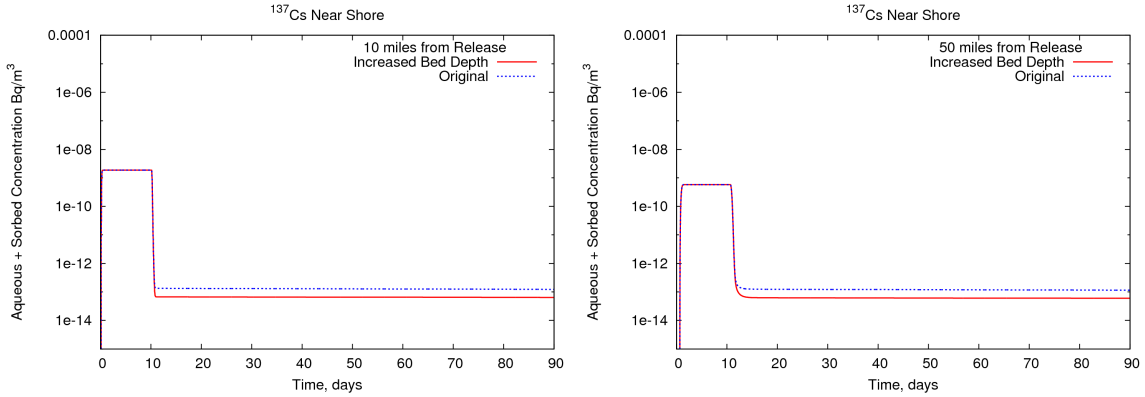

Figure B-96. Comparison of increased bed and original simulated ^{137}Cs activity concentrations at 10 (left) and 50 (right) miles from the release

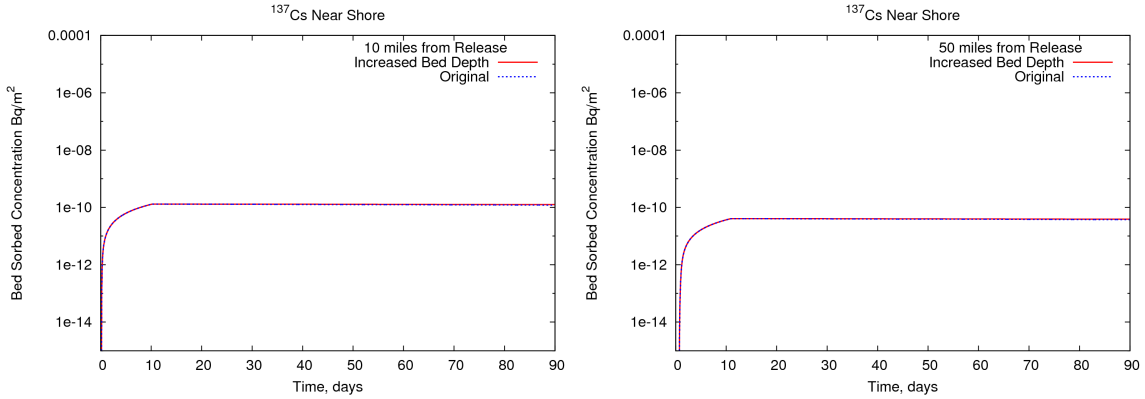

Figure B-97. Comparison of increased bed and original simulated ^{137}Cs activity concentrations in the bed at 10 (left) and 50 (right) miles from the release.

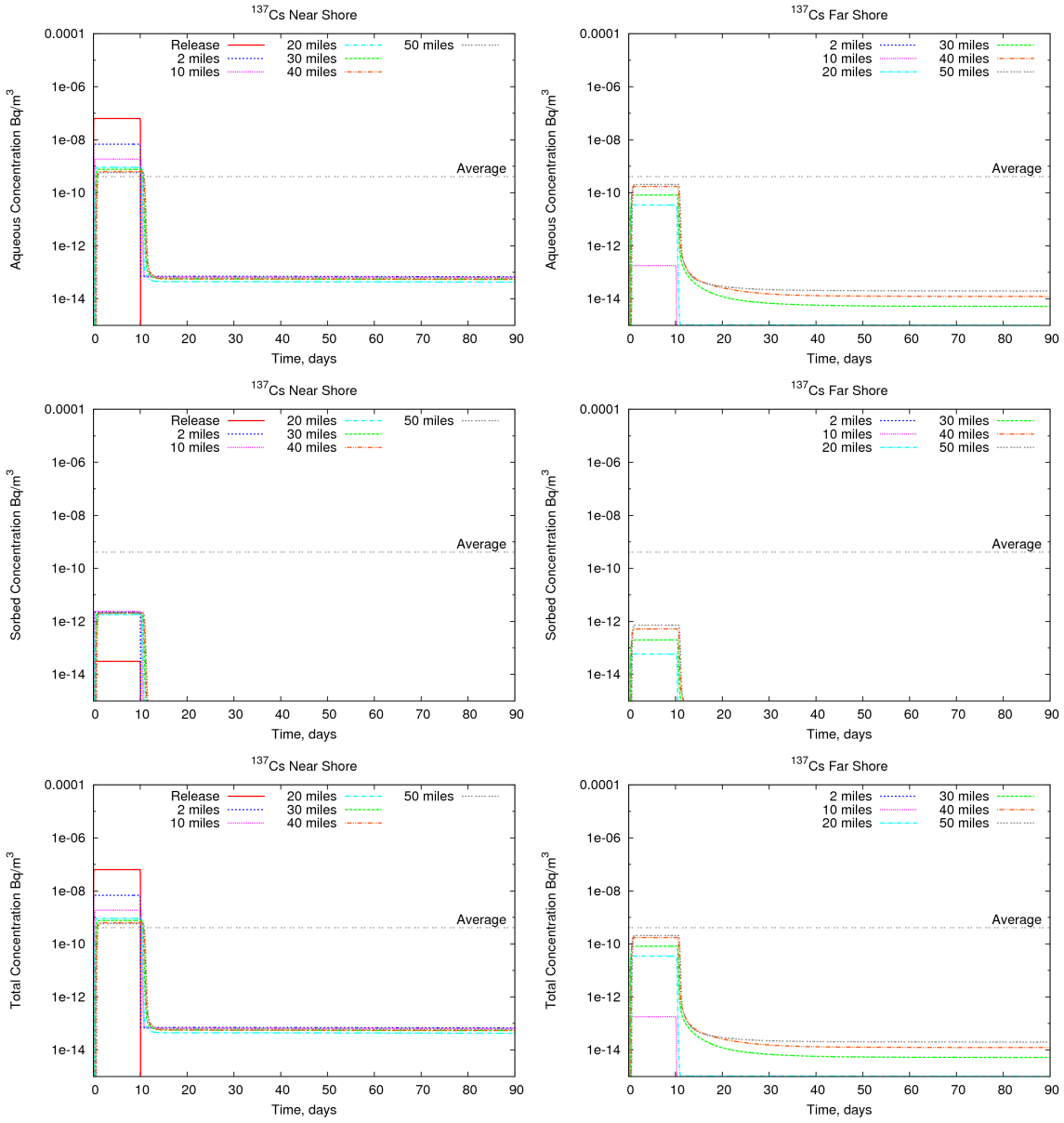

Figure B-98. Simulated increased bed depth large river aqueous (top), sorbed (middle), and total (bottom) ^{137}Cs activity over a full year at several locations along the same shore as the release (left) and the opposite shore (right).

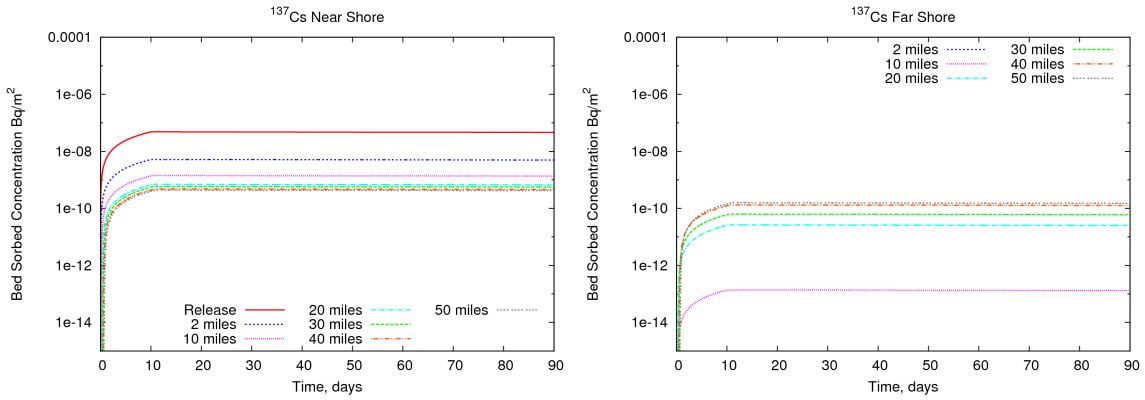

Figure B-99. Simulated increased bed depth large river bed-sorbed ^{137}Cs activity over a full year at several locations along the same shore as the release (left) and the opposite shore (right).

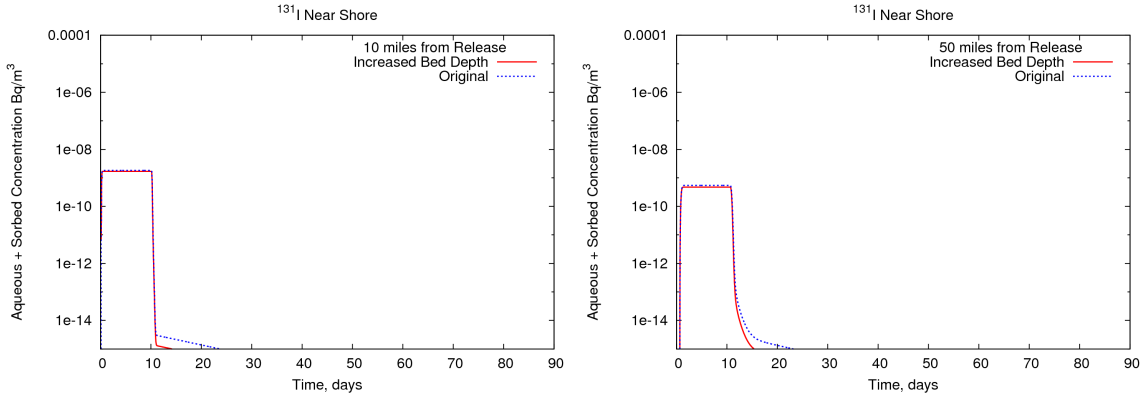

Figure B-100. Comparison of increased bed and original simulated ^{131}I activity concentrations at 10 (left) and 50 (right) miles from the release

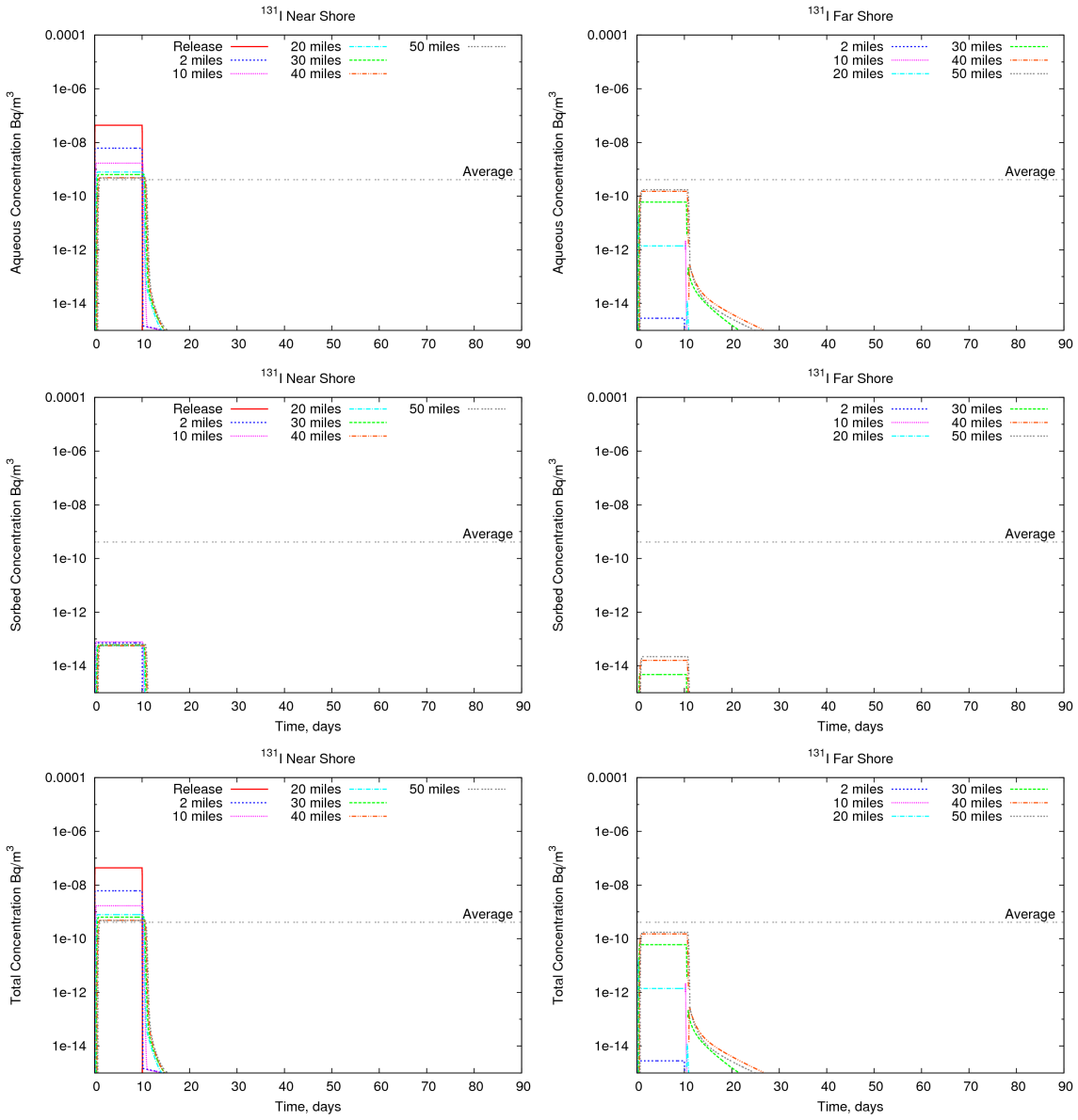

Figure B-101. Simulated increased bed depth large river aqueous (top), sorbed (middle), and total (bottom) ^{131}I activity over a full year at several locations along the same shore as the release (left) and the opposite shore (right).

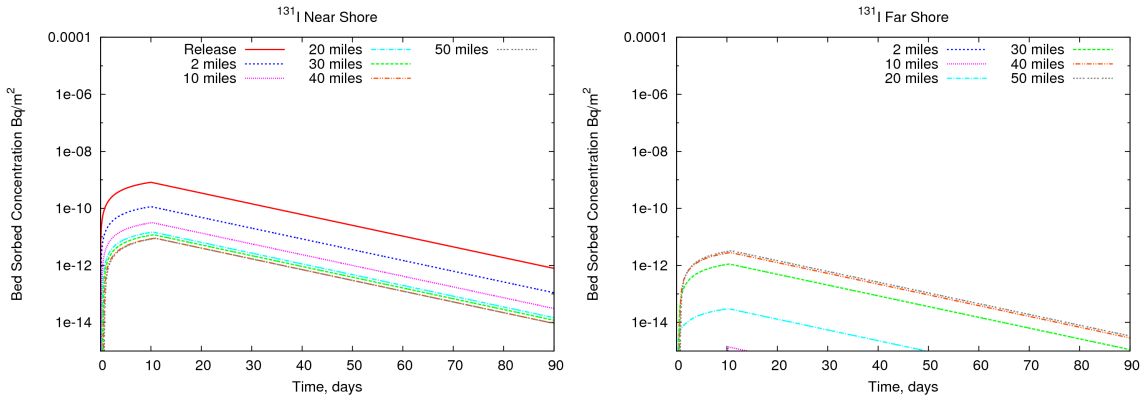

Figure B-102. Simulated increased bed depth large river bed-sorbed ^{131}I activity over a full year at several locations along the same shore as the release (left) and the opposite shore (right).

B.3.4.3 Increased Sediment Load

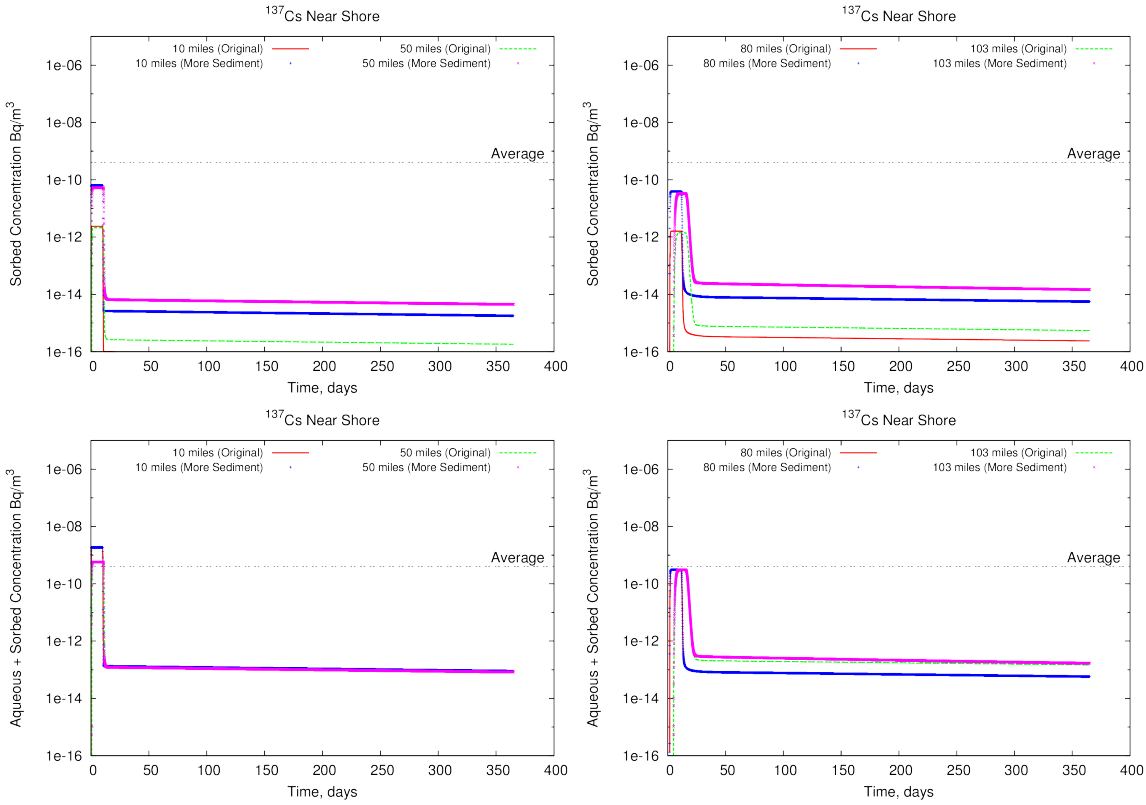

Figure B-103. Comparison of water column activity concentration from the original one-year large river and increased sediment load simulation. Sorbed phase (top) and total (bottom) ^{137}Cs activity concentrations at 10 and 50 (left) and 80 and 103 (right) below the release location are shown.

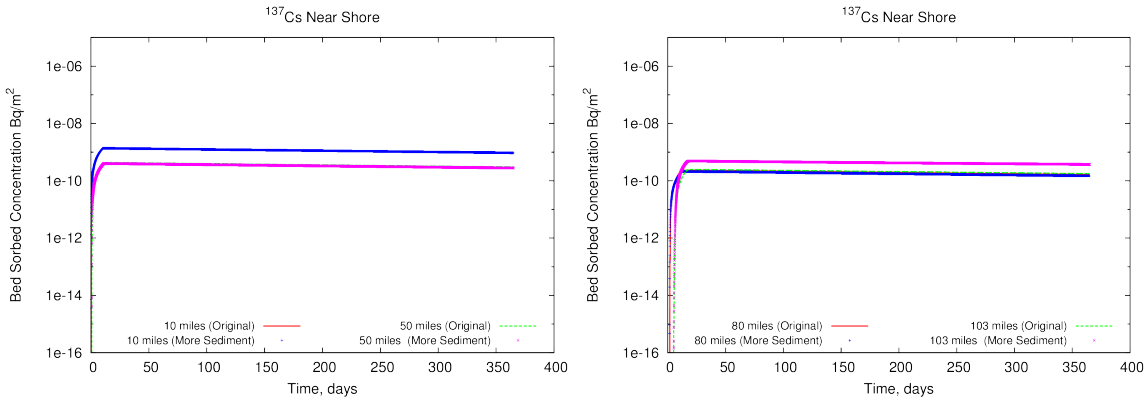

Figure B-104. Comparison of bed activity from the original one-year large river and increased sediment load simulation at 10 and 50 (left) and 80 and 103 (right) below the release location are shown.

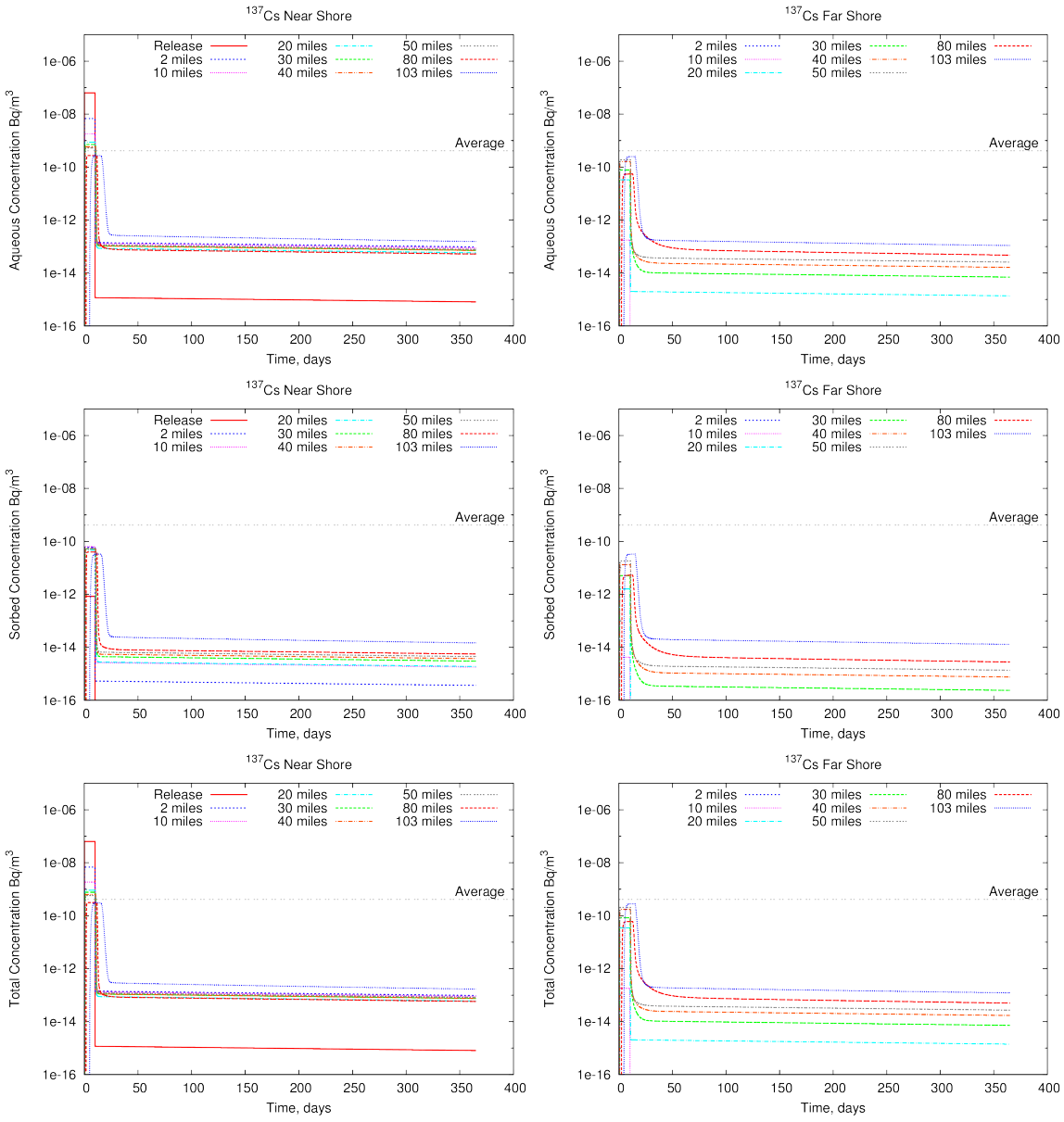

Figure B-105. Simulated increased sediment load large river aqueous (top), sorbed (middle), and total (bottom) ^{137}Cs activity over a full year at several locations along the same shore as the release (left) and the opposite shore (right).

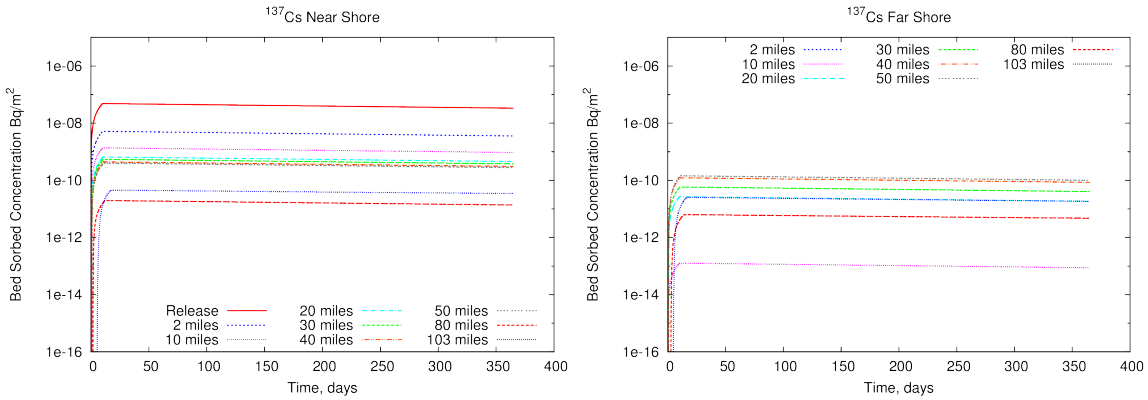

Figure B-106. Simulated increased sediment load large river bed-sorbed ^{137}Cs activity over a full year at several locations along the same shore as the release (left) and the opposite shore (right).

NRC FORM 335
(12-2010)
NRCMD 3.7

U.S. NUCLEAR REGULATORY COMMISSION

BIBLIOGRAPHIC DATA SHEET

(See instructions on the reverse)

1. REPORT NUMBER
(Assigned by NRC, Add Vol., Supp., Rev., and Addendum Numbers, if any.)

NUREG/CR-7231

2. TITLE AND SUBTITLE

Modeling of Radionuclide Transport in Freshwater Systems Associated with Nuclear Power Plants

3. DATE REPORT PUBLISHED

MONTH	YEAR
April	2017

4. FIN OR GRANT NUMBER

V6366

5. AUTHOR(S)

S. B. Yabusaki, B. A. Napier,
W. A. Perkins, M. C. Richmond, C. L. Rakowski,
S. F. Snyder, and L. F. Hibler

6. TYPE OF REPORT

Technical

7. PERIOD COVERED (Inclusive Dates)

2015-2016

8. PERFORMING ORGANIZATION - NAME AND ADDRESS (If NRC, provide Division, Office or Region, U. S. Nuclear Regulatory Commission, and mailing address; if contractor, provide name and mailing address.)

Pacific Northwest National Laboratory
Richland, Washington 99352

9. SPONSORING ORGANIZATION - NAME AND ADDRESS (If NRC, type "Same as above", if contractor, provide NRC Division, Office or Region, U. S. Nuclear Regulatory Commission, and mailing address.)

Division of Risk Analysis
Office of Nuclear Regulatory Research
U.S. Nuclear Regulatory Commission
Washington, DC 20555-0001

10. SUPPLEMENTARY NOTES

11. ABSTRACT (200 words or less)

The potential consequences of radionuclides that have been directly released into a surface water body, as happened in the 2011 Fukushima Daiichi nuclear power plant accident, are not well understood, especially for the lake and river settings where most U.S. nuclear power plant reactors are sited. Accordingly, hypothetical scoping analyses were performed to better understand how radionuclide transport in freshwater systems might be affected by the interaction of radionuclide-specific decay and sorption with hydrologic and sediment conditions. Eight radionuclides, 137Cs, 134Cs, 131I, 90Sr, 3H, 106Ru, 125Sb, and 144Ce, were selected for these analyses based on a methodology that estimated the partitioning of the reactor core inventory to water as a function of reactor type, mass of uranium fuel, and fuel burnup. Transport simulations for each radionuclide were based on the release of a 10-day pulse of 1,000 m3 of water with 1 Bq (providing fractional concentrations) of activity into small lake, small river, and large river settings. The small lake setting was based on a reservoir impounded by a dam on a river that provided a large water volume but limited transport, which led to high concentrations at early times. The small river setting examined relatively low flow and slow average velocity conditions, resulting in less dilution (i.e., higher concentrations) and longer transit times for the 10-day radioactive release. The large river scenario examined conditions where relatively high flow resulted in lower concentrations but faster downriver transport. Modeled transport processes included advection, mixing/dispersion, decay, sediment transport, and sediment-radionuclide interaction (i.e., adsorption/desorption); modeled features included the impact of tributaries, dams, and impoundments.

12. KEY WORDS/DESCRIPTORS (List words or phrases that will assist researchers in locating the report.)

severe reactor accident, freshwater, aqueous release, transport, sediment radionuclide interaction,

13. AVAILABILITY STATEMENT

unlimited

14. SECURITY CLASSIFICATION

(This Page)

Federal Recycling Program

UNITED STATES
NUCLEAR REGULATORY COMMISSION
WASHINGTON, DC 20555-0001

OFFICIAL BUSINESS

NUREG/CR-7231

Modeling of Radionuclide Transport in Freshwater Systems Associated with Nuclear Power Plants

April 2017